Development of Novel Sorbent Beads for Removal of Radionuclides and Organic Contaminants

By

Charu Dwivedi

(CHEM01200704001)

Bhabha Atomic Research Centre, Mumbai

A thesis submitted to the

Board of Studies in Chemical Science Discipline

In partial fulfillment of requirements

For the Degree of

DOCTOR OF PHILOSOPHY

of

HOMI BHABHA NATIONAL INSTITUTE

August, 2012

Homi Bhabha National Institute

Recommendations of the Viva Voce Board

As members of the Viva Voce Board, we certify that we have read the dissertation prepared by **Charu Dwivedi** entitled **Development of novel sorbent beads for removal of radionuclides and organic contaminants** and recommend that it may be accepted as fulfilling the dissertation requirement for the Degree of Doctor of Philosophy.

Chairman- Dr. P. N. Bajaj — Date: 21.11.2012

External Examiner- Dr. Nand Kishore — Date: 21.11.2012

Manmohan Kumar

Guide/Convener- Dr. Dr. M. Kumar — Date: 21-11-2012

Co-Guide - Shri. P. K. Wattal — Date: 21-11-2012

Member - Dr. T. N. Das — Date: 21-11-2012

Yk Bhardwaj

Member - Dr. Y. K. Bharadwaj — Date: 21/11/2012

Final approval and acceptance of this dissertation is contingent upon the candidate's submission of the final copies of the dissertation to HBNI.

I hereby certify that we have read this dissertation prepared under our direction and recommend that it may be accepted as fulfilling the dissertation requirement.

Date: 21/11/2012

Place: Bhabha Atomic Research Centre, Mumbai, India

STATEMENT BY AUTHOR

This dissertation has been submitted in partial fulfillment of requirements for an advanced degree at Homi Bhabha National Institute (HBNI) and is deposited in the Library to be made available to borrowers under rules of the HBNI.

Brief quotations from this dissertation are allowable without special permission, provided that accurate acknowledgement of source is made. Requests for permission for extended quotation from or reproduction of this manuscript in whole or in part may be granted by the Competent Authority of HBNI when in his or her judgment the proposed use of the material is in the interests of scholarship. In all other instances, however, permission must be obtained from the author.

Charu Dwivedi

Charu Dwivedi

DECLARATION

I, hereby declare that the investigation presented in the thesis has been carried out by me. The work is original and has not been submitted earlier as a whole or in part for a degree / diploma at this or any other Institution / University.

Charu Dwivedi
Charu Dwivedi

Dedicated to…….

………My Parents

Acknowledgment

I would like to express my heartfelt gratitude and regards to my worthy supervisor, Dr. M. Kumar, for his luminous guidance, encouragement and support in executing this project from conception to completion

In equal measure, I extend my gratitude to Dr. P. N. Bajaj of Bhabha Atomic Research Centre (BARC) whose continual encouragement helped me to endure the process. He has also been an influential mentor to me and his wise input, invaluable comments and suggestions were integral to the successful completion of this thesis.

I am thankful to the Director Chemistry Group, Dr. T. Mukherjee, for providing necessary facilities during the course of work. I am indebted to him for rendering all the help and encouragement throughout my endeavor.

I extend many thanks to my co-guide, Mr. P. K. Wattal, and the doctoral committee members, Dr. T. N. Das and Dr. Y. K. Bhardwaj, for their part in guiding and supporting this work.

I would also like to thank Dr. S. K. Sarkar, Head, Radiation & Photochemistry Division, Dr. D. B. Naik and all the members of the Radiation & Photochemistry Division, for their kindness and gracious assistance.

I also want to express my gratitude to Dr. A. Kumar, Dr. S. C. Tripathi and Mr. S. K. Pathak who were kind enough in extending the facilities for radioanalytical measurements.

I would also like to express my thanks to Dr. C. G. S. Pillai and Mr. J. Nuwad for the assistance of scanning electron microscopy.

My sincerest thanks are due to Chetan, Krishankant, Suraj, Juby, Farheen and Ridhima, for their moral support and providing a soothing hand when it was needed.

I am eternally grateful to my parents and brother, for their love, patience, care, encouragement and blessings.

Last but not the least, I am thankful to Almighty for all time blessings.

Charu Dwivedi
Charu Dwivedi
(August, 2012)

Table of Contents

Chapter-2: Experimental and Techniques 40

Synopsis

Development of novel sorbent beads for removal of radionuclides and organic contaminants

Man not only survives and functions in his environment, he shapes it and he is shaped by it (René Dubos). Development of science and technology has changed the human lifestyle and his environment immensely. Since the industrial revolution, human has become more and more reliant on technology. In today's world, superior technologies contribute to build robust economies, and in a well-functioning robust economy, economic excess naturally flows into the greater use of technology. Technology has become such an inseparable part of human society, especially its economic aspects, funding sources for technological endeavors are virtually unlimited. All these advancements in technologies and industrialization have negative impact on the environment, which undoubtedly has affected the people. The negative impact of industrialization and technological developments on the environment include the depletion of nonrenewable natural resources, such as petroleum, coal, ores etc., pollution of air, water and land, depletion of ozone layer, increased global warming, reduced vegetation, climate change, natural habitat destruction, etc.[1] It is rightly said that, civilization has wrecked the planet, from the seafloor to the stratosphere. With every new development in the technology, new types of waste are generated, which were previously unknown to humans, such as toxic waste, radioactive waste, electronic waste, etc. To have a sustainable development and clean environment, it is required to develop effective ways, to remove these pollutants on a large scale expediently. These pollutants have polluted air, soil and water greatly. Especially, water pollution has affected all the living beings on this planet. The importance of water for all the living beings is well realized from ancient times. It is well mentioned in Atharav Veda, “Water is the elixir of life, and water contains medicines”. Perhaps access to water has been the most essential ingredient for any viable civilization to grow and sustain. Almost all the great civilizations of the world were founded and flourished around water sources, and water still has influence on the economy, society and the overall development of any nation. With the advancements in the science and technology, the quality of life has improved, but this development also has adverse impact on environment, especially on water resources. Various human activities have polluted water tremendously, in which the contribution from different industries is the largest.[2-3] It is essential to minimize the discharge of toxic contaminates from various industrial waste streams into environment, for sustainable growth.

The waste from industries can be broadly classified into two categories, nuclear waste and non nuclear waste. The nuclear waste comprises the radioactive contaminants coming from the use of radioactive materials. The main sources of radioactive wastes include large sealed radiation sources used in medicine, industry, agriculture and the food industry, for diagnostic and therapeutic purposes, materials testing, pasteurization and sterilization.[4-5] However, the largest contributor is the nuclear power generation industry. Nuclear power is considered as economically competitive and environmentally clean way of power generation, as compared to most of the other forms of energy used for electricity production. The nuclear waste is categorized on the basis of its physical, chemical and radiochemical properties, and accordingly, given different treatments.

The waste water stream, free of radioactive contaminants, is termed as non nuclear waste. But, the origin and nature of the pollutants in these waste streams are different for different industries. The various waste streams from these industries include employees' sanitary waste, process waste from manufacturing, product washing water, spills and leakages, heating and cooling water operations. Depending on the source of origin, the wastewater constituents may include dissolved organics, ammonia, fluoride, nitrate, organic nitrogen, phosphorus, aluminum, potassium, sulfur and heavy metal ions.

The commercially employed waste water treatment procedures for nuclear and non-nuclear waste include evaporation, chemical precipitation/flocculation, solid-phase separation and ion exchange.[6-7] Concerted and sincere efforts are required from the scientific fraternity, to focus on the development of new methods and technologies for controlling water pollution, and to improve the existing waste water treatment technologies. Along with other branches of science, chemistry plays a very important role in understanding the source, nature, and effects of the various pollutants coming from different industrial waste streams, on the environment. With deep knowledge and application of the concepts of chemistry in waste treatment and disposal, it is possible to develop new technologies to check and control water pollution.

The main objective of the thesis is to develop novel sorbent beads for removal of radionuclides and other toxic pollutants from the various waste water streams from nuclear and non nuclear industries. Special emphasis is given for removal of radio-cesium from different types of nuclear waste streams. The synthesis procedures proposed here are novel, use simple chemicals and ambient synthesis conditions. The thesis focuses on the development of novel methods of synthesis of various organic and inorganic sorbents, using polymers, directly into a more appropriate and efficient physical form, for removing radioactive and toxic metal ions from the waste waters.

The thesis has been organized into six chapters, elaborating the work done on the above mentioned theme.

Chapter 1

The introduction chapter deals with some basic knowledge of industrial waste and their classifications, based on source, origin, physical state, and radioactivity. This chapter also elaborates the importance of nuclear power plants, and nuclear fuel reprocessing. Further, it describes various methods of treatment for industrial waste water streams, and the role of chemistry in the development of new methodologies for water remediation technologies.

This chapter also elaborates the necessity of cesium removal from various waste streams coming from nuclear industry, and the various methods currently being employed, or proposed, for its efficient removal. The objective of the present work is described, along with an overview of the literature reports in the relevant areas.

Chapter 2

This chapter describes the general methods used for the synthesis of organic resins, inorganic sorbents, and inorganic sorbent-polymer composites, as well as the techniques which have been used for the characterization of the synthesized materials. Different polymer resins and inorganic sorbent-polymer composites, in the form of beads, have been synthesized, for removal of cesium ions from various nuclear waste streams. For characterization of the synthesized materials, various techniques, such as X-Ray diffraction (XRD), infrared spectroscopy, scanning electron microscopy (SEM), thermal analysis and

BET surface area analysis, have been employed. Radioanalytical technique of analysis has been used, to investigate the sorption of cesium ions onto various synthesized sorbents, using ^{134}Cs and ^{137}Cs as radiotracers. The degradation of dye has been monitored, employing UV-Visible absorption spectroscopy.

Chapter 3

This chapter describes the use of resorcinol formaldehyde resin in nuclear industry, for removal of cesium ions from alkaline waste. Three new synthetic approaches have been proposed for synthesizing RF resin directly into spherical bead form. The characterization and application of the beads is also discussed in detail. The chapter is divided into two sections, one for the synthesis of pure RF beads, and the other for the synthesis of RF beads by using spherical template beads of XAD-4 and calcium alginate.

Section 1

This section deals with synthesis of spherical resorcinol-formaldehyde beads, using suspension polymerization technique, characterization and application, thereof.

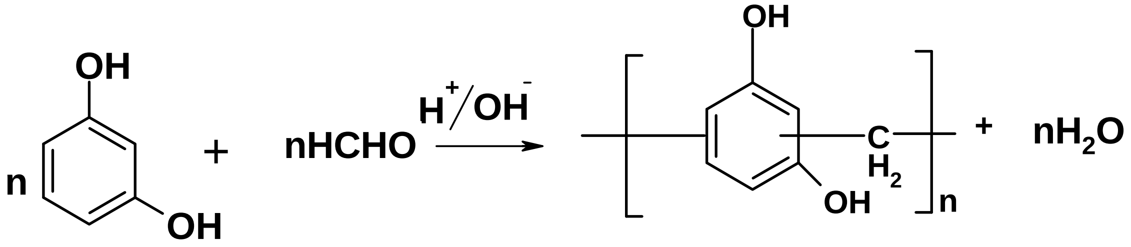

For preparation of spherical RF beads, the RF pre-condensate was prepared by the reaction of resorcinol with formaldehyde in the presence of alkaline catalyst. When this pre-condensate attained a suitable viscosity, it was suspended in a stabilizing bath of a suitable polymer solution with continuous stirring. It was observed that, on addition of the aqueous RF pre-condensate into the polymeric solution, the polymer precipitated on the surface of aqueous RF pre-condensate, and acted as a protective shield, preventing agglomeration of the RF droplets. The further condensation reaction of the RF pre-condensate occurred within these polymer coated beads, and after complete curing, the protective polymer coating was washed off by using suitable solvent. With this method spherical resorcinol formaldehyde beads, with better control on their mean size, can be synthesized. The effect of various synthesis parameters such as, viscosity of the RF pre-condensate at the time of mixing, agitation intensity, organic to aqueous ratio and the amount of the stabilizing polymer, on the mean diameter of the synthesized beads was investigated. These RF beads can be used, to develop sorbents for chromatographic columns and as cation exchanger, for removal of radioactive cesium from alkaline nuclear waste. The synthesized beads were characterized by IR and TGA techniques. The mechanical strength of these beads was measured, using a universal testing machine. The mechanical strength of the beads was found to be quite high as compared to the conventional RF grounded particles.

The potential of theses beads in removing cesium ions from alkaline waste was studied in batch mode. Equilibrium isotherm studies were carried out, by varying the initial concentration of non-radioactive cesium in the solution, from 0.1-50 mM. The liquid to solid phase ratio of ~100 :1 was maintained for all the experiment and the contact time was 6 hr, for most of the experiments. The equilibrium data were fitted to Langmuir, Freundlich and Temkin isotherm models. It was observed that Langmuir isotherm explains sorption process nicely. Using Temkin model, the spontaneous nature of the sorption process was established. The effect of the resin mesh size on percentage uptake of cesium ion was also investigated, and 20-40 mesh size was found to be optimum. The kinetics of the sorption was studied at different initial cesium ion concentrations, and the kinetics data were fitted to various kinetic models. The cesium ion sorption was found to follow pseudo second-order kinetics. The mechanistic steps involved were found to be complex, consisting of both film diffusion and intraparticle diffusion.

Section 2

This section describes synthesis of resorcinol-formaldehyde (RF) resin in spherical form, of required mesh size, using pre-formed spherical beads as template. Here, RF pre-condensate was loaded onto two different templates, vis-a-vis commercially procured XAD-4 beads, and, in-house prepared calcium alginate beads. The synthesized RF-coated XAD (RF-XAD) beads and RF beads synthesized, using alginate (RF^A) beads were characterized, by different techniques. Suitable size and mechanical stability, along with their spherical shape, make these beads the most appropriate for column operation. The efficiency of these beads was evaluated for removal of cesium, from alkaline medium, in batch conditions, using radioanalytical technique. The effect of operating variables, such as initial cesium ion concentration, sodium ion concentration, and contact time was also investigated. It was observed that, there is a decrease in the K_d value for Cs^+ ions with increase in Na^+ ion concentration, in the case of both the resin beads. The equilibrium data were fitted to different isotherm models, and were found to be represented well by the Langmuir isotherm equation, with a monolayer sorption capacity values of 287 mg/g and 458.7 mg/g, respectively, for RF-XAD and RF^A beads.[8] Kinetic modeling analysis, using various models, show that the pseudo-second order equation was the most appropriate model for description of the sorption of cesium ions onto the RF-XAD beads over the entire studied range. Whereas, for RF^A beads, at higher initial cesium ion concentration, the pseudo first order kinetic was followed. Further analysis of the kinetics data showed that the process mechanism was complex, consisting of both film diffusion and intraparticle diffusion, with film diffusion as rate limiting step.

Chapter 4

This chapter deals with the studies carried out on transition metal hexacyanoferrates for their potential application in removal of cesium ions from nuclear waste streams. It describes the synthesis of copper hexacyanoferrate (CuHCF) and potassium copper hexacyanoferrate (KCuHCF) particles of controlled size, and their incorporation in different polymeric matrices, characterization and applications thereof. The chapter comprises two sections, describing the synthesis, characterization and applications of copper hexacyanoferrate sorbent beads. The first section describes the synthesis and sorption studies carried out with the copper hexacyanoferrates-loaded polyethersulfone (KCuHCF-PS) beads, while the second section synthesis and sorption studies carried out using potassium copper hexacyanoferrate loaded hydrogel (KCuHCF-Gel) beads, for removal of cesium ions.

Section 1

A novel method has been developed for preparation of different sorbent-polymer composite beads under simple laboratory conditions. Copper hexacyanoferrate was synthesized, and its composite beads of required composition and size were prepared by phase inversion technique, using polyethersulfone as the polymer matrix. Further, the results of TGA, IR, SEM and BET surface area analysis of the beads have been discussed in the chapter. The efficiency of these composite beads for the removal of cesium was tested, using radioanalytical technique, in batch method. The effect of pH, the initial metal ion concentration and contact time was also investigated. The synthesized composites beads perform best in the pH range 5-9. Different sorption isotherm models were applied to the experimental data. Equilibrium data are found to be represented well by the Langmuir isotherm equation, with a monolayer sorption capacity of 1.57 mg/g of the swollen beads. Kinetic modeling analysis, by fitting the data in the pseudo first-order, pseudo second-order, and intraparticle diffusion equations, show that the pseudo second-order equation is the most appropriate model for the description of sorption of cesium ions onto the composite beads. The rate constants at different initial cesium ion concentrations has been determined. The process mechanism is found to be complex, consisting of both intraparticle diffusion and film diffusion.

Section 2

Potassium copper hexacyanoferrate-hydrogel beads were synthesized by using PVA and sodium alginate as a binding matrix. The synthesized beads were characterized, and their potential for removal of cesium from aqueous solution was investigated, using ^{137}Cs radiotracer. Maximum removal was observed in the pH range 3-9, and the beads were found to be stable under normal operating conditions of the extraction. The experimental results were analyzed, using Langmuir and Freundlich sorption isotherms, and monolayer capacity of the beads towards cesium was determined to be 1.6 mg/g of the swollen beads, which corresponds to 16 mg/g of the dry beads. The batch sorption kinetics was studied at various initial cesium ion concentrations, and the data were analyzed in terms of the different kinetic models. The kinetic data are described best by the pseudo second-order kinetic model, and the mechanism of sorption is found to be complex, and influenced by both external diffusion and intraparticle diffusion. The effect of the interfering ions on the sorption of cesium ions was also quantified in the interfering ion concentration range 0-48 mg/L. A decrease of ~5 % in the efficiency of beads for removal of cesium ions, was observed in the presence of Na^+& K^+, and 10% in the presence of Ca^{2+}& Ba^{2+} ions.

Chapter 5

This chapter deals with the synthesis, characterization and application of potassium cobalt hexacyanoferrate (KCoHCF) and potassium nickel hexacyanoferrate (KNiHCF) hydrogel-sorbent composite beads in removal of cesium. These beads were synthesized, using PVA containing sodium alginate as binding matrix. The characterization of these beads was carried out, using TGA and SEM techniques. The sorption of cesium ions onto these synthesized beads was studied. All the studies were conducted by a batch method, to determine equilibrium sorption and kinetic parameters at different initial cesium ion concentrations. The experimental isotherm data were analyzed, using the Langmuir and Freundlich sorption isotherms. The sorption process was described the best by Langmuir sorption isotherm, and the monolayer capacities of KCoHCF-Gel and KNiHCF-Gel beads, for sorption of cesium ions, were found to be 2 mg/g and 8 mg/g of the swollen beads, respectively. Sorption kinetics data were analysed, using pseudo first-order, pseudo second-order and intraparticle diffusion models. Kinetic studies show that the sorption follows a pseudo second-order reaction, in the case of both the gel beads. The initial sorption rate, pseudo first-order, pseudo second-order and intraparticle diffusion rate constants were evaluated, for different initial cesium ion concentrations, and discussed. The sorption mechanism is found to be complex.

Chapter 6

The technological applications of titanium dioxide (TiO_2) range from sensors and electronic devices to catalyst development. Especially, photo-catalysis by TiO_2 has received an increasing attention, since the photo-catalyst absorbs light, and causes various chemical reactions, and brings about the degradation of environmental pollutants. In this chapter, a new method of synthesis of mesoporous titanium dioxide microspheres, for photo-catalytic degradation of the dyes, by the sol-gel templating method, using calcium alginate as a sacrificial template, is described.[9-10] The effect of the synthesis conditions, such as calcining temperature, atmosphere and polymer content on the composition, crystallinity, phase and surface morphology, were investigated by TGA, XRD, SEM and EDX techniques. The effect of polymeric content on the surface area and the pore size of the titania beads was evaluated by BET surface area analysis. The results showed that N_2 atmosphere and high temperature influence the phase content and morphology of the microsphere significantly. Anatase-to-rutile phase transformation and formation of calcium titanate took place under nitrogen atmosphere at lower temperature, as compared to that under air atmosphere. To examine the applications of these synthesized microspheres, photo-catalytic activity was evaluated, by carrying out photo-degradation of methylene blue (MB) dye. The microsphere showed good photo-catalytic activity towards degradation of MB dye. These beads can be used for degradation of other dyes, and removal of toxic metals, such as arsenic.

Summary

The thesis gives a brief account of the sources of various industrial waste water streams, their classifications, as well as the approaches used for the treatment of such waste waters. It describes the necessity of removal of cesium ions from aqueous waste, which has different origins in nuclear industry, and is a constituent of almost all kinds of aqueous waste coming from nuclear power plants. Further, it briefly describes the literature survey on various methods used for removal of cesium ions from nuclear waste. The main goal of this Ph.D. programme is to focus on the applications of polymers, along with the development of new chemical methods, for the synthesis of organic and inorganic sorbents, and their polymeric composites, for removal of radionuclides, such as cesium, from the aqueous solutions. The resultant sorbents have been characterized, using several instrumental techniques. In addition to this, TiO_2 ceramic beads have been synthesized, and used for photo-degradation of dyes, such as metheylene blue.

References

1. A. J. Hunt, E. H. K. Sin, R. Marriott and J. H. Clark, *ChemSusChem*, 2010, **3**, 306-322.
2. D. Angel and M. T. Rock, *Technological Forecasting and Social Change*, 2009, **76**, 229-240.
3. J. Roy and S. Pal, *Current Opinion in Environmental Sustainability*, 2009, **1**, 192-200.
4. C. F. Schmidt, W. K. Nank and R. V. Lechowich, *Journal of Food Science*, 1962, **27**, 77-84.
5. P. Warde, *Medicine*, 2008, **36**, 15-18.

6. V. M. Nurchi and I. Villaescusa, *Coordination Chemistry Reviews*, 2012, **256**, 212-221.

7. H. Lal, J. A. Delgado, C. M. Gross, E. Hesketh, S. P. McKinney, H. Cover and M. Shaffer, *Environmental Science & Policy*, 2009, **12**, 1028-1039.

8. C. Dwivedi, A. Kumar, J. K. Ajish, K. K. Singh, M. Kumar, P. K. Wattal and P. N. Bajaj, *RSC Advances*, 2012, **2**, 5557-5564.

9 C. Dwivedi, N. Raje, M. Kumar, A. Reddy and P. Bajaj, *Journal of Radioanalytical and Nuclear Chemistry*, 2011 (Article in Press).

10. C. Dwivedi, N. Raje, J. Nuwad, M. Kumar and P. N. Bajaj, *Chemical Engineering Journal*, 2012, **193–194**, 178-186.

Figures

Tables

Chapter-1

Introduction

Man not only survives and functions in his environment, he shapes it and he is shaped by it (René Dubos). Development of science and technology has changed the human lifestyle and the environment immensely. Since the industrial revolution, human beings have become more and more reliant on technology. In today's world, superior technologies contribute to build robust economies, and in a well-functioning robust economy, economic excess naturally flows into greater use of the technology. Technology has become such an inseparable part of the human society, especially its economic aspects, funding sources for technological endeavors are virtually unlimited. All these advancements in technologies and industrialization have negative impact on the environment, which undoubtedly has affected the people. The negative impact of industrialization and technological developments on the environment include the depletion of nonrenewable natural resources, such as petroleum, coal, ores etc., pollution of air, water and land, depletion of the ozone layer, increased global warming, reduced vegetation, climate changes, natural habitat destruction, etc.[1] Richard Bach has rightly quoted that, civilization... wrecks the planet, from seafloor to stratosphere. With every new development in the technology, a new set of waste is created, which was previously unknown to human beings, such as toxic waste, radioactive waste, electronic waste, etc. To have a sustainable development and clean environment, it is required to develop effective ways to remove these pollutants on a large scale expediently. These pollutants have polluted air, soil and water greatly. Especially, water pollution has affected all the living beings on this planet. The importance of water for all the living beings is well realized from ancient times, and is rightly mentioned in Atharav Veda, “Water is the elixir of life, and water contains medicines”. The access to water has been the most essential ingredient for any viable civilization to grow and sustain. The importance of water for human society is symbolized by the fact that almost all the ancient great civilization originated, and flourished along the banks of major rivers, such as the Tigris, the Euphrates, the Ganges and the Nile. In the present times also, water remains the most essential natural resource for keeping the health and pleasant lives of people, and for making valuable natural and industrial products. The macroeconomic policies and the development strategies of a country have an intimate relationship with the demand and the investment in water related activities, including industries, agriculture and public sector services. The various human activities have polluted water tremendously, in which the contribution from different industries is the largest.[2-3] Water pollution is generally defined as any physical, chemical, or biological, alteration in water quality that has a negative impact on the living organisms. The sources of water pollution can be divided into the following two categories

i. **Point source:** Point source is contamination that enters the environment through any discernible, confined, and discrete conveyance, directly into the waterway, such as industrial plant discharges and municipal sewage treatment plant discharges. Point-source pollutants mainly pollute the surface waters, like rivers, lakes, seas, and are usually found in a **plume** that has the highest concentrations of the pollutant nearest the source, and their concentrations decrease with the increase in the distance from the source.

ii. **Non point source:** Nonpoint source pollution generally results from land runoff, precipitation, atmospheric deposition, drainage, seepage, or hydrologic modification. Nonpoint sources are the main contributors to the pollution of the ground water resources. The exact origin of the non point source usually cannot be traced, as it is spread over a large area.

The releases from the point source can be treated by wastewater treatment plants, but, the releases nonpoint sources can only be minimized. Municipal sewage treatment plant discharges and industrial plant discharges are the main sources of point source contaminants. Municipal point sources are the result of the community sewage treatment plants, wherein wastewater is treated in various steps, to make free of solid and organic matter and microorganisms, and then, often discharged to surface water. But, all the solids and organic matter are not removed during treatment, and this discharge acts as potential point source pollutant.

Industries are the major contributors to the point source water pollution. The sources of wastes in industrial process are numerous, and also extremely variable, both in quantity and quality. These waste water streams are treated and managed differently, depending on the characteristics of the wastes and the process producing these. With the development in science and technology, numerous industries are established, and growing worldwide, such as textile industry, cement manufacturing, chemical industries, dairy products processing, leather tanning and finishing, fertilizer manufacturing, metal products, machinery oil, gas extraction, paper and paperboard, hospital, nuclear industry, etc. Though, the spectrum of the pollutants in the waste water streams coming from these industries is very wide, still these pollutants can be classified into two categories, nuclear waste and non nuclear waste.

1.1 Nuclear Waste

As global trend for nuclear power and reprocessing continues, the research is geared towards removal and recovery of the fission products from the nuclear waste streams. The development and use of nuclear technology, beginning in the early 1940s, has led to a substantial inventory of nuclear waste.[4] The term nuclear waste embraces all the residues from the use of radioactive materials. The sources of radioactive wastes include large sealed radiation sources used in medicine, industry, agriculture and the food industry, for diagnostic and therapeutic purposes, materials testing, pasteurization and sterilization.[5-6] However, the largest contributor is the nuclear power generation industry.

As the worldwide demand for electricity is continuously increasing, the need for large-scale sustainable power sources is also increasing continuously. Concern has also grown over finding an energy source that will not produce large quantities of harmful greenhouse gases, as the power plants based on fossil fuel do. When used for energy production, fossil fuels, such as coal, oil and natural gas, emit massive amounts of carbon dioxide, which leads to global warming, as well as sulfur dioxide and nitrogen oxides, which cause acid rain and smog. Nuclear power plants do not emit these hazardous pollutants into the environment. Though, the elements used in nuclear fuel are non-renewable resources, nuclear power plants have promise for longer operation, with much smaller fuel requirement than the conventional thermal power plants based on the non-renewable fossil fuels. Nuclear power has environmental, economic, and security benefits over the fossil-fuelled power. The progress of a country depends on the electricity consumption per capita. Electricity demand in India also is increasing rapidly, and the 830 billion kilowatt hours (kWh) produced in 2008 was triple the output in 1990, though still represented only some 700 kWh per capita for the year. Coal provides 68% of the India's electricity at present, but the reserves are limited. Gas provides 8%, and hydro 14% of the total production. Nuclear power supplied 15.8 billion kWh of India's electricity in 2007 from 3.7 GWe (of 110 GWe total) capacity. The per capita electricity consumption figure is expected to double by 2020, with 6.3% annual growth, and reach 5000-6000 kWh by 2050.[7] From the current global energy consumption, it can be predicted that the oil reserves may last for only 40 more years, the natural gas reserves can support only 65 more years of energy production, and the coal reserves can last over 150 years. It is projected that uranium reserves for nuclear power are sufficient to meet the world's energy demands for 85 years, with the once-through open fuel cycle approach.[8] However, the closed nuclear fuel cycle, i.e., the recycling of nuclear fuel has the potential to increase the lifetime of nuclear power, from 85 years to more than 4000 years. Considering all the factors, the nuclear power emerges as a better option than the fossil-fuelled power, from environmental, economic and longevity perspectives. But, for nuclear energy to sustain as an attractive option for meeting the growing energy demands, practical solutions must be found for reprocessing of the used fuel, and disposal of the nuclear waste. Nuclear fuel reprocessing would benefit in multiple ways. It will recover the useful fissile and fertile materials from the waste, and also reduce the volume and toxicity of the waste, that requires long-term storage. But, handling of the highly radioactive waste, and that too in the large volumes, makes industrial reprocessing of the used nuclear fuel one of the most complex and challenging chemical processes, carried out on a large scale.[9] Therefore, for the safe, systematic and convenient management and treatment, the nuclear waste has been divided into different categories. Table 1 describes the categorization of the nuclear waste, based on its physical, chemical and radiochemical properties.

Table 1.1: Categorization of the nuclear waste based on its physical chemical and radiochemical properties

Physical Properties	Chemical Properties	Radiochemical Properties
Physical State	Chemical Reactivity	Types of Radioactivity: α, β, γ
Thermo-physical Property	Chemical Composition	Half-Life of Radionuclides Present
Mechanical Strength	Leachability	Specific Activity
Fluidity	Pyrophoric Quality	Isotopic Composition
Homogeneity		Maximal Energy of γ Radiation
		Heat Release
		Radiotoxicity

The waste classified in terms of its physical form, i.e., solid, liquid or gaseous form, is always processed separately. During fuel reprocessing, solid waste originates from the insoluble residue of the fuel elements, solid materials used in the technology and structural parts of the equipment. Gaseous wastes make up 90 % of the total activity of radionuclides discharged into the environment from nuclear power plants. The radioactivity present in these wastes comes from the dust from conveyer belts, crushers, chemical preparations, product drying, etc., aerosols, fumes from solution and leaching processes.[10]

Liquid wastes includes acidic or neutralized waste solutions from acidic leaching, waste from alkaline leeching, small volumes of liquid wastes from laboratories, waters which have been used for washing floors and equipment, seepage from the ore slurry dams, leaching from heaps and decantation solutions from the slurry dams. The different liquid wastes create the greatest problems with regard to both processing and waste disposal.

Table 1.2: Classification of radioactive waste

Category of waste	Specific radioactivity (Bq/g)		
	β radionuclides	**α radionuclides**	**Transuranic radionuclides**
LLW	Less than 10^3	Less than 10^2	Less than 10
ILW	More than 10^3 but less than 10^7	More than 10^2, but less than 10^6	More than 10^2, but less than 10^5
HLW	More than 10^7	More than 10^6	More than 10^5

The categorization of nuclear waste, based on its source, the amount and the type of the radioactive species that it contains, is an internationally accepted classification, and according to this, nuclear waste is of three types (i) high level waste (HLW) (ii) intermediate level waste (ILW) and (iii) low level waste (LLW) (Table 1.2). Table 1.3

gives the volumes of the wastes produced by a closed nuclear fuel cycle, excluding the decommissioning stage.[11]

Table 1.3: Closed nuclear fuel cycle-back end waste generation

Stage	Waste type	Quantity (m^3/GW year)
Hulls/Hardware	Solids	15
Feed Sludge	Solids	0.02
Tritium Containing Effluent	Liquid	70
HLW	Liquid	28
ILW	Liquid	25
LLW	Liquid	15
	Solids	65

1.1.1 High level waste (HLW)

High-level waste is highly radioactive, and contains mainly the fission and the neutron capture products of the nuclear fuel cycle. It may be in the form of spent fuel, liquid and solid products from the reprocessing waste streams, unprocessed spent fuel, or from the isolation of fissile radionuclides from irradiated materials associated with nuclear production of weapons. HLW generates a significant amount of heat, and contains long-lived radionuclides. Typically, these aqueous waste streams are treated by the principle of “concentrate and contain”, as the HLW is normally further processed, and solidified into either a glass (vitrification), or a ceramic, matrix waste form. About 95% of the total radioactivity found in nuclear waste is contained in the HLW.[12]

Table 1.4: Composition of Indian HLW

Component	Concentration (g/L)
Na	6.6
K	0.2
Fe	0.5
Ni	0.1
Cr	0.1
SO_4^{2-}	0.5
NO_3^-	4.1
Fission Products	1.1
Transuranic Elements	7.6

HLW contains a number of constituents, including uranium fission products, fuel alloying elements, including cladding elements, transuranic elements, and the process chemicals, such as kerosene, tributyl phosphate and related organic materials. Table 1.4 gives composition of Indian HLW.[13]

1.1.2 Intermediate-level waste (ILW)

ILW contains lower amounts of radioactivity than HLW, but still requires the use of special shielding, to assure safety of the workers. It typically comprises resins, chemical sludges and metal fuel cladding, as well as the contaminated materials from reactor decommissioning. Smaller items and any non-solids may be solidified in concrete, or bitumen, for disposal. It makes up about 7% of the volume, and has 4% of the radioactivity of entire radioactive waste.[14] The most common management option is "delay to decay", for short-lived waste, but, for the long-lived waste, the "concentrate and contain" principle (solidification for deep geologic disposal) is employed.

1.1.3 Low-level waste (LLW)

The largest volume of the radioactive waste from nuclear power production is that of the low-level waste (LLW). LLW is also generated from hospitals and industry. It comprises paper, rags, tools, clothing, filters, etc., which contain small amounts of mostly short-lived radioactivity. It does not require shielding during handling and transport. It comprises about 90% of the volume, but only ~1% of the radioactivity of all the radioactive waste, and is suitable for shallow land burial.[12] To reduce its volume, it is often compacted, or incinerated, before disposal. However, wastes, containing small amounts of long-lived radionuclides, are also included under the LLW classification. The disposal options for this class of waste are near-surface burial, depending on the level of radioactivity. The various radioactive nuclides present in the large volumes of LLW include Cs, Sr, Tc, etc. The removal of these radionuclides, before discharge or disposal, to bring the level of the radioactivity within the permissible limits, is very important.

Among all the radionuclides present in the various radioactive streams, cesium is of main concern, due to its long half-life and the high energy of its emitted gamma radiation. Cesium is a soft, silvery white-gray metal that occurs in nature as cesium-133. The natural source, yielding the greatest quantity of cesium, is the rare mineral pollucite. Although it is a metal, cesium melts at a relatively low temperature of 28 ºC (82 ºF). So, like mercury, it is liquid at moderate temperatures. Cesium, like most of the alkaline metals, reacts explosively when it comes in contact with cold water. The concentration of cesium in the earth's crust is 1.9 mg/kg, and the concentration in seawater is about 0.5 µg/kg. Naturally occurring cesium is entirely non-radioactive.[15] There are 11 major radioactive isotopes of cesium, but only three have relatively long half-lives: ^{134}Cs, ^{135}Cs and ^{137}Cs. Each of these decays by emitting a beta particle, and their half-lives range from about 2 years to 2.3 million years (Table 1.5).[15]

Table 1.5: Half-life, specific activity, decay mode, and radiation energy of various isotopes of cesium

Isotope	Half-life	Specific Activity (Curie/g)	Decay Mode	Radiation Energy (MeV)		
				Alpha (α)	Beta (β)	Gamma (γ)
Cs-134	2.1 y	1300	β	-	0.16	1.6
Cs-135	2. 3 million y	0.0012	β	-	0.067	-
Cs-137	30 y	88	β	-	0.19	-
Ba-137 m	2.6 min	540 million	Isomeric Transition	-	0.065	0.60

The isotopes ^{134}Cs, ^{135}Cs and ^{137}Cs are produced by nuclear fission, but the yields of ^{134}Cs and ^{137}Cs are relatively high, about 7% and 6%, respectively. The radioactive cesium isotopes are introduced in the terrestrial environment, in large amounts, by the authorized discharge of nuclear waste, accidental release from nuclear facilities, and testing of nuclear weapons. In the spent nuclear fuel and in radioactive wastes associated with the operation of nuclear reactors and fuel reprocessing plants, cesium-137 is a major radionuclide present. A smaller quantity of ^{137}Cs-containing waste is also generated in medical, academic, or commercial facilities. ^{137}Cs has important medical and industrial applications because of its long half-life.[16] ^{137}Cs has been used to sterilize medical supplies, milk and other food items.[17] Industrial applications of ^{137}Cs include the production of plastic shrink tubing, as the irradiated plastic develops the tendency to shrink on heating due to the cross-linking induced by gamma irradiation, radiography to inspect metal castings and welds for flaws and material defects (such as cracks in steel pipes), radioactive measurement gauges for thickness of liquids or solid (e.g. gauging of automobile sheet steel), treatment of sewage sludge, to kill bacteria and viruses, and radiotherapy, to kill cancerous tissue. ^{137}Cs has a half-life of 30.17 years, and emits one to two high-energy beta particles.[18-20] Fig. 1.1 shows the decay scheme of ^{137}Cs.

Cesium is a highly electropositive and alkaline element, and thus, forms ionic and electrovalent bonds with nearly all inorganic and organic anions. The common chemical compounds of ^{137}Cs are water-soluble, and readily move with ground water. In the environment, cesium preferentially adheres to soil, particularly to clay minerals, in very high concentrations.[21-23] Cesium, being highly water soluble, can easily enter the food chain and water supply, and ultimately reach the human body. Absorption of cesium by human beings takes place primarily through the digestive tract.[24-26] Cesium and potassium, both being alkali metals, have similar chemical properties. One of the problems with radioactive cesium is that it affects the potassium levels in the body, in addition to its radiation affects on the various body tissues. Essentially, all cesium that is ingested is absorbed into the blood stream through the intestines, and can damage the organs by initiating radiation induced chemical reactions in the tissues. So, its removal from the waste streams, before discharge to the environment, is necessary.

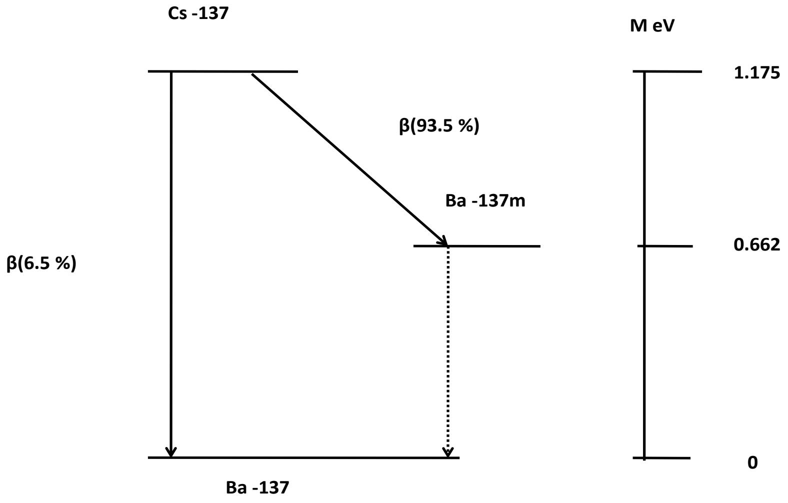

Fig. 1.1: Decay scheme of Cs-137 isotope

1.2 Non Nuclear Waste

The waste water streams, free of radioactive contaminants, come under this category. But, the origin and nature of the pollutants in these waste streams are different for different industries. Various waste-streams from different industries consist of process wastes from manufacturing, product washing water, spills and leakages, heating and cooling water operations, employees' sanitary waste, etc.[7] Depending on the nature of the industry, the wastewater constituents may include dissolved organics, ammonia, fluoride, nitrate, organic nitrogen, and phosphorus, aluminum, potassium, sulfur, heavy metal ions, etc. In many industries, such as textiles, rubber, paper, plastics, cosmetics, etc., dyes are widely used, to color the products. The dyes, even in low concentrations, affect the aquatic life and food web. Among these pollutants, heavy metals need special attention, as these cannot be destroyed, or degraded, and after entering into the living organisms, these heavy metals start bio-accumulating. Bio-accumulation means an increase in the concentration of a chemical in a biological organism over time, as compared to the chemical's concentration in the environment. Major industries, containing heavy metals in their waste waters, include leather tanning industry, electroplating units, paper mills, metal manufacturing industry, textile industries, paint plastics, batteries, fertilizers production plants, etc. Heavy metals such as lead, cadmium, zinc, mercury, arsenic, silver, chromium, copper, iron, etc., impose potential health hazard, if these enter the body, above the safe limit. The nature of the effects of the heavy metal poisoning could be toxic (acute, chronic, or sub-chronic), neurotoxin, carcinogenic, mutagenic or teratogenic.[27-30] The heavy metals tend to bio-accumulate, and interfere with the normal functioning of the metabolic processes, and affect the normal bio-chemistry.

1.3 Waste Water Treatment

Due to the various deleterious effects imposed by the industrial waste water on the environment and human beings, it is very important to treat the waste water, to bring the concentrations of the contaminants below the safe limits, before discharging into the environment. Numerous methods/technologies have been developed over the years, to treat these industrial wastes. Broadly, these technologies can be divided into three categories: chemical methods, physical methods, and biological methods.

i. **Chemical methods** include chemical precipitation, chemical oxidation or reduction, sorption, formation of an insoluble gas, followed by stripping, and other chemical reactions that involve exchanging or sharing electrons between the atoms. These methods make use of the two types of properties of the pollutants, (a) the chemical nature of the pollutants, regarding their reactivity towards the chemicals used for treatment, and (b) the physical characteristics, such as solubilities, volatilities, etc., of the reaction products, generated in the reaction between the pollutants and treatment chemicals during the water treatment. One of the chemical methods which have gained interest over the years is advanced oxidation processes (AOP). Advanced chemical oxidation processes make use of (chemical) oxidants, to reduce chemical oxygen demand/ biological oxygen demand levels, and to remove both organic and oxidisable inorganic components. Different AOPs such as ozone, Fenton's oxidation, electron beam radiation and ultrasound, have been identified as the most promising options for the in-situ generation of highly reactive transient species, like H_2O_2 , $OH^{\cdot}$, $O_2^{-\cdot}$, O_3 , for mineralization of refractory organic compounds, water pathogens and disinfection of by-products.[31] Among these AOPs, heterogeneous photo-catalysis, employing semiconductor catalysts (TiO_2, ZnO, Fe_2O_3, CdS, GaP and ZnS) has demonstrated efficiency in degrading a wide range of refractory organics into readily biodegradable compounds, and eventually mineralizing these to innocuous carbon dioxide and water.[32]

ii. **Physical methods** of the treatment of waste waters include filtration, sedimentation, flotation, stripping, dialysis and other processes that bring about the removal of the pollutants present in the waste waters, without necessarily changing their chemical structures.

iii. **Biological** methods involve the use of living organisms, to remove, or degrade, the pollutants from the waste waters. Biological treatment mainly is of three types: aerobic, anaerobic and anoxic. Aerobic biological treatment involves retardation in the growth of biomass, by the action of the microbes in presence of oxygen. These microorganisms catalyze the oxidation of biodegradable organics and other contaminants, such as ammonia, and degrade these into harmless by-products, such as carbon dioxide, water and excess biomass (sludge). Whereas anaerobic (without oxygen) and anoxic (oxygen deficient) treatment modes do not require addition of oxygen from outside, to assist the microbes for degradation of the pollutants.

1.4 Role of Chemistry In Waste Water Treatment

Chemistry plays very important role in understanding the source, nature and effects of various pollutants, emanating from different industrial waste streams, on the environment. With the deep knowledge and application of the underlying concepts of chemistry in the waste treatment and disposal, it is made possible to develop effective technologies, to check and control water pollution. Advancement in chemistry has also helped in getting better throughput from conventional and non conventional methods of treatment, such as precipitation, oxidation, coagulation, microfiltration, nanofiltration, ultrafiltration, etc. Advanced adsorbents are being developed to remove contaminants from waste waters more selectively and effectively. Worldwide, chemists are doing research, to design such processes and products which require minimum water and energy during their production and use.

1.5 Cesium Removal

Chemistry, in general, and polymeric materials, in particular, play very important role in waste treatment and recovery of precious elements/isotopes therefrom. A variety of methods, based on precipitation, liquid/liquid extraction, solid/liquid extraction, ion-exchange processes, etc., have been proposed/used for the removal/recovery of ^{137}Cs from nuclear waste. A few widely used methods are discussed here.

1.5.1 Precipitation

Precipitation is a method of separation of metal ions from the waste, containing higher concentrations of metals. In this method, various coagulants, such as alum, lime, iron salts and organic polymers, are added to bring about precipitation of the contaminant ions present in the aqueous phase.[33-34] The main disadvantage associated with this process is that, it results in generation of a large amount of sludge, containing toxic compounds. In one of such proposed treatment processes, radioactive ^{137}Cs is removed from the highly radioactive waste supernatant, by precipitation of cesium and potassium cations with sodium tetraphenylborate (NaTPB).[35-36] The precipitation reaction can be written as

$$Cs_{aq}^{+} + Na[B(C_6H_5)_4]_{Solid} = Cs[B(C_6H_5)_4]_{Solid} + Na_{aq}^{+} \qquad (1.1)$$

Cesium tetraphenyl borate has lower solubility, and settles down. The radioactive slurry thus generated is finally vitrified into durable borosilicate glass. However, the low stability of NaTPB has been observed in acidic solutions through acid hydrolysis.[37] Even in strongly basic solution, NaTPB decomposes, on reaction with certain component or conditions, which include copper (II), light, and temperatures greater than ambient temperature. Another bulky anion used for precipitation of cesium from HLW is phosphotungstate, which forms cesium phosphotungstate precipitates with the dissolved cesium from liquid waste.

$$3Cs_{aq}^{+} + H_3[PW_{12}O_{40}]_{aq} = Cs_3[PW_{12}O_{40}]_{solid} + 3H_{aq}^{+} \quad (1.2)$$

The precipitation reaction is carried out in 0.5-2.0 M HNO_3. Phosphotungstate can exist in various forms in aqueous medium, but $[PW_{12}O_{40}]^{3-}$ form is reported to give maximum precipitation yield.

1.5.2 Liquid-liquid extraction or solvent extraction

Solvent extraction is the process of moving one, or more compounds of interest, (analytes) from their original location (usually referred to as the sample or matrix in the form of a liquid phase) to a physically separate location (usually another liquid phase which is immiscible with the first liquid), where further processing and analysis can be carried out.[38] This process has a long history of success in reprocessing of the spent nuclear fuel and recovery of plutonium. Solvent extraction is also known as liquid-liquid extraction, or partitioning. The removal of the nuclides, in this process, is based on the differences between their solubilities in the aqueous stream solution and that in the organic solvent. Generally, the process consists of several steps. First, the solvent (organic) is contacted with the aqueous stream solution, containing the nuclides, in continuous mode, to transfer (extract) these from the aqueous stream solution to the organic solvent. Second, the solvent, containing the target nuclides, is contacted with another aqueous stream (strip), and the nuclides are removed selectively from the solvent. Third, the nuclide-free solvent is recycled, and directed to the head of the process.[39] Despite several advantages, such as long successful experience of application in nuclear industry and the possibility of remote control, there are some specific shortcomings associated with the solvent extraction process. Such processes require more inventory, and hence, high capital investment, large volume of the secondary waste generation, etc. There are a number of organic extractants used for removal of cesium from aqueous waste, and among these, dicarbolides, crown ethers and calixarenes have shown good potential for removal of cesium ions from nuclear waste. Cobalt dicarbolides, $[3{,}3\,Co(1{,}2-C_2B_9H_{11})_2]^-$, especially hexachloro cobalt dicarbolides (CCD), has been reported to have good radiation, thermal and acid stability. CCD is highly polar in nature, and has good solubility in various low polarity solvents. But, the best results have been reported, using nitrobenzene as a solvent. The CCD anion does not take part in the extraction process, but it associates with cations, to form neutral compounds, sparingly soluble in water, but much more soluble in polar dissociating diluents, such as nitrobenzene. Poorly hydrated dicarbollide anions transfer the cesium ion from the aqueous phase to organic phase. The selectivity for cesium ions over other cations present in the waste comes from the lowest Gibbs energy of transfer of cesium to polar organic solvents, as compared to other cations in the waste.[40]

$$M_{aq}^{n+} + nH_{org}^{+} + nCoB_{2\,org}^{-} \leftrightarrow nH_{aq}^{+} + M_{org}^{n+} + nCoB_{2\,org}^{-} \qquad (1.3)$$

Crown ethers are another class of organic compounds which have been considered for efficient removal of cesium ions from nuclear waste. These are macrocyclic polyether compounds, which selectively complex with alkali and alkaline earth cations. Crown ethers, containing alkyl or aryl groups, such as dicyclohexano-18-crown-6 (DC18C6) and dibenzo-21-crown-7 (DB21C7), have less hydrophilicty, and can be used for solvent extraction. McDowell et al. have reported that, rigid benzocrown ethers preferentially extract monovalent cations, and cyclohexano crowns are more effective for divalent cations.[41] DB21C7 is considered as the most efficient crown ether for extraction of cesium ion from ILW.

1.5.3 Solid-liquid extraction

Solid-liquid extraction/solid phase extraction (SPE) is a very popular technique in waste water treatment. SPE is the most widely used technique, mainly due to the variety of materials employed as sorbents. Many of the problems associated with liquid–liquid extraction, such as incomplete phase separations, less-than-quantitative recoveries, and disposal of large quantities of organic solvents, can be circumvented by using SPE. In addition, easily automated extractions provide better yields.[42-43] SPE is used in nuclear industry for the treatment of various waste streams, using different sorbents and ion exchangers.

1.5.3.1 Sorption

The phenomenon of the accumulation of concentration at a surface is termed as adsorption. This is essentially an attraction of the solute molecules (a gaseous or liquid component) to an adsorbent surface (a porous solid). The preferential concentration of molecules in the proximity of a surface arises, because the surface forces of an adsorbent solid are unsaturated. Both short range (repulsive) and longer range (attractive) forces between the solute and the sorbent become balanced, when adsorption occurs.[44] The term “adsorption” was first introduced into literature by H. Kayser, in 1881, and in 1909, J. W. McBain introduced a similar term, i.e. “absorption”, to determine an uptake of hydrogen by carbon, which is much slower than adsorption. He proposed the term “sorption” for both adsorption and absorption.[45] Depending on the type of bonding involved, sorption can be classified as follows.

(a) Physical sorption. In physical sorption (or physisorption), no exchange of electrons is observed; and the sorbate adheres to the surface only through van der Waals (weak intermolecular) interactions. Physiosorption is characterized by interaction energy comparable to heat of vaporization (condensation), and multiple layers may be formed, with approximately the same heat of sorption. The heat of physisorption is, at the most, a few kcal/mole, and, therefore, this type of sorption is stable only at temperatures below 150 °C, depending on the sorbate-sorbent pair.

(b) Chemical sorption. Chemical sorption (or chemisorption) involves an exchange of electrons between the sorbate molecules and the specific surface sites, and as a result, a chemical bond is formed. Chemisorption is characterized by interaction energy between the surface and the sorbate to be comparable to the strength of a chemical bond (tens of kcal/mol), and, consequently, is much stronger, and more stable at high temperatures, than physisorption. Generally, only a single molecular layer can be sorbed.

(c) Electrostatic sorption (ion exchange). This is a term reserved for Coulomb attractive forces between ions and charged functional groups, and is commonly classified as ion exchange.

The sorption of various sorbates onto sorbents is a surface phenomenon. The surface can be characterized either as external, when it involves bulges, or cavities, with width greater than the depth, or as internal, when it involves pores and cavities that have depth greater than the width.[46-47] All these surfaces are not really smooth, and there are many sources of surface heterogeneity, e.g., the polycrystalline character of the solid, growth steps, crystal edges and corners, vacancies, existence of various atoms, or functional groups at a surface, irregularities in a crystalline structure of the surface, chemical contaminants, etc. In these areas of heterogeneity, the atoms of the solid can attract atoms, or molecules, from a fluid nearby. The most important property of the sorbent materials, which ultimately decides the technical effectiveness of any sorbent in a commercial separation process, is the pore structure. Generally, the pores are divided into macro-, meso- and micro-pores (Table 1.6). [46]

Table 1.6: Classification of the pores on the basis of pore width (w)

Type of Pore	Pore Width
Micro	w < 2.0 nm
Meso	2.0 nm < w < 50.0 nm
Macro	50.0 nm < w

Sorbate molecules transport through the macropores to the mesopores, and finally, enter the micropores. The micropores usually constitute the largest portion of the internal surface, and contribute the most to the total pore volume. As the attractive forces are stronger in the micropores, these pores are filled at low relative pressures/concentrations. Therefore, most of the sorption of gaseous sorbates occurs within this region. The total number of the pores, their shape and size determine the sorption capacity, and even the dynamic sorption rate of a sorbent material. The sorbate molecules experience the first resistance by the film which is external to the sorbent particle, and, then, it has to pass through the macroporous structure into the micropores, where the bulk of the molecules are sorbed. A general structure of a sorbent particle and the associated resistances are shown in Fig. 1.2.

The practical application of sorption process is based mainly on the selective uptake of the individual components from a mixture, by the sorbent. The sorbent must also have good mechanical properties, such as strength and resistance to attrition. In most applications, the sorbent must be regenerated after use, without any significant damage to its mechanical and sorptive properties. The raw materials and methods for producing sorbents must ultimately be inexpensive, for the sorption process to compete successfully, on economic grounds, with alternative separation processes.

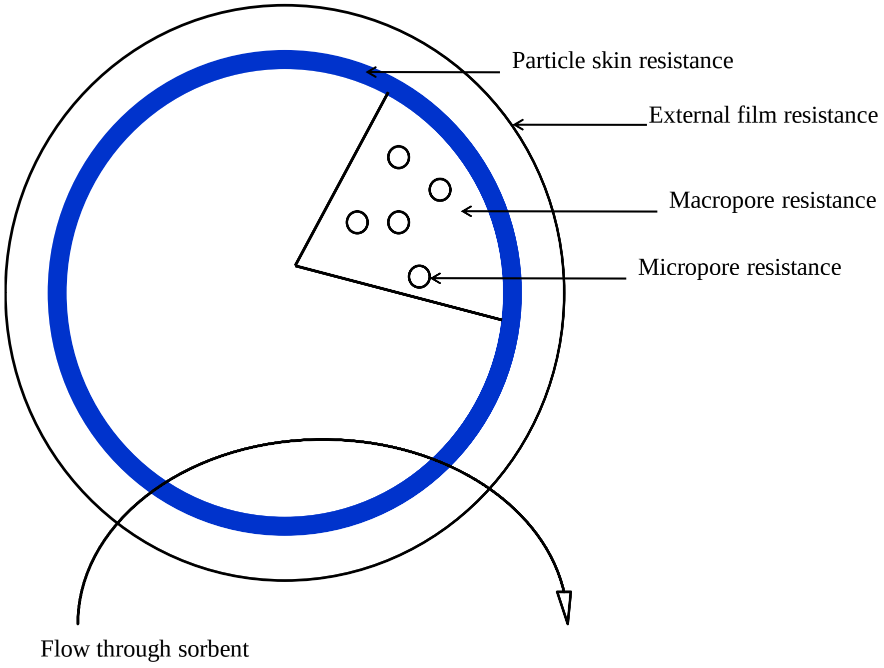

Fig. 1.2: General structure of the sorbent and the associated resistances towards the uptake of the sorbate

1.5.3.2 Ion exchange

An ion exchange reaction may be defined as reversible interchange of the ions between a solid phase (the ion exchanger) and a solution phase. The ion exchanger is insoluble in the medium, in which the exchange is carried out.[48] The ability to exchange the ions is due to the properties of the materials. Although ion exchange is similar to sorption, since a substance is captured by a solid, in both the processes, it is a stoichiometric process which differentiates it from the sorption process, i.e., for every ion that is removed, another ion of the same sign is released into the solution.[49] In contrast, in sorption, no replacement of the solute takes place. The removal of ions by solids can involve more phenomena, for example, in inorganic natural materials, ion uptake is attributed to ion exchange, sorption processes, or even internal precipitation mechanisms.[50]

1.5.3.3 Sorbents and ion exchangers used for removal/recovery of cesium ions

Over the years, a variety of methods have been developed for efficient removal/ recovery of cesium from different nuclear waste streams. Among the operational techniques in water and wastewater treatment, sorption has been proved to be an excellent way, to treat industrial waste effluents, offering significant advantages, like the low-cost, availability, profitability, easy operation, efficient enough to achieve decontamination factors of several orders of magnitude, simple, compact, and not requiring any hazardous organic solvents. Several materials, both inorganic and organic sorbent/ion exchangers, are being considered for use in the cesium removal processes. Some of the most common ones are biosorbents, activated carbon, chelating resins, clays, functionalized silica, zeolites, crystalline silicotitanate, ammonium molybdophosphate Duolite CS-100, resorcinol formaldehyde resin, etc. [51-54]

1.5.3.3.1 Biosorbents

The ability of biological materials to accumulate metals ions from wastewater through metabolically mediated or physico-chemical pathway of uptake is termed as bio-sorption.[55] The binding of the metal ions/sorbate onto the biosorbent is governed by various complex mechanisms. Depending on the cell's metabolism, biosorption mechanisms can be of two types, (i) metabolism dependent and (ii) metabolism independent. The biosorption can be classified into extra cellular accumulation, cell surface sorption and intracellular accumulation, according to the location of the metal ion sorbed on the biosorbent. Biosorbents have many advantages over other methods of waste water treatment, including low cost, minimization of chemical or biological sludge, more environment friendly, possibility of metal recovery, etc. The major advantages of biosorption technology are its effectiveness in reducing the concentration of the heavy metal ions to very low levels. The disadvantages of biosorbents are; a long time is required for removal of metals, their regeneration for further biosorption is difficult, and, moreover, biosorbents do not function that effectively in harsh alkaline and acidic environment. Algae, bacteria, fungi, yeasts, aquatic plants, seaweeds and agricultural wastes have proven to be potential metal biosorbents for removal of radionuclides from aqueous waste.[56-57] Kuyucak and Volesky, in 1988, demonstrated that the biosorption of uranium, cadmium, zinc, copper and cobalt by dead biomasses of algae, fungi and yeasts, is governed by the electrostatic interactions between the metal ions in solutions and the cell walls of the microbial cells.[58] Chakraborty et al., in 2007, have reported the potentiality of *O. basilicum* seeds in removing the radionuclides cesium-137 and strontium-90 from aqueous solution.[59] *Pseudomonas fluorescens* C-2 (exopolymer) is also reported as an efficient biosorbent for the removal of Cs(I) ions from aqueous solution, by Mao et al.[60] Mishra and coworkers have reported the use of dead bio mass, such as rice hulls, Mango (Mangifera indica), and Neem (Azadirachta indica) bark samples, in the removal of Sr and Cs ions from waste waters.[61]

1.5.3.3.2 Inorganic sorbents /ion exchangers

The inorganic ion exchangers offer many advantages over the organic ion exchangers, such as better chemical, thermal and radiation stability, and higher mechanical strength. The uniform structure of the inorganic ion exchangers gives these remarkable selectivity and efficiency, making the simple single-pass operation feasible. Moreover, after its useful operational life cycle, an inorganic ion exchanger/sorbent loaded with radionuclides can be easily converted into a stable waste form, for the final disposal. The different types of inorganic sorbents/ ion exchangers are discussed ahead.

1.5.3.3.2.1 Clays

Among the inorganic ion exchangers, the swelling clays or smectites tend to be relatively nonselective ion exchangers, and are difficult to separate from aqueous media due to their small particle size and tendency to form dispersions. The cation exchange capacity of the smectites is in the range of 0.5-1.3 meq/g, but more commonly 0.8-1.2 meq/g.[62] This low capacity implies a low negative layer charge and low selectivity. These disadvantages experienced with natural clays can be addressed by bringing about some modification in the clay, using inorganic pillars, e.g., alumina and others.[63-68] Pillared clays have relatively high surface areas and uniformly-sized pores. These clays do not swell, or disperse, and can be handled much more easily in aqueous media. Sylvester et al. reported the synthesis of silica-pillared montmorillonite, using 3-aminopropyltrimethoxy silane and an alumina-pillared montmorillonite, for the removal of ^{137}Cs and ^{89}Sr from simulated nuclear waste and groundwater solution.[69] The authors found that though the pillared clays did not show the high selectivity for ^{137}Cs or ^{89}Sr in the simulated wastes, the K_d values for both the radionuclides were very high, as compared to that of the natural parent clays. In 2011, Ma et al. demonstrated the application of phosphate-modified montmorillonite clay for removal of Cs^+ from aqueous solutions.[70] The modification of montmorillonite with KH_2PO_4 increased its monolayer capacity for sorption of cesium ions, from 0.4 mmol/g to 0.7 mmol/g.

1.5.3.3.2.2 Crystalline silicotitanate

Crystalline silicotitanate (CST) is another inorganic sorbent, composed of sodium, silicon, titanium and niobium oxides, which is considered to be a primary candidate for use in the cesium removal process, due to its high chemical and radiation stability.[71-72] It was jointly developed by Sandia National Laboratory and Texas A&M University.[73] The initial reports revealed that CST has high affinity for removal of Cs, Sr, and several other radionuclides from highly alkaline solutions (pH >14), containing high Na^+ concentrations. CST exists as a fine powder, which is not suitable for industrial applications as such, and, therefore, its engineered, granular form, known as IONSIV IE-911, has been developed, and it is commercially available.[73] Cesium-loaded CST (IE-911) has also been shown to be suitable for vitrification into a final waste form. But, the exchange of Cs ions is almost irreversible, and, therefore, CST is not considered to be elutable or reusable.

1.5.3.3.2.3 Metal phosphates/Acid salts of group (III) and (IV) metals

Metal phosphates and the salts of group (III) and (IV) metals are a well-studied class of inorganic ion exchangers. These exhibit the general formula

$M(IV)(HXO_4)_2 \cdot nH_2O$, where M(IV) = Zr, Ti, Sn, Ce, Th, etc., and X= P, Mo, W, As, Sb, etc. [74-77] The exchangeable sites in these salts are structural hydroxy protons, i.e., the H^+ of the –OH, and a number of cations can be exchanged with this H^+. These transition metal salts can be synthesized in amorphous and crystalline forms.[78] Zirconium phosphate is one such ion exchanger, which is used for removal of cesium from radioactive wastes.[79-80] Numerous reports are available in literature, assessing the use of zirconium molybdate, zirconium tungstate, stannic molybdo-phosphate, crystalline silicotitanate, titanium phosphate, zirconium phosphosilicate, sodium titanate and combination of thereof as sorbents, for the removal of radioactive cesium and other radionuclides. [81-84] Mishra and co-workers synthesized stannic phosphate, by mixing of stannic chloride solution and sodium dihydrogen phosphate solution at room temperature, followed by vigorous stirring. In a similar manner, they prepared zirconium phosphate, by reacting zirconyl chloride and phosphoric acid solution at 55 °C, under constant stirring conditions.[79] The gelatinous precipitate of both stannic and zirconium phosphates were washed with water, dried, ground and sieved, to get desirable mesh size. The cesium ion sorption studies on these phosphates revealed that zirconium phosphate is relatively more effective for the removal of Cs(I), and its sorption behavior is almost unaffected by the change in temperature, pH, irradiation, and by added anions, viz., sulphate, phosphate, glycine, EDTA, etc. The sorption efficiency of the phosphates of Zr, Ti and Sn towards cesium ions increases with increase in pH, and, therefore, these phosphates are better suited for treatment of alkaline waste.[79]

For removal of cesium ions from acidic solution, an insoluble salt of dodecaheteropolyacid, ammonium molybdophosphate, $[(NH_4)_3Mo_{12}O_{40}.xH_2O]$, (AMP) has been found to be highly effective.[85] Ammonium molybdophosphate becomes soluble in solutions, with pH more than 4, and, therefore, is only applicable to acidic solutions. Cesium can be eluted from AMP with concentrated ammonium salt solutions (NH_4NO_3, NH_4Cl, etc.). Smit et al. were the first who discovered ion-exchange properties of AMP for cesium. Since then, this ion-exchanger has been extensively studied for removal/pre-concentration of cesium ions from samples of various origins. AMP contains NH_{4s}^+ ions, which can be exchanged for Cs^+ and other heavy alkali metal cations, such as Rb^+ and K^+.[85,86] However, the affinity of AMP for Cs^+ is so high that it can sorb cesium ions quantitatively from the solutions, containing large concentrations of potassium and rubidium.[85] Moreover, AMP has a very large separation factor for Cs^+/Na^+ ion pair. Other advantages of AMP include its rapid sorption rate of cesium, high radiation stability, ease of preparation, and availability at low cost.[87-88] Salts of other dodecaheteropolyacids, such as salts of dodecatungstophosphoric acid and dodecatungstosilicic acid, are also reported to have similar selectivity for cesium, as AMP in acidic solutions.[79, 88-89] The main disadvantage of ammonium molybdophosphate is its microcrystalline structure, which makes the column operation difficult. This problem has been addressed by many researches by making a composite of AMP with some organic or inorganic matrix. Alumina supported AMP, in which alumina acts as a binder, has also been tested for removal of cesium from acidic solutions.[90]

1.5.3.3.2.4 Metal hexacyanoferrates

The potential of metal hexacyanoferrates, for removal of cesium ions, has been extensively investigated by many researchers throughout the world. This class of mixed-valence compounds can be represented by the general formula $A_hM_k[Fe(CN)_6]_l.mH_2O$, where A is alkali metal cation and M is transition metal ion, and *h*, *k*, *l*, *m* are the stoichiometric numbers.[91]

Synthesis and structure of hexacyanoferates

In general, these sorbents are prepared by the reaction of soluble ferrocyanide ($Fe(CN)_6^{4-}$ or $Fe(CN)_6^{3-}$)) compounds of K, Na, NH_4, or H, with the salts of divalent transition metal ions, and are obtained as small-sized, sparingly soluble precipitates. Metal hexacyanoferrates have a face-centered cubic lattice (unit cell length ~10.2 Å), with octahedral co-ordination of the M and Fe ions by -N≡C and -C≡N ligands, respectively (Fig. 1.3).[92]

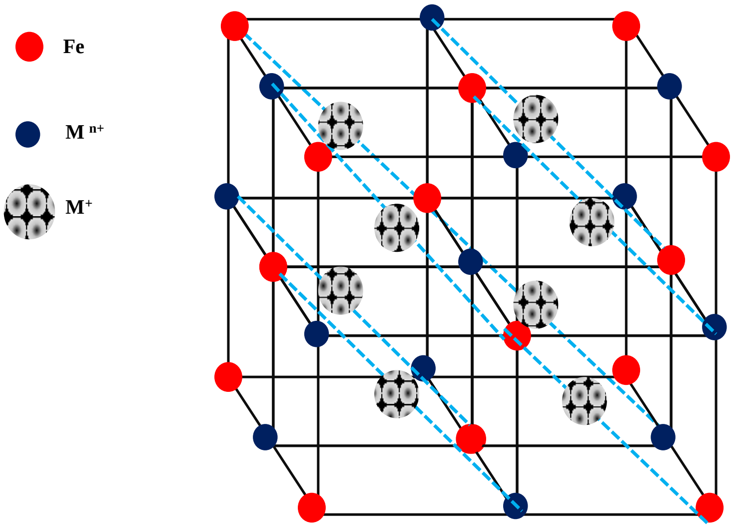

Fig. 1.3: Crystal structure of metal hexacyanoferrate

Fe and M ions are located at the corners of the elementary cubes, while cyano groups are on the edges. The site in the cube center can be occupied by an alkali metal cation, to achieve charge neutrality in the lattice, which may also contain co-ordinated water molecules and anions, in some cases. Since the structure of the metal hexacyanoferrate is mainly governed by the large cyanide ions, the average inner diameter of the channels of all cubic structured metal hexacyanoferrates is ~320 pm. All of the alkali metal ions are not exchangeable with cesium ions, but only those in the surface layer of the crystals are labile.[93]

Mechanism of cesium uptake

Cesium ions are sorbed onto the insoluble hexacyanoferrates in two main steps.[92, 94] The first step involves diffusion-controlled transfer of the cesium ions from the bulk solution to the solid surface. In the second step, cesium ions are sorbed within the hexacyanoferrate solids. The mechanism of this process is complicated. It strongly depends on the composition and crystal structure of the starting solid. It may be a fast ion exchange reaction, or some other slower chemical reaction, leading to a change in the crystal structure of the solid phase. Due to these different mechanisms, hexacyanoferrates have different sorption kinetics and capacities. Loos-Neskovic and co-workers investigated the mechanisms involved in the sorption of cesium ions onto hexacyanoferrate compounds of Zn (II), Ni (II), Cu(II) and Cu(III). $Ni_2^{II}Fe^{II}(CN)_6$, $Cu_2^{II}Fe^{II}(CN)_6$ and $Cu_3^{III}[Fe^{III}(CN)_6]_2$ compounds have cubic structures, with iron vacancies that can be occupied by water, or salt molecules.[94-95] The cesium sorption capacity of $Cu_2^{II}Fe^{II}(CN)_6$ is higher than that of $Cu_3^{III}[Fe^{III}(CN)_6]_2$. The cubic crystal structure of Cu (III) hexacyanoferrate differs from that of $Cu_2^{II}Fe^{II}(CN)_6$, in terms of the position of the copper atoms. In the latter, copper atoms occupy two different lattice sites.[94] One copper atom is linked to CN framework, and another copper atom partially occupies the interstitial position. This second copper atom plays a major role in the sorption of cesium ions. The diffusion of ion pair of Cs^+ and NO_3^- into the solid takes place, and this ion pair is hosted in the vacancies of the structure, resulting in the reorganization of the solid, and hence, formation of a new solid phase. The structure of zinc hexacyanoferrates is quite different. $Zn_2Fe^{II}(CN)_6.2H_2O$, has a trigonal and compact structure, while $M^I{}_2Zn_3[Fe(CN)_6]_2$, (M^I=Na, K, Cs), has a zeolitic rhombohedral structure, with cavities that can host alkali metal ions and water molecules. The sorption of cesium ions onto these compounds takes place mainly through ion exchange. Since the alkali metal ions are not a part of Zn-Fe frame work, therefore, a rapid exchange of Cs with M^I is observed. $K_2[CoFe(CN)_6]$ is another member of the metal hexacyanoferrates class, with a proven potential for removal of cesium. The $K_2[CoFe(CN)_6]$ also has a cubic structure, with cobalt and iron located at the corners of the elementary cubes, and cyanide groups placed between the iron and cobalt atoms.[96] The exchangeable potassium ions are at the body centre. The exchange of K^+ ions with Cs^+ ions is quite fast, and does not bring about any drastic changes in the crystal structure. But, all of these potassium ions do not take part in the exchange process, only those ions which are closest to the crystal surface are capable of participating in the exchange process. Therefore, the effective capacities of cobalt hexacyanoferrates of different stoicheiometries are between 0.24-1.24 meq./g, which is much lower than the theoretical capacity of 5.73 meq./g.[97] The rate of reaction also depends upon the physical properties, such as surface area, etc., of the hexacyanoferrate particles.

1.5.3.3.3 Organic sorbents

1.5.3.3.3.1 Resorcinol formaldehyde resin

The resorcinol formaldehyde resin was first developed by Savannah River Laboratory, in the early 1980s, for the removal of cesium from alkaline nuclear waste.[98] Since then, it has been used effectively in nuclear industry for treatment of alkaline nuclear waste. Resorcinol-formaldehyde resin has emerged out as a satisfactory option for removal of Cs^+ ions from highly alkaline media because of low cost, safety, availability, selectivity, easy operation and efficiency considerations.

Synthesis

Resorcinol-formaldehyde resin is prepared by condensation polymerization of resorcinol and formaldehyde in alkaline media, at ambient temperature and pressure conditions. Resorcinol, also known as 1,3-dihydroxy benzene, has two hydroxyl groups on the same benzene ring, as shown in the following structure

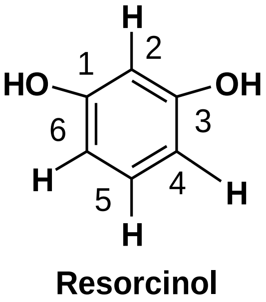

Empirical formula: $C_6H_6O_2$

Molecular weight: 110.11

Fig. 1.4: Resorcinol molecule

The presence of two hydroxyl groups enhances electron density at the 2-, 4- and 6-positions, and, therefore, resorcinol can undergo all the typical reactions of phenol, that too, at much faster rates. The substitutions primarily occur at the 4- and 6-positions, because the 2nd-position is sterically hindered by the adjacent hydroxyl groups. Resorcinol reacts with aldehyde to produce resin, under both acidic and basic conditions. Base catalyzed resins are called resols, and these have both methylol and methylene-bridged resorcinolic structures, and are self-curing. Resinous compounds, prepared under acidic conditions, have methylene-bridged structures, and are often called novolak materials. These resins have no reactive methylol group in their structures, and, therefore, cannot be self-cured, like the phenolic resols. The fixed-ionic groups in resols or RF resins are the ring hydroxyl groups, which can be used for ion-exchange only at higher pH regimes, due to the high pK_a of the phenolic -OH group.

Mechanism of polymerization

The following mechanism has been proposed for the formation of resorcinol formaldehyde polymeric structures from the base catalyzed RF reaction, as shown in Figs. 1.5-1.7. In general, the formation of resorcinolic resins from the RF reactions can take place in three stages.

i. Addition reaction

The first step of the RF reaction is called an addition reaction, in which resorcinol combines with formaldehyde to form hydroxymethyl (or methylol) resorcinol. Under basic condition, this step involves the formation of a resorcinate ion. The addition rate of formaldehyde to resorcinol depends on the concentration of the resorcinate ion. This resorcinate ion now activates the benzene ring, and the electron density at the 4 (or 6) position increases, for the formaldehyde attack and formation of methylol group.[99] The introduction of a methylol group into the ring increases the activity of the other nuclear positions.

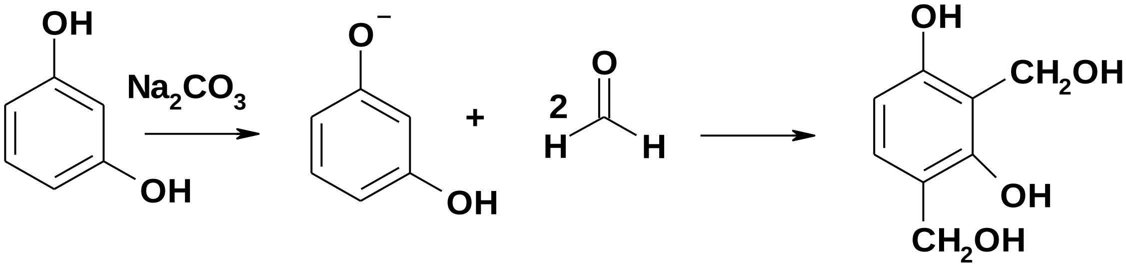

Fig. 1.5: Addition reaction of resorcinol and formaldehyde in presence of basic catalysts

ii. Condensation reaction

In the second stage, the condensation of methylol groups takes place, forming the methylene (-CH_2-) and methylene ether (or benzylether)(-CH_2O-) bridged structures.[100-101] In RF reactions, there is a greater tendency for the methylol group, or formaldehyde, to continue to react as long as there are active sites in the resorcinol molecule, or RF resin.

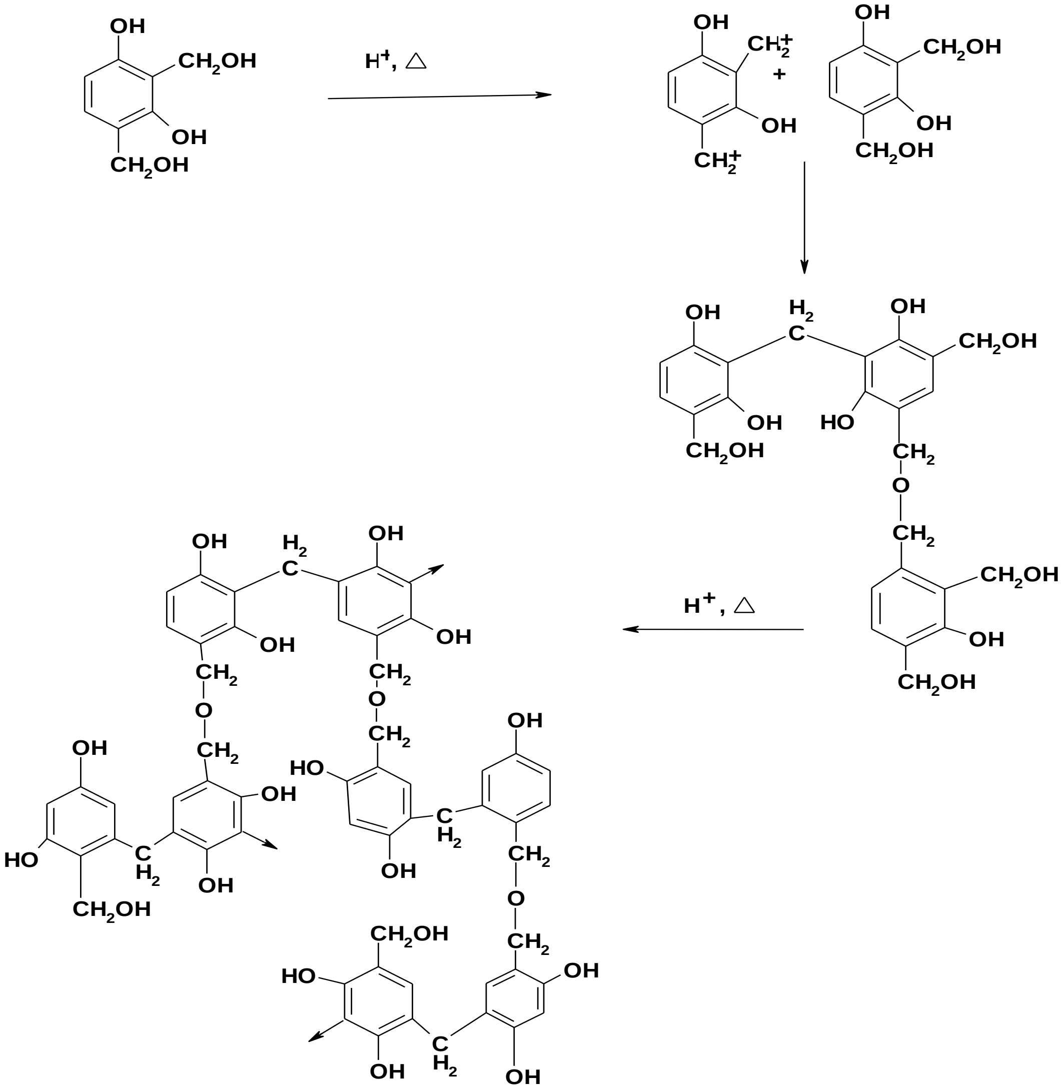

Fig. 1.6: Condensation reaction of resorcinol

iii. Disproprotionation reaction

Finally, in the disproportionation reaction, the benzylether structures are decomposed, to produce the methylene bridged structures and formaldehyde.[102]

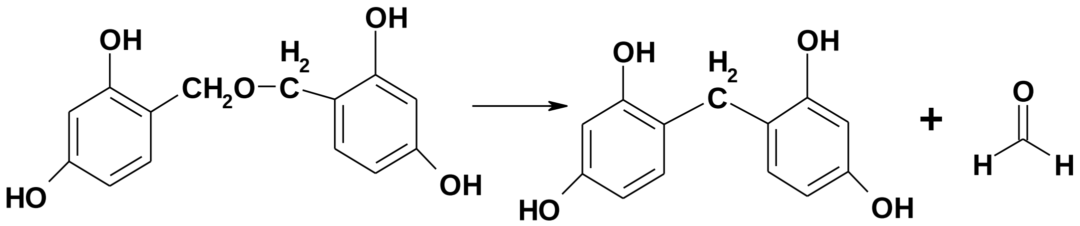

Fig. 1.7: Disproprotionation reaction

This cross-linked RF resin is obtained as a bulk mass, which is ground and sieved, to get the granular RF particles of the desirable size. Many patents and reports are available on the synthesis of resorcinol formaldehyde resin in granular form. Indian patent No. 97,345 discloses a method of the reacting phenol with formaldehyde, in presence of sulphuric acid, to form bulk gel, and then breaking the gel into small pieces of required mesh size. U.S. Pat. Nos 4,423,159 and 5,441,991 disclose a method of reaction of resorcinol with formaldehyde under basic conditions, heating the reaction mixture at 60-90 ºC, to cure the gel, and then crushing the dried gel to the required mesh size.

Stability of RF resin

The protonated form of RF resins is observed to be more stable than the metallated form under alkaline conditions. In the first step of the degradation process of RF resin, the methylene bridge is attacked by an oxygen molecule, to form the hydroperoxide group.[98] This hydroperoxide, subsequently, decomposes into radicals. The free radical formed on the polymer main chain decomposes the molecule, and produces an aldehyde and phenolic radical, which, on further reaction, produces a mixture of organic molecules, containing carbonyl group. This study clearly showed that hydroperoxides and radicals could be more easily formed in the metallated form than in the protonated form of RF resin. RF resin also gets degraded in the presence of concentrated nitric acid.[103] The studies on the acidic degradation of RF in the presence of different concentrations of nitric acid have shown that 2 M HNO_3 induces significant changes in the structure of RF resin. For RF resin, left in contact with high concentrations of nitric acid, visually evident partial dissolution of the polymer into the solution, and effervescence are observed. It is believed that the nitration reaction occurs, along with independent oxidative reactions. A portion of the organonitrate functionalities thermally decomposes, which results in degradation of the polymer network with continued acid contact.

Synthesis of spherical resorcinol-formaldehyde resin

Conventionally prepared RF resin gives big chunks of the polymeric resin, which are then ground and sieved, to get desirable mesh size for column operation.[104] But, these ground gel particles are of irregular shape, have broad particle size distribution, and exhibit poor column hydraulic behavior. These problems can be solved by using spherical resin material. Various patents are available in literature, suggesting different methods of synthesis of resorcinol-formaldehyde resin beads. In the patent, U.S. Pat. No. 5,908,896, method of synthesis of spherical resorcinol formaldehyde resin is disclosed, in which resorcinol is reacted with formaldehyde under basic conditions in the presence of surfactant, containing mineral oil. The reaction mixture is heated till complete curing of the gel, and then, the oil is washed off with toluene.[105] U.S. Pat. Nos. 2,186,369;

2,675,336, 2,489,336, and 3,850,868, have reported methods of reacting phenol with formaldehyde in aqueous medium, under basic conditions, to form a pre-polymer. This pre-polymer was blended with polyvinyl alcohol (a protective colloid), and polymerized by acidifying and heating.[106-109] The mixture was heated under agitation, to form inert beads, and the water was removed. Gum Arabic is also used as a protective colloid in aqueous alkaline medium, for the production of resol in powder form.[110] U.S. Pat. No 4,206,095 discloses a method of reaction of a phenol and hexaethylenetetraamine with formaldehyde, in presence of gum Arabic, and then washing the cured polymer with water, to get free-flowing resol powder of mesh size much above 100.[111] These powders have classical applications, such as fiber bonding, molding, adhesives, etc. U.S. Pat. No. 4,237,107 discloses a method of production of cellular, spherical beads, having high carbon content, by collecting droplets of phenoplast in a hot, vibrated bed of talcum.[112] U.S. Pat. No. 4,317,901 discloses a method, in which aqueous resol dispersion is produced in the presence of a surfactant and a protective colloid. Then, a polyvalent cationic precipitant is added to the resulting reaction mixture.[113] The resulting precipitate is filtered, washed with water, and dried, to recover the spherical resin. U.S. Pat. Application No. 444840 discloses a method of preparation of mesoporous phenolic resin beads, by dissolving polymerizable liquid precursor and hexamine (crosslinker) in polar solvent, and suspending these in transformer oil, and allowing these to polymerize in the laminar flow of suspension medium.[114] U.S. Pat. No. 4,873,218 discloses a method of polycondensation of resorcinol with formaldehyde under alkaline conditions, and then, supercritical drying of the gel, followed by carbonization, to get low density carbon foam.[115] All these methods have their associated disadvantage, such as multi-step synthesis, low yield of the desired size beads, tedious washing of oil from the beads, and generation of a large amount of waste. So, there is a need to develop better synthetic methods, to produce spherical RF particles of appropriate mesh size.

1.6 Scope of Thesis

A concise survey is presented in the thesis, describing the impact of industrialization on water quality, various sources of water pollution and nuclear and non nuclear waste. The role of chemistry in water remediation, and the different methods and techniques applied for removal of cesium ions from nuclear waste streams are also discussed.

An introduction to inorganic and organic sorbents and the relevant techniques for the synthesis of these have been discussed. One of the main goals of this Ph. D. programme is to synthesize sorbent polymeric extractant systems for removal of radionuclides and toxic metal ions from various wastewater streams. Solid liquid extraction has some advantages over the conventional liquid-liquid extraction method. The conventional solvent extraction technique has some problems, like poor phase separation, reduction in extraction efficiency, waste generated from the large volumes of organic solvents used, etc. Thus, polymer-extractant system, mainly in the form of beads/resin, can give an alternative route for extraction of metal ions. Solid-liquid extraction is a better substitute for solvent extraction, to overcome some of these difficulties, and polymers can play a very important role in providing the solid support in the development of such systems. In the thesis, new methods have been developed to synthesize conventional sorbents, with better mechanical strength and spherical shape, to overcome some of the mentioned difficulties. The different organic and inorganic sorbents are loaded into various polymeric matrices. Resorcinol formaldehyde resin has been synthesized in spherical form by using suspension polymerization technique and also by coating onto pre-formed polymer beads. Among the inorganic sorbents, different metal hexacyanoferrate composites have been synthesized by using polymeric binders.

Another important objective is to study the potential of these sorbent-polymer systems for removal of cesium ions. The effects of various experimental conditions on the sorption efficiency, kinetics, mechanism of the sorption process have also been investigated, using the synthesized beads.

Generally, photo-catalysts are synthesized and used in the form of fine powder, or films, for photo degradation of organic contaminants. Although fine powders are easy to disperse in the solution, and give better results due to their high surface area, these form slurry with the water, and are very difficult to remove from the treated water. There are chances that these may even act as potential contaminants, if not completely removed from the treated water. Moreover, films of photo-catalyst do not have good mechanical strength, and cannot be used effectively for treating large volumes of waste. Conventional photo-catalysts, like titanium dioxide, can be synthesized in spherical bead form, with good mechanical strength and high surface area, by using sacrificial polymeric templates. These bead can be easily removed from water after its treatment.

In conclusion, this thesis is dedicated to synthesis of novel composite sorbent-beads, their characterization and potential applications in removal of toxic metal ions from waste streams, and degradation of dyes.

Chapter-2

Experimental & Techniques

2.1 Introduction

Organic polymeric resins, inorganic extractant polymeric composites and photo-catalyst beads have been synthesized for potential technological applications in the removal of radionuclides, and photo-catalytic degradation of dyes. This chapter deals with the methodologies that were used for the synthesis of these materials, and details of the various techniques that were employed for their characterization, and sorption and photo-degradation studies.

2.2 Materials

Resorcinol, formaldehyde, copper sulphate, potassium hexacyanoferrate, polyvinyl alcohol (PVA) [Mol. Wt. = 1,25,000], N-methyl pyrrolidone (NMP), nickel sulphate, cobalt sulphate, nitric acid, titanium isopropoxide, 2-propanol, glutarldehyde, methylene blue, cesium nitrate, sodium hydroxide and sodium carbonate were procured from the local suppliers, and were used as received. Polyethersulfone (PES), (Gafone PES 3200P), was procured from Gharda Chemicals Limited, India. All the chemicals were of AR grade. Sodium alginate (80% hydrolyzed) and Amberlite XAD-4 were purchased from SD Fine Chemicals, India.

The dye solutions were freshly prepared, and kept in dark, to avoid any photochemical reaction. Aqueous solutions were prepared, using water, with conductivity of 0.6 µS cm^{-1}, or lower, purified by a Millipore-Q water purification system, and were purged with nitrogen, wherever required. Glassware was cleaned, using chromic acid, followed by rinsing with distilled water, and then, with water, purified by Millipore-Q water purification system, and dried in an oven at 110 ^{0}C.

2.3 Synthetic Strategies

2.3.1 Synthesis of resorcinol-formaldehyde (RF) beads

Many methods have been reported for the synthesis of resorcinol formaldehyde (RF) polymer, using different base catalysts. The uncontrolled reaction of formaldehyde with resorcinol in basic medium results in the formation of big chunks of resol polymer by bulk polymerization reaction, which can be ground into smaller resin particles. The methods reported in the literature, for the synthesis of spherical resorcinol-formaldehyde beads of desirable size, make use of intricate inventory, and involve multiple-steps. In the present study, new and simple chemical methods were developed for the synthesis of spherical RF beads, *viz.*, pure RF resin beads, RF coated XAD beads (RF-XAD) and RF beads, using alginate beads as a template (RF^{A}) of desirable size. Synthesis of pure RF resin beads was carried out, by the reaction of resorcinol and formaldehyde, using sodium carbonate as base catalyst. The size of the beads was controlled by mixing the pre-polymer of RF in a stabilizing polymer solution. RF-coated XAD beads were synthesized by coating RF pre-polymer onto the commercially available XAD-4 (polystyrene-divinylbenzene copolymer) beads. Similar strategy was employed to synthesize RF^A, using pre-formed beads of the biopolymer calcium alginate as a base template. The details of the procedures and the experimental parameters will be discussed in chapter 3. The synthesized resin beads were characterized by different techniques, as discussed in the subsequent sections.

2.3.2 Synthesis of metal hexacyanoferrate-polymer composite beads

Copper hexacyanoferrate (brown-colored) powder was prepared, by reacting copper sulphate with potassium hexacyanoferrate in the presence of PVA stabilizer in aqueous medium. The precipitates of CuHCF were separated by centrifugation, and washed with double-distilled water. These precipitates were air-dried, to obtain CuHCF powder. This powder was used to prepare sorbent-polymer composite beads by phase inversion technique, using PES as the binding matrix, NMP as a good solvent and water as non-solvent for PES. For preparation of KCuHCF-Gel beads, KCuHCF was formed in the presence of PVA, using the same reactants as described above, but at a different molar ratio. To this PVA-KCuHCF sol, aqueous solution of sodium alginate was added, to form homogenous slurry. This slurry was dropped through a needle into calcium chloride (4%) aqueous bath, through a 0.8 mm needle, using a syringe pump, to form spherical gel beads, containing uniformly distributed KCuHCF. These were further gellified by cross-linking the PVA, present in the beads, with glutaraldehyde in the presence of acid. Similar strategy was used to prepare potassium cobalthexacyanoferrate and potassium nickel hexacyanoferrate gel beads, only difference being that the PVA used in the process was not further cross-linked. The experimental parameters will be discussed in detail in the respective chapters.

2.3.3 Synthesis of TiO_2 beads

Mesoporous titanium dioxide microspheres were synthesized by the sol-gel templating method, using calcium alginate as a sacrificial template, and subjecting the pre-formed swollen beads to different temperatures, under various atmospheres. Titanium isopropoxide (TIP) was used as a titanium precursor, and the pre-formed calcium alginate beads were equilibrated with ethanol, isopropanol and TIP, sequentially. These TIP-equilibrated beads were treated with distilled water, to bring about the hydrolysis of the titania precursor, and then, these beads were heated under controlled conditions of temperature and atmosphere, to obtain template-free porous ceramic titania beads.

2.4 Analytical Methods

Several techniques have been used for the physical and chemical characterization of the synthesized sorbents and photo-catalytic beads, sorption and photo-catalytic degradation studies.

2.4.1 X-ray diffraction (XRD)

X-rays were discovered, in 1895, by Wilhelm Röntgen, for which he received the first Nobel Prize in Physics in 1901. X-ray diffraction was first theorized to be possible, in 1912, by the German physicist Max von Laue. Amongst one of the discoveries was a diffraction-like effect, on exposure of crystalline materials to X-rays. Laue had noticed that the diffraction was obtained, after passing X-rays through a grating, with spacing of the order of a few angstroms. The spacing is roughly the same, as the spacing between atoms in a crystal. Based on these results, he theorized that a crystal could be used as a diffraction grating in three dimensions, as opposed to the normal two-dimensional grating. However, the physicists William Henry Bragg and his son William Lawrence Bragg worked out the relationship between the patterns of the spots produced on the photographic plate and the arrangement of the atoms in a crystal. Since then, X-ray diffraction (XRD) has emerged as a very important experimental technique for structural characterization of condensed matter. It is the most commonly used technique for fingerprint characterization of the crystalline materials, as well as for determination of their unit cell, lattice parameters, phase and probable crystal structure.[116] The theory of diffraction is based on the Bragg's law, which describes how the electromagnetic waves of a certain wavelength λ interfere with a regular lattice. At a certain angle of incidence, also called as Bragg′s angle (θ), with regard to a set of parallel crystal planes, which are, therefore, called reflectors, constructive interference take place according to the equation

$$n\lambda = 2d_{hkl}sin\theta \qquad (2.1)$$

where n is a positive integer, d_{hkl} represents the inter planer spacing between the crystal planes that cause constructive interference, and λ is the wavelength of the incident X-ray beam.

In XRD, the sample is irradiated by a monochromatic X-ray beam, which are generated by a cathode ray tube, by heating a filament to produce electrons, accelerating the electrons toward a target, by applying a voltage, and bombarding the target material (Cu, Fe, Mo, Cr) with the electrons. When the electrons have sufficient energy, to dislodge inner shell electrons of the target material, characteristic X-ray spectra are produced. These X rays are then collimated, and directed toward the sample. The interaction of the incident rays with the sample produces constructive interference (and a diffracted ray), when conditions satisfy the Bragg's law.[117] These diffracted X-rays are then detected, processed and counted. By scanning the sample through a range of 2θ angles, all the possible diffraction directions of the lattice should be attained due to the random orientation of the powdered material. The conversion of the diffraction peaks to d-spacings allows identification of the material, because each material has a set of unique d-spacings. Typically, this is achieved by comparison of the d-spacings with the standard reference patterns. The intensity distribution of the peaks is governed by the nature and the kind of distribution of the atoms/ions in the unit cell. The absolute intensities of the peaks depend on the source intensity and counting time, in addition to the nature and the kind of distribution of the atoms/ions in the unit cell. A schematic diagram of XRD diffractometer is given in Fig. 2.1.

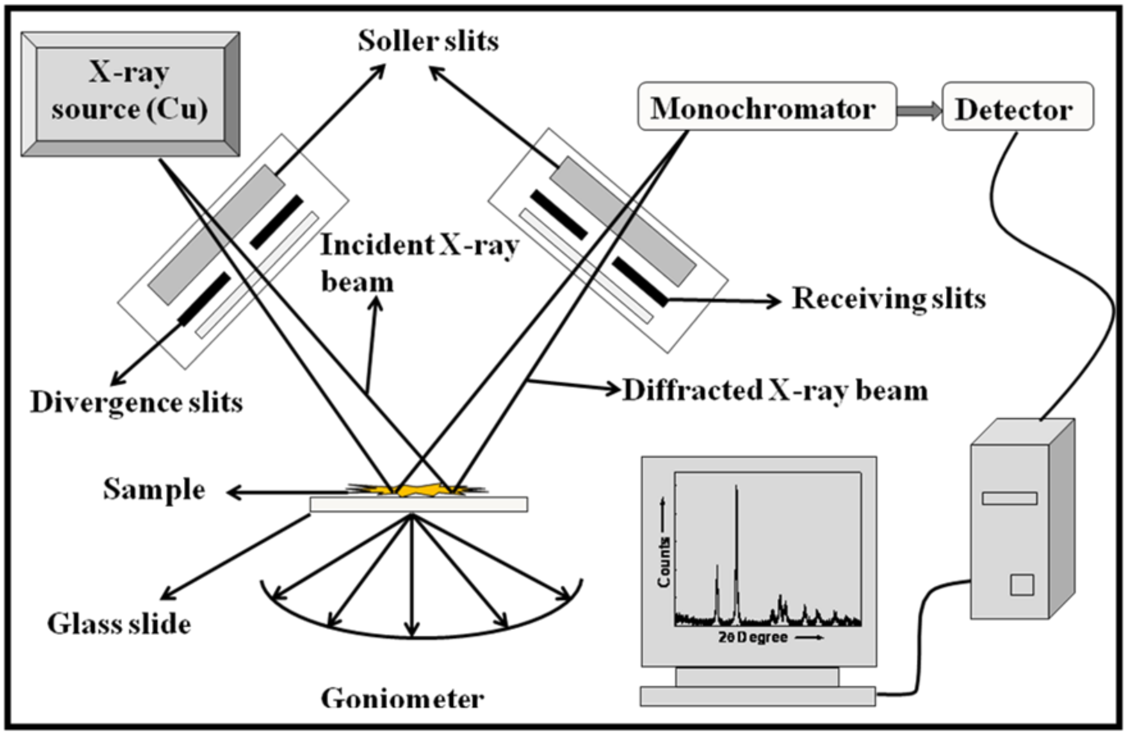

Fig. 2.1: A schematic diagram of X-ray diffractometer

2.4.1.1 Particle size estimation by X-ray diffraction

The approximate average size of the particles can be calculated from the broadening of the X-ray diffraction peak. Generally, for crystals of thickness less than ~ 2000 Å, the Scherrer formula has been widely used for estimating the crystallite size of nano-crystalline compounds from the diffraction peak width, as given by the equation (2.2).[118-119]

$$d = \frac{0.9\lambda}{\beta cos\theta} \qquad (2.2)$$

where d is the thickness of the crystal, λ is the wavelength of the x-ray used and β is the FWHM (Full Width at Half Maxima) in radians.

The line broadening, β, is measured from the peak width at half the peak height, and is obtained from the Warren formula:

$$\beta^2 = \beta_M^2 - \beta_S^2 \qquad (2.3)$$

where β_M is the measured peak width in radians at half peak height and β_S is the measured width of the peak of the standard material, mixed in the sample, having a diffraction peak near the relevant peak of the sample.[120] Based on this concept of broadening of the XRD peak of the nanocrystalline compound, its approximate crystallite size can be determined.

In the present thesis, X-ray powder diffraction patterns (XRPD) were recorded on a Philips X-ray diffractometer, model-PW 1710, with Ni-filtered Cu Kα radiation (λ = 1.5406Å), using silicon as an external standard. The measurements are performed in the range of 10°-80° in a continuous scan mode, with a step width of 0.02°, and scan rate of 1° per minute. The measurement of the values corresponding to each peak position and the peak intensity forms the basis of the method of identification of materials, with the help of JCPDS-ICDD (Joint Committee on Powder Diffraction Standards-International Centre for Diffraction Data) files.[121]

2.4.2 Scanning electron microscopy (SEM)

The first Scanning Electron Microscope was debuted in 1942, while the first commercial instrument came only in 1965. Its late development was due to the electronics involved in scanning the beam of electrons across the sample.[122] SEM gives information about topography, morphology, composition and crystallographic details of the arrangement of the atoms in a material. In a typical SEM, a source of electrons is focused into a beam of a very fine spot size of ~5 nm, and having energy ranging from a few hundred eV to 50 KeV, to examine a very small area of an object.

Electrons from a filament in an electron gun are beamed at the specimen in a vacuum chamber. As the electrons strike and penetrate the surface, a number of interactions occur that result in the emission of secondary electrons and photons from the sample, and SEM images are produced by collecting the emitted electrons on a cathode ray tube (CRT). The images formed by the scanning electron microscope are from secondary electrons, backscattered electrons, characteristics x-rays, Auger electrons, and other electrons that are emitted by the sample. Secondary electrons (SE), defined as being those with energies between 0 and 50 eV, are easy to collect, and can be employed over a very wide range of incident beam energies. These are generated when the primary (exciting) electrons interact with electrons in the specimen, and cause the latter to eject, with some amount of kinetic energy, which is lower than that of the primary electrons.

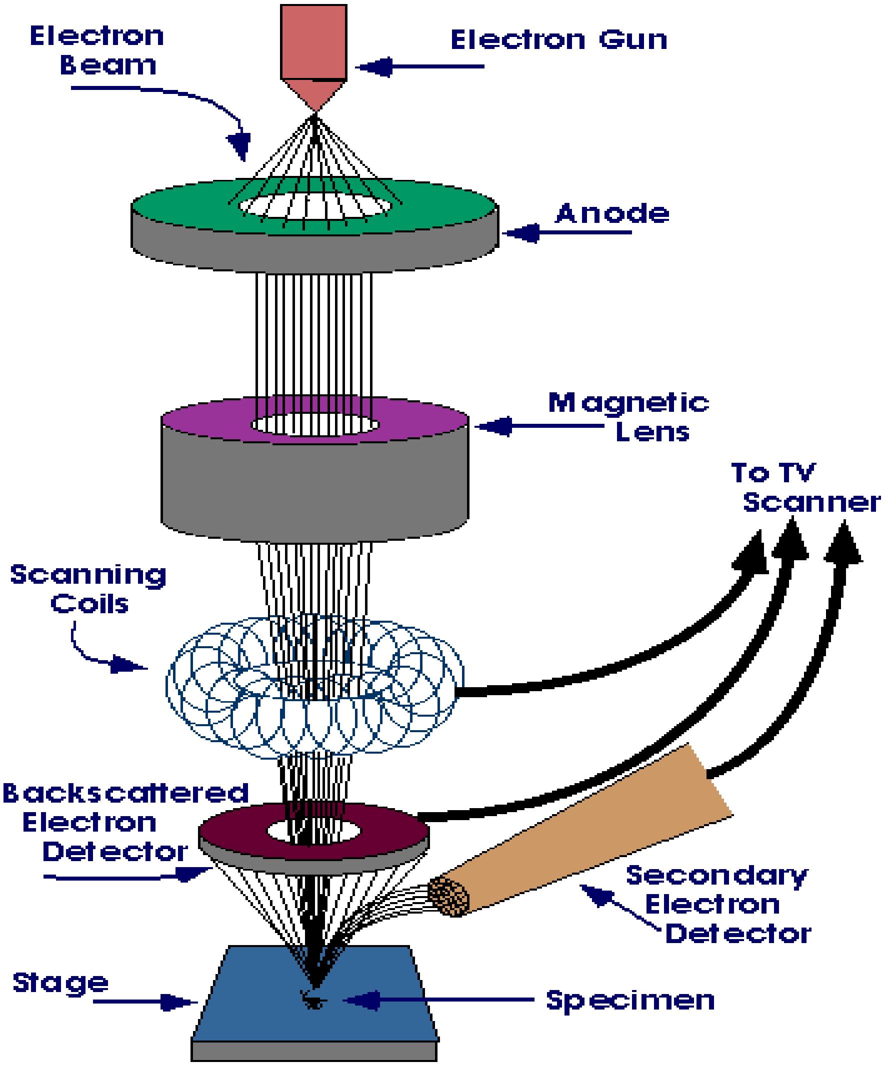

Fig. 2.2: Various components of SEM.

SEs are created near the surface, and are sensitive to the topography of the sample. In addition, SEM image may contain information about the chemistry, and the electrical and magnetic state of the sample. Backscattered electrons constitute all the other electrons emitted from the specimen. The BSE are generated, if the primary electrons interact with the nucleus of a sample atom, and get scattered in any direction with little loss of energy. These backscattered electrons (BSEs) are much more energetic than SEs, and so, may escape from a greater depth within the sample. Therefore, compared to SEs, the backscattered signal will neither carry much information about sample topography nor will it be highly resolved in space. Contrast in the BSE image is directly sensitive to the atomic number of the sample, as well as to its magnetic and crystallographic nature, and comes from the bulk rather than from the surface of the sample. The BSE signal carries information about distribution of heavy elements. The one common problem encountered during recording the SEM images of the organic or non conductive samples is the destruction of the sample due to build-up of charges, or the strong electric currents produced by the electron beam. This problem can be rectified efficiently by coating the non-conductive specimens with a thin layer of conductive material, before recording the scanning electron micrograph.

In the present thesis, the surface morphology of the sorbents has been analyzed, using AIS2100 SERON Tech. SEM from South Korea, equipped with energy dispersive X-ray (EDX) spectrometer (Model: INCA E350 from Oxford, UK).

2.4.3 Thermal analysis

Thermal analysis refers to a variety of techniques in which a property of a sample is continuously measured as the sample is programmed through a predetermined temperature profile. Today, it is an important analytical tool in various branches of chemistry, geology, fuel science, ceramics, and material science.[123] The recent years have seen major advances in this thermal analysis technique through improved furnace technology, microcomputer-based electronics, and the addition of microcomputer data handling systems.

There are multiple methods in thermal analysis, and each is defined as a technique, depending on the type of properties of the sample that are measured. Of these techniques, for measuring the properties, the five shown in Table 2.1, are the commonly used techniques of thermal analysis.

Table 2.1: Thermal analysis techniques

Name of the Technique	Measurement Object	Unit	Uses
Differential thermal analysis	Temperature difference	^{0}C µV*	Phase changes Different reactions
Differential scanning calorimetry	Thermal Flow	W=J/sec	Heat capacity Phase changes Reactions
Thermaogravimetry	Mass	mg	Decompositions Oxidation
Thermomechanical analysis	Deformations	µm	Softening Expansion
Dynamic thermomechanical measurements	Elasticity	Pa, dyn/cm^2	Phase changes Polymer cureing

2.4.3.1 Thermogravimetric analysis (TGA)

TGA is a technique in which the mass of a substance is monitored as a function of temperature or time, as the sample specimen is subjected to a controlled temperature program. It can be used to study any physical, or chemical process that causes a material to lose or gain mass. This technique is used to detect evaporation, sublimation, oxidation, thermal degradation and other effects of temperature that cause mass change. The processes which do not result in a change in sample mass are not detected by this technique. TGA can be carried out by using either a heating ramp (dynamic mode) or a constant test temperature (isothermal mode). Provision for changing the test atmosphere by gas switching enables polymer decomposition to be studied under inert, oxidizing, or reducing conditions. The basic instrumental requirements are simple: a precision balance, a programmable furnace, and a recorder and/or a computer (Fig. 2.3). Modern instruments, however, tend to be automated and include software for data processing. In addition, provisions are made for surrounding the sample with an air, nitrogen, or an oxygen atmosphere.

A schematic layout of TGA instrument is shown in Fig. 2.3

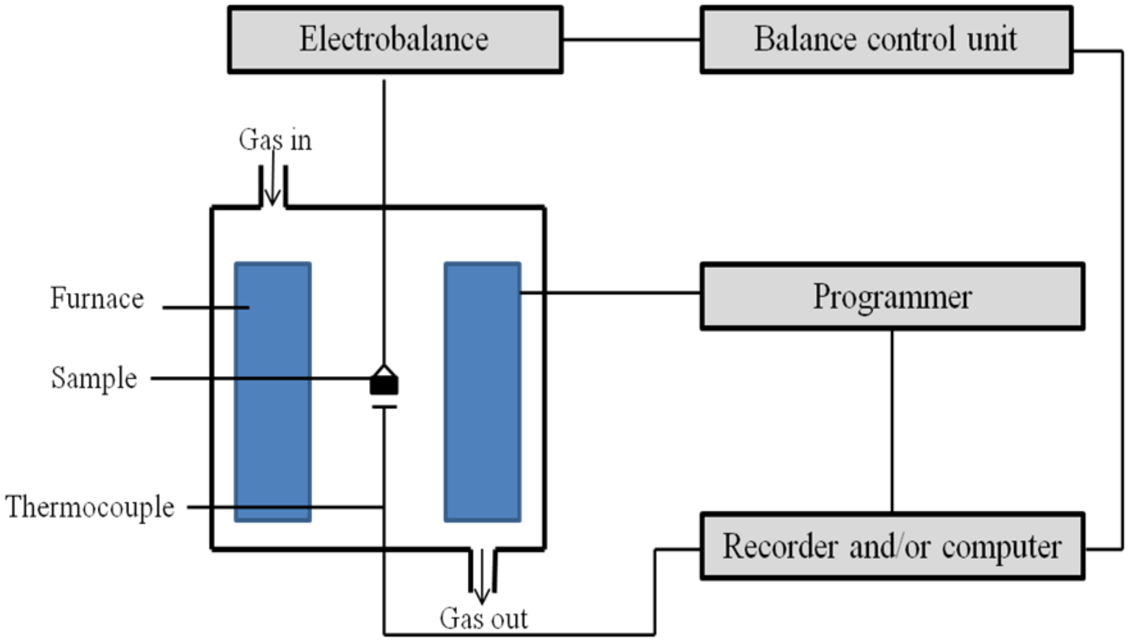

Fig. 2.3: Schematic layout of TGA instrument

In the present studies, thermo gravimetric analysis (TGA) measurements have been carried out, using Mettler Toledo TGA/DSC STAR E1 thermal analysis system. The details of the thermal programming, used in studying the individual systems will be discussed in the relevant sections.

2.4.4 Scintillation detector

In 1908, Rutherford and Geiger established the reliability of a method of counting α -particles, by observing visually the flashes of luminescence produced in a thin layer of ZnS by the α-particles.[124] Since the development of reliable *photomultiplier* tubes (PMT) in 1946, scintillating counting technique has played an important role in nuclear science.

Scintillation detector consists of a *scintillator*, or *phosphor*, optically coupled to a PMT. Scintillators are the materials, in which a large fraction of the incident energy carried by striking particles, or radiation, is absorbed, and transformed into detectable photons (visible or near visible light), and later, converted into an electric signal.

2.4.4.1 Mechanism

The scintillating materials, used in scintillator detectors, can be an inorganic crystal, an organic solid, a liquid, or a gas. Scintillation detectors for beta radiation are often organic scintillators. Organic scintillators operate at the molecular level, which means that the light emission occurs as a molecule undergoes radiative transition from an excited level, following excitation by energy absorption from ionizing radiation, to the ground state. Molecules such as anthracene, trans-stilbene, para-terphenyl, and phenyl oxazole derivatives are among the many organic species that have useful scintillation properties. Crystalline inorganic scintillators are usually used for detection of gamma radiation. In the inorganic scintillators, the mechanism of scintillation depends on the energy states of the material in the crystal lattice. The valence band contains electrons that are bound at the lattice sites (as shown below in Fig. 2.4). Electrons in the conduction band are free to move throughout the crystal. The passage of gamma rays through the crystal may produce ionization of the crystal, if the incoming particle transfers sufficient energy to a valance electron to move it into the conduction band, leaving a hole in the valence band. If the incoming energy is not high enough, the electron of the valence band will not reach the conduction band, and will form with the hole a bound state called exciton. The excitons are located in an exciton band below the conduction band (Fig. 2.4). If impurities are present these can create energy levels between the valence and the conduction bands. Therefore, small amounts of an impurity are commonly added to inorganic scintillators. Such deliberately added impurities, called activators, create special sites in the lattice at which the normal energy band structure is modified from that of the pure crystal. As a result, there will be energy states created within the forbidden gap through which the electron can de-excite back to the valence band. The de-excitation from this level back to the valence band may occur through phosphorescent photon emission. Again, since this photon would have energy smaller than the difference between the valence and conduction bands, these crystals are transparent to their own radiation.

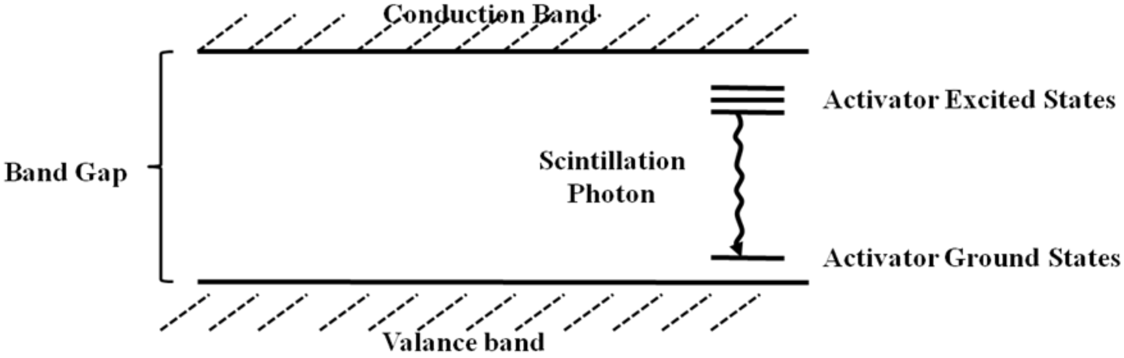

Fig. 2.4: Band gap model of scintillator

2.4.4.2 Well type NaI(Tl) scintillator detector

To be useful as a scintillator, a substance must possess certain properties. First, there must be a reasonable probability of absorption of the incident energy. The high density in solid and liquid scintillators meets this condition. Following absorption, emission of luminescence radiation must occur with high efficiency, and the scintillator must be transparent to its own radiation. Finally, the radiation must have a wavelength that falls within the spectral region to which the PMT is sensitive. The scintillator must be coupled optically to the PMT, so that there is a high efficiency of transfer of the light photons to the PMT photo-cathode. Since most of PMTs are sensitive to light in the visible wavelength region, both scintillator and PMT must be protected from visible light. Fig. 2.5 shows the schematic diagram of a well type NaI(Tl) scintillator detector.

Robert Hofstadterw was first to demonstrate that crystalline sodium iodide, in which a trace of thallium iodide had been doped in the melt, produced an exceptionally large scintillation light output, as compared with the organic materials that had previously received primary attention.[125] The sodium iodide (NaI) scintillator has a high attenuation coefficient for the interaction of gamma rays, and gives high efficiency and good energy resolution of gamma rays. NaI(Tl) usually contains about 0.1% of thallium. The most prominent property of NaI(Tl) detector is its excellent light yield. The high atomic number of iodine in NaI results in high efficiency for gamma ray detection. The best resolution achievable is about 7% for the 662-keV gamma ray from Cs-137, for a 3-inch diameter by 3-inch long NaI crystal. Besides, NaI (Tl) is almost linear in its energy response. Scintillators of unusual size, or shape, can also be fabricated by pressing small crystallites of NaI together. But, NaI(Tl) is hygroscopic, and will deteriorate due to water absorption, if exposed to the atmosphere. When the charged particle pass through the scintillator medium, these generate a large number of free electrons, free holes and electron-hole pairs, which move around in the crystal lattice until these reach an activator center (Tl). These transform the activation center into an excited state. The subsequent decay of this excited state of the activator center to its ground state produces emission of light, known as scintillation photons, in 0.23 microseconds. The excited states decay by emitting flashes of light.[126] After the scintillation photons strike the photocathode, photoelectrons are ejected from the photocathode. The light sensitive photo cathode of the PMT is semitransparent layer of a material, such as Cs_3Sb, which emits electrons when struck by visible light.

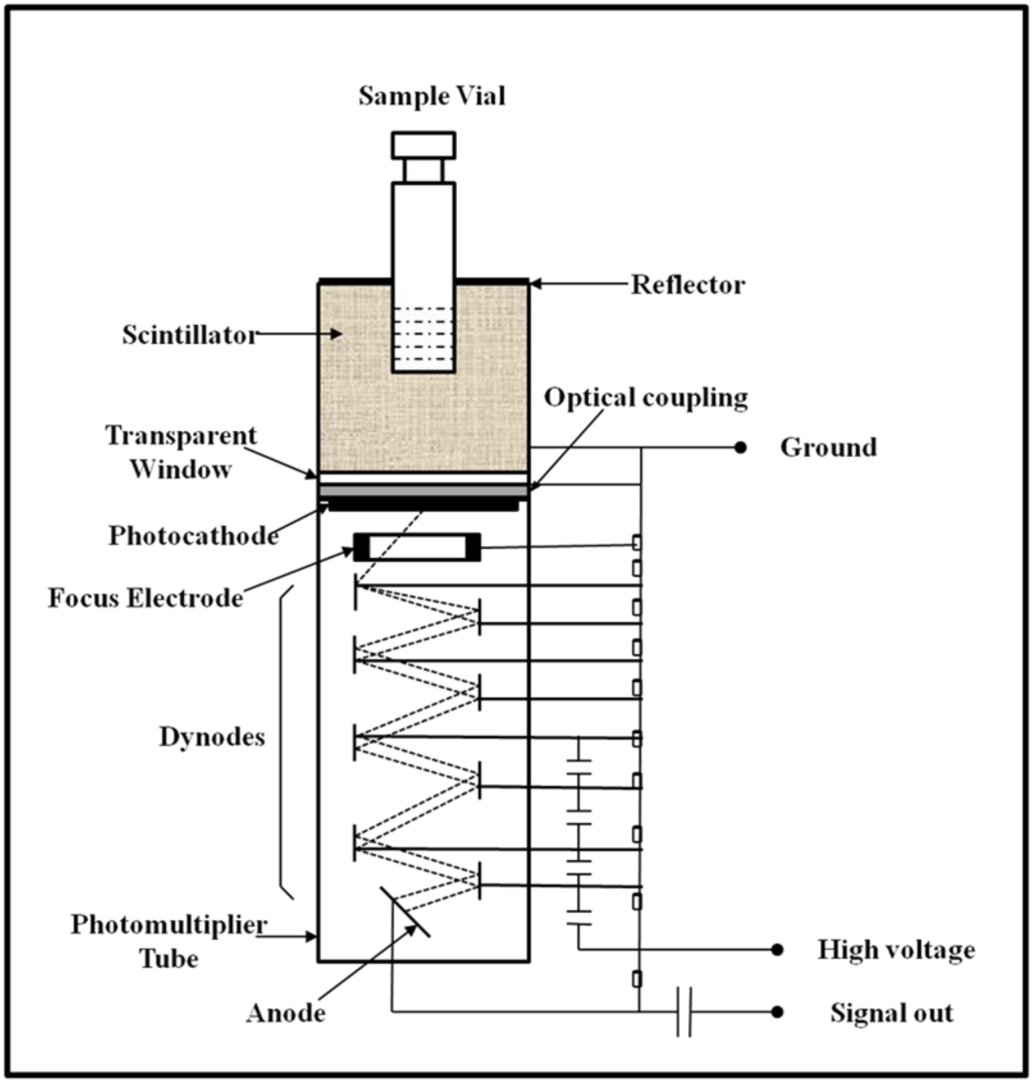

Fig. 2.5: Schematic diagram of well type NaI(Tl) scintillator detector

The number of photoelectrons produced is proportional to the energy of the gamma ray. The emitted photoelectrons are accelerated through a series of 10-14 electrodes (dynodes), between which a constant voltage difference is maintained. When the photoelectrons strike the nearest dynode, secondary electrons are emitted, as the dynodes are also coated with Cs_3Sb or MgO, etc. Consequently, there is a multiplication of electrons at each dynode stage, and at the last dynode, the numbers of original electrons have been increased by about a factor of 10^6-10^8 over a total voltage drop in the photo tube of 1000-2000 V. The electrical signal is normally generated from a voltage change between the ground and the anode caused by a resistor between anode and bias supply. As compared to GM tubes, these have the advantage of shorter resolution time and higher efficiency, although these require a more stable high voltage supply. If m_1,m_2,…..m_n are the multiplication factors of the respective dynodes, the total gain of the PMT is given by equation (2.4)

$$G = m_1 \, . \, m_2 \, \ldots \ldots \, m_n \tag{2.4}$$

In the present study, to investigate uptake of cesium on various synthesized sorbents, cesium solutions, spiked with Cs-134 and Cs-137 radiotracer, have been used, and the gamma counting of the samples, before and after sorption, has been carried out, using NaI (Tl) detector, from ECIL-India, connected to a single-channel analyzer,.

2.4.5 UV-visible absorption spectroscopy

Ultraviolet and visible spectrophotometers has been in general use, for many decades, and over this period, has become the most common analytical instrument in the modern day laboratory. Since its inception by Cary and Beckman, in the 1940s, UV-vis spectroscopy has revolutionized the field of molecular spectroscopy. In many applications, other techniques could be employed, but none rival UV-visible spectrometry for its simplicity, versatility, speed, accuracy and cost-effectiveness. Over the decades, numerous improvements have been made with respect to optical designs, including dual-beam optics, variable slit resolution, noise suppression, and integrated electronics. The principle of UV-visible absorption spectroscopy is based on the *"Beer-Lambert's Law"*, which states that *"A beam of light passing through a solution of absorbing molecules* *transfers energy to the molecules, as it proceeds, and, therefore, decreases progressively in intensity. The decrease in the intensity, or irradiance, (dI), over the course of a small volume element is proportional to the irradiance of the light entering the element, the concentration of absorbers (C), and the length of the path through the element, (dl)*

Mathematically, it can be expressed as,

$$-dI \propto Icdl \tag{2.5}$$

or $$-\frac{dI}{I} = kcdl \tag{2.6}$$

where k is the proportionality constant. It is called absorption coefficient.

Integrating the equation (2.6), one gets

$$-lnI = kcl + C_1 \tag{2.7}$$

where I is the transmitted intensity, l is the optical path length and C_1 is the constant of integration.

Since, when l=0, I =I_0, the incident intensity

$$-lnI_0 = C_1 \tag{2.8}$$

Therefore, equation (2.7) can be written as

$$-lnI = kcl - lnI_0 \tag{2.9}$$

or,

$$ln\frac{I_0}{I} = kcl \tag{2.10}$$

or,

$$log\frac{I_0}{I} = \frac{k}{2.303}cl = \varepsilon cl \tag{2.11}$$

where $\varepsilon = k/2.303$ is the molar absorptivity, or extinction coefficient.

For a solution of an absorbing substance, absorbance, A, at a monochromatic wavelength is defined as,

$$A = log\frac{I_0}{I} \tag{2.12}$$

From equations (2.11) and equations (2.12), one gets

$$A = \varepsilon cl \tag{2.13}$$

When the energy of the incident photon matches with the energy of the excited state of an atom, a molecule, radical or an ion the resonance occurs, and the intensity of the transmitted light is decreased. Depending on the energies of the excited states and the absorbed photons a sorption band is observed.

In the present studies, UV-visible optical absorption spectra have been recorded, using a double beam spectrophotometer from Chemito, model Spectroscan 2600 and UV-visible diffuse reflectance spectra of the beads and P25 Degussa powder have been recorded in the 200–700 nm region, employing a JASCO Model 605 spectrometer.

2.4.6 Surface area

Brunauer-Emmett-Teller (BET) surface area of the titania beads was determined by N_2 adsorption-desorption measurement, using Quantachrome Autosorb Automated Gas Sorption System. The titania sample beads were out-gassed at 150 ºC in vacuum, before the measurement. The surface area of rest of the sorbent beads was determined by using SORPTOMATIC 1990' analyzer, from CE Instruments, Italy. Samples were out-gassed at 100 ºC in vacuum, before the measurement. The conditioning of these samples was done at relatively lower temperature of ~100 ºC, to avoid thermal decomposition of the polymer matrix.

2.4.7 Dynamic light scattering (DLS)

Particle size analysis of the metal hexacyanoferrate particles was carried out by Dynamic light scattering (DLS) method, using VASCO$^{\gamma}$ particle size analyzer at 25ºC (laser wavelength 658 nm).

2.4.8 Universal testing machine (UTM)

The mechanical strength of the synthesized resins was analyzed by Lyods LRX plus universal testing machine, using 500 N load cell. The diameter of the sample beads was measured by a vernier caliper. The mechanical strength of the sample beads was determined in duplicate.

2.4.9 Fourier transform infra-red spectroscopy (FT-IR)

The FT-IR spectra of the samples have been recorded, using Diamond ATR on IR Affinity, Shimadzu spectrophotometer. The spectra were recorded with a resolution of 4 cm^{-1}, and an average of 60 scans.

2.4.10 Rheology studies

Rheology is defined as the science involved in the study of flow and deformation of materials.[127] It is a powerful tool that can be used, to characterize a wide range of materials, solutions, melts, gels, particulate systems, among others. It can also be used to provide information, and characterize microstructure of many materials. Rheological measurements can be performed either in steady or dynamic mode. In the steady mode, rheology measurements are performed by subjecting a sample to a steady shear at a constant shear rate (γ), resulting in a generation of shear stress (τ). The corresponding shear stress (τ) on the sample is measured, using a torque transducer. The viscosity (η) is measured as a function of the steady shear rate (γ), and is defined as:

$$\eta = \tau / \gamma \qquad (2.14)$$

In the present study, the viscosity of the resorcinol formaldehyde samples have been measured on a rheometer from Anton Paar, Germany, model MCR 101, at constant shear rate, at 25 ºC.

2.5 Sorption Studies

Sorption studies were carried out, by adding a fixed amount of the sorbent (m) into equilibration tubes, each containing a fixed volume (V) of the sorbate solution of different concentrations. After agitation for known time, a small portion of the aqueous phase was separated, and counted for radio-activity. Equilibrium sorption capacity, qe, was determined, using equation (2.15)

$$\boldsymbol{q_e = (C_o - C_e)\frac{V}{m}} \tag{2.15}$$

where C_o and C_e are the initial and the equilibrium concentrations, respectively, of the sorbate in the solution.

2.5.1 Sorption isotherms

Various theoretical models have been proposed over the years, to describe the sorption process in detail. By analyzing the experimental data, using these models, various important parameter can be determined, which help in building a thorough understanding about the sorption system under investigation.

2.5.1.1 Langmuir isotherm

Langmuir was the first to propose a coherent theory of sorption onto a flat surface based on a kinetic viewpoint.[45] The Langmuir sorption model is one of the best known and most frequently applied isotherms. The Langmuir equation initially was formulated on the basis of a dynamic equilibrium between the sorbent and the sorbate, that is, the rate of sorption (which is the striking rate at the surface multiplied by a sticking coefficient, sometimes called the accommodation coefficient) is equal to the rate of desorption from the surface.

The assumptions of the Langmuir model are:

1. Surface is homogeneous, that is, sorption energy is constant over all the sites

2. Sorption on the surface is localized, that is, atoms or molecules are sorbed at definite, localized sites

3. Each site can accommodate only one molecule, or atom

Langmuir proposed that the rate at which the sorbate molecules (B) strike a surface of a sorbent (A) is proportional to the product of the concentration of the sorbent and the fraction of the surface remaining uncovered by sorbate.

To derive Langmuir Equation, a parameter ‘θ’ is introduced. Let θ be the fraction of the number of the sites on the surface which are covered with sorbate molecules. Therefore, the fraction of surface which is unoccupied will be (1 – θ).

Now, the rate of the forward direction depends upon two factors: The fraction of sites available on the surface of sorbent, (1-θ), and the concentration, C. Therefore, the rate of the forward reaction is directly proportional to both the mentioned factors.

$$\text{Rate of sorption} \propto C(1-\theta) \tag{2.16}$$

$$\text{or, Rate of sorption} = K_a\, C(1-\theta) \tag{2.17}$$

Similarly, the rate of the backward reaction or rate of desorption depends upon number of the sites occupied by the sorbate molecules on the sorbent,

$$\text{i.e. Rate of desorption} \propto \theta \tag{2.18}$$

$$\text{or, Rate of desorption} = K_d\theta \tag{2.19}$$

At equilibrium, the rate of sorption is equal to the rate of desorption.

$$K_a\, C_e\, (1 - \theta) \; = \; K_d\, \theta \tag{2.20}$$

On solving the above equation for θ, we get

$$\theta = \frac{K_a C_e}{K_d + K_a C_e} \tag{2.21}$$

On rearranging the above equation, and substituting K_a/K_d with K_L (Langmuir constant)

$$\theta = \frac{K_L C_e}{1 + K_L C_e} \tag{2.22}$$

This is known as Langmuir sorption equation.

θ can be expressed in terms of equilibrium sorption capacity, q_e, and maximum monolayer capacity, q_m, as given in equation (2.22)

$$\theta = \frac{q_e}{q_m} \tag{2.23}$$

Therefore, on substituting θ from equation (2.21), and rearranging, equation (2.22) becomes

$$q_e = \; q_m \frac{K_L C_e}{1 + K_L C_e} \tag{2.24}$$

The linearized form of the Langmuir sorption isotherm can be presented as

$$\frac{1}{q_e} = \frac{1}{q_m} + \frac{1}{K_L q_m C_e} \tag{2.25}$$

From the linear plot of $1/q_e$ vs $1/C_e$, the values of q_m and K_L can be calculated from the intercept and the slope, respectively.[128]

The basic characteristics of Langmuir equation have been often represented in terms of a dimensionless separation factor, (R_L), defined as [129]

$$R_L = 1/(1 + K_L C_0) \qquad (2.26)$$

The value of parameter R_L indicates the nature of the isotherm as given below.

$R_L > 1$	unfavorable sorption
$0 < R_L < 1$	favorable sorption
$R_L = 0$	irreversible sorption
$R_L = 1$	linear sorption

2.5.1.2 Freundlich isotherm

Freundlich isotherm is an empirical equation. This equation is also one among the most widely used isotherms for the description of sorption equilibrium. In contrast to the Langmuir equation, the Freundlich isotherm assumes sorption onto sorbent surfaces, which are characterized by heterogeneous sorption sites. It is also assumed that the stronger binding sites are occupied first, and that the binding strength decreases with increase in the degree of site occupation.

At low concentration, the amount of the sorbate sorbed is directly proportional to concentration of the sorbate (raised to power one).

$$q_e \propto C_e \qquad (2.27)$$

At high concentration, the amount of the sorbate sorbed is independent of concentration, i.e., C_e raised to power zero

$$q_e \propto C_e^0 \qquad (2.28)$$

Therefore, at an intermediate value of concentration, sorption is directly proportional to the concentration raised to power 1/n. Here, n is a variable, the value of which is greater than one.

$$q_e = K_F C_e^{1/n} \tag{2.29}$$

The above equation is known as Freundlich sorption equation.[130] The linearized form of the above equation can be represented as

$$\log q_e = \log K_F + \frac{1}{n} \log C_e \tag{2.30}$$

The linear plot of log q_e versus log C_e has a slope of $1/n$ and an intercept of log K_F. However, in other case, when $1/n \neq 1$, the K_F value depends on the units in which q_e and C_e are expressed. On average, a favorable sorption tends to have Freundlich constant n between 1 and 10. Larger value of n (smaller value of $1/n$) implies stronger interaction between the sorbate and the sorbent, while $1/n$ equal to 1 indicates linear sorption, leading to identical sorption energies for all the sites.

2.5.1.3 Temkin isotherm

Temkin sorption isotherm considers a heterogeneous surface, where no molecular interaction exists. It is based on Langmuir sorption isotherm. However, like Langmuir model, it does not take into account the lateral interaction between the sorbates. Temkin isotherm assumes that the decrease in the heat of sorption as a function of temperature is linear rather than logarithmic.[131] The heat of sorption of all the molecules in the layer would decrease linearly with coverage due to sorbate-sorbent interactions.[130] The linear form of the Temkin model is given as,

$$q_e = \frac{RT}{b} lnK_T + \frac{RT}{b} ln\, C_e \qquad (2.31)$$

where K_T is Temkin isotherm constant, b is a constant related to heat of sorption, R is the gas constant, and T is the absolute temperature. A linear plot of q_e versus ln (C_e) enables the determination of the isotherm constants K_T and b, from the intercept and slope, respectively.

2.5.1.4 Dubinin-Redushkevich isotherm

Dubinin and his co-workers conceived this equation for subcritical vapor in microporous solids, where the sorption process follows a pore filling mechanism onto energetically non-uniform surface. According to this model, the characteristic sorption curve is related to the porous structure of the sorbent.[132] The Dubinin–Radushkevich (D-R) equation is excellent for sorption equilibrium of interpenetrating organic compounds (in gas phase condition) in porous solids. It has several advantages:

- it predicts quite fairly the experimental data over a wide concentration range
- it includes the effect of temperature
- it is based on physical parameters
- easy application.

This isotherm is generally expressed as follows:

$$lnq_e = lnq_m - K_{DR}\varepsilon^2 \qquad (2.32)$$

where q_m is the theoretical maximum capacity, K_{DR} is the D-R model constant (mol^2/kJ^2), related to the mean free energy of the sorption, and ε is the Polanyi potential, and is equal to

$$\varepsilon = RT \ln (Co/Ce) \tag{2.33}$$

The plot of ln q_e vs ε^2 gives a straight line, from the intercept and the slope of which, q_m and K_{DR}, respectively, can be obtained. The mean free energy of sorption per mole of the sorbate, as it is transferred to the surface of the sorbent from infinite distance in the solution, E, is calculated by the following equation

$$\mathrm{E} = (2(K_{DR}))^{-1/2} \tag{2.34}$$

The apparent free energy of sorption, for the physiosorption process is upto 40 kJ/mol, and a negative value indicates the exothermic nature of the sorption process.

2.6 Sorption Kinetics

Sorption kinetics describes the time-dependent evolution of the sorption process until equilibrium is reached. Such studies yield information about the possible mechanism of the sorption and the different transition states involved on the way to the formation of the final sorbate-sorbent complex. The results of such study help to develop appropriate mathematical models, to describe the interactions. Among the most popular kinetic models/equations are the so-called "pseudo first-order" and "pseudo second-order" rate expressions.

2.6.1 Pseudo first-order kinetic model

Lagergren equation is probably the earliest known one, describing the rate of sorption in the liquid-phase systems. This equation is called the pseudo first-order equation, or the Lagergren's rate equation, and can be written as [133-135]

$$\frac{dq_t}{dt} = k_1(q_e - q_t) \tag{2.35}$$

where q_t is the amount of sorbate sorbed at time t, and k_1 is the rate constant of the first order sorption. After integration and applying the boundary conditions, $q_t = 0$ at $t = 0$, the equation (2.35) can be written as

$$log\ (q_e\text{-}q_t)= log(q_e)\text{-}\ \frac{k_1}{2.303}t \tag{2.36}$$

The values of k_1 and q_e can be determined from the slope and intercept, respectively, of the straight line plot of log (q_e - q_t) versus t. Determining q_e accurately is a difficult task, because, in many sorbate-sorbent interactions, the chemisorption becomes very slow, after the initial fast response, and it is difficult to ascertain whether equilibrium is reached or not. Therefore, it has been reported that, many sorption processes follow Lagergren pseudo first-order model only for the initial 20 to 30 min of interaction. The value of k_1 parameter, also called time-scaling parameter, decides how fast the equilibrium in the system can be reached. The experimental studies have confirmed that the value of k_1 parameter can be both dependent and independent of the applied operating conditions. Its value depends on the initial concentration of the sorbate. It usually decreases with the increasing initial sorbate concentration in the bulk phase.[136] Since the model does not describe the interactions for the whole range of contact time, in many cases, higher order kinetic models are employed to analyze the experimental results.[137-139]

2.6.2 Pseudo second-order kinetic model

The pseudo second-order kinetics is usually associated with the situation, when the rate of direct sorption/desorption process (seen as a kind of chemical reaction) controls the overall sorption kinetics. The pseudo second-order kinetic model is expressed as [140]

$$\frac{dq_t}{dt} = k_2(q_e - q_t)^2 \tag{2.37}$$

Where k_2 is the rate constant of the pseudo second-order sorption. After integration and applying the similar boundary conditions, the equation (2.39) can be written as

$$\frac{t}{q_t} = \frac{1}{k_2 q_e^2} + \frac{1}{q_e} t \tag{2.38}$$

The above equation can be further simplified by substituting h for $k_2q_e^2$, where h can be considered as the initial sorption rate, when $t/q_t \to 0$, and, hence the final form of the equation can be written as

$$\frac{t}{q_t} = \frac{1}{h} + \frac{1}{q_e} t \tag{2.39}$$

The plot of t/q_t vs t gives a straight line, from the slope and intercept of which, the values of q_e and h, respectively, can be determined.[141] once the value of h is known, the value of k_2 can be determined therefrom. Many reports are available in literature, indicating that the value of k_2 has strong dependence on the applied operating conditions, such as the initial solute concentration, pH of solution and temperature, etc.[137-139, 142-143]

The value of k_2 is usually strongly dependent on the applied initial solute concentration, and it decreases with the increase in C_o, i.e., the higher is the C_o value, the longer time is required to reach an equilibrium. The sorption kinetics is very complex in nature, and the importance of the various factors varies from one system to another. Any change in the pH and temperature brings about the changes in the equilibrium state. Due to these reasons, the influence of pH and temperature on the k_2 value has not yet been theoretically studied.[136]

2.6.3 Kinetic steps

Mass transport, or migration, of the sorbate can be divided into four consecutive steps until it reaches the interior surface of the pores. A schematic representation of all the mass transport steps is given in Fig. 2.6

i. Bulk transport

This is transport of the sorbate from the solution phase to the subsurface, which is built up around the sorbent. This step is usually very rapid due to mixing of the flow.

ii. Film transport

This step involves diffusion of the solute across the so-called liquid film/sub surface surrounding the sorbent particles. This step is also known as external diffusion.

iii. Intraparticle transport

The third step in sorption involves the transport or diffusion of the solute in the liquid contained in the pores of sorbent particle, and along the pore walls.

iv. Sorption of the solute on active sites

This is the final step in the sorption process, and involves sorption and desorption of the solute molecules on/from the sorbent surface, which is quite fast.

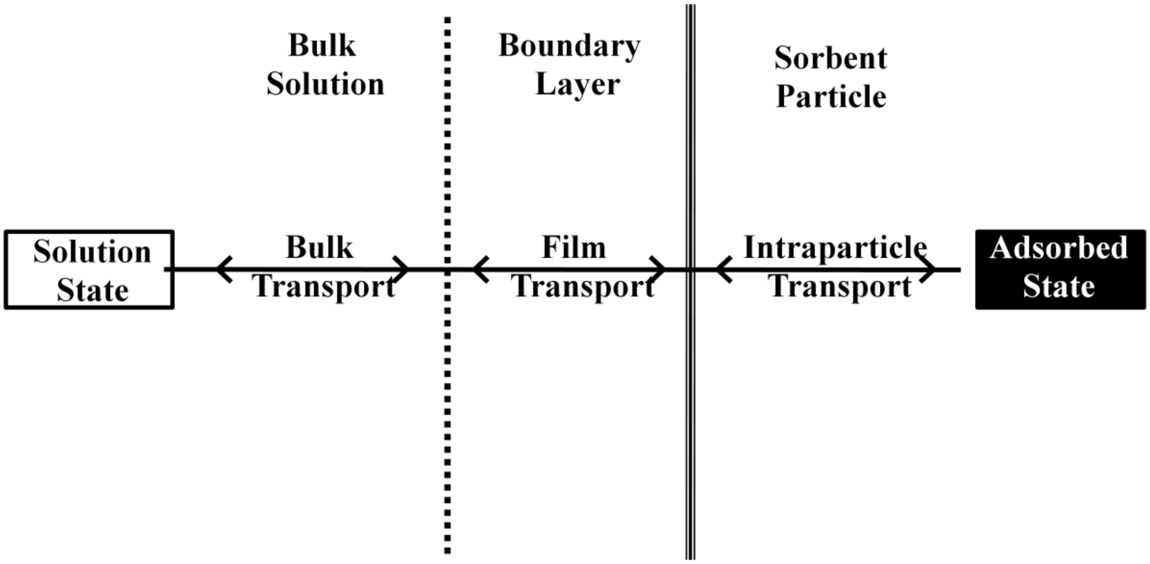

Fig. 2.6: Schematic of mass transport steps involved in a porous sorbent

The overall sorption rate may mainly be governed by any one of these steps, or a combination of two or more steps. Usually, the sorbate-sorbent system is under rapid mechanical mixing, and hence, the effect of the transport in the solution is eliminated. Therefore, the involvement of bulk transport step on the overall sorption rate can be neglected. Thus, the sorption rate is governed by external diffusion or internal diffusion. Internal diffusion step actually involves intraparticle diffusion and intercrystalline diffusion, or the sorption of the solute on the active sites.[144] Generally, the control by liquid-phase mass transfer/film diffusion is favored by

- low liquid-phase concentration (small driving force in the liquid)
- high ion-exchange capacity (large driving force in the exchanger)
- small particle size (short mass transfer distances in the bead)

- open structure of the exchanger, e.g., low cross-linking (little obstruction to diffusion in the exchanger)
- ineffective agitation of the liquid (low contribution of convection to liquid-phase mass transfer).

All of these mechanisms may also occur in parallel, which makes the determination of the dominating step difficult. In order to determine the contribution of the steps involved, numerous kinetic models have been compared to predict the behavior of the experimental data.

2.6.4 Intraparticle diffusion model

This model is represented by the following equation[145]

$$q_t = k_{id} t^{1/2} + I \tag{2.40}$$

where k_{id} is the intraparticle diffusion rate parameter and I (mg/g) is a constant that gives an idea about the thickness of the boundary layer. The values of k_{id} and I can be determined from the slope and the intercept, respectively, of the plot of q_t vs $t^{1/2}$. Intraparticle diffusion process involves the migration of ions into the internal surface of the sorbent particles through pores of different sizes. Boundary layer diffusion and the rate of surface sorption affect the intraparticle diffusion. These factors, along with the intraparticle diffusion rate, are dependent on surface characteristics of the sorbent.

2.6.5 Boyd's plot

In order to further confirm whether the sorption proceeds via film diffusion or intraparticle diffusion mechanism, the kinetic data can be analyzed, using the kinetic expression given by Boyd et al.[146]

$$F(t) = 1 - \frac{6}{\pi^2} \sum_{n=1}^{\infty} \frac{1}{n^2} \exp\left(-\frac{D_i \pi^2 t n^2}{r_o^2}\right) \quad (2.41)$$

$$F(t) = 1 - \frac{6}{\pi^2} \sum_{n=1}^{\infty} \frac{1}{n^2} \exp(-n^2 Bt) \quad (2.42)$$

where $B = \pi^2 D_i / r_o^2$ and F is the fractional attainment of equilibrium, i.e., the ratio of the solute sorbed at times t, to that at equilibrium ($F = q_t / q_e$), D_i is the effective diffusion coefficient of the sorbate, r_o is the radius of the sorbent and n is an integer.

Solutions to the equation (2.42), depending on the value of F, are given as equation (2.43) and equation (2.44).[147]

$$Bt = 2\pi - \frac{\pi^2 F}{3} - 2\pi\left(1 - \frac{\pi F}{3}\right)^{1/2} \quad (2.43)$$

$$Bt = -0.4977 - \ln(1 - F) \quad (2.44)$$

Thus, the value of Bt can be calculated for each value of F, using equation (2.43) for F values upto 0.85 and equation (2.44), for higher F values.[147] The linearity of Bt vs. t plot provides useful information to distinguish between the film diffusion and the intraparticle diffusion rates of sorption.[148] A straight line passing through the origin is indicative of sorption processes only governed by intraparticle-diffusion mechanisms, otherwise, it is governed by film diffusion.[149]

Chapter-3

Resorcinol Formaldehyde Resin Beads

3.1 Introduction

Resorcinol formaldehyde (RF) resin is the most widely used organic ion exchanger for removal/recovery of cesium from alkaline nuclear wastes. RF resin was developed in Savannah River National Lab, for its use in nuclear industry. Since then, it has been considered as a satisfying option for removal of Cs^+ ions from highly alkaline media because of low-cost, safety, availability, profitability, easy operation and efficiency considerations.[150] RF resin has exceptionally high affinity for Cs^+ ions, which can be attributed to the presence of -OH groups, which ionize under high alkaline condition. Conventionally, RF resin is prepared by bulk polymerization reaction between resorcinol and formaldehyde in alkaline medium, to get big chunks of the polymeric resin, and then, these chunks are ground and sieved, to get desirable mesh size.[104] But, these ground gel particles are of irregular shape, have broad particle size distribution, and exhibit poor column hydraulic behavior. These problems can be solved by using spherical resin material. The literature survey suggests that, the earlier research in the synthesis of RF resin involves specific inventory, such as vibrating column, laminar flow, supercritical drying, etc. Some inventors have used oil as a stabilizing media, to produce beads, with control over size, but washing out of the oil is a tedious step, and, moreover, it also generates secondary waste in considerable amount. We have developed new and simple methods for the synthesis of resorcinol formaldehyde beads, with good control over size. Two approaches have been used for the synthesis of spherical RF resin beads:

- **Suspension polymerization**: Synthesis of spherical RF resin beads by suspension polymerization, involves use of a suitable stabilizing polymer solution as a suspension medium, in which the aqueous droplets of required size, containing precursor of RF resin, are stablized.
- **Templating method**: In this method, a suitable pre-formed spherical template, such as beads of XAD-4, or calcium alginate, is used as base material which is equilibrated with the precursors of RF resin, to synthesize spherical RF resin beads. Depending upon the nature of the template, it may be retained in the final beads or removed by a suitable treatment, to incorporate porosity, and hence, increase the surface area for efficient sorption.

The methods do not require any sophisticated equipment, and the beads can be made free of unwanted contaminants by easy washing. The synthesis, characterization and sorption studies, carried out with these beads, are described in this chapter.

3.2 Materials

Resorcinol, formaldehyde (37% in methanol) and sodium hydroxides were obtained from Merck. Amberlite XAD-4, sodium alginate and calcium chloride were procured from S. D. Fine chemicals, India. All the other solvents and the chemicals used were of analytical grade. Water obtained from Millipore-Q water purification system, with conductivity < 0.3 μS/cm, was used in all the experiments. ^{134}Cs and ^{137}Cs radiotracers were procured from the Board of Radiation and Isotope Technology (BRIT), Mumbai, India.

3.3 Synthesis

3.3.1 Synthesis of pure RF resin beads

The resorcinol-formaldehyde pre-condensate was prepared, by reacting resorcinol with formaldehyde in a suitable proportion under alkaline conditions.[151] The pre-condensate was allowed to polymerize until it attained appropriate viscosity, and then, it was added to the stabilizing polymer solution, with optimum stirring. After stirring for certain time, the reaction mixture was kept undisturbed, for complete curing of the RF polymer. The cured RF beads were recovered from the reaction vessel, by washing out the polymer with a suitable solvent for the stabilizing polymer and then washing the beads with distilled water, and drying at room temperature. The cured beads of specific size were separated, using test sieves. Fig. 3.1 represents the schematic diagram of the steps involved in the synthesis of RF beads. Patent for the detail method of the synthesis of RF resin beads is in process.

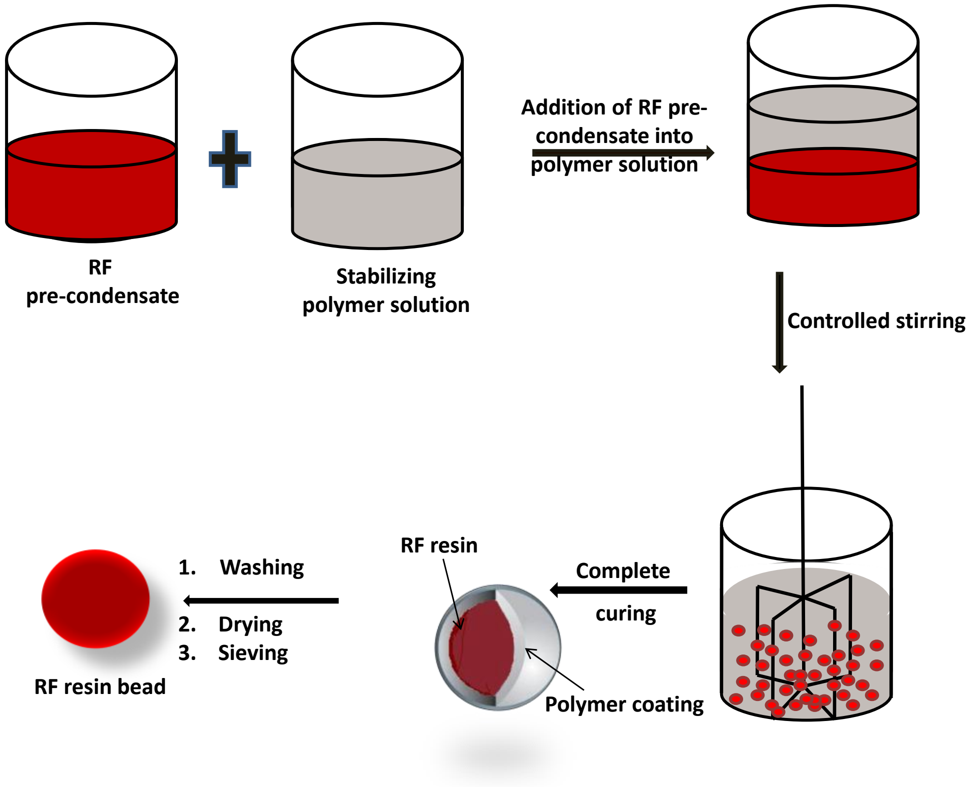

Fig. 3.1: Schematic diagram for the synthesis of RF beads.

3.3.2 Synthesis of RF-XAD resin beads

Resorcinol formaldehyde pre-condensate was prepared by reacting resorcinol and formaldehyde in aqueous media, using NaOH as a catalyst. An aqueous solution, with resorcinol : formaldehyde : catalyst in the molar ratios of 1 : 3 : 6, was prepared, and allowed to react for some time. Then, the XAD beads were equilibrated with this RF pre-condensate solution, for 2 hours. The equilibrated beads were separated from the rest of the RF pre-condensate solution, and the solution sorbed onto the beads was allowed to cure completely.[152] After complete curing at 105 °C, for 4 hours, brown-colored RF-coated XAD beads were obtained. The synthesized beads were in the sodium form, and hence, were dark-colored. These resin beads were converted into the hydrogen form, by mixing these with 0.5 M HNO_3 in a 3:1 ratio of liquid-to-resin volumes, for 1 hour, with occasional gentle shaking. After that, the resin beads were separated**,** and washed with water thoroughly, to remove any residual acid, till pH of the washing became near neutral. This acid treatment turned the resin into a light-colored hydrogen form. This hydrogen form of the resin was air-dried, and stored. It was used as such, without any further pre-treatment, in all the sorption experiments.

3.3.3 Synthesis of alginate assisted RF (RF^A) beads

In order to synthesize RF^A beads, template alginate beads were first synthesized. For that, 2.0% (w/v) aqueous solution of sodium alginate was obtained, by dissolving 2.0 g of sodium alginate in 100 ml of water, which was then, dropped into a calcium chloride solution (4%) through a syringe needle of 0.8 mm internal diameter, forming gelified calcium alginate microspheres. These beads were kept overnight in the calcium chloride solution, for complete curing, and then, washed with water. Resorcinol formaldehyde pre-condensate was prepared by reacting resorcinol and formaldehyde in aqueous media, using $NaCO_3$ as a catalyst. An aqueous solution, with resorcinol: formaldehyde: catalyst in the molar ratios of 1: 2: 0.05, was prepared, and was allowed to react for ~15 min. The pre-formed water-swollen alginate beads were equilibrated with this RF pre-condensate solution, for 3 hours, and then, separated from the rest of the RF pre-condensate solution. The solution adsorbed on the beads was allowed to cure completely. After complete curing at 105 ºC, for 4 hours, the brown-coloured RF^A beads were obtained.[153] These dark-coloured beads were in sodium form, and were converted into hydrogen form, by the method mentioned earlier for the RF-XAD beads, before carrying out the sorption experiments.

3.4 Sorption Studies

The solutions of the radiotracers, ^{134}Cs and ^{137}Cs, were further diluted to the required concentrations, as and when required. The sorption experiments on RF resin beads were carried out, by equilibrating 0.05g of RF resins beads with 5 mL of the $CsNO_3$ solution of appropriate concentration, containing ^{137}Cs as a radiotracer. The solutions were stirred, using a mechanical shaker, for 6 hours. The sorption experiments with RF-XAD and RF^A resin beads were carried out, using ^{134}Cs as a radiotracer, for 4 hours of contact time, keeping the sample volume to the resin mass ratio same, as mentioned earlier. The contact time was found to be sufficient for attaining equilibrium. However, for studying the kinetics of sorption, the equilibration time was varied from 0 to 4 hours. All the test solutions, containing cesium ions, were prepared in 0.1 N NaOH solution, to maintain similar alkalinity of the solutions. After the equilibration, a small portion of the aqueous phase (1 ml) was separated, and taken for counting gamma activity. The gamma activity measurements were carried out in a well-type NaI (T1) [ECIL] detector, connected to a single-channel analyzer. The sorption capacity at equilibrium, q_e, was calculated by the equation (3.1)

$$q_e = \frac{(C_o - C_e)V}{m} \tag{3.1}$$

where C_o and C_e are, respectively, the initial and the equilibrium concentrations of cesium ions, V is the volume of the solution, and m is the mass of the sorbent used.

3.5 Results and Discussion

3.5.1 RF resin beads

3.5.1.1 Characterization

3.5.1.1.1 Optical microscopy and SEM studies

Fig. 3.2(a) and (b) show the optical microscope image of RF ground gel and RF beads of size 20- 40 mesh (0.8-0.4 mm), respectively. Fig. 3.2(c) depicts the SEM image of the outer surface of a RF bead. There are some big pores on the outer surface of the bead, which might have formed due to water loss during curing. These pores will offer higher surface area to the sorbate during sorption process, and hence, will increase its capacity.

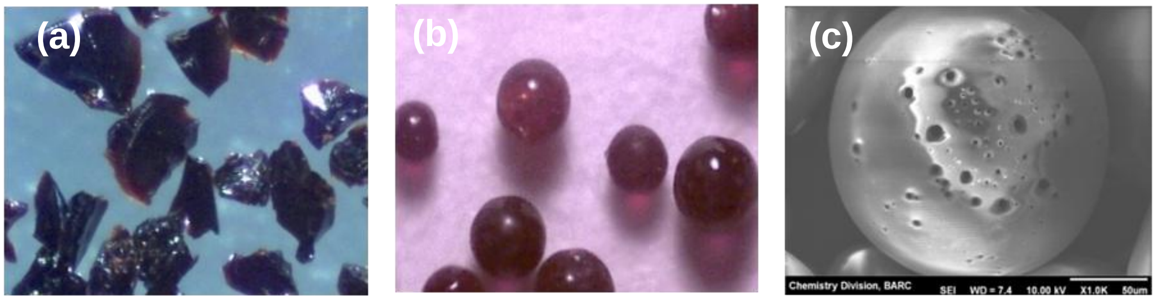

Fig. 3.2: Optical microscope image of (a) the RF ground gel, and (b) the RF resin beads, and (c) SEM image of a RF bead

3.5.1.1.2 Mechanical strength

Mechanical strength of the synthesized RF beads was tested, and compared with that of the conventional ground RF gel particles, using a universal testing machine. The measurement was carried out, by applying the load in the range of 0- 250 N, using a 500 N load cell. The spherical RF beads showed the first break at a load of 12-14 N, for the different samples. Under similar experimental conditions, the first breakage for the ground RF gel was observed at 2.5-5 N, and different breakages were seen in the range of 2.5-15 N, depending on the shape and the size of the granular RF particles. The irregular-sized ground gel particles have some sharp and weak edges, which are the most susceptible for breaking under pressure, and result in generation of fine powder that leads to choking of column. These results suggest that the synthesized RF resin beads offer better mechanical strength, and are expected to work better in column mode of operation.

3.5.1.1.3 Water content and surface area analysis

The moisture content of the synthesized RF beads was determined by thermogravimetry technique. For this measurement, a pre-weighed amount of the RF beads was heated isothermally at 100ºC, under N_2 atmosphere, for 2 hours, and the loss in the weight was determined. The water content of these beads was found to be 18% of the total weight. The specific surface area and the pore volume of the beads were determined by BET N_2 adsorption method. The nitrogen adsorption-desorption isotherms were measured at 77 K, at a relative partial pressure (i.e. P/P_o) of N_2 of 0.98, after degassing the samples at 100 ºC, for 5 hours. The surface area of the beads was determined to be 273.6 m^2/g. The higher surface area of the beads, along with 18 % moisture content, indicates towards its better sorption efficiency for removal of cesium ions.

3.5.1.1.4 Ion-exchange capacity

About 0.5 g of the H^+-form, air-dried RF resin beads were equilibrated with 100 ml of 0.1 M NaOH solution, containing 5% NaCl. From the amount of NaOH consumed, the total H^+-Na^+ ion-exchange capacity was determined to be 6.15 milliequivalents/g of air-dried, H^+-form RF resin beads.

3.5.1.2 Sorption studies

3.5.1.2.1 Effect of the size of the resin

The effect of the size of the synthesized RF resin on the sorption of cesium was determined, by agitating 0.05 g of the RF resin beads of different sizes, ranging from less than 20 to more than 80 mesh, with 5 mL of 0.005 mmol/L cesium ion solution in 0.1 M

NaOH in separate equilibration tubes, using a shaker, at 20 °C. Agitation was provided at a constant speed of 150 rpm, for 6 hours, which is sufficient to reach equilibrium. The percentage removal of cesium ions can be calculated as follows

$$\% \text{ Removal} = \frac{C_o - C_e}{C_o} \times 100 \tag{3.2}$$

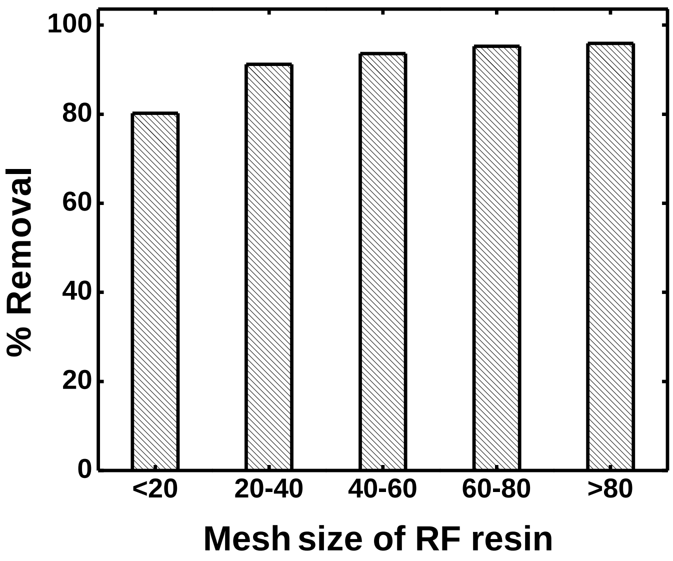

Fig. 3.3: Effect of the mesh size of the RF resin beads on % removal of cesium ions

Fig 3.3 shows the effect of the size of the RF resin beads on % removal of cesium ions from alkaline solution (0.1 M NaOH). With increase in the mesh size, i.e., decrease in the particle size, of the RF resin beads, the % removal of cesium ions increases gradually. In the case of bigger size RF resin beads (less than 20 mesh), 80% cesium is removed, whereas under similar experimental condition, ~ 91 to 96% cesium is removed, in the case of higher mesh size resin beads. The increase in percentage removal of cesium ions with the decrease in particle size (from 20-40 mesh to more than 80 mesh) of the sorbent is very small ~ 5.0%. Hence, a reduction of the particle size, from less than 20 mesh to 20-40 mesh size, leads to increased removal of cesium due to increased availability of the sorption sites, but further decrease in the resin size does not show much improvement. So, the optimum particle size for the sorbent may be considered as 0.4–0.8 mm, corresponding to 20-40 mesh size, which was selected for all the further sorption experiments. Particle size of this range has been also reported in literature for removal of cesium from alkaline waste.[104]

3.5.1.2.2 Effect of Na^+ ion concentration

The effect of the presence of the Na^+ ions on equilibrium uptake capacity of the RF resin beads, for Cs^+ ions, was studied at 0.02 mM initial cesium ion concentration, at 20 °C. Fig. 3.4 shows that the sorption of cesium ions decreases with increase in sodium ion concentration up to the studied concentration of 3.0 M. These results indicate that the q_e value for cesium ion is significantly affected by the presence of Na^+ ions in the solution, due to the competition offered by Na^+ ions for the available exchange sites. But, the observed q_e value of ~0.4 mmol/g at 2 M Na^+ ion concentration is sufficient, to remove the amount of cesium usually present in the low-level alkaline waste.

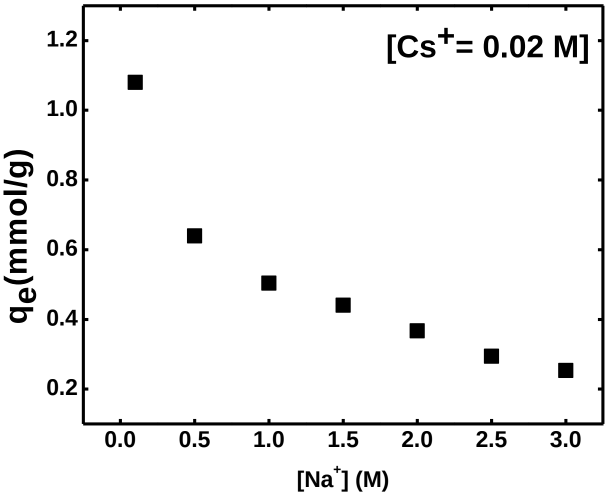

Fig. 3.4: Effect of Na^+ ion concentration on the sorption of cesium ions

3.5.1.2.3 Effect of cesium ion concentration

The sorption of cesium ions by the beads at different initial concentrations, ranging from 0.5 to 50 mM, at 20 °C, is illustrated in Fig 3.5. It is evident that the amount of cesium ions sorbed increases with the increase in the concentration of cesium ions in the solution, but the percentage sorption decreases (Fig. 3.5 (b)). When the initial cesium concentration increases from 0.5 to 50 mM, the sorption uptake of cesium ions increases from 0.04 to 1.79 mmol/g, i.e., 5.3 to 238 mg/g (Fig. 3.5(a)).

A higher initial concentration provides an important driving force, to overcome all resistances to the cesium ions between the aqueous and solid phase, and thus, increasing the uptake. Moreover, with increase in the initial cesium ion concentration, there is an increase in the number of collisions between the cesium ions and the active sites of the RF resin, which results in both increase in the rate of sorption and enhanced equilibrium sorption capacity. While the percentage removal of cesium ions decreases from 99.3 to 35.9%, as the initial concentration increases from 0.5 to 50 mM (Fig. 3.5(b)). This is because the total number of active sites are finite due to the fixed amount of the resin taken for sorption studies.

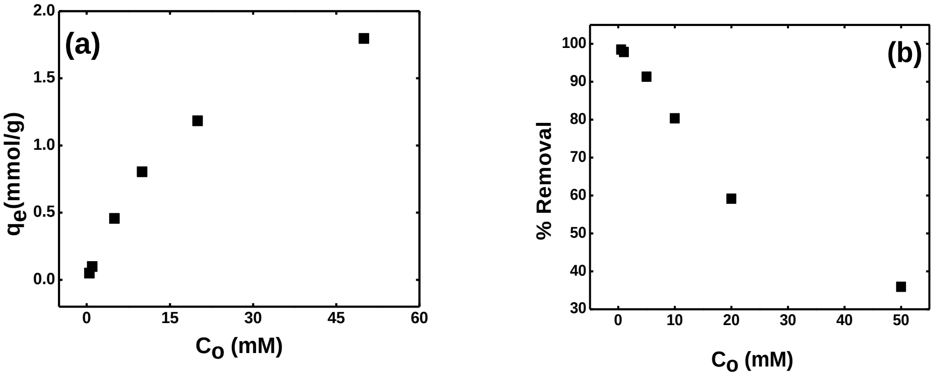

Fig. 3.5: Effect of the initial cesium concentration on (a) equilibrium sorption capacity and (b) percentage removal of cesium ions by the RF resin

3.5.1.3 Sorption isotherms

The sorption data were analyzed, using the Langmuir and the Freundlich sorption isotherm models. The Langmuir sorption isotherm is the simplest model for the sorption of a solute from a liquid solution.[154] The Langmuir sorption model is based on the assumption that maximum sorption corresponds to a saturated monolayer of the solute molecules on the sorbent surface.[130, 154] The linearized expression of the Langmuir model is

$$\frac{1}{q_e} = \frac{1}{q_m} + \frac{1}{K_L q_m C_e} \tag{3.3}$$

Where q_m is the maximum monolayer loading capacity, and K_L is a constant related to the affinity of the binding sites.

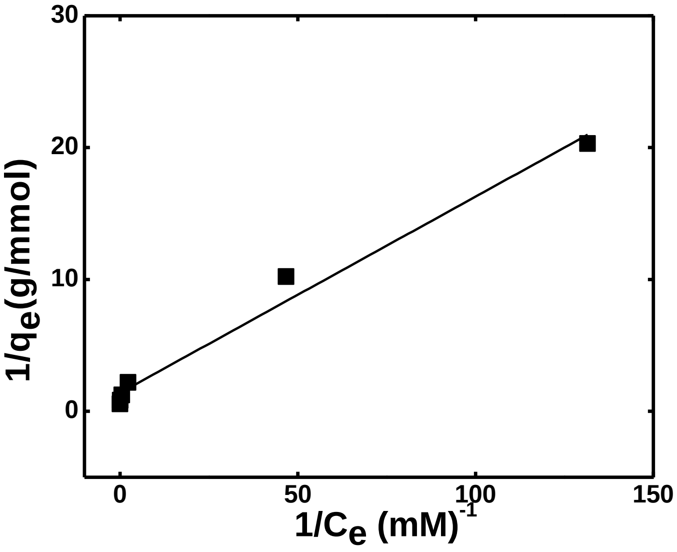

Fig. 3.6: Langmuir plot for sorption of Cs^+ ions onto the RF resin beads at 293 K

The linear plot of $1/q_e$ verses $1/C_e$, with R^2 value of 0.9794 (Fig. 3.6), shows that the sorption seems to obey the Langmuir model. The Langmuir constants q_m and K_L are determined from the intercept and slope of the plot, respectively, and are given in Table 3.1.

The Freundlich model is an empirical equation that assumes heterogeneous sorption due to the diversity of the sorption sites.[130, 154] The Freundlich equation is expressed as

$$\log q_e = \log K_F + \frac{1}{n}\log C_e \tag{3.4}$$

where K_F is related to the sorption capacity and 1/n is the sorption intensity. The magnitude of the exponent, 1/n, gives an indication of the favorability of the sorption. The values of K_F and n are calculated from the intercept and slope, respectively, of the linear plot of log q_e vs. log C_e (Fig. 3.7), and are listed in Table 3.1

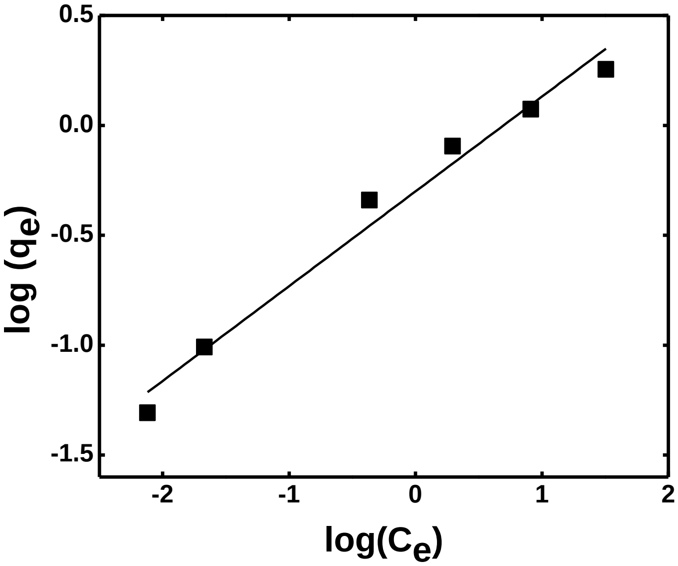

Fig. 3.7: Freundlich isotherm plot for sorption of Cs^+ onto RF resin beads at 293 K

The regression correlation coefficients obtained for both the Langmuir and the Freundlich models are almost similar, but the maximum monolayer capacity determined from the Langmuir model is less than the experimentally determined equilibrium capacity. Therefore, the Langmuir model is not the best model, to describe the sorption of cesium ions onto the synthesized beads. From Table 3.1, it can be seen that the value of Freundlich isotherm parameter ‘n’ lies between 1 and 10, which indicates favorable sorption. From the high R^2 value for Freundlich model, and fractional value of 1/n, it can be concluded that Freundlich isotherm explains sorption process well. The predicted expressions for the q_e, corresponding to the Langmuir and the Freundlich models, for sorption of ions onto the RF resin beads, useful for design calculations, can be given by equations (3.6) and (3.7), respectively

Langmuir: $$q_e = \frac{0.7158C_e}{1+9.3835C_e} \tag{3.6}$$

Freundlich: $$q_e = 0.50066C_e^{0.43123} \tag{3.7}$$

Table 3.1: Langmuir and Freundlich isotherm parameters for sorption of cesium ions onto the RF resin beads

Isotherm model	Parameters	
Langmuir	q_m	0.715 mmol/g
	K_L	0.852 L/mmol
	R^2	0.9793
Freundlich	K_F	0.481 mmol/g
	1/n	0.431
	R^2	0.9754

3.5.1.4 Sorption kinetics

The effect of contact time on the removal of cesium ions by the RF resin, studied at three different initial concentrations, in the range 0.5–10 mM, at 20 °C, shows rapid sorption of cesium ions in the initial period of 2 hours (Fig. 3.8(a)). About 96 % and 64 % removal of cesium ions is observed for the initial concentrations of 0.5 and 10 mM, respectively, during this time period (Fig. 3.8(b)). Such short times, coupled with high % removals, indicate a high degree of affinity of the RF beads for the cesium ions, pointing towards chemisorption. The decrease in sorption rate is observed with increase in contact time, and gradually, sorption reaches equilibrium value in about 3 to 6 hours, depending on the initial cesium ion concentration. For cesium ion solution, with initial concentrations of 5 mM, the contact time of 5 hours is sufficient to attain equilibrium. The time required to attain the state of equilibrium is termed as the equilibrium time, and the amount of cesium ions sorbed at the equilibrium time reflects the maximum cesium sorption capacity of the sorbent, under these particular conditions.

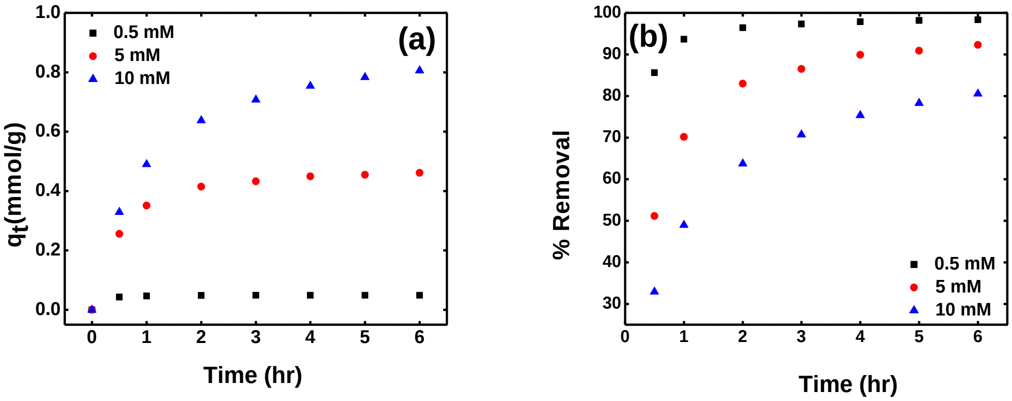

Fig. 3.8: Effect of contact time on (a) the sorption capacity, and (b) the percentage removal of cesium ions by RF resin beads, at different cesium ion concentrations

Various kinetic models have been proposed, to determine the mechanism of the sorption process, which provides useful data, to improve the efficiency of the sorption and feasibility of scale-up of the process.[155] In order to analyze the sorption kinetics of cesium ions onto RF resin, the pseudo first-order, pseudo second-order, and intraparticle diffusion models, given by equations (3.8), (3.9) and (3.10), respectively, were used.

$$\log (q_e - q_t) = \log(q_e) - \frac{k_1}{2.303} t \qquad (3.8)$$

$$\frac{t}{q_t} = \frac{1}{k_2 q_e^2} + \frac{1}{q_e} t \qquad (3.9)$$

$$q_t = k_{id} t^{1/2} + I \qquad (3.10)$$

where q_t is the amount of the cesium ions sorbed at time t, k_1, k_2 and k_{id} are the rate constants of the pseudo first-order, the pseudo second-order sorption and the intraparticle diffusion model, respectively, and I gives an idea about the boundary layer thickness.[156]

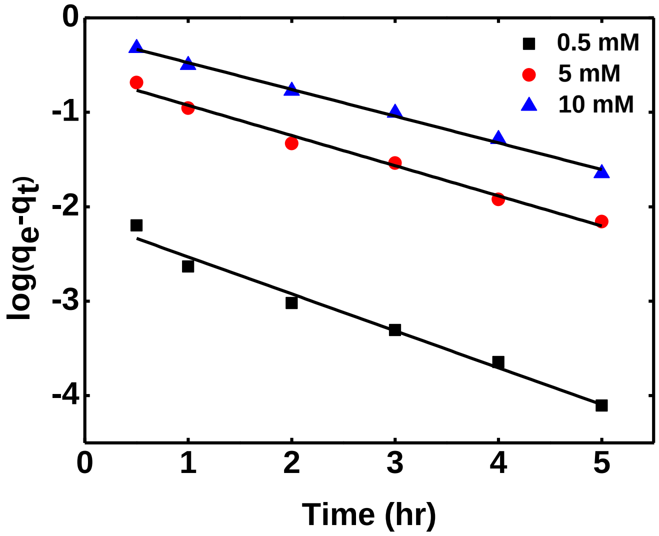

Fig. 3.9: Pseudo first-order kinetic plots for sorption of cesium ions onto the RF resin

Fig. 3.9 shows the plots of log (q_e-q_t) vs t, for sorption of cesium ions onto the RF resin, along with the fitted straight lines. The values of the pseudo first-order sorption rate constant (k_1) for the sorption of cesium ions onto RF resin, and the sorption capacity (q_e) were determined from the slopes and the intercepts, respectively, of the corresponding straight lines of the Fig. 3.9. The parameters of the pseudo first-order model are summarized in Table 3.2. Although the correlation coefficient, R^2, for the application of the pseudo first-order model is reasonably high in some cases, the calculated q_e values do not match with the experimental q_e values, suggesting that the sorption of cesium ions onto the RF resin does not follow the pseudo first-order kinetics, at the studied initial concentrations of cesium ions.

The kinetic data were further analyzed, using the pseudo second-order relation proposed by Ho and McKay,[156] equation (3.9). Fig. 3.10 shows the plots of t/q_t vs t, for the sorption of cesium ions onto the RF resin beads, along with the fitted straight lines. From the slope of the straight line, the corresponding value of the sorption capacity, (q_e) can be determined. Once the value of q_e is known, the rate coefficient k_2 can be determined from the intercept of the straight line.

Table 3.2: Comparison of the kinetic constants and the calculated and the experimental q_e values for the sorption of cesium ions onto the RF resin beads at different initial concentrations

C_o (mM)	Pseudo first-order kinetic model				Pseudo second-order kinetic model		
	$q_{e,exp}$ (mmol/g)	k_1 (/h)	$q_{e,cal}$ (mmol/g)	R_1^2	k_2 (g/mmol h)	$q_{e,cal}$ (mmol/g)	R_2^2
0.5	0.049	0.901	0.0072	0.97729	288.796	0.049	0.9999
5.0	0.461	0.736	0.2474	0.98516	4.756	0.498	0.9997
10.0	0.805	0.652	0.6435	0.99454	1.196	0.925	0.9999

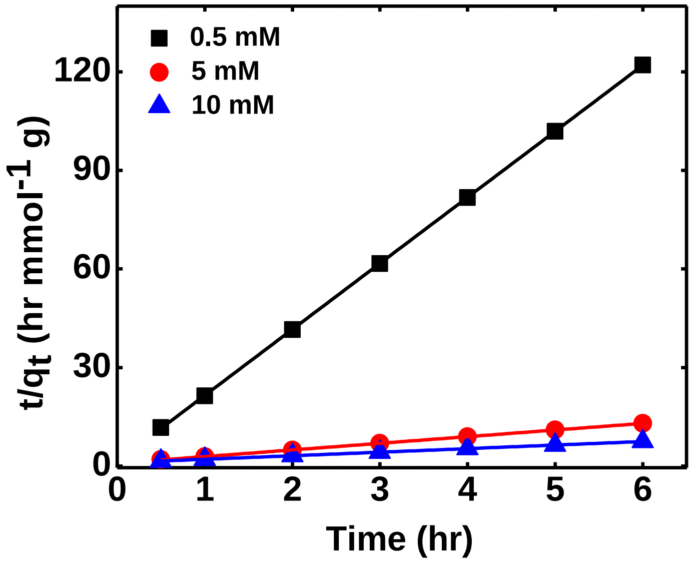

Fig. 3.10: Pseudo second-order kinetic plots for sorption of cesium ions onto the RF resin

It is evident from these results that the correlation coefficients for the pseudo first-order kinetics model, obtained at all the studied concentrations, are a bit lower than those for the pseudo second-order model. Moreover, the theoretical q_e values calculated from the pseudo second-order kinetic model are closer to the experimentally determined q_e values, whereas the theoretical q_e values obtained from the pseudo first-order model do not seem to be reasonable. These results indicate that the sorption of cesium ions onto the RF resin beads is chemisorption, and follows pseudo second-order kinetics. From Table 3.2, it is observed that the pseudo-second-order rate constant (k_2) decreases significantly with the increase in the initial cesium concentration.

3.5.1.5 Mechanism

In order to identify the sorption mechanism, the intraparticle diffusion model, equation 3.10, proposed by Weber and Morris, was applied to the kinetic data.[145] According to this theory, if the intraparticle diffusion is followed, then, the plot of q_t vs $t^{1/2}$ plot will be linear, and if this straight line passes through origin, then, only the intraparticle diffusion can be considered as the rate limiting step, otherwise, some other mechanism may also be involved. Fig. 3.11 shows the plots of q_t vs. $t^{1/2}$, for various initial cesium ion concentrations. These plots are multilinear. The value of k_{id} and I can be determined from the slope and intercept, respectively, of the second linear portion of the corresponding plot. The values of intraparticle diffusion rate constant and I values are given in Table 3.3, for the different initial concentrations of cesium ions..

It can be seen from Table 3.3 that the R^2 values are >0.92, but the plots do not pass through the origin, suggesting that sorption involves intraparticle diffusion, though that is not the only rate-controlling step. Other kinetic steps also may govern the sorption rate. The value of the intraparticle diffusion rate constant, k_{id}, for the studied system, is observed to increase with increase in the initial cesium ion concentration, from 0.5 to 10 mmol/L. The boundary layer thickness also increases with increase in the initial cesium ion concentration.

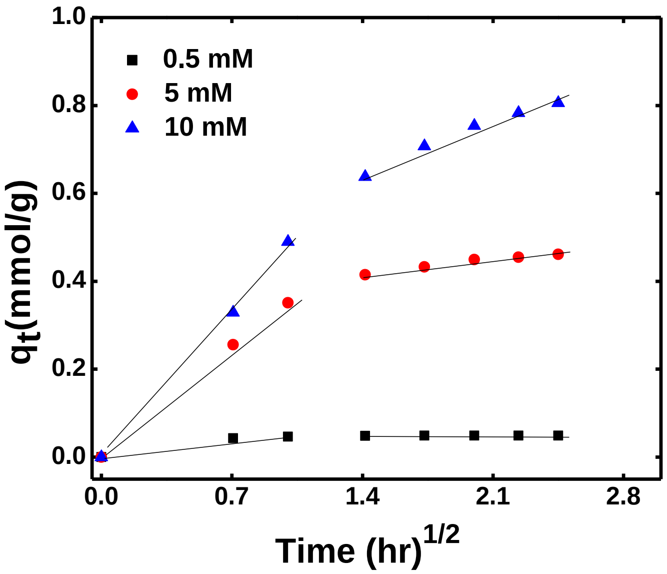

Fig. 3.11: Intraparticle diffusion plots for sorption of Cs^+ ion onto the RF resin beads

Table 3.3: Intraparticle diffusion parameters at different initial cesium ion concentrations, for its sorption onto the RF resin beads

Initial conc. (mg/L)	k_{id} (mmol/g h$^{1/2}$)	I (mmol/g)	R^2
0.5	0.001	0.048	0.93885
5.0	0.039	0.368	0.91901
10.0	0.137	0.475	0.97996

In order to predict whether the sorption proceeds via film diffusion or intraparticle diffusion mechanism, the kinetic data were further analyzed, using the kinetic expression given by Boyd et al.[146]

$$Bt = 2\pi - \frac{\pi^2 F}{3} - 2\pi(1 - \frac{\pi F}{3})^{1/2} \qquad (3.11)$$

$$Bt = -0.4977 - \ln(1 - F) \qquad (3.12)$$

The value of Bt was calculated for each value of F, using equation (3.11), for F values upto 0.85, and equation (3.12), for F values higher than 0.85.[147] The calculated Bt values are plotted against time (Fig. 3.12). The linearity of this plot provides useful information to distinguish between the film diffusion and the intraparticle-diffusion rates of sorption.[148] A straight line passing through the origin is indicative of sorption process governed by intraparticle diffusion mechanism.[149] In the present case, all the plots are linear, with R^2 value >0.98, in the whole studied initial concentration range, but do not pass through the origin, indicating that the sorption process is of complex nature, consisting of both film diffusion and intraparticle diffusion steps, with film diffusion mainly governing the rate-limiting process in the studied solute concentration range.

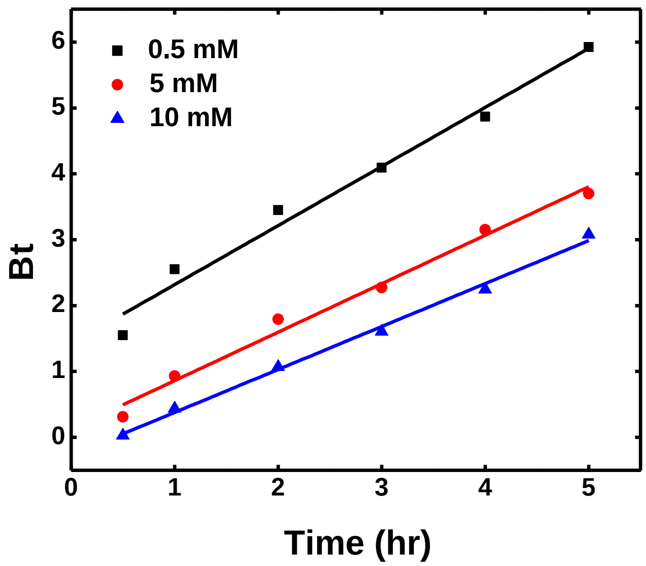

Fig. 3.12: Boyd's plots for sorption of cesium ions onto the RF resin beads

3.5.2 RF-XAD Resin beads

3.5.2.1 Characterization

3.5.2.1.1 Optical microscopy and SEM studies

Figs. 3.13 and 3.14 represent the optical microscope and SEM images of the XAD and RF-XAD beads, respectively, and confirm the coating of RF on the pre-formed XAD beads. The SEM image (Fig. 3.14 (a)) of the outer surface of a RF-XAD bead shows porosity. This porous nature of the beads, which is also corroborated from the results of the TGA study discussed ahead, is a desirable feature, as it will contribute to better sorption behavior. The SEM image of a cross-section of the RF-XAD bead does not show any distinct boundary, or contact between the RF coating and the XAD template, indicating that the RF has penetrated inside the XAD-4 beads (Fig. 3.14 (b)). This supports the observations from the studies on the testing of the mechanical strength of the beads.

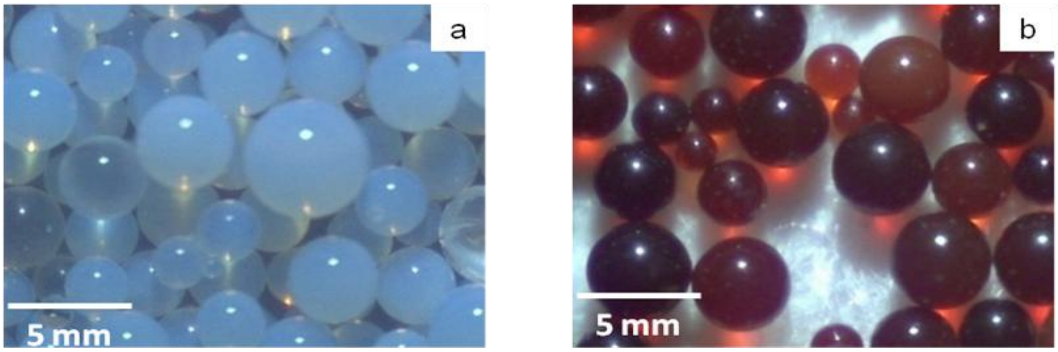

Fig. 3.13: Optical microscope image of (a) XAD beads and (b) RF-XAD beads (10X magnification)

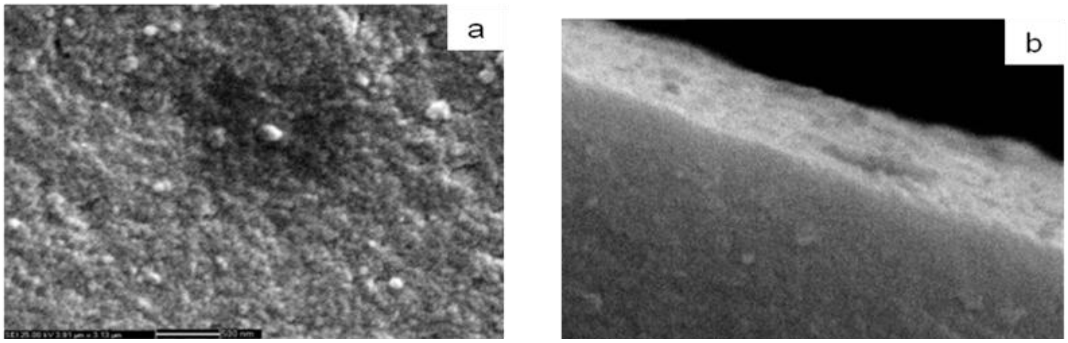

Fig. 3.14: SEM image of (a) the surface and (b) the cross-section of RF-XAD bead (scale bar 500 nm)

3.5.2.1.2 Mechanical strength testing

Mechanical strength of the synthesized RF-XAD beads was tested, and compared with that of the conventional ground RF gel particles and the blank XAD beads, using universal testing machine. The XAD blank beads showed the first breakage at an applied load of 2 N, and second breakage at 4 N; at this stage, the XAD bead was completely compressed, and no machine extension was observed for even higher applied load. Spherical RF-XAD beads showed the first break at a load of 13-15 N, for the different samples tested, while the same for the ground RF gel was observed at 2.5-5 N. The increase in the mechanical strength of RF-XAD beads suggests that, the RF is present not only on the surface of the XAD template beads, but it has also penetrated in the pores of the XAD beads, and solidified. This observation supports the results from BET surface area analysis discussed subsequently. The synthesized RF-XAD beads are spherical in size, and have better mechanical strength as compared to that of the currently used ground RF resin gel particles, making these more suitable for column operation.

3.5.2.1.3 Thermogravimetric analysis

Thermo gravimetric analysis (TGA) of the synthesized RF-XAD beads was performed at a heating rate of 10°C/min, in nitrogen atmosphere, from ambient conditions to 900 °C. Fig. 3.15 shows typical TGA profiles of the granular RF gel, XAD and RF-XAD beads. The thermal decomposition profile of pure granular RF particles is continuous, and unlike that of XAD and RF-XAD beads, it does not show well-defined decomposition steps (trace a, Fig. 3.15). After heating upto 110 °C, a weight loss of about 8% is observed, which could be due to the absorbed water. Additional 7 % weight loss is observed upto 216 °C, which could be due to decomposition of RF. With further increase in temperature, a continuous decrease in the weight takes place, and at the end of the heating cycle, a charred mass is obtained, which is about 37 % of the initial weight taken. The thermal decomposition of XAD beads takes place in two major steps (trace b, Fig. 3.15). In the first step, (30 to 86 °C), there is a weight loss of 8.7 %, corresponding to evaporation of the sorbed water. Then, the second step starts at 343 °C, in which degradation of XAD matrix takes place, and additional weight loss of ~72 % is observed at the end of this step at 560 °C. The TGA profile of RF-XAD beads (trace c, Fig. 3.15) also can be divided into two main stages. The first stage is from 30 to 118 °C, over which a weight loss of about 36% is observed, due to dehydration. The weight loss in the same range of 343-560 °C, as that in the case of XAD beads, is of about 38 %, due to simultaneous degradation of RF and XAD. The TGA profiles of XAD and RF-XAD appear similar, but the extent of thermal degradation of the composite beads is much lower than that of the XAD beads, and the water content in the blank XAD is less than that in the RF-XAD beads.

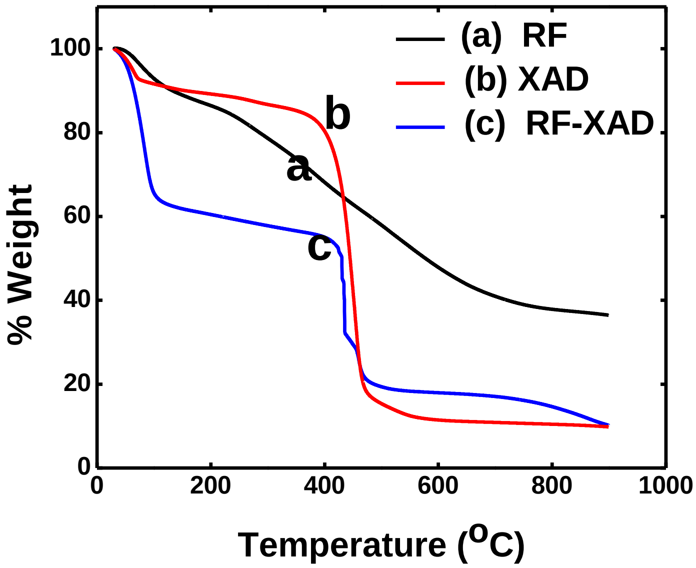

Fig. 3.15: TGA profiles of (a) granular RF gel, (b) XAD beads and (c) RF-XAD beads

The enhanced thermal stability of the composite beads can be attributed to the presence of RF, which is more thermally stable than XAD. In addition, the factors, such as the RF coating affecting the release of the gases from the XAD core, and the difference in the heat transfer behavior due to the new surface, may also be contributing, to some extent. The higher water content indicates hydrophilic and porous nature of the RF coating. These characteristics of the RF-XAD beads improve efficiency of Cs^+ ion sorption, from alkaline aqueous waste.

3.5.2.1.4 BET surface area

The specific surface area and the pore volume of the beads were determined by BET N_2 sorption method, as described earlier. The surface area was found to be 170 m^2/g, and the pore volume was found to be 0.19 cc/g. The pore radius was determined to be ~20 Å, confirming mesoporous nature of the synthesized beads. The surface area of the blank Amberlite XAD-4 beads, as per specifications, is 750 m^2/g, with an average pore diameter of 100 Å. The reduction in the surface area and the pore diameter of the template beads in the RF-XAD beads suggest the presence of the RF inside the pores also.

3.5.2.1.5 Ion-Exchange Capacity

The ion exchange capacity of the RF-XAD beads was determined by the method described in section 3.5.1.1.4. From the amount of NaOH consumed, the total H^+-Na^+ ion-exchange capacity was found to be 2.35 milliequivalents/g, i.e., 2.35 mmol/g of air-dried, H^+-form RF-XAD resin. The capacity of the template XAD-4 beads was also tested, using ^{134}Cs radiotracer, and it was confirmed that blank XAD-4 beads do no pick up cesium ions from aqueous solution.

3.5.2.2 Sorption studies

3.5.2.2.1 Effect of Na^+ ion concentration

The competitive effect of Na^+ ions on the sorption of Cs^+ ions onto the RF-XAD beads was investigated, by varying Na^+ ion concentration, at a constant Cs^+ ion concentration of 0.02 M, at 300 K. The solutions were prepared in aqueous 0.1 M NaOH, and the concentration of Na^+ ions was varied, using $NaNO_3$, as a source of Na^+ ions. The batch distribution coefficient (K_d) was calculated, using equation (3.13)

$$K_d = \frac{A_o - A}{A} \times \frac{V}{m} \tag{3.13}$$

where A_0 and A are the initial and the final activities, respectively, of the solution, V is the volume of equilibrating solution (10 ml), and m is the weight of the resin beads taken (0.1 g).

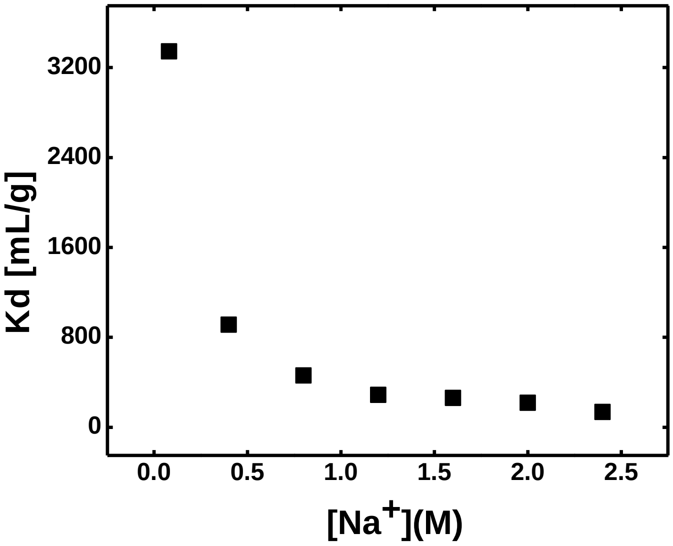

Fig. 3.16: Effect of the Na^+ ion concentration on the sorption of Cs^+ ions (at 0.02 M) onto the RF-XAD beads at 300 K

3.5.2.2.2 Effect of Cs^+ ion concentration

The sorption capacity of the RF-XAD beads for cesium ions was determined, by studying the sorption as a function of cesium ion concentration, at 300 K, in a batch experiment. The concentration of inactive cesium ions in the aqueous solution was increased from 0.1 to 250 mM, and the q_e was determined. It is observed that, q_e

increases gradually with increase in cesium ion concentration, and reaches a saturation value of ~1.5 mmol/g at 250 mM, as shown in Fig. 3.17. The initial concentration provides an important driving force, to overcome all the mass transfer resistances to the Cs^+ ions between the aqueous and the solid phases. Therefore, a higher initial Cs^+ ion concentration will enhance the sorption process. The observed results can be explained by the fact that, with increase in concentration, the incremental increase in cesium ion uptake by sorbent will be more initially, as a large number of active sites are available, but, with further increase in concentration it decreases, as the number of the available active sites decreases, and finally, it becomes zero.

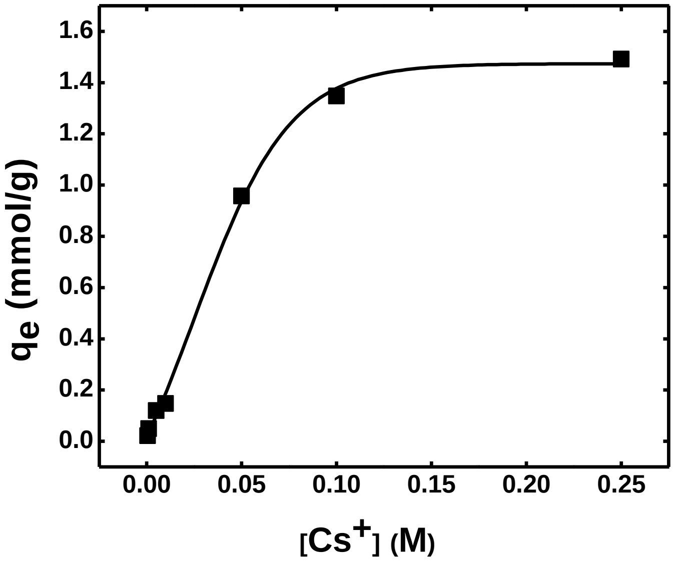

Fig. 3.17: Effect of the initial metal ion concentration on the sorption of Cs^+ ions onto the RF-XAD beads at 300 K

3.5.2.3 Sorption isotherms

To evaluate the nature of the sorption, the data were fitted to the Langmuir and the Freundlich isotherm models, equations (3.6) and (3.7), respectively. The plot of $1/q_e$ vs $1/C_e$ for sorption of cesium ions onto the RF-XAD beads is a straight line (Fig. 3.18).

The value of correlation coefficient R^2 is 0.9981, which indicates a good agreement between the experimental data and the Langmuir sorption model. The maximum sorbing capacity of the RF-XAD beads, for Cs^+ ions, is determined to be 2.17 mmol/g, i.e., 287 mg/g of the resin.[152] The sorption coefficient, K_L, which is related to apparent energy of sorption of Cs^+ ions onto the RF-XAD, is determined to be 0.66 L/mmol. The high sorption capacity of the synthesized beads can be attributed to the high surface area of the RF-XAD beads.

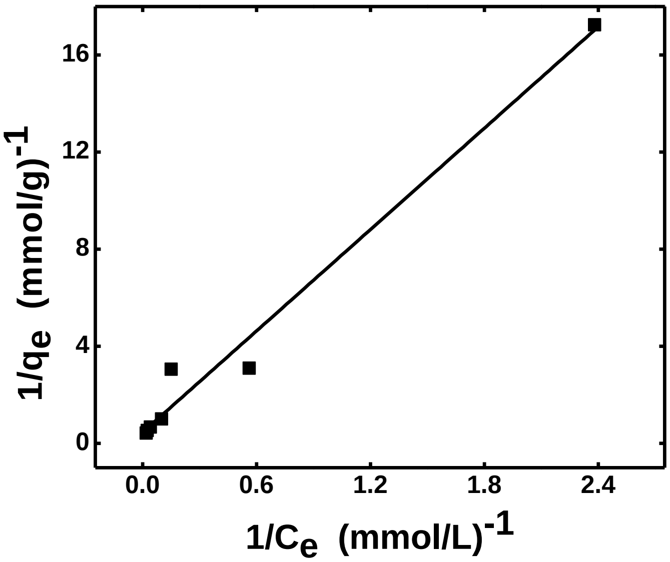

Fig. 3.18: Langmuir isotherm plot for sorption of Cs^+ ions onto the RF-XAD beads, at 300 K

The favorability of sorption of Cs^+ ions onto the RF-XAD beads can be expressed in terms of a dimensionless constant, (R_L), called separation factor, using the essential features of the Langmuir isotherm, as given below

$$R_L = \frac{1}{1+K_L C_o} \tag{3.14}$$

The calculated values of R_L are less than one (in the range of 0.94 to 0.15), indicating that the RF-XAD beads are good sorbent for Cs^+ ions, and the sorption process is favorable for efficient removal of Cs^+ ions from alkaline aqueous waste solutions.

The data were also analyzed, using the Freundlich isotherm, and from the slope and the intercept of log (q_e) vs log (C_e) straight line, the values of 1/n and K_F, respectively, were determined (Fig. 3.19). The correlation function value R^2 for this plot is 0.9302, which suggests that the correlation between the experimental data and the Freundlich isotherm model is not as good as that of the Langmuir sorption model. The different sorption parameters, obtained by fitting the experimental data to both the models, are given in Table 3.4.

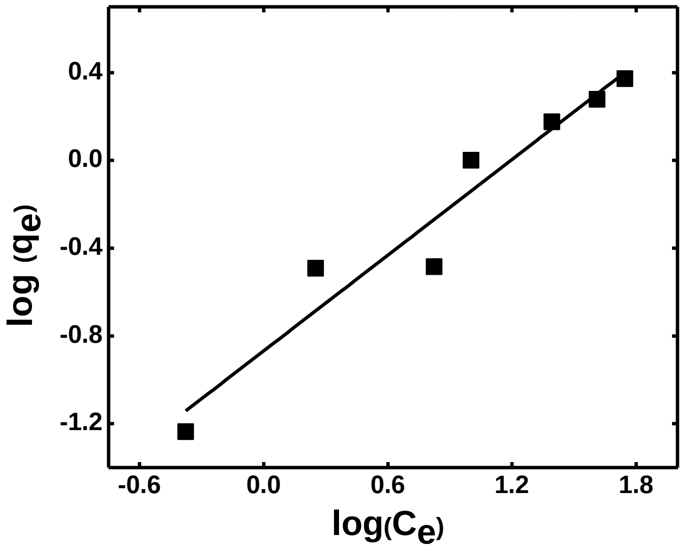

Fig. 3.19: Freundlich isotherm plot for the sorption of Cs^+ ions onto the RF-XAD beads at 300 K

Table 3.4: Langmuir and Freundlich isotherm parameters, for sorption of cesium ions onto the RF XAD beads

Isotherm model	Parameters	
Langmuir	q_m	2.17 mmol/g
	K_L	0.66 L /mmol.
	R^2	0.99815
Freundlich	K_F	136 mmol/g.
	n	1.38
	R^2	0.93023

3.5.2.4 Sorption kinetics

The kinetics of sorption describes the law governing the rate of the sorbate uptake by the sorbent, and this rate governs the equilibrium time. The kinetics of an sorbate uptake is required for selecting optimum operating conditions for the full-scale batch process. Therefore, the effect of equilibration time on the sorption of cesium ions, from aqueous solutions, was also studied. The sorption increases with increase in contact time (Fig. 3.20).

The uptake of Cs^+ ions is rapid in the initial 2 hours, and the equilibrium is reached in ~4 hours, indicating a quite fast sorption rate. The initial rapid sorption can be related to the abundant availability of the active sites in the initial stage. Later on, as both the availability of the sites and the concentration of the solute decrease, the process becomes relatively slower, and equilibrium conditions are reached in about 4 hours. At this point, the amount of the cesium ions being sorbed onto the sorbent is in dynamic equilibrium with the amount of the cesium ions desorbing from the sorbent. The time required to attain this equilibrium is termed as the equilibrium time, and the amount of cesium ions sorbed at the equilibrium time is the equilibrium sorption capacity of the sorbent under those operating conditions. As the equilibrium stage is attained in 4 hours, further batch experiments, for uptake determination, were carried out at 4 hours of equilibration time. The experimental q_e values, at the three studied concentrations of 100, 500 and 1000 μM, were found to be 6.7, 23.8 and 36.8 μmol/g, respectively.

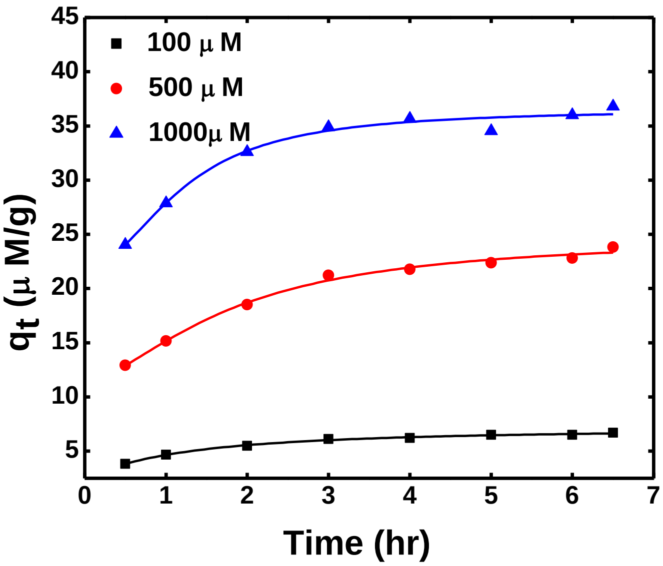

Fig. 3.20: The effect of equilibration time on the sorption of Cs^+ ions onto the RF-XAD beads, at three different initial concentrations

In order to investigate the sorption process of cesium ions onto the RF-XAD beads, three kinetic models, namely, pseudo-first-order (equation (3.8)), pseudo-second-order (equation (3.9)), and intraparticle diffusion models (equation (3.10)), were used. Fig. 3.21 depicts the pseudo first-order plots for the sorption of cesium ions onto the RF-XAD beads. The data were fitted, with correlation coefficient values in the range of 0.81 to 0.98, depending on the initial concentration, which indicates that the rate of sorption of cesium ions onto the RF-XAD beads cannot be explained by the pseudo first-order kinetic model, for the entire studied range of the initial cesium ion concentration. The q_e values obtained from this model, 3.33, 12.54 and 12.08 μmol/g, respectively, at the three studied initial concentrations of 100, 500 and 1000 μM, are significantly lower than the corresponding experimental q_e values of 6.7, 23.8 and 36.8 μmol/g. the results are listed in Table 3.5.

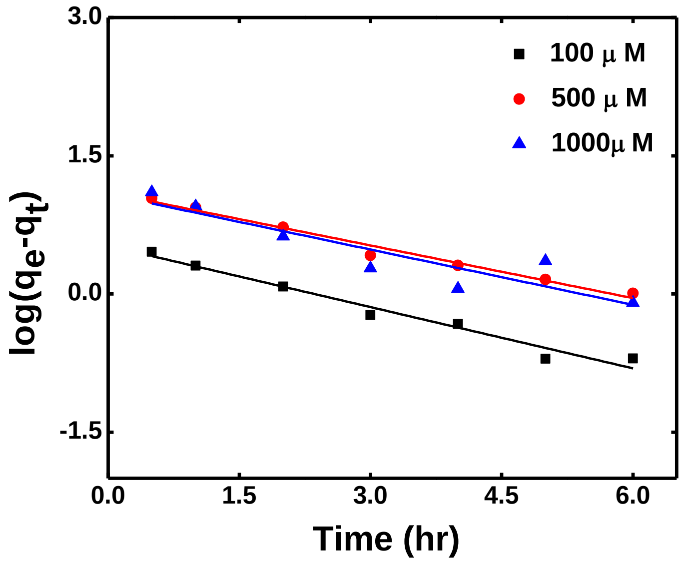

Fig. 3.21: Pseudo first-order plots for sorption of Cs^+ ions onto the RF-XAD beads, at three different initial Cs^+ ion concentrations.

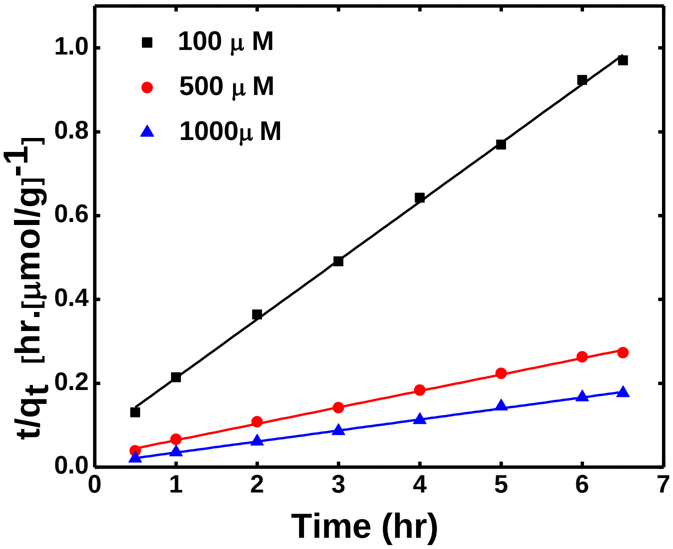

Fig. 3.22: Pseudo second-order plots for the Cs^+ ion sorption onto the RF-XAD beads at three different initial concentrations of Cs^+ ions

Pseudo second-order plots for the Cs^+ ion sorption are shown in Fig. 3.22. the parameters obtained from the plots are given in Table 3.5. It is clear that k_2 decreases with increase in the initial Cs^+ ion concentration. The values of R^2 for the pseudo second-order kinetic model are higher than that for the pseudo first-order kinetic model, for all the studied concentrations of cesium ions. And, the values of q_e calculated, using this model, are also in good agreement with the actual experimental values. Therefore, this model can be applied to the sorption process in the entire studied concentration range, and it can be concluded that the sorption process obeys pseudo second-order kinetics.[152]

3.5.2.5 Mechanism

The experimental data were further analyzed using the intraparticle diffusion model, equation (3.10). Fig. 3.23 shows that the plots of q_t vs $t^{1/2}$ are multilinear, and hence, intraparticle diffusion is also involved in the sorption process. The value of K_{id} is calculated from the slope of the second stage, and its value, for the studied system, is found to increase with increase in the initial concentration, from 100 to 1000 μmol /L. The boundary layer also increases with increase in the initial cesium ion concentration. In order to predict whether sorption proceeds via film diffusion or intraparticle diffusion mechanism, the kinetic data were further analyzed, using the solutions, equations (3.11 and 3.12), of the kinetic expression given by Boyd et al. On plotting the calculated values of Bt vs t, as per Boyd's equation, it is found that the fitted lines, for all the concentrations studied, do not pass through origin, indicating that the sorption process is mainly governed by the film diffusion (Fig. 3.24).

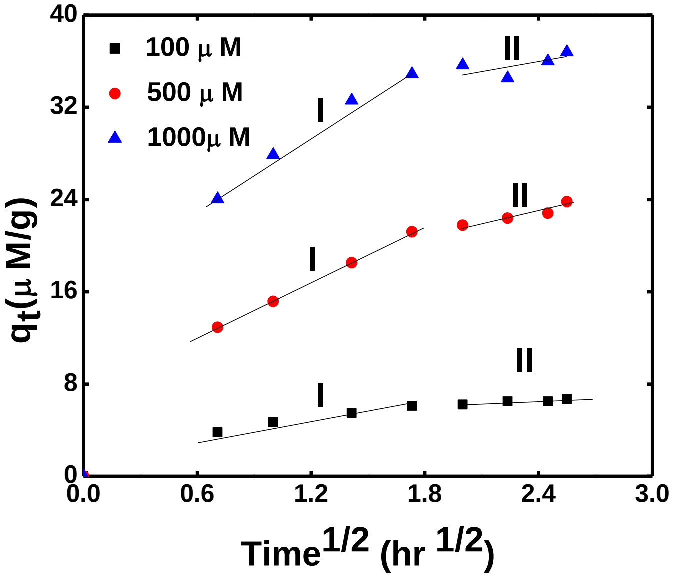

Fig. 3.23: Intraparticle diffusion plots for sorption of Cs^+ ions onto the RF-XAD beads at three different initial concentrations of Cs^+ ions

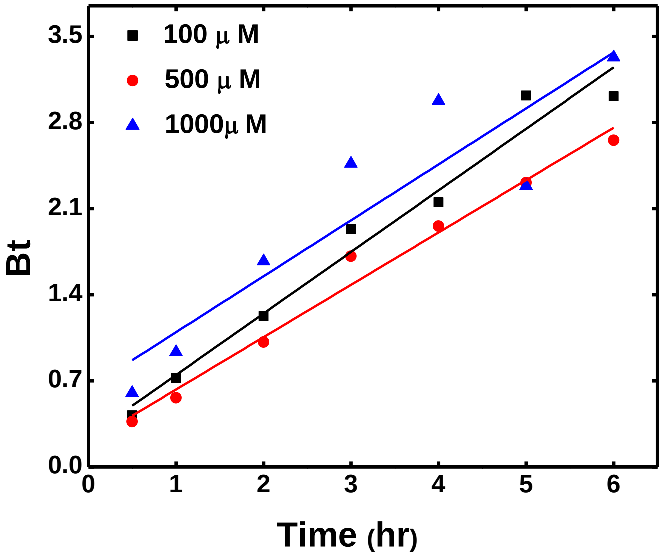

Fig. 3.24: Boyd's plots for sorption of Cs^+ ions onto the RF-XAD beads at three different initial concentrations of Cs^+ ions

Table 3.5: Kinetic parameters of the different models for the sorption of cesium ions onto the RF-XAD resin beads at different initial cesium ion concentrations

Kinetic model	**Parameters**	**C_o**		
		100 µM	**500 µM**	**1000 µM**
	$^{experimental}q_e$ (µmol /g)	6.7	23.8	36.8
Pseudo-1st order	k_1 (hr^{-1})	0.51	0.44	0.46
	q_e (µmol/g)	3.33	12.54	12.08
	R^2	0.9653	0.9777	0.8084
Pseudo-2nd order	k_2 (g μmol^{-1} hr^{-1})	0.27	0.06	0.08
	q_e (µmol /g)	7.14	25.55	38.05
	R^2	0.9989	0.9973	0.9982
Intraparticle diffusion	k_{id} (g μmol^{-1} $hr^{-1/2}$)	2.2	8.09	10.68
	I (µmol /g)	2.36	7.13	16.90
	R^2	0.9876	0.9995	0.9818

3.5.3 RF^A resin beads

3.5.3.1 Characterization

3.5.3.1.1 Optical microscope and SEM studies

Figs. 3.25(a) and (b) represent the optical microscope images of the alginate and RF^A beads, respectively, confirming the loading of RF on the pre-formed alginate beads. Fig. 3.25(c) shows the SEM image of the outer surface of the RF^A beads. On the surface itself, long connecting channel-like features are visible. These channels may provide better accessibility to the exchangeable sites, which will ultimately lead to better sorption properties.

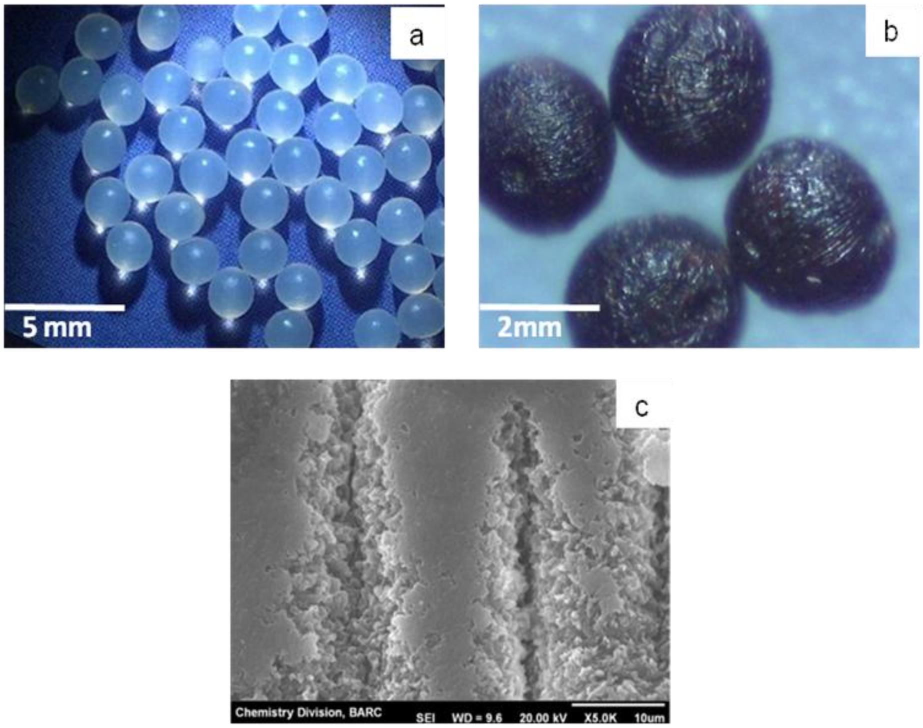

Fig. 3.25: Optical microscope images of (a) the alginate beads and (b) the RF^A beads at 60X magnification, and (c) SEM image of the outer surface of a RF^A bead

3.5.3.1.2 Mechanical strength testing

Mechanical strength of the synthesized RF^A beads was analyzed, employing universal testing machine, and it was observed that spherical RF^A beads showed first break at a load of 24-29 N, for the different samples tested. Thus, the mechanical strength of the RF^A beads is much better as compared to the ground gel particles currently in use, having first break at much lower load of 4-5 N, as mentioned earlier. From the mechanical strength studies, it can be concluded that the RF^A beads are more appropriate for column operation.

3.5.3.1.3 Thermogravimetric analysis

Thermo gravimetric analysis (TGA) of the synthesized beads was performed at a heating rate of 10 °C/min, in nitrogen atmosphere, from ambient conditions upto 700 °C. TGAs of the RF ground gel and the synthesized RF^A beads were carried out, using the prepared material as it is, without any pre-treatment, whereas that of the alginate beads was carried out, after just removing the surface water present on the swollen beads, using a filter paper. Fig. 3.26 shows typical TGA profiles of the alginate beads, RF ground gel and RF^A beads. The thermal degradation of the blank alginate beads occurs in two steps (Fig. 3.26, trace a). In the first step, (30 °C to110 °C), there is a weight loss of ~62 %, which is due to the loss of the absorbed water. Then, an additional weight loss of 3.7 %, due to thermal degradation of alginate, is observed in the temperature range 200-700°C. Fig. 3.26, trace b shows degradation of the RF ground gel. The thermal decomposition of RF ground gel does not have clear degradation steps, but only a gradual degradation profile. The weight loss (~9 %) observed upto 110 °C may be due to the absorbed water. Then, a continuous weight loss is observed till the highest temperature investigated. TGA profile of the RF^A beads (Fig. 3.26, trace c), too, has the same features as that of the RF ground gel, and does not show any well-defined degradation steps. After heating upto 110 °C, a weight loss of ~ 9 % is observed, which could be due to the absorbed water. The TGA profiles of the RF ground gel and the RF^A beads are overlapping till 200 °C, and after that, a slightly more %weight loss is observed for the RF^A beads, as compared to that for the RF ground gel in the temperature range of 200 to 473 °C. This could be due to the simultaneous decomposition of the remaining alginate, along with that of RF. But, at the end of 700°C, about 46% of the total weight is left as charred residue, in the case of RF, as compared to 41 %, in the case of RF ground gel. Similar nature of the TGA profiles of the RF ground gel particles and the synthesized RF^A beads indicates the presence of negligible amount of alginate in the synthesized beads.

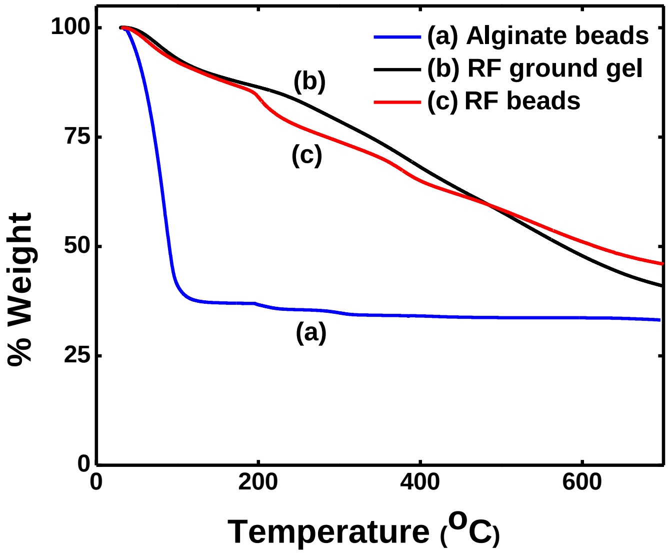

Fig. 3.26: TGA profiles of (a) alginate beads, (b) RF ground gel and (c) RF^A beads

3.5.3.1.4 Ion-exchange capacity and BET surface area

The total H^+-Na^+ ion-exchange capacity of the beads was determined to be 2.84 milliequivalents/g, i.e., 2.84 mmol/g of air-dried H^+ form of the RF^A resin. The specific surface area and the pore volume of the beads were determined by BET N_2 sorption method. The surface area was found to be 568.45 m^2/g, and the pore volume was found to be 0.19 cc/g. The observed high surface area of the synthesized beads supports the observations from SEM studies.

3.5.3.2 Sorption studies

3.5.3.2.1 Effect of Na^+ ion concentration

From Fig. 3.27, it is observed that, in the studied concentration range 0.1-3.0 M, q_e decreases abruptly with increase in the Na^+ ion concentration upto 1 M. After that, the q_e value remains almost unaffected upto 2.0 M Na^+ ion concentration. Thereafter, further decrease of q_e value to 46.47 mg/g is observed. These results indicates that the q_e value for cesium ion is affected by presence of Na^+ ion in the solution due to the competitive sorption of Na^+ ions onto the available exchange sites. The capacity of the RF^A beads, even at 3.0 M NaOH is enough to remove/extract cesium ions from aqueous solution.

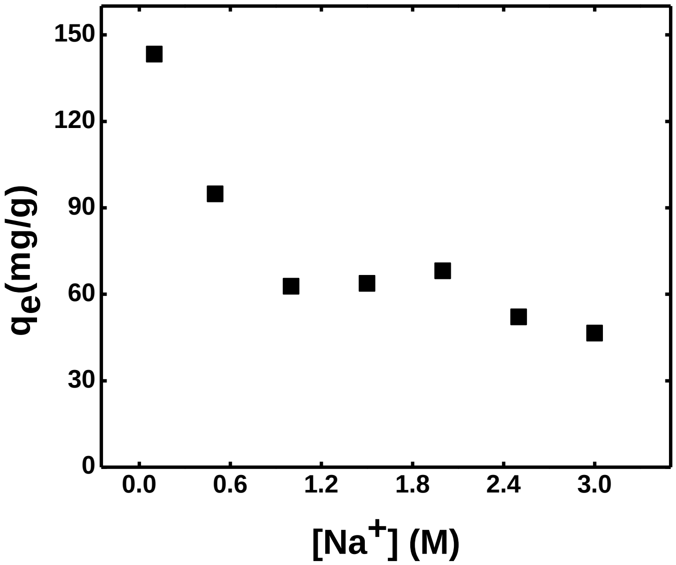

Fig. 3.27: Effect of the Na^+ ion concentration on the removal of cesium ions

3.5.3.2.2 Effect of cesium ion concentration

The sorption capacity of the RF^A beads for cesium ions was determined, by studying the sorption as a function of cesium ion concentration, at 300 K, in a batch experiment. The concentration of inactive cesium ions in the aqueous solution was increased from 5 to 400 mM, and the q_e was determined. It is observed that, initially, q_e increases almost linearly, with increase in Cs^+ ion concentration, because the available active sites on the sorbent are sufficient, and the amount of cesium ions sorbed depends on the number of cesium ions transported from bulk to the sorbent. But, with further increase in the cesium ion concentration, the number of available active sites decreases, and consequently, the incremental increase in q_e drops exhibiting deviation from linearity in the q_e vs C_o plot. An equilibration value of ~ 326 mg/g is obtained at 400 mM, as shown in Fig. 3.28. The initial concentration provides an important driving force, to overcome all the mass transfer resistances to the Cs^+ ions between the aqueous and the solid phases. Therefore, a higher initial Cs^+ ion concentration will enhance the sorption process.

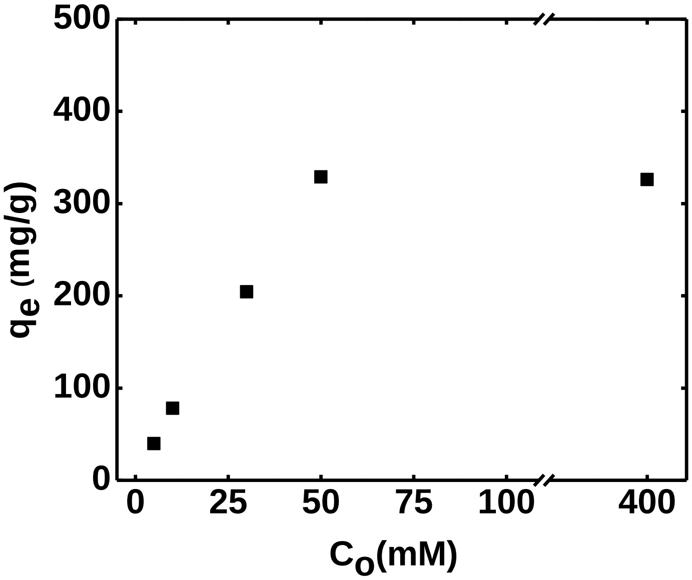

Fig. 3.28: Effect of the initial metal ion concentration on sorption of Cs^+ ions onto the RF^A beads at 300 K

3.5.3.3 Sorption isotherms

The sorption isotherm data were further analysed, using the Langmuir and the Freundlich isotherm models, equations (3.3) and (3.4), respectively. Figs. 3.29 (a) and (b) show the Freundlich and the Langmuir isotherm plots, respectively, along with the fitted straight lines. From these figures, it is observed that the equilibrium data fit to the Freundlich and Langmuir expressions, with a correlation coefficient values of 0.631 and 0.994, respectively. The higher correlation coefficient of 0.994 for the Langmuir isotherm shows that the sorption process conforms to the Langmuir isotherm, which predicts monolayer coverage of cesium ions onto the RF^A resin. Table 3.6 gives the results of the fitting of the sorption data to the Langmuir and the Freundlich isotherm models, after 4 hours of equilibration. Based on the Langmuir model, the maximum sorption capacity q_m (mg/g) of the RF^A beads for sorption of cesium is 490.2 mg/g.[153]

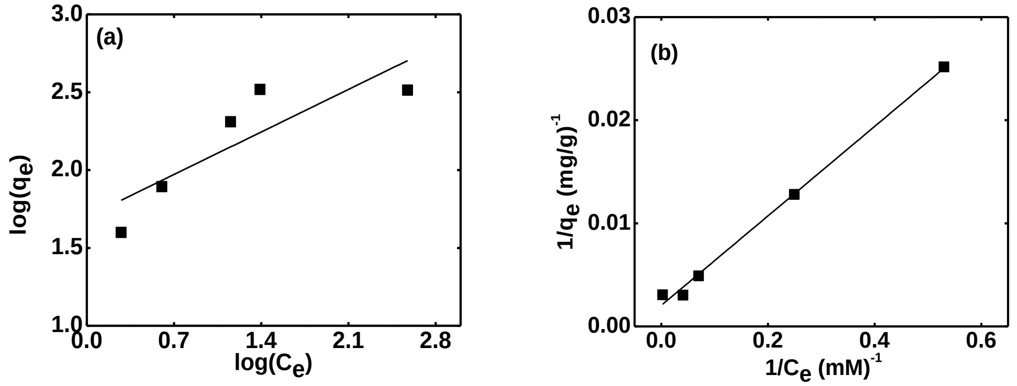

Fig. 3.29: (a) Freundlich and (b) Langmuir isotherm plots for sorption of Cs^+ ions onto the RF^A beads at 300 K

The predicted Langmuir isotherm equation, for sorption of cesium onto the RF^A at 300 K, useful for design calculations, is given by

$$\textbf{Langmuir: } q_e = \frac{23.04C_e}{1+0.047C_e} \tag{3.13}$$

Table 3.6: Sorption isotherm constants for sorption of cesium ions onto the RF^A beads

K_F (mmol/g)	1/n	$R^2_{(Freundlich)}$	K_L (L/mmol)	q_m	R^2 Langmuir
5.46	0.3902	0.631	0.047	490.2 mg/g	0.994

3.5.3.4 Sorption kinetics

Fig. 3.30 shows the effect of contact time on the removal of cesium ions at different initial cesium ion concentrations. It is observed that the % removal of cesium ions decreases with increase in the initial cesium ion concentration. For a contact time of 4 hours, the % cesium ion removal decreases from 87.7% to 15.4%, for an increase in the initial Cs^+ ion concentration from 0.5 to 5 mM. Also, from the figure, it is observed that, at all the studied initial cesium ion concentrations, the rate of removal of Cs^+ ions is very rapid for the initial period of about 90 min, and thereafter, the sorption rate decreases, and finally, becomes negligible after about 240 min. This is due to the combined effect of the decrease in flux (concentration gradient) with time due to transfer of the solute onto the solid phase, and availability of lesser vacant sorption sites.

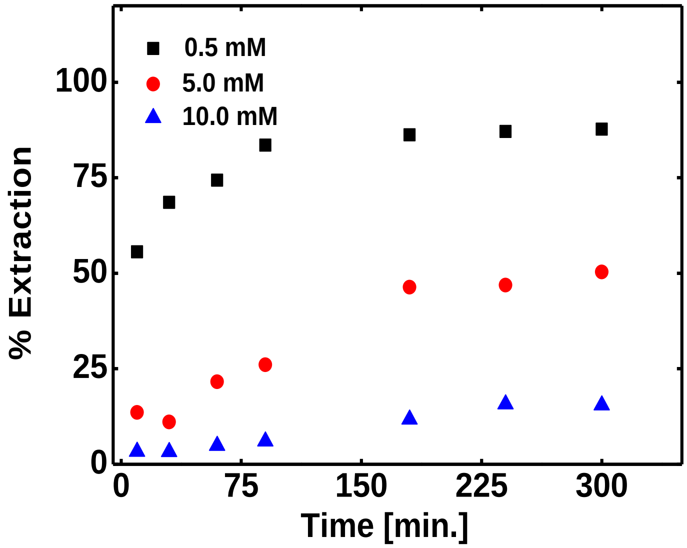

Fig. 3.30: The effect of equilibration time on the sorption of Cs^+ ions onto the RF^A beads at different initial Cs^+ ion concentrations

Fig. 3.31 shows the Lagergren pseudo first-order kinetic plots, equation (3.8), at two initial cesium ion concentrations of 0.5 and 5 mM. It is observed that Lagergren first-order kinetic model describes the sorption process well only for the first 90 min, at both the initial cesium ion concentrations, and thereafter, the sorption deviates from the model, more so, at the lower studied concentration. In other words, the sorption data are well represented by the model only in the region where rapid sorption takes place, i.e., for the first 90 min. Ho and McKay,[143] too, reported that the sorption data were represented well by the Lagergren first-order kinetic model only for the rapid initial time period. This confirms that it may not be appropriate to use only the Lagergren first-order kinetic model, to describe sorption of cesium ions onto the RF^A resins over the entire sorption period and at all the initial concentrations. The parameters and the coefficients obtained, by applying the pseudo first-order kinetic model to the experimental data, are given in Table 3.7.

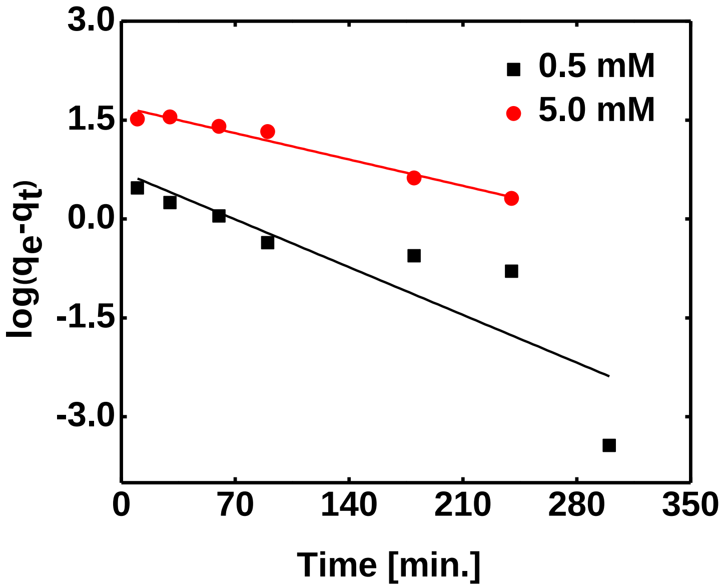

Fig. 3.31: Pseudo first-order kinetic plots for the sorption of Cs^+ ions onto the RF^A beads, at two different initial Cs^+ ion concentrations

Fig. 3.32 shows the pseudo second-order kinetic plots, equation (3.9), for the sorption of cesium ions onto the RF^A beads at the two different initial concentrations of cesium ions. The results show that, at lower initial cesium ion concentration, i.e., 0.5 mM, R_2^2 value is found to be higher than that for the pseudo first-order kinetic plot, whereas the R_2^2 value for the higher concentration (5 mM) is less than that for pseudo first-order kinetic plot. Moreover, the value of q_e calculated from the pseudo second-order plot is in agreement with the experimental q_e value of 7.93 mg/g at 0.5 mM initial cesium ion concentration. But, the q_e value calculated from the pseudo first-order plot is closer to that determined experimentally (45.3 mg/g) for 5 mM initial cesium ion concentration (Table 3.7). These observations suggest that the sorption process is explained best by pseudo second-order kinetics at the lower initial cesium ion concentration, whereas at the higher initial cesium ion concentration, pseudo first-order kinetics is followed.[153, 157]

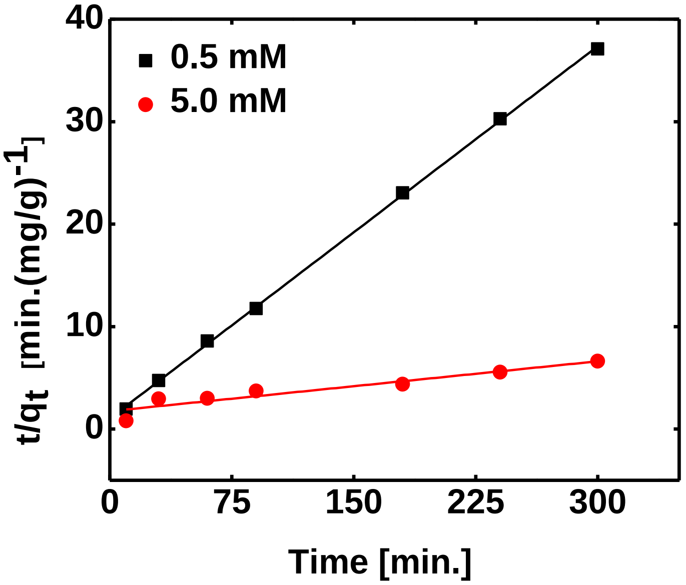

Fig. 3.32: Pseudo second-order kinetic plot for sorption of cesium ions onto the RF^A beads, at two different initial Cs$^+$ ion concentrations

3.5.3.5 Mechanism

The intraparticle diffusion plots for the sorption of cesium onto the RF^A beads, as given in Fig. 3.33, for the different initial concentrations of cesium ions, show multilinearity. The first linear portion is followed by a second linear portion, representing the different stages in the sorption, followed by the intraparticle diffusion of the cesium ions onto the RF^A beads. The intraparticle diffusion parameter, K_{id}, at the two studied initial concentrations, is determined from the slope of the corresponding second linear region of the Fig. 3.33, whereas the intercept of this second linear portion gives an idea about the boundary layer thickness. The calculated K_{id} and I values at different cesium ion concentrations are given in Table 3.7.

Table 3.7: Kinetic constants for the sorption of cesium ions onto the RF^A beads

C_o, (mM)	Pseudo first-order model			Pseudo second-order model			Intraparticle diffusion model	
	k_1, min^{-1}	R_1^2	$q_{e,cal}$ (mg/g)	k_2, g/(mg min)	R_2^2	$q_{e,cal}$ (mg/g)	K_{id}, mg/(g $min^{1/2}$)	I (mg/g)
0.5	0.024	0.7172	5.21	0.014	0.9996	8.23	0.032	7.44
5.0	0.013	0.9634	50.00	0.001	0.8807	61.65	4.392	13.01

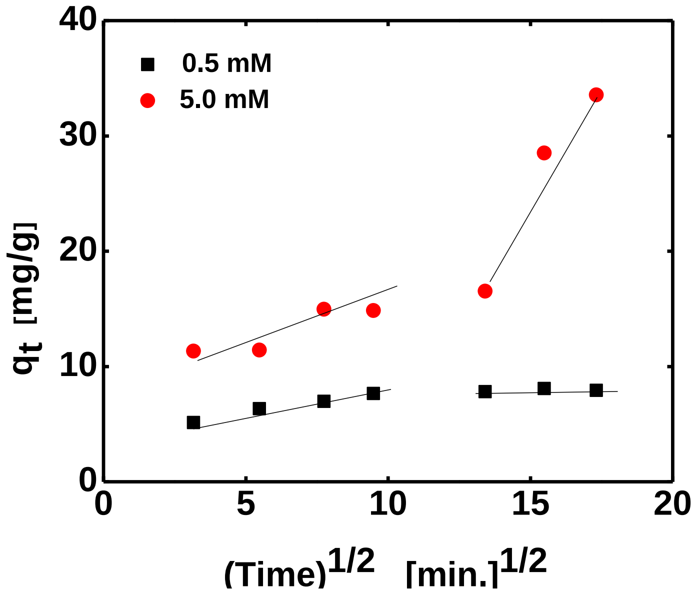

Fig. 3.33: Intraparticle diffusion plots for sorption of the Cs^+ ions onto the RF^A beads at two different initial Cs^+ ion concentrations

As can be seen from Fig. 3.33, the plots of q_t vs $t^{1/2}$, for both the concentrations, are neither straight line nor pass through origin. This indicates some degree of boundary layer control, and also that, the intraparticle diffusion is not the only rate-limiting step, but other kinetic processes also may govern the rate of sorption, all of which may be operating simultaneously. Therefore, in order to find what the actual rate-controlling step, involved in the cesium ion sorption process, is, the sorption data were further analyzed by the kinetic expression given by Boyd et al., the solutions of which are given by equations (3.11 and 3.12). The calculated values of Bt were plotted against time

(Fig. 3.34). In the present case, the plots are non linear, and do not pass through the origin, indicating that, the sorption process is of complex nature, consisting of both film diffusion and intraparticle diffusion steps, and film diffusion being mainly the rate-limiting process for the studied solute concentration range.

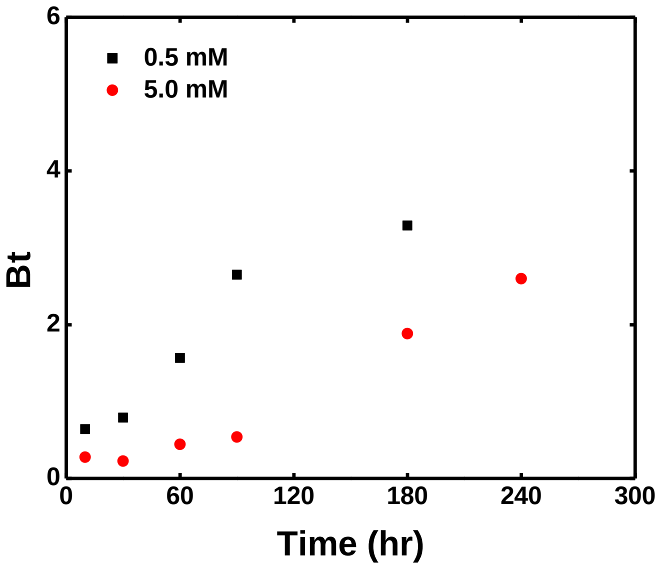

Fig. 3.34: Boyd's plots for the sorption of cesium ions onto the RF^A beads at two different initial cesium ion concentrations

3.5.3.6 Desorption studies

Desorption experiments of the sorbed cesium ions were carried out, using 0.5M HNO_3. First, 0.5 mM alkaline solution of cesium ions was equilibrated with the synthesized resin beads, for 4 hours, keeping V/m ratio same as in the other experiments. The sorbed cesium ions were then eluted, by equilibrating the resin with 5 ml of 0.5 M HNO_3 solution, and suitable aliquots of this solution were counted at different intervals of time. It was observed that, in ~ 10 min of elution time, 100% desorption of the sorbed cesium from the RF^A beads was achieved. This indicates that the beads can be regenerated, and complete recovery of the sorbed cesium is possible.

3.6 Comparison of the Resin Beads

Three different methods have been developed for the synthesis of RF resin directly in the spherical beads form. In the first method, spherical RF beads have been synthesized by suspension polymerization, using a suitable polymer solution, both as a suspension media and a protective polymer. In the other two methods, pre-formed beads of XAD-4 and calcium alginate were used as templates. The difference in the use of the two templates is that, in the case of alginate template, a negligible amount of alginate is retained in the final product, and the RF resin beads obtained are almost pure. From the TGA profile of the RF^A beads also, it is clear that the TGA profile of RF^A is almost similar to that of the RF particles, and hence, the effective presence of alginate in the final product is negligible. On the other hand, RF-XAD beads are actually composite beads, in which RF is present only on the surface, and in the pores of the XAD beads.

The surface area of the different resin beads increases in the order RF-XAD < RF< RF^A. During the synthesis of the RF-XAD beads, the RF pre-condensate penetrates in the pores inside, in addition to that on the surface of the template, and gets solidified on curing. This clogs the pores of XAD beads, and results in the drop of the surface area. While in the case of the alginate-assisted synthesis of the RF beads, the leaching of the alginate from the matrix during the synthesis generates connected pores, leading to high surface area. Probably, due to this high surface area, the cesium ion capacity of the RF^A is also the highest among the three types of the synthesized beads. The mechanical strength of all the resin beads is higher than that of the conventional RF granules. The sorption capacity of the RF^A is highest among all of the synthesized RF resins. Kinetics of sorption is fast, in the case of all the three resin beads, and follows pseudo second-order kinetics. Only RF^A beads are observed to follow pseudo first-order kinetics at higher cesium ion concentration. The mechanism of the sorption of cesium ions onto these beads is complex, and involves both film diffusion and intraparticle diffusion, with the former as the rate determining step.

3.7 Conclusions

The results described in the present studies show that the RF resin beads can be synthesized directly into spherical form, with good control over the size, by varying the various synthesis parameters, using three different methods. The methods of synthesis described here are new, novel and simple, and do not require any intricate machinery. The beads can be made free of unwanted contaminants by easy washing. The mechanical strength, water content and the surface area of the beads are quite high. The cesium ion sorption capacity of the beads is also very high, and even in the presence of high sodium ion concentration, all the resin beads showed good sorption capacity. The q_e values for RF resin, RF-XAD and RF^A resin beads are 238 mg/g, 287 mg/g and 326 mg/g, respectively. Kinetics of the sorption of cesium onto these beads is quite fast, and almost completes in ~4 hours, depending on the system and the initial cesium ion concentration. Analysis of mechanistic steps, involved in the sorption process, confirms that the sorption process involves multiple steps, including film diffusion and intraparticle diffusion, with the film diffusion as the rate governing step. The results from the different sorption studies suggest that these synthesized sorbent beads have good potential for sorption of cesium ions from alkaline waste, and can be used in both batch and column modes.

Chapter-4

Copperhexacyanoferrate-Composite Beads

4.1 Introduction

With growing interest in nuclear power and the development of nuclear science and technology, an enormous amount of nuclear waste is being produced worldwide. These radioactive contaminants threaten the human environment seriously.[158-160] Among all the fission products, ^{137}Cs is one of the most critical radionuclide, as this radionuclide has a long half-life, and is a biological hazard.[24, 161-162] Many sorbents have been developed over the years, to remove cesium from the nuclear waste. Most of the commercialized sorbents are organic resins, having their own limitations, such as poor thermal and radiation stability and mechanical strength. On the other hand, inorganic sorbents have better thermal, chemical, mechanical and radiation stability, and, moreover, after their effective use, these can be solidified, before the ultimate disposal. But, because of their fine morphology, or gel-like nature, these create excessive pressure drop across the fix bed and low hydraulic conductivity, and hence, cannot be used as such in any flow-through system.[163] The above limitations of the inorganic sorbents can be overcome, by introducing composite resins, consisting of inorganic sorbents and organic binding matrices. In literature, a considerable number of reports are available on the use of synthetic inorganic sorbents, which have a strong affinity for one or more radionuclides over a wide pH range. The major classes of the inorganic ion exchange materials include aluminosilicates,[164] phosphates,[165] ferrocyanides and hydrous oxides of multivalent cations.[166-168] Among these, transition metal hexacyanoferrates are well known, for their high affinity towards cesium over a wide range of pH.[169-173] These inorganic sorbents can be used for removal of cesium from the waste streams in three different modes, (1) as co-precipitating agents, (2) slurry and (3) dry powder or granular form. The first two mods of usage have associated disadvantages, such as generation of radioactive colloidal sludge. Therefore, their use as exchangers is preferred over that as co-precipitating agents. These metal hexacyanoferrates are synthesized in granular form of irregular size, but their efficiency in the column operation decreases due to their poor mechanical properties. During column operations, these granules wear out, which leads to clogging of the bed.[174]

Transition metal ferrocyanides are usually prepared in the form of colloids, by reacting soluble ferrocyanide, $K_4Fe(CN)_6$, with the divalent transition metal salts, such as $CuSO_4$, $Co(NO_3)_2$, etc. This reaction can be represented as

$$\mathrm{Fe(CN)_6^{4-} + 2M^{2+} + xH_2O \rightarrow M_2Fe(CN)_6xH_2O} \qquad (4.1)$$

where M stands for the divalent elements.

The properties and chemical composition of the prepared metal hexacyanoferrate depend on the synthesis procedure, the ratio and the nature of the salts used, and the after-treatment given to the precipitates. Depending on these synthesis variables, different products are obtained. Therefore, the general formula of the metal hexacyanoferrates can be represented as $A_{2n}M_{2-n}Fe(CN)_6.xH_2O$, in which A stands for Na^+ or K^+, and *n* indicates one of the numbers, 0,1, or 2.[175] The precipitates obtained have poor mechanical stability, which makes these unsuitable for column usage. In order to improve their mechanical strength, the researchers have tried, various support materials. Milonjic et al. synthesized copper hexacyanoferrate/polymer/silica composites beads, after coating silica beads with a polymer binder, and studied the uptake of cesium ions from aqueous solution.[176] They have reported a sorption capacity of 0.15 mmol/g of the synthesized sorbent. Koichi prepared copper hexacyanoferrate/amberlite XAD-7 composite ion exchanger, using trioctylalkylammonium chloride as a mediating agent, for separation of cesium from waste solutions.[177] Nilchi et al. used polyacrylonitrile (PAN) as a matrix material for CuHCF ion exchanger, in order to separate cesium from liquid wastes.[178] Huang et al. used vermiculite as a support material for CuHCF.[175] Wang and co workers reported loading of potassium copperhexacyanoferrate (KCuHCF) particulates on the porous matrix of granular coconut-shell activated carbon, by repeated precipitation reaction of $CuSO_4$ with K_4 [Fe $(CN)_6$].[179] Most of these composites make use of some inert supports, which increases the required volume of the resin, as the content of the loaded active material is quite less. Moreover, there are chances that the deposited sorbent material may wear off from its support, after repeated use. Considering these facts, we have developed two new methods of synthesis of CuHCF-polymer and KCuHCF-polymer composites, by using two different approaches. These composites were used to synthesize directly spherical composite beads of different sizes. The potential of the developed materials for removal of cesium was evaluated radioanalytically. The data obtained were fitted to different sorption and kinetics models, to get better understanding of the sorption process.

- In the first method, polyether sulfone (PES) was used as a binding matrix for the pre-formed dry CuHCF powder, and the beads of CuHCF-loaded PES were synthesized by phase inversion technique. PES was chosen as the binding matrix because of its high radiation and chemical stability.

- In the second method, KCuHCF was prepared in the form of a slurry in the presence of PVA as a stabilizing polymer. This slurry was further mixed with sodium alginate solution, from which the KCuHCF-Gel beads were finally prepared.

The aim of the study is to explore the use of unconventional and novel polymeric materials as a binder, or a support, to improve the mechanical strength and column hydraulics of the copper hexacyanoferrate powders. The synthesized sorbent beads were characterized by X-ray diffraction (XRD), energy dispersive x-ray analysis (EDAX), thermo gravimetric analysis (TGA), scanning electron microscopy (SEM) and BET surface area analysis. The efficiency of the beads, for the sorption of cesium ions, was investigated radioanalytically, using ^{134}Cs and ^{137}Cs as radiotracers. The effect of pH, contact time and the initial cesium ion concentration on the sorption kinetics and sorption equilibrium was also studied. Further, the data were analyzed, using different kinetic and sorption isotherm models.

4.2 Materials

Polyethersulfone (PES) (Gafone PES 3200P) was procured from Gharda Chemicals Limited, India. Sodium alginate and poly vinyl alcohol (Molecular weight 1,25,000) were purchased from SD Fine Chemicals, India. Cesium nitrate, potassium hexacyanoferrate (KHCF), copper sulphate, and N, N- methyl pyrrolidone (NMP), and glutaraldehyde (AR grade) were obtained from Merck. All the solvents and the chemicals used were of analytical grade. Water obtained from Millipore-Q water purification system, with conductivity < 0.3 µS/cm, was used in all the experiments. ^{134}Cs and ^{137}Cs radiotracers were procured from the Board of Radiation and Isotope Technology (BRIT), Mumbai, India.

4.3 Synthesis

4.3.1 Synthesis of CuHCF-PES composite beads

Copper hexacyanoferrate powder was prepared by reacting solution of copper sulphate (10 wt %) with potassium hexacyanoferrate (10 wt %), in the presence of PVA stabilizer (6 wt %), in aqueous medium. The copper sulphate solution was added drop wise to the potassium hexacyanoferrate solution, with continuous stirring. Brown-coloured precipitate of copper hexacyanoferrate started to appear, on mixing the two solutions. PVA acts as a stabilizer in controlling the particle size of the CuHCF precipitate. The effect of PVA concentration on the particle size of the CuHCF precipitate was studied by particle size analyzer. It was observed that, in the absence of PVA, the average size of the synthesized CuHCF was ~ 450 nm, and by varying PVA concentration, from 0 to 10 wt %, the size of CuHCF particles varied from 450 to 145 nm. The precipitate was separated from the mother liquor by ultracentrifugation, and washed off with water several times, to remove PVA and the leftover reactants. This precipitate was air-dried, to obtain a freely flowing fine brown powder. This powder was used to prepare sorbent–polymer composite beads. The synthesized CuHCF powder was dispersed in PES/NMP solution, to form homogenous slurry of appropriate viscosity. The polymeric composite beads, containing CuHCF, were produced by controlled precipitation of PES, present in the slurry, in the form of drops of required size, in a suitable aqueous bath. The blank PES beads were synthesized by the similar method, without adding the CuHCF powder in the polymer solution. The beads were allowed to cure for ~ 10 hours in the aqueous bath, before washing with water. The synthesized sorbent beads were used, in the swollen state, for TGA and sorption experiments, whereas IR, SEM, EDXRF and BET surface area studies were carried out, after air-drying the composite beads.

4.3.2 Synthesis of KCuHCF-Gel beads

A strong three-dimensional network of interpenetrating hydrogel of the cross-linked alginate and PVA can be formed by making use of calcium chloride and glutaraldehyde as specific cross-linkers in step-wise manner. This approach has been used here in synthesizing composite beads of KCuHCF, using sodium alginate and PVA together as a binding matrix. KCuHCF was prepared by the reaction of KHCF and $CuSO_4$ in 2:1 molar ratio, in the presence of PVA solution (5 weight %), to control the size of KCuHCF precipitates. To this brown-coloured KCuHCF sol, aqueous solution of sodium alginate was added, such that the final ratio of the weight % of PVA to that of sodium alginate became 2.5:1. This solution was used to prepare KCuHCF containing polymer composite beads, by dropping it into an aqueous bath, containing 4 weight % $CaCl_2$ aqueous solution, through a 0.8 mm diameter needle, using a syringe with a pump. Thus formed beads were kept in the same $CaCl_2$ solution for ~3 hours, for complete conversion of sodium alginate to calcium alginate. Then, the beads were separated from the solution, and washed with water. These beads were further equilibrated with aqueous solution, containing 0.01M HCl and 0.02% glutaraldehyde, for 3 hours, to bring about cross-linking of the PVA present in the beads. The cross-linked beads were washed with excess water, to remove the leftover reactants. The blank alginate-PVA cross-linked gel beads were synthesized in the similar manner, without adding KCuHCF sol. The synthesized sorbent beads were used, in the swollen state, for TGA and sorption experiments, whereas IR, SEM, EDXRF and BET surface area studies were carried out with air-dried composite beads.

The effect of the presence of PVA in controlling the size of KCuHCF particles during its formation, was studied, by varying the concentration of PVA (0-10 wt%), and keeping the concentrations of KHCF and $CuSO_4$ constant. It was observed that, in the presence of PVA, there was no significant change in the rate of reaction of the KHCF with $CuSO_4$. The reaction between the two precursors occurred instantly, resulting in the formation of brown-coloured KCuHCF precipitate, irrespective of the concentration of the PVA in the reaction mixture. However, there was a significant variation in the size of the precipitates formed in the presence of PVA. Fig. 4.1 depicts the plot of the average diameter, measured by the particle size analyzer, vs. the PVA concentration. From this plot, it is clear that the size of the KCuHCF particles can be effectively controlled by introducing PVA in the reaction mixture. No significant change in the size of KCuHCF particles was observed in the presence of PVA concentration above 3%. Hence, the precipitation of KCuHCF sorbent, for the synthesis of composite beads, was carried out in the presence of 5% PVA.

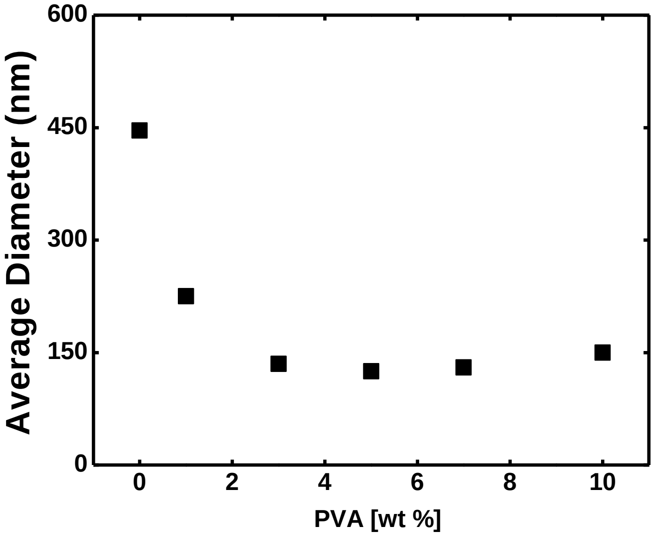

Fig. 4.1: Effect of PVA concentration on the size of KCuHCF particles

4.4 Sorption studies

The radiotracer solutions of ^{134}Cs and ^{137}Cs were further diluted to the required concentrations, as and when required. The batch capacities of the resin beads were determined, by shaking 0.05 g of the sorbent beads with 5 mL of $CsNO_3$ solution of appropriate concentration, containing cesium radiotracer. The solution was stirred continuously, using a mechanical shaker, for 4 hours, in the case of CuHCF-PES beads, and, for 2 hours, in the case of KCuHCF-Gel beads, which were found to be sufficient for attaining respective equilibria. However, for kinetic studies, the samples were equilibrated for different time intervals. After the equilibration, a small portion of the aqueous phase was separated, and taken for counting gamma activity. The gamma activity measurements were carried out in a well-type NaI (T1) [ECIL] detector, connected to a single-channel analyzer.

Equilibrium sorption capacity, $q_{e,}$ was calculated, using the following equation

$$q_e = \frac{(C_o - C_e)V}{m} \qquad (4.2)$$

where C_o is initial cesium ion concentration, C_e is equilibrium cesium ion concentration, V is the volume of the aqueous solution and m is the weight of the sorbent.

4.5 Results and Discussion

4.5.1 CuHCF-PES composite beads

4.5.1.1 Characterization

The synthesized composite beads of copper hexacyanoferrate-polymer were characterized, using various techniques.

4.5.1.1.1 Thermogravimetric analysis

Thermo gravimetric analysis (TGA) of the synthesized beads was performed, at a heating rate of 10 °C/min, in nitrogen atmosphere, from ambient conditions up to 750 °C. Fig. 4.2 shows typical TGA profiles of the CuHCF powder, the blank PES beads and CuHCF-PES beads. The TGA profile of CuHCF powder (Fig. 4.2(a)) can be divided into three main stages. The first stage is from 30 to 148 °C, over which a mass loss of about 33% is observed due to dehydration.[180] The second stage, from 148 to 200 °C, experiences an additional mass decrease of about 8%, due to loss of the last traces of water. In the temperature range 200-750 °C, additional weight loss of ~24%, due to degradation of CuHCF, is observed. The residual mass of 35% is left, after 750 ºC. Fig. 4.2(b) shows the TGA profile of the water-swollen blank PES beads. This profile consists of two steps. The first step, from 30 ºC to 143 ºC, corresponds to 84% decrease in the weight due to water loss. The degradation of PES starts at 522 ºC, whereas no change is seen in the weight after 625ºC, and 7% residual charred mass is obtained at the end of the sample run. Fig. 4.2(c) depicts the thermal degradation profile of CuHCF-PES beads, which is similar to that of the blank PES beads, but the onset and the completion of decomposition of PES have shifted from 522 to 490 ºC, and from 625 to 593 ºC, respectively. The observed shift in the onset, and the completion of decomposition of PES in the CuHCF-PES beads could be due to the presence and simultaneous degradation of copper hexacyanoferrate, along with that of the PES. The water content of the beads was determined, by heating the beads isothermally, for 3 hours, under N_2 flow of 50 ml/min, at 130 ºC, and the change in the weight was determined. The results are summarized in Table 4.1. These values of water content match very well with those determined from the corresponding TGA profiles.

Table 4.1: Feed loading of the sorbent and water content of the synthesized CuHCF-PES beads

Beads	Feed loading of the sorbent	Water content
CuHCF-PES	28.57 %	78.20%
Blank PES	00.00%	83.55%

The observed high water content in the synthesized beads indicates that a large volume of the beads is occupied by water, i.e, the beads are highly porous, and the loaded

CuHCF sorbent is easily available for exchange throughout the swollen beads. As synthesis of the composite beads was carried out, using a feed mixture, containing 28.6 weight percentage of CuHCF with respect to the polymer taken, the expected loading of CuHCF in the dry beads is 28.6 weight percentage, or lower. However, the estimation of the CuHCF loading in the synthesized beads could not be carried out from these TGA results, because of overlapping of the thermal degradation profiles of the polymer and CuHCF powder.

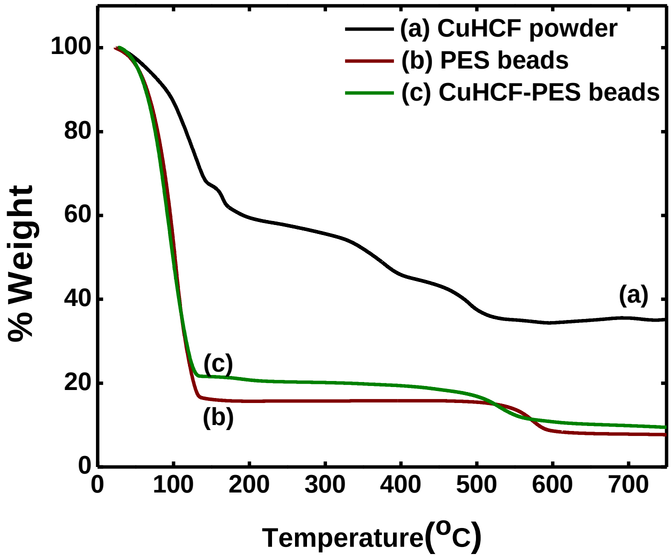

Fig. 4.2: TGA profiles of (a) CuHCF powder, (b) PS beads and (c) CuHCF-PES beads

4.5.1.1.2 XRD and IR studies

The crystal structure of the synthesized CuHCF was confirmed by XRD analysis (Fig. 4.3). The XRD pattern of the synthesized CuHCF matches well with that previously reported,[181] and indicates the crystalline nature of the synthesized sorbent.

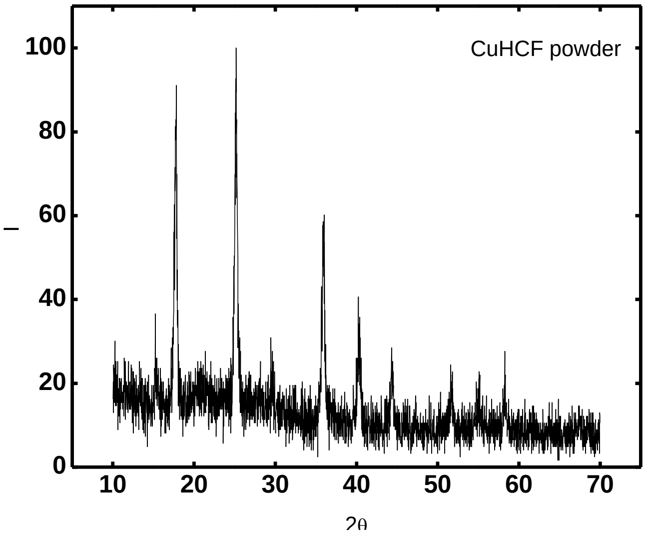

Fig. 4.3: XRD pattern of the synthesized CuHCF powder

Fig. 4.4(a) represents IR spectrum of CuHCF dry powder. The most relevant and characteristic bands in the sample are at 595 cm^{-1} (medium), 3400-3600 cm^{-1} (broad) and 2090 cm^{-1} (strong). The last one corresponds to Fe(II)-CN stretch.[181] The low-intensity peak at 1610 cm^{-1} could be due to the lattice water. Figs. 4.4(b) and 4.3(c) represent IR spectra of the blank PS beads and the CuHCF-PES beads, respectively. The strong peak at 2090 cm^{-1}, due to Fe-CN stretch, though present, is diminished in Fig. 4.4(c). This is due to less loading of CuHCF powder in comparison to PES matrix. There is also a shift of about 2 cm^{-1} in the peaks due to the presence of SO_2 stretching of the sulfone groups and aromatic -C-O-C ether stretching. These shifts could be due to the interaction of CuHCF with PES.

The presence of CuHCF in the beads was further confirmed by Energy dispersive X-ray fluorescence technique (EDXRF) using EDXRF, Jordan Valley (EX3600M). (Fig. 4.5). Energy dispersive X-ray fluorescence spectrum of CuHCF-loaded polyethersulfone beads shows peaks corresponding to copper and iron present in the composite beads (Fig. 4.5). The peak due to sulfur arises from the sulfur present in the polymer binding matrix, i.e., polyethersulfone. Rhodium peak is originates from the rhodium target used. This study indicates that the CuHCF powder is successfully loaded into the polymer matrix.

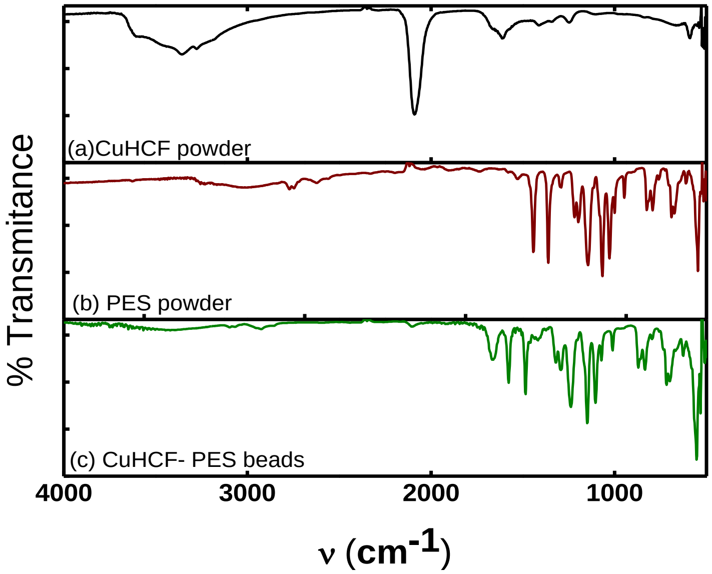

Fig. 4.4: IR spectra of (a) CuHCF powder, (b) PES powder and (c) CuHCF-PES beads

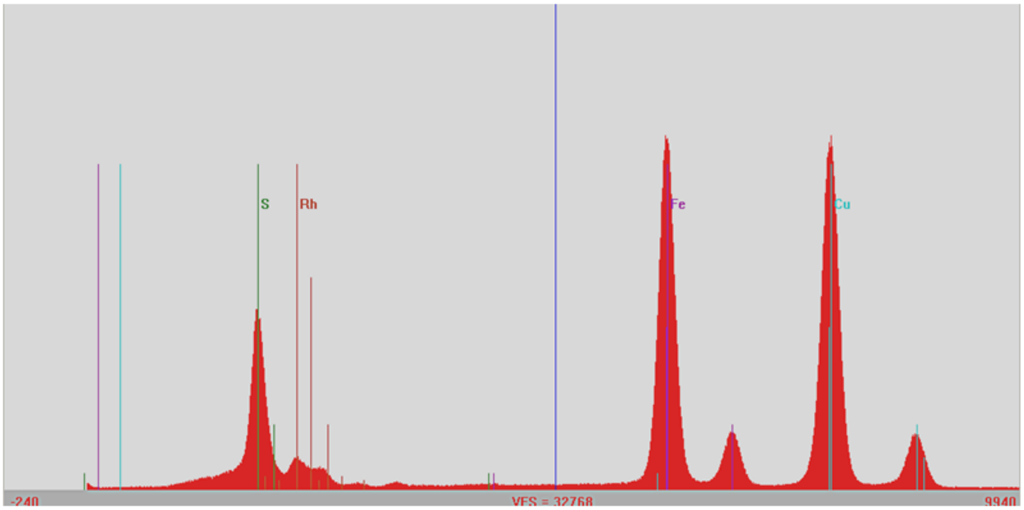

Fig. 4.5: EDXRF spectrum of CuHCF-PES beads

4.5.1.1.3 BET surface area

The specific surface area and the pore volume of the beads were determined by BET N_2 adsorption method. The surface area was found to be 479 m^2/g, and the pore volume was found to be 1.767 cc/g. The surface area and the pore volume measured are for the dried beads, but the actual sorption experiments are carried out, using the swollen beads. Therefore, the effective surface area and the pore volume of the swollen beads are expected to be still higher. This high value of the surface area could be due to the porous nature of the binding polymer. During the synthesis of the beads by phase inversion, the solvent (NMP) is exchanged by the water in the aqueous bath, and precipitation of the PES polymer starts. This process is very fast at the surface of the droplets, but as the polymer at the surface of the beads starts precipitating, the rate of exchange of NMP from inside the bead with water starts slowing down. The extractant, i.e., CuHCF particles remains embedded in the polymer matrix, whereas the slow exchange of the solvent (NMP) with water generates porosity in the beads. The higher surface area value is indicative of the higher number of the available active sites, which will increase efficiency of the sorption process.

4.5.1.1.4 Optical microscopy and SEM studies

Fig. 4.6 presents the optical microscope and SEM images of the synthesized CuHCF-PES beads. From these images, it can be inferred that the synthesized beads are spherical in shape, and have almost monodisperse size. The outer surface of these beads is quite porous, as depicted by Fig. 4.6(c). The porous nature of the beads is a desirable feature, as it will lead to better sorption properties.

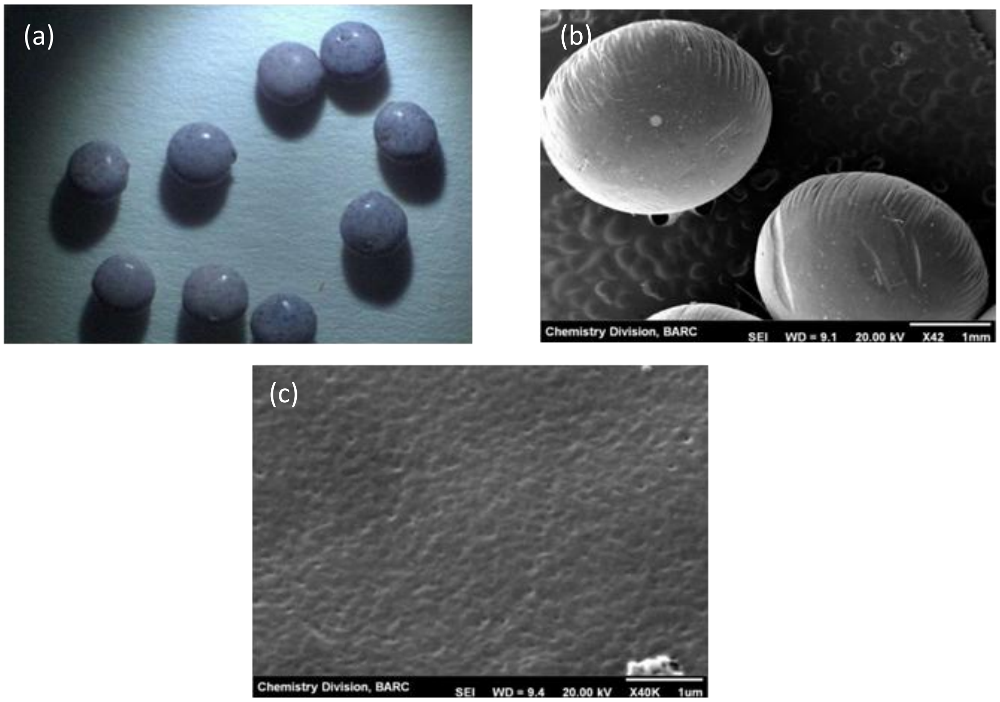

Fig. 4.6: (a) Optical microscope and (b) SEM images of the CuHCF-PES beads, and (c) SEM image of the surface of a bead

4.5.1.2 Sorption studies

The removal of cesium ions, using copper hexacyanoferrate sorbent, proceeds by two mechanisms, involving (a) incorporation of cesium and nitrate ions into the CuHCF matrix, and (b) exchange of the cesium ions with copper ions. Among these two, the sorption of cesium and nitrate ion-pair is the predominant mechanism, which is a complex process, and includes at least two steps, namely, (i) diffusion of Cs^+ and NO_3^- ion-pairs into the solid, and (ii) formation of a new phase. Loos-Neskovic and co-workers proposed that copper occupies two different types of sites in copper hexacyanoferrate, one of the Cu(II) ions is in the position linked to Fe(II) through CN groups, and the other Cu(II) ion, not linked to the CN groups, partially occupies the interstitial position, which seems to play a favorable role in the sorption.[94] The ion-pairs, Cs^+ and NO_3^-, are probably hosted in the vacancies of the structure, replacing the water molecules. The diffusion of the ion-pairs is the main process, which occurs during the initial stages (< 72 hours) of the contact, whereas destruction of the old crystal structure, and formation of a new phase is a very slow process, and takes place only after several months of contact with cesium solution.[94] True ion exchange is also one of the processes taking place in the sorption system, but it plays very minor role. To get a further insight into the sorption system, the sorption of cesium ions onto the synthesized beads was studied in detail, in the present work, and sorption and kinetic data were analyzed, using various models. Batch experiments were carried out, to investigate the effect of pH, Cs^+ ion concentration and equilibration time, using $CsNO_3$ salt as a source of cesium ions, and ^{134}Cs as a radiotracer.

4.5.1.2.1 Effect of pH

pH is one of the important factors in controlling the sorption of metal ions on a sorbent. The sorption of Cs^+ ions from aqueous solution of 25 mg/L concentration onto the CuHCF-PES composite beads was studied in the pH range 1.8-12.2. The results, as depicted in Fig. 4.7, reveal that the amount of cesium ions sorbed per unit mass of the sorbent at equilibrium (q_e) increases with increase in pH till pH 9, and then, it decreases. The observed findings can be explained on the basis of the fact that, both at low pH (< 2), and at high pH (>10), the decomposition of the CuHCF sorbent takes place.[182] This is the main reason for the observed lower Cs^+ ions uptake at pH 12. From these studies, it can be concluded that these beads work best for the removal of cesium ions in the pH range 5-9.

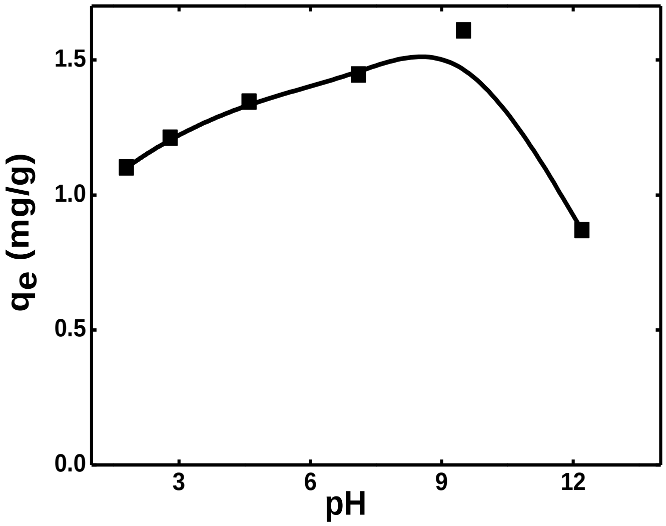

Fig. 4.7: The effect of pH on the sorption of Cs^+ ions onto CuHCF-PES beads

4.5.1.2.2 Effect of Cs^+ ion concentration

The sorption capacity of the CuHCF-PES beads for cesium ions was determined, by studying sorption, as a function of cesium ion concentration, at 27 ºC in batch experiment mode. It is observed that, q_e, the amount of Cs^+ ions sorbed per unit mass of the sorbent, in mg/g, increases, with increase in the concentration of Cs^+ ions, as shown in Fig. 4.7 (a). However, the percentage sorption decreases, with increase in the concentration of Cs^+ ions, as shown in Fig. 4.7 (b).The initial concentration provides an important driving force, to overcome all the mass transfer resistances to the cesium ions between the aqueous and the solid phases. Therefore, a higher initial cesium ion concentration will enhance the sorption process. It is observed that, the q_e value for sorption of cesium ions increases with increase in the initial cesium ion concentration, and then, starts attaining saturation, after a concentration of 25 mg/L. This can be explained by the fact that, the cesium ion uptake by the sorbent is initially linear, as enough number of active sites are available, but it decreases with the increase in the concentration eventually, as competition for the available active sites intensifies due to paucity of the available active sites.

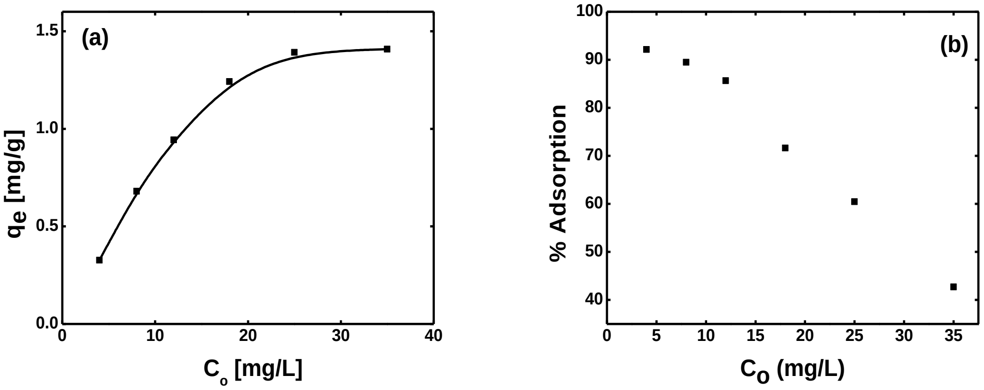

Fig. 4.8: Effect of the initial metal ion concentration on the sorption of Cs^+ onto CuHCF-PES beads

4.5.1.3 Sorption isotherms

Since the quantity of the metal ions sorbed by the sorbent is a function of both the metal ion concentration and the temperature, the amount of cesium ions sorbed was determined as a function of the initial metal ion concentration at a constant temperature, and the sorption equilibrium data were fitted to various sorption isotherm models. Sorption isotherms are important in determining important sorption parameters, which can be used for sorption design purpose. The sorption equation parameters and the underlying thermodynamic assumption describe the surface properties and affinities of the sorbent, and how the solute interacts with the sorbent. The experimental isotherm data were analyzed by Langmuir, Freundlich, Temkin, and Dubinin-Redushkevich isotherms

4.5.1.3.1 Langmuir sorption isotherm

The Langmuir sorption isotherm is the simplest model for sorption of a solute from a liquid solution. It is described by the single site-single sorbate species, and given by the equation[154]

$$\frac{1}{q_e} = \frac{1}{q_m} + \frac{1}{K_L q_m C_e} \qquad (4.3)$$

where q_m is the maximum monolayer capacity of the sorbent beads, K_L is the sorption coefficient and C_e is the equilibrium concentration of the metal ions in the solution. The plot of $1/q_e$ vs $1/C_e$ is a straight line (Fig. 4.9) for sorption of cesium ions onto the CuHCF-PES beads. The value of correlation coefficient R^2 is 0.9981, which indicates a good correlation between the experimental data and the Langmuir sorption model. The values of q_m and K_L can be calculated from the intercept and the slope, respectively, of the straight line. The maximum sorption capacity of the CuHCF beads for Cs^+ ions is determined to be 1.56 mg/g of the resin. The sorption coefficient, K_L, is determined to be 0.852 L/mg. The results are summarized in Table 4.2.

The favorability of the sorption of Cs^+ ions onto the CuHCF beads can be expressed in terms of a dimensionless constant, (R_L), called separation factor, using the essential features of the Langmuir isotherm, as given below

$$R_L = 1/(1+K_L C_o) \qquad (4.4)$$

The calculated values of R_L lie between 0.54 and 0.02, for the concentration investigated in the present work which indicates that the CuHCF- PES beads are good sorbent for Cs^+

ions, and the sorption process is favorable for efficient removal of Cs^+ ions from aqueous waste solutions.

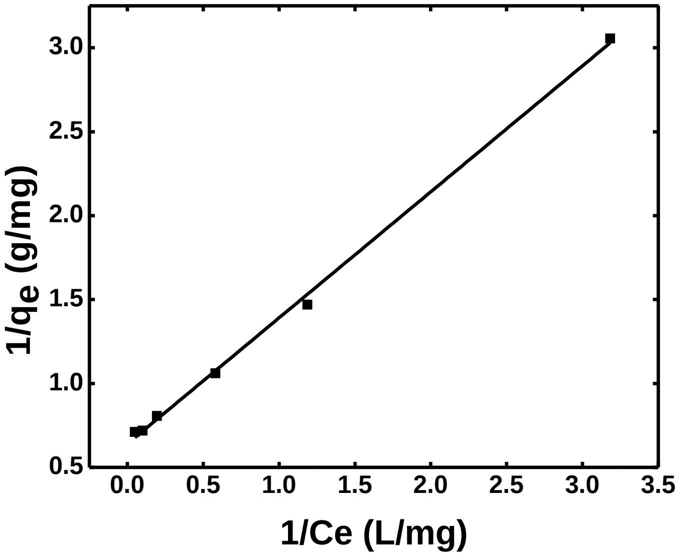

Fig. 4.9: Langmuir isotherm plot for sorption of Cs^+ onto the CuHCF-PES beads at 300 K

4.5.1.3.2 Freundlich isotherm

Freundlich isotherm is an empirical model which can be used to describe non-ideal sorption occurring in heterogeneous sorption systems. This model assumes that the stronger binding sites are occupied first, and that the binding strength decreases with increase in the degree of site occupation. The sorption data were also analyzed by the linearized form of Freundlich isotherm, which is given by the equation,[130]

$$log q_e = \log K_F + \frac{1}{n} \log C_e \qquad (4.5)$$

where, K_F is a Freundlich constant related to the sorption capacity, and n is Freundlich parameter.

The plot of log (q_e) vs log (C_e) is a straight line, as shown in Fig. 4.10. From the slope and the intercept of this straight line, respectively, the values of 1/n and K_F are determined. The correlation coefficient R^2 for this plot is 0.8465, which suggests that the correlation between the experimental data and the Freundlich isotherm model is not as good as that of the Langmuir sorption model. The values of K_F and n are determined to be 0.633 mg/g and 2.9, respectively (Table 4.2).

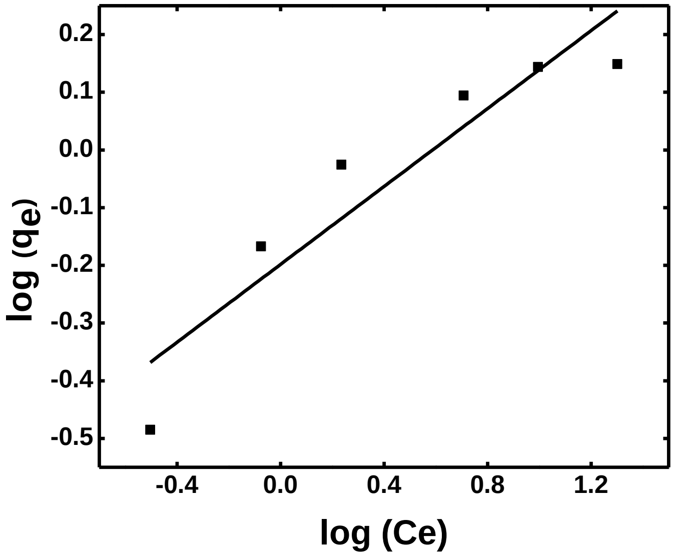

Fig. 4.10: Freundlich isotherm plot for sorption of Cs^+ ions onto CuHCF-PES beads at 300 K

4.5.1.3.3 Temkin sorption isotherm

Temkin sorption isotherm considers a heterogeneous surface, where no molecular interaction exists. It is based on the Langmuir sorption isotherm. Like the Langmuir model, it does not take into account the lateral interaction between the sorbates. For the synthesis of the CuHCF-PES beads, CuHCF powder is loaded on PES matrix. Therefore, it is highly probable that the sorption sites are energetically non-equivalent. The experimental data were also analyzed by applying Temkin model.[130] The linear form of the model is given as,

$$q_e = \frac{RT}{b} lnK_T + \frac{RT}{b} ln\,(C_e) \tag{4.6}$$

where K_T (L/g) is Temkin isotherm constant, b (J/mol) is a constant related to heat of sorption, R is the gas constant (8.314 J/mol/K) and T is the absolute temperature (K). A plot of q_e versus ln (C_e) enables the determination of the isotherm constants K_t and b, from the intercept and the slope, respectively.

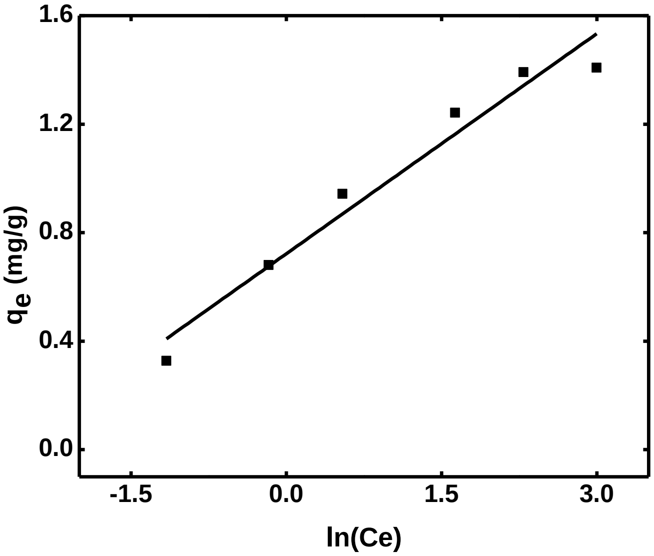

Fig. 4.11: Temkin isotherm plot for sorption of Cs^+ ions onto the CuHCF-PES beads at 300 K

Fig. 4.11 shows that the plot of the ln q_e vs ln C_e is a straight line, with the correlation coefficient R^2 value of 0.9573. It shows that, the experimental equilibrium data are in good correlation with Temkin model also. The Temkin constant, b, is determined to be 9.21 kJ/mole. The typical range of the binding energy for ion exchange mechanism is 8-16 kJ/mole.[130] The isotherm parameters are listed in Table 4.2. The lower value of b, obtained in the present study, indicates weak interaction between the sorbate and the sorbent.

Table 4.2: Isotherm parameters of the different models for sorption of cesium ions onto the CuHCF-PES beads

Sorption isotherm model	**Parameters**	
Langmuir	q_m	1.56 mg/g
	K_L	0.85 L/mg
	R^2	0.9981
Freundlich	K_F	0.633 mg/g
	1/n	0.334
	R^2	0.8465
Temkin	b	9.21 kJ/mol
	K_T	14.45
	R^2	0.9573
D-R	q_D	1.748 mg/g
	K_{DR}	0.037
	R^2	0.8745

4.5.1.3.4 Dubinin-Redushkevich isotherm

The experimental data were analyzed in terms of D-R isotherm model also, to determine the porosity and the apparent free energy of the sorption. D-R isotherm assumes that the characteristics of the sorption curves are related to the porosity of the sorbent.[132] The linearised form of D-R isotherm is given as

$$lnq_e = lnq_m - K_{DR}\varepsilon^2 \tag{4.7}$$

where q_m is the theoretical maximum capacity (mg/g), K_{DR} is the D-R model constant (mol^2/ kJ), related to the mean free energy of the sorption, and ε is the Polanyi potential, and is given by

$$\varepsilon = RT \ln (C_o/C_e) \tag{4.8}$$

Fig. 4.12 shows that the plot of ln (q_e) vs ε^2, for sorption of cesium ions onto the CuHCF-PES beads, is a straight line, with a correlation coefficient R^2 of 0.8745. From the intercept and the slope of the straight line, the values of K_{DR} (also known as the porosity factor) and q_m of the CuHCF-PES beads for Cs^+ ions are determined to be 0.037 and 1.75 mg/g, respectively. The K_{DR} value less than unity implies that the synthesized beads have fine micro pores, and indicates surface heterogeneity. The results of these sorption isotherms are summarized in Table 4.2.

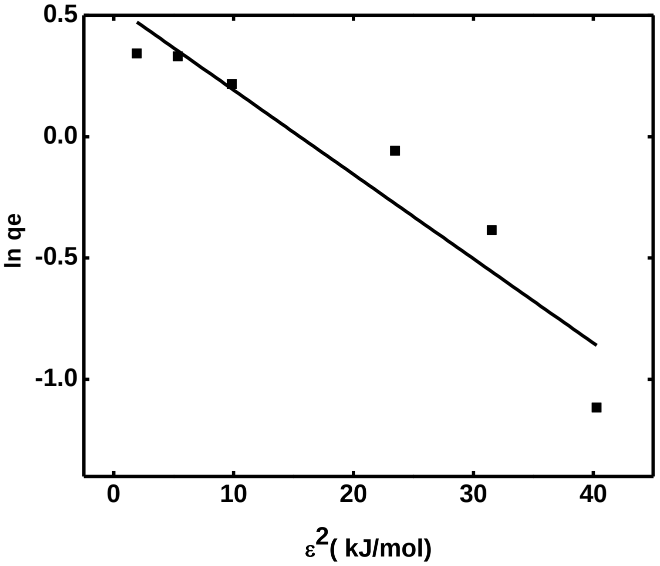

Fig. 4.12: D-R isotherm plot for sorption of Cs^+ ions onto the CuHCF-PES beads at 300 K

4.5.1.4 Sorption kinetics

4.5.1.4.1 Effect of equilibration time

The effect of equilibration time on the sorption of cesium ions from aqueous solutions onto the CuHCF-PES beads, at neutral pH, is presented in Fig. 4.13. The sorption increases with increase in contact time. The uptake of Cs^+ ions is rapid in the first 30 minutes, and then, it becomes slow until a state of equilibrium is reached. In the first 30 minutes, nearly 48 to 70% of the total cesium ion uptake appears to have taken place, depending on the initial cesium ion concentration taken. The initial rapid stage is due to the abundant availability of the active sites in the initial stage. Later on, the process becomes relatively slower, and equilibrium is reached in 120-240 minutes. At this point, the amount of the cesium ions being sorbed onto the sorbent is in dynamic equilibrium with the amount of the cesium ions being desorbed from the sorbent. The time required to attain this state of equilibrium is termed as the equilibrium time, and the amount of cesium ions sorbed at the equilibrium time is the equilibrium sorption capacity of the sorbent under those operating conditions. Therefore, all the further batch experiments were carried out at 240 minutes of equilibration time.

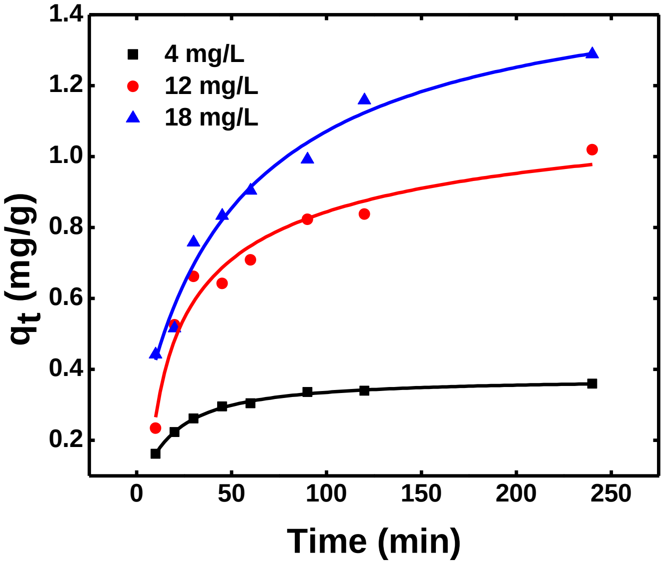

Fig. 4.13: The effect of equilibration time on the sorption of Cs^+ ions onto CuHCF-PES beads, at different initial concentrations

Sorption kinetic studies are important from the view point of both understanding the sorption process and applications thereof. In order to investigate the sorption of cesium ions onto the CuHCF-PES beads, three kinetic models, namely the pseudo first-order model, the pseudo second-order and the intraparticle diffusion models, were employed.

4.5.1.4.2 Pseudo first-order rate model

The linearized form of the pseudo first-order kinetic model can be written as[133]

$$\log(q_e - q_t) = \log(q_e) - \frac{k_1}{2.303}t \qquad (4.9)$$

where q_t is the amount of the cesium ions sorbed at time t, and k_1 is the rate constant for the pseudo first-order sorption process.

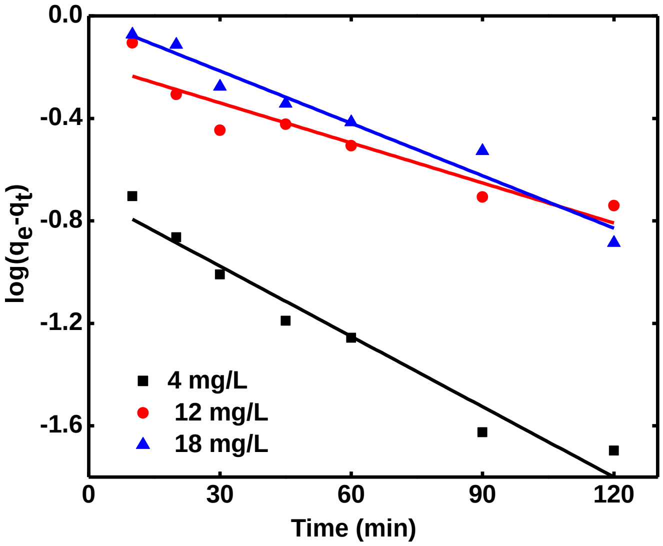

Fig. 4.14: Pseudo first-order kinetic plots for sorption of Cs^+ ions onto the CuHCF-PES beads, at different initial Cs^+ ion concentrations

The values of k_1 and q_e can be determined from the slope and the intercept, respectively, of the corresponding straight line plot of log (q_e - q_t) versus t (Fig. 4.14).These values are given in Table 4.3. The data are fitted with a poor correlation coefficient, indicating that the rate of removal of cesium by the CuHCF-PES beads does not follow pseudo first-order kinetics in the entire studied range. The value of q_e determined from this model is also much lower than the experimentally determined value.

4.5.1.4.3 Pseudo second-order kinetic model

The linearized form of the pseudo second-order kinetic equation is expressed as[140]

$$\frac{t}{q_t} = \frac{1}{k_2 q_e^2} + \frac{1}{q_e} t \tag{4.10}$$

where k_2 is the rate constant of the pseudo second-order sorption (g/mg/min). The plot of t/q_t vs t gives a straight line, from the slope and intercept of which, the values of q_e, and k_2, respectively, can be determined. Fig. 4.15 shows that the plots of t/q_t vs t, for sorption of Cs^+ ions onto the CuHCF-PES beads, are linear, with correlation coefficient R^2 greater than 0.9888. The values of q_e and k_2 determined from the plot are given in Table 4.3. The rate is directly proportional to the number of the active sites on the surface of the sorbent. From the Table 4.3, it is clear that k_2 decreases with increases in the initial Cs^+ ion concentration. The values of q_e thus obtained match very well with the experimental values, and the value of R^2 suggests that the model can be applied to the sorption process in the entire studied concentration range.

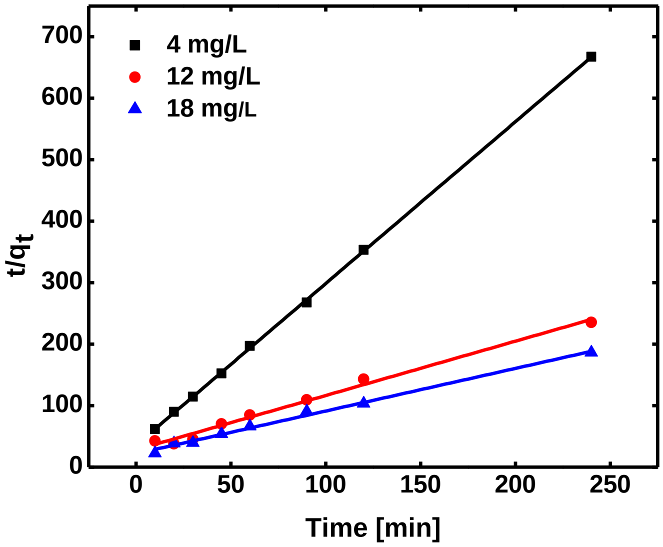

Fig. 4.15: Pseudo second-order kinetic plots for the sorption of Cs^+ ions onto the CuHCF-PES beads at three different initial concentrations of Cs^+ ions

Table 4.3 Kinetic parameters for the sorption of cesium ions onto the CuHCF-PES beads, at different initial cesium ion concentrations

Kinetic model	**Parameters**	**C_o= 4mg/L**	**C_o= 12mg/L**	**C_o= 18mg/L**
	$^{experimental}q_e$	0.359 mg/g	1.019 mg/g	1.256 mg/g
Pseudo –1st order	k_1 (min^{-1})	0.021	0.042	0.024
	q_e (mg/g)	0.198	0.907	0.946
	R^2	0.9476	0.8499	0.9524
Pseudo -2nd order	k_2 (g mg^{-1} min^{-1})	0.193	0.039	0.022
	q_e (mg/g)	0.380	1.132	1.441
	R^2	0.9888	0.9998	0.9931
Intraparticle diffusion	k_{id} (g mg^{-1} $min^{-1/2}$)	0.015	0.065	0.056
	I (mg/g)	0.191	0.204	0.461
	R^2	0.9462	0.9999	0.9863

4.5.1.5 Mechanism

The transfer of the sorbate from the solution phase onto the surface of the sorbent particles is a gradual process, and completes after several steps, such as film or external diffusion, surface diffusion, pore diffusion, and sorption on the pore surface. The overall sorption process may be controlled by one step, or a combination of more than one step. From Fig. (4.16), it is clear that, with increase in the contact time, there is an increase in the sorption capacity of the CuHCF-PES beads for Cs^+ ions, which indicates that the sorption process can be intraparticle diffusion controlled. Therefore, such a possibility was explored by using the intraparticle diffusion model. This model is represented by the following equation [156]

$$q_t = k_{id} t^{1/2} + I \tag{4.11}$$

where k_{id} is the intraparticle diffusion rate parameter and I (mg/g) is a constant that gives an idea about the thickness of the boundary layer. If the intraparticle diffusion occurs, then the plot of q_t vs. $t^{1/2}$ is linear, and, if this straight line passes through origin, then, the intraparticle diffusion is the rate controlling step, otherwise, some other mechanism may also be involved.

As shown in the Fig. 4.16, the plot of q_t vs $t^{½}$ is a multi-linear plot, indicating that the sorption process consists of multiple stages. The first stage is indicated by the small portion of the curve with steep slope. Then, the stage of intraparticle diffusion control starts, indicated by the portion of the curve with gentle slope. This stage is referred to as intraparticle diffusion step. Generally, the slope of stage II is called the intraparticle diffusion rate constant k_{id}. The calculated values of k_{id} and I are given in Table 4.3

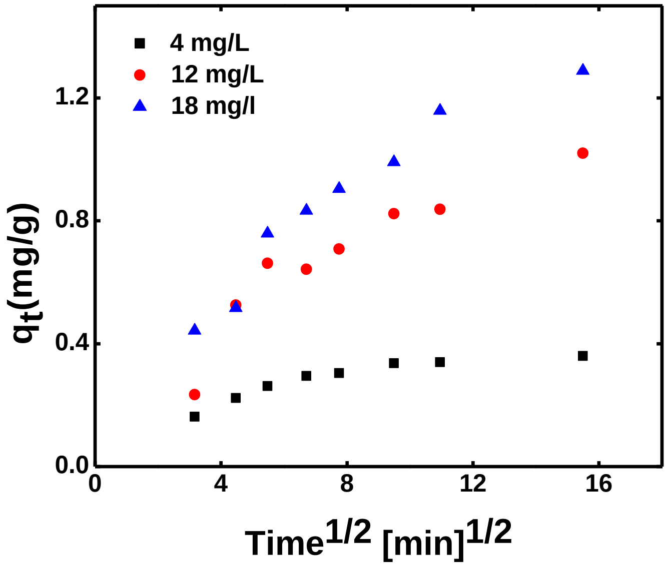

Fig. 4.16: Intraparticle diffusion plots for sorption of Cs^+ ions onto the CuHCF-PES beads, at three different initial concentrations of Cs^+ ions

In order to further confirm whether the sorption proceeds via film diffusion or intraparticle diffusion mechanism, the kinetic data were further analyzed, using equations (4.12) and (4.13), which, depending on the value of F, the fractional attainment of equilibrium, are the solutions of the kinetic expression given by Boyd et al.[146]

$$Bt = 2\pi - \frac{\pi^2 F}{3} - 2\pi(1 - \frac{\pi F}{3})^{1/2} \tag{4.12}$$

$$Bt = -0.4977 - \ln(1 - F) \tag{4.13}$$

The values of Bt were calculated for each value of F, using the equations (4.12), for F values upto 0.85, and equation (4.13) was used for higher F values.[147] The calculated Bt values were plotted against time (Fig. 4.17). The linearity of this plot provides useful information to distinguish between the film diffusion and the intraparticle-diffusion as the rate governing step of the sorption.[148] A straight line passing through the origin is indicative of the sorption process being governed by intraparticle-diffusion mechanism.[149] Fig. 4.17 represents the Boyd's plots for the sorption of cesium ions onto the synthesized beads at different initial metal ion concentrations. It is clear from the Fig. 4.15 that, the lines, for all the studied concentrations, do not pass through origin, and the points are scattered. These results indicate that the sorption process is governed by the film diffusion.

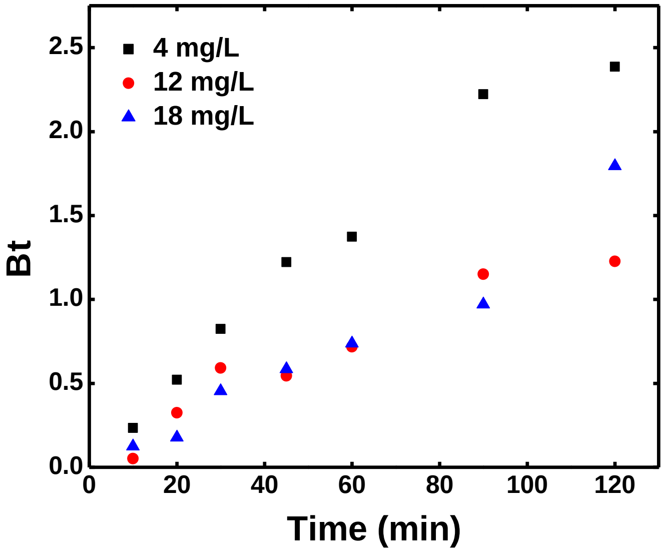

Fig. 4.17: Boyd's plots for sorption of cesium ions onto CuHCF-PES beads at three different initial concentrations of Cs^+ ions

4.5.2 KCuHCF-Gel beads

Alginates are linear unbranched copolymers of β-d-mannuronic acid (M) and α-l-guluronic acid (G) units, in which the M and G monomers have 1→4 glycosidic linkage. These linkages can result in the formation of homopolymeric M- or G-segment, or copolymeric MG segments. Alginates form gels in the presence of a number of polyvalent cations, such as Ca^{2+}, Cu^{2+}, Zn^{2+}or Al^{3+}, etc. The cross-linking of the segments takes place via co-operative bonds between the metal ions and the polymeric segments. The cations act as bridges between the anionic polymer segments, and form a dense hydrogel network. Calcium ions are the most commonly used cross-linker for alginates. It preferentially interacts with G segments, due to structurally favorable chelation of the corrugated chains, and the binding of calcium ion takes place with the carboxyl groups by primary valency, and with the hydroxyl groups via secondary valencies. This kind of binding of calcium ions with the G segments is popularly referred to as "egg-box" model (Fig. 4.18 (a)), in which the cavity formed by diaxially linked G-segments acts as a binding site for the calcium ions. During gelation, dimerisation of the segments takes place, followed by aggregation of the dimers, resulting in a three-dimensional network. After gelation, the water molecules are physically trapped inside the polymeric network, but still can migrate in and out of the solid matrix, which can be very advantageous during the sorption process. Whereas the cross-linking of PVA by chemical methods, using difunctional aldehydes, such as glutaraldehyde, involves bonding of PVA through its pendant hydroxyl groups to glutaraldehyde, by rapid condensation reaction, in the presence of an acid, forming a chemically cross-linked network (Fig. 4.18(b)). Figs. 4.19 (a) & (b) show the schematic representation of the bead and the actual optical microscope image of the swollen KCuHCF-Gel beads, respectively. From the optical microscope image at 10X magnification (Fig. 4.19(b)), it can be inferred that, the method is capable of synthesizing beads of spherical shape, with good control over size. The diameter of the synthesized swollen beads is ~2 mm.

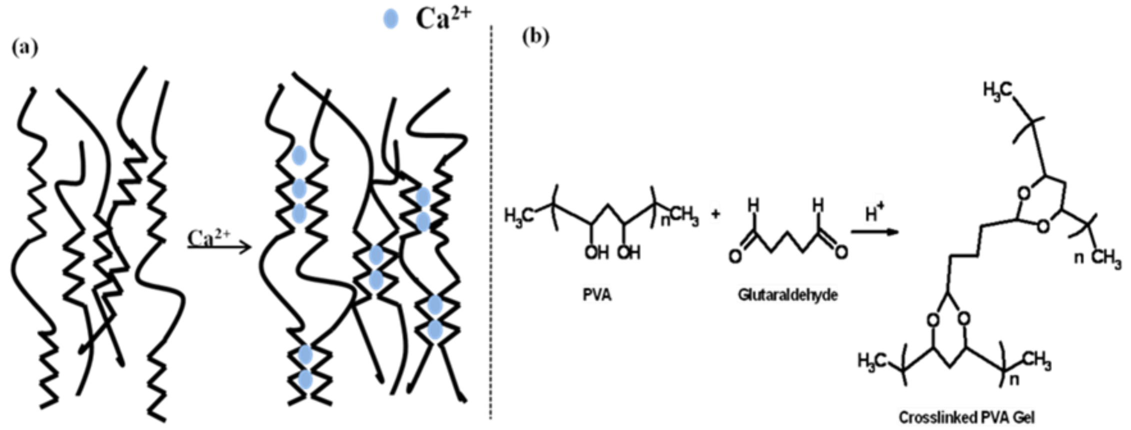

Fig. 4.18: (a) Egg-box model for alginate gel formation in presence of calcium ions and (b) cross-linking of PVA with glutaraldehyde

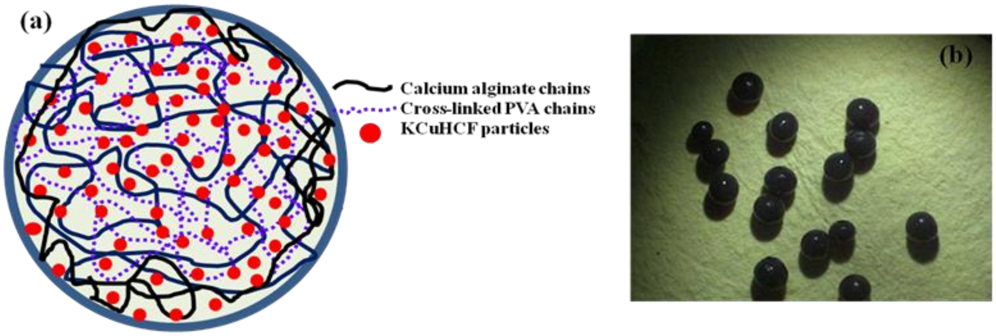

Fig. 4.19: (a) Schematic representation of the bead, and (b) the optical microscope image of the swollen KCuHCF-Gel beads at 10X magnification

4.5.2.1 Characterization

4.5.2.1.1 SEM and EDX study

Fig. 4.20 presents the SEM images of the outer surface and a cross-section of a KCuHCF-Gel bead. These SEM images of a dried KCuHCF-Gel bead depict the porous nature of the synthesized beads, and the uniformly distributed random-sized KCuHCF particles in the beads. The presence of KCuHCF in the synthesized beads was also confirmed by EDX measurement, which showed peaks corresponding to K, Cu and Fe, as given in Fig. 4.21. A thin coating of gold was applied to the beads, before recording SEM images and EDX spectra, to prevent charging of the sample. The peak corresponding to gold in the EDX spectrum originates from this coating only. The calcium peak is also seen due to calcium present in the cross-linked gel beads.

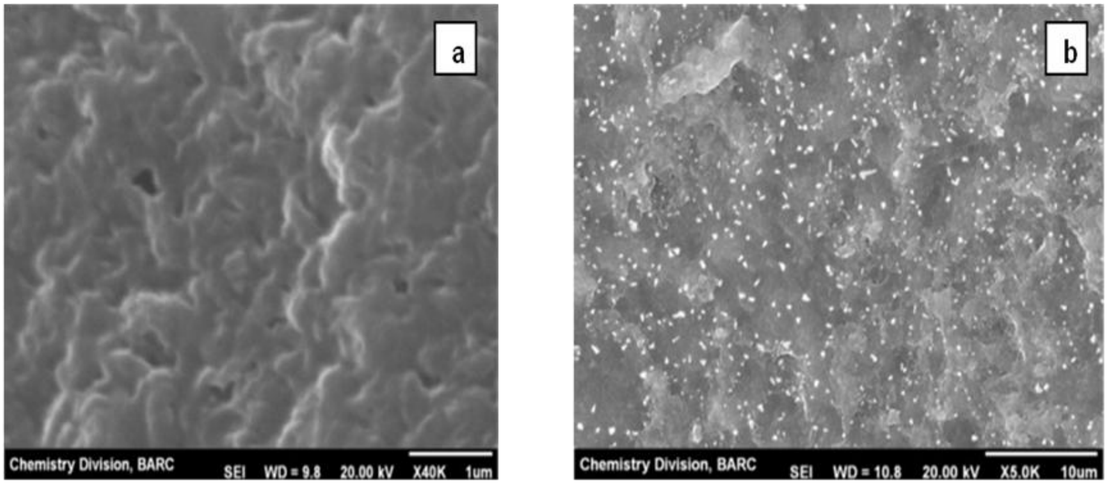

Fig. 4.20: SEM images of (a) the outer surface and (b) a cross-section of a dried KCuHCF-Gel bead, at 40,000 X and 5000 X magnifications, respectively

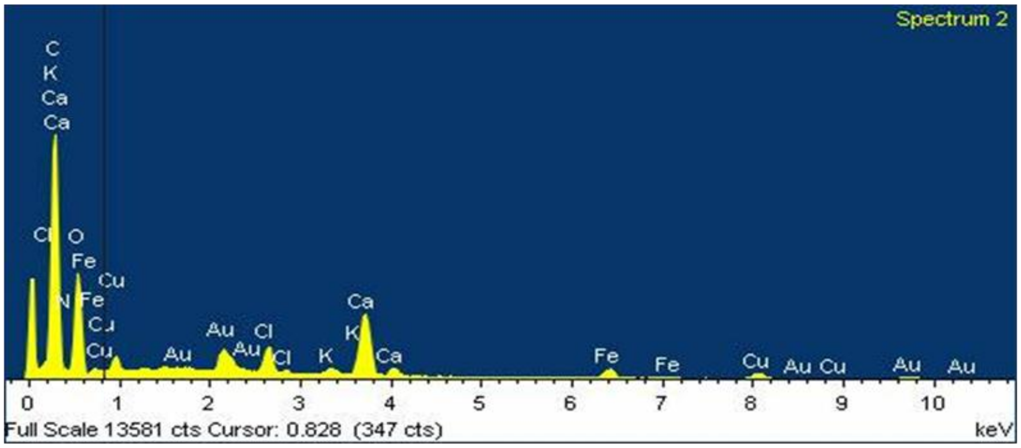

Fig. 4.21: EDX spectrum of KCuHCF-Gel bead

4.5.2.1.2 Thermogravimetric analysis

Thermo gravimetric analysis (TGA) of the synthesized beads was performed at a heating rate of 10 °C/min, in nitrogen atmosphere, from ambient conditions upto 750 °C. Fig. 4.22 shows typical TGA profiles of the blank gel and the KCuHCF-Gel beads. The first step in the TGA profile of the blank gel beads corresponds to a weight loss of 91.13%, due to the absorbed water in the water-swollen beads. After this step, simultaneous thermal degradation of PVA and alginate components takes place, and the degradation of the blank gel beads completes at 484 °C. At the end, ~6% residue is left as charred mass

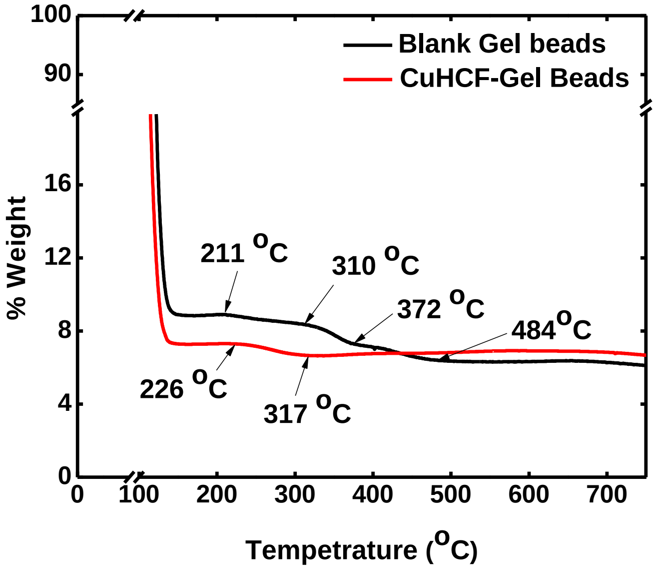

Fig. 4.22: TGA profiles of the blank gel beads and the KCuHCF-Gel beads

TGA profile of KCuHCF-Gel beads also shows similar weight loss of 92.88%, due to the absorbed water. After that, the thermal degradation of the sorbent beads completes in two steps, starting at 226 and 317 °C, respectively. After heating upto 750 °C, ~7% residue is left. The weight loss observed is due to the simultaneous degradation of the KCuHCF, PVA and alginate components of the beads. The separate individual degradation peaks are not visible in the TGA profile of the synthesized beads, due to the small amounts of the individual components, and overlapping thermal degradation profiles of some of the components present. From these results, it can be concluded that the synthesized KCuHCF-Gel beads are stable upto 226°C, and the water content of these beads is very high, indicating extremely hydrophilic and porous nature. On the other hand, the water content of the metal hexacyanoferrate composites, synthesized by using other conventional polymers, is much lower.[183] Therefore, the synthesized sorbent beads will have enhanced sorption efficiency towards the metal ions from the aqueous waste solutions.

4.5.2.1.3 FTIR study

Infrared spectroscopy was used to determine the loading of KCuHCF in the synthesized beads. Fig. 4.23 shows IR spectra of the blank gel beads and the KCuHCF-Gel beads. The spectrum of the blank gel beads shows peaks at 1023, 1716 and 2920 cm^{-1}, corresponding to C-O-C, C=O and C-H stretching vibrations, respectively.[184-185]And, the peaks at 1412 and 1597 cm^{-1} correspond to symmetric and antisymmetric carboxylate vibrational frequencies, respectively, for calcium-carboxylate complex.[186] The stretching band from 3042 to 3566 cm^{-1} corresponds to intermolecular and intramolecular hydrogen bonding in the glutaraldehyde cross-linked PVA chains and alginate beads. The IR spectrum of the KCuHCF-Gel, in the region 600-3600 cm^{-1}, is very similar to that of the blank gel beads, except for the presence of a peak at 2100 cm^{-1}, corresponding to the C≡N stretching vibration.

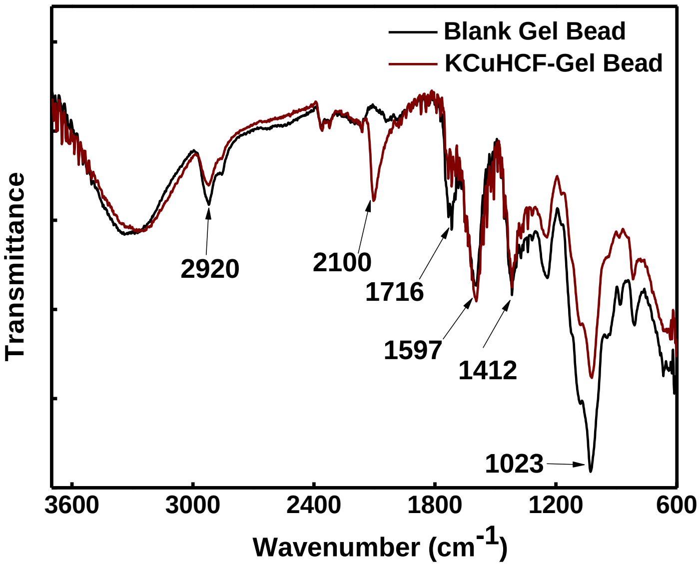

Fig. 4.23: Infrared spectra of the blank gel beads and the KCuHCF-Gel beads

4.5.2.1.4 XRD study

In the X-ray powder diffraction pattern of the synthesized KCuHCF-Gel beads, three main diffraction peaks were observed at 2θ values of 17.72°, 25.22° and 35.84°, which match well with those of $K_2Cu[Fe(CN)_6]$ (JCPDS Card No. 20-0376). The intensity of the peaks observed in the diffraction pattern was not high, which could be due to the lower loading or nanocrystallite size of the KCuHCF particles, as evident from the results of particle size analysis.

4.5.2.1.5 BET surface area

The specific surface area and the pore volume of the beads were determined by BET N_2 sorption method. The surface area was found to be 304.6 m^2/g, and the pore volume was found to be 1.262 cc/g. The surface area and the pore volume measured are for the dried beads, but the actual experiments are carried out, using swollen beads.

Therefore, the effective surface area and the pore volume of the swollen beads are expected to be much higher.

4.5.2.2 Sorption studies

The sorption of cesium ions by KCuHCF sorbent, in neutral solutions, proceeds by an exchange of potassium ions by cesium ions. But, in acidic solutions, the mechanism is different, and involves change in the crystal structure due to dissolution-precipitation.[187] The potential of the KCuHCF-Gel beads was tested for quantitative sorption of cesium from neutral aqueous solutions, and the effect of pH on the sorption efficiency was also studied.

4.5.2.2.1 Effect of pH

pH is one of the important factors in controlling the sorption of metal ions on a sorbent. The sorption of cesium ions, from a solution of concentration 10 mg/L, onto the KCuHCF-Gel beads, was studied in the pH range 1-12. The results, as depicted in Fig. 4.24, reveal that, the amount of cesium ions sorbed per unit mass of the sorbent at equilibrium (q_e) is practically the same in the pH range 3-9, but experiences a steep decrease at pH 12. The observed finding suggests that the competition offered by excess H^+ ions is insignificant in this particular system. While under alkaline conditions, above pH 9, the decomposition of the sorbent (KCuHCF) starts, which accounts for the observed decrease in the uptake of Cs^+ ions at higher pH.[188] Therefore, the beads can be used for sorption/removal of cesium ions in the pH range 3-9.

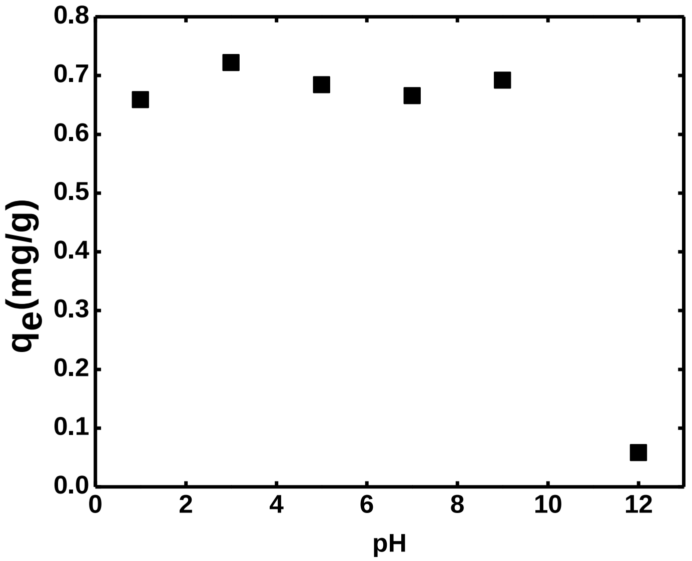

Fig. 4.24: The effect of pH on the sorption of Cs^+ ions onto the KCuHCF-Gel beads

4.5.2.3 Sorption isotherms

Equilibrium studies were carried out, to determine optimum conditions for maximum removal of cesium by KCuHCF-Gel beads. Fig. 4.25(a) shows the equilibrium isotherm, which indicates that, the amount of cesium ions sorbed at equilibrium increases from 0.04 to 2.1 mg/g, for an increase in the initial cesium ion concentration from 1 to 100 mg/L. As the swollen beads, used in the present study, contain more than 90% water, the equilibrium amounts of the cesium ions sorbed with respect to the dry weights will be more than 10 times of these values. The higher initial cesium ion concentration provides an important driving force to overcome all the mass transfer resistances to the cesium ions between the aqueous and the solid phases, thus increasing the rate of sorption and the uptake capacity of the sorbent (Fig. 4.25(a)). However, the percentage uptake shows a decreasing trend, as the initial concentration of the cesium ions is increased (Fig. 4.25(b)). At lower concentration, all the sorbate ions present in the sorption medium can interact with the binding sites, and hence, resulting in higher percentage uptake. But, at higher concentration, the availability of the vacant active sites decreases, and the competition for the available active sites intensifies, and, therefore, % uptake decreases (Fig. 4.25(b)).

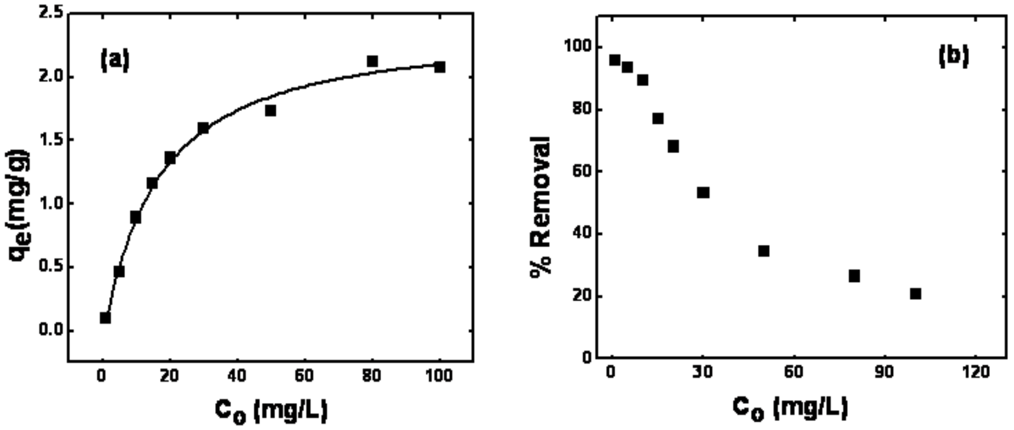

Fig. 4.25: Effect of the initial metal ion concentration on the sorption of Cs^+ ions onto the KCuHCF Gel beads at 293 K, (a) sorption capacity of the beads, and (b) percentage uptake

The Langmuir (equation (4.2)) and the Freundlich (equation (4.4)) equilibrium sorption models were used to fit the experimental data, and determine sorption parameters.[189] Fig. 4.26 shows that the Langmuir model (Fig. 4.26(a)) gives a better fit to the experimental sorption isotherm than the Freundlich model (Fig. 4.26(b)), on the basis of the regression coefficient values (R^2_L=0.9984, and R^2_F = 0.8699, respectively, for the Langmuir and the Freundlich model). The Langmuir parameters determined from the Fig. 4.26(a) are: q_m= 1.60 mg/g and K_L= 1.481 L/mg, while the Freundlich parameters are: K_F = 0.560 and n = 2.71.

The predicted Langmuir and Freundlich sorption isotherm equations for sorption of cesium ions onto the KCuHCF-Gel beads, at 20 °C, useful for design calculations, can be represented as

Langmuir: $\mathrm{q_e} = \frac{2.3639\mathrm{C_e}}{1+1.4812\mathrm{C_e}}$ (4.17)

Freundlich: $q_e = 0.5604C_e^{0.3689}$ (4.18)

The better fitting of the equilibrium data to the Langmuir isotherm expression confirms the monolayer sorption of cesium ions onto the KCuHCF-Gel beads.

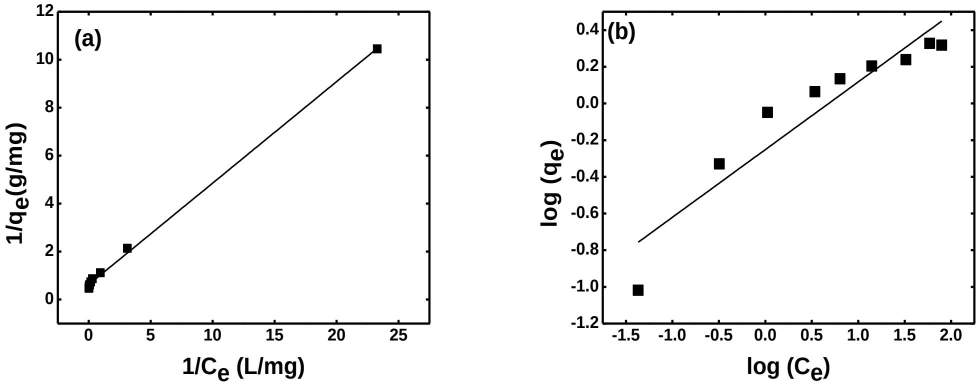

Fig. 4.26: (a) Langmuir and (b) Freundlich isotherm plots for sorption of Cs^+ ions onto the KCuHCF-Gel beads, at 293 K

4.5.2.4 Sorption kinetics

The study of kinetics of a sorbate uptake is required for obtaining essential information, to evaluate the suitability of the sorbent to be used in practical treatment systems, and selecting optimum operating conditions for full-scale batch process. Therefore, the effect of equilibration time on the sorption of cesium ions, from aqueous solutions, was also studied. The sorption increases with increase in contact time (Fig.

4.27). Four models for metal ion sorption kinetics, namely, (i) the pseudo first-order model (Lagergren), (ii) the pseudo second-order model, (iii) intraparticle diffusion model and (iv) Boyd's plot, were used, to fit the experimental results, to determine kinetic parameters for sorption of cesium ions onto the KCuHCF-Gel beads, and delineate the steps involved in the sorption mechanism.

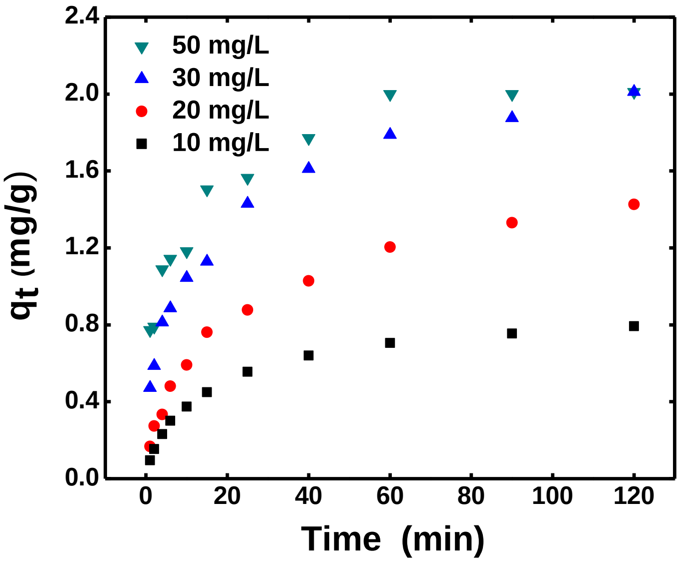

Fig. 4.27: The effect of equilibration time on the sorption of Cs^+ ions onto KCuHCF–Gel beads, at 293 K, for different initial cesium ion concentrations

In the first case, the rate constant of cesium ion removal is determined from the pseudo-first order rate expression (equation 4.9) given by Lagergren.[133] Fig. 4.28 shows the pseudo first-order plots for sorption of cesium ions onto KCuHCF-Gel beads at different initial concentrations of cesium ions. The values of k_1 and q_e can be determined from the slope and the intercept, respectively, of the straight line plot of log (q_e - q_t) versus t (Fig. 4.28).

The values of k_1, q_e and the correlation coefficient (R^2) values obtained by fitting the data to the first-order rate model at different concentrations are presented in Table 4.4. The poor fitting of the data, at different initial concentrations of cesium ions (Fig. 4.28), suggests that the process of cesium ion sorption does not follow pseudo first-order kinetics. Moreover, the values of q_e obtained from the equation differ substantially from those measured experimentally, further supporting the above conclusion.

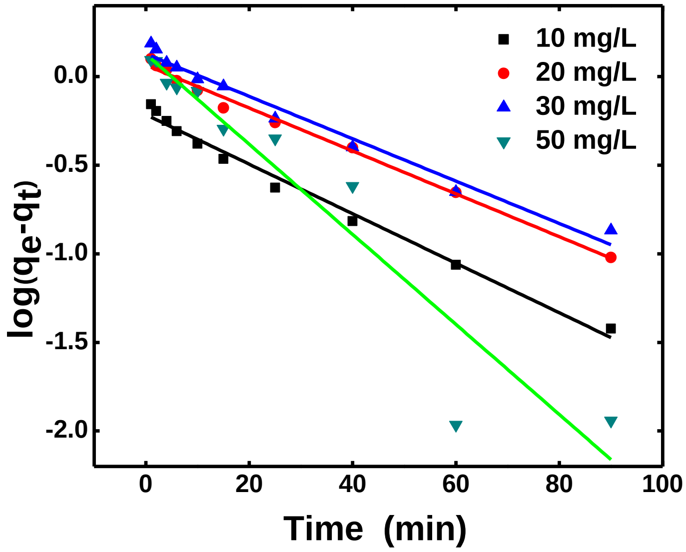

Fig. 4.28: Pseudo first-order plots for sorption of Cs^+ ions onto the KCuHCF-Gel beads, at 293 K, for four different initial Cs^+ ion concentrations

Fig. 4.29 shows the pseudo second-order plots for sorption of cesium ions onto the KCuHCF-Gel beads. The results show that, at all the initial cesium ion concentrations, and for the entire sorption time investigated, the values of linear regression correlation coefficient R_2^2 are found to be higher than that in the case of pseudo first-order plots, and are in the range of 0.9897 to 0.9974. The calculated values of q_e are also in agreement with the experimental values of 0.79, 1.43, 2.01 and 2.012

mg/g at C_o values of 10, 20, 30 and 50 mg/g, respectively. The value of q_e thus determined increases with an increase in the initial cesium ion concentration, and attain an equilibration value of ~2.1 mg/g at the highest studied initial concentration. The higher R_2^2 values confirm that the sorption data are well represented by the pseudo second-order kinetic model.

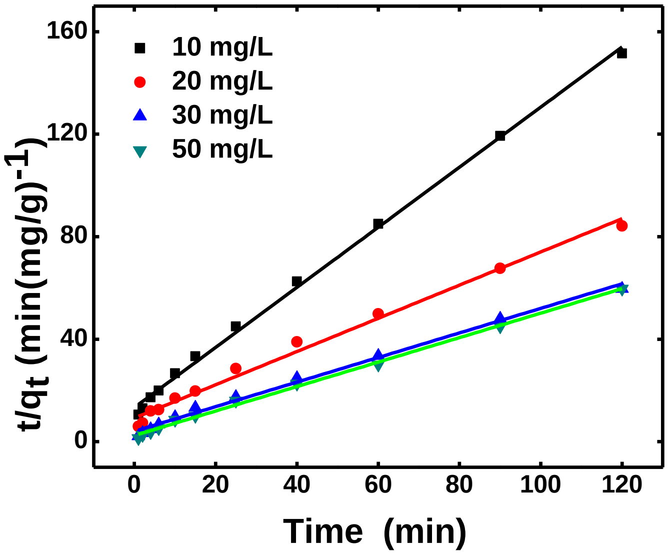

Fig. 4.29: Pseudo second-order plots for sorption of cesium ions onto the KCuHCF-Gel beads, at 293 K, for four different initial Cs^+ ions concentrations

The data were further analyzed by using intraparticle diffusion model, expressed as equation (4.11), to identify the steps involved during the sorption. Fig. 4.30 shows that the plots of q_t against $t^{1/2}$ consist of two separate linear regions, which confirms that intraparticle diffusion is not the only process involved in this system. Generally, the slope of stage II is the intraparticle diffusion rate constant K_{id}, and its value for the system studied presently increases with increase in the initial cesium ion concentration, in the range 10 to 30 mg/L, and then, decreases at 50mg/L. The values of I also increases with increase in the initial metal ion concentration (Table 4.4).

Table 4.4: Kinetic parameters for the sorption of cesium ions onto the KCuHCF-Gel beads at different initial cesium ion concentrations

Kinetic model	Parameters	C_o (mg/L)			
		10	20	30	50
	$^{experimental}q_e$ (mg/g)	0.79	1.43	2.01	2.012
Pseudo –1st order	k_1 (min^{-1})	0.032	0.028	0.027	0.059
	q_e (mg/g)	0.601	1.161	1.341	1.337
	R^2	0.9867	0.9918	0.9757	0.9038
Pseudo -2nd order	k_2 (g mg/min)	0.103	0.045	0.057	0.095
	q_e (mg/g)	0.853	1.5437	2.085	2.094
	R^2	0.9974	0.9897	0.9929	0.9968
Intraparticle diffusion	K_{id} (g/mg/min)	0.039	0.092	0.094	0.073
	I (mg/g)	0.383	0.442	1.001	1.291
	R^2	0.9502	0.9745	0.9607	0.6941

In order to know whether the sorption proceeds via film/external diffusion or intraparticle diffusion mechanism, the kinetic data were further analyzed, using the kinetic expression given by Boyd et al.[146] The value of Bt were calculated for each value of F, as explained in section 4.5.1.4. The calculated Bt values were plotted against time, for different concentrations (Fig. 4.31). All the plots do not pass through the origin, and the points are scattered, indicating some degree of boundary layer control, and also that, intraparticle diffusion is not the only rate-limiting step, and the process of sorption of cesium ions onto the sorbent gel beads is governed by film diffusion step.

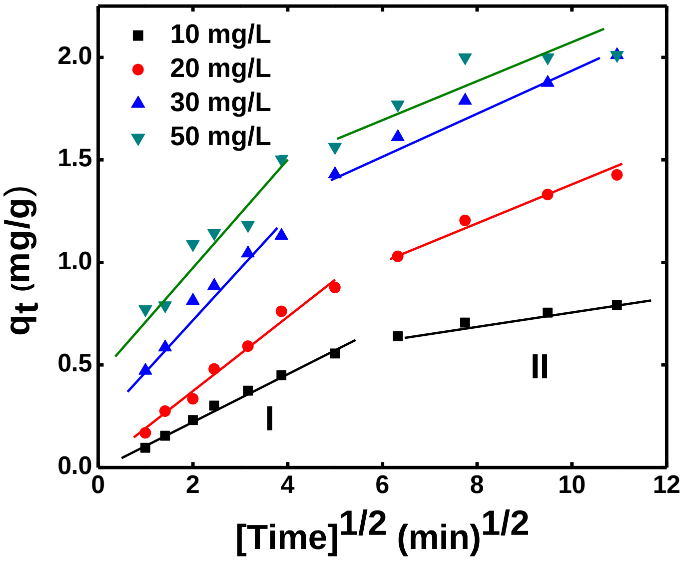

Fig. 4.30: Intraparticle diffusion plots for Cs^+ ions sorption onto the KCuHCF-Gel beads at 293 K, for four different initial concentrations of Cs^+ ions

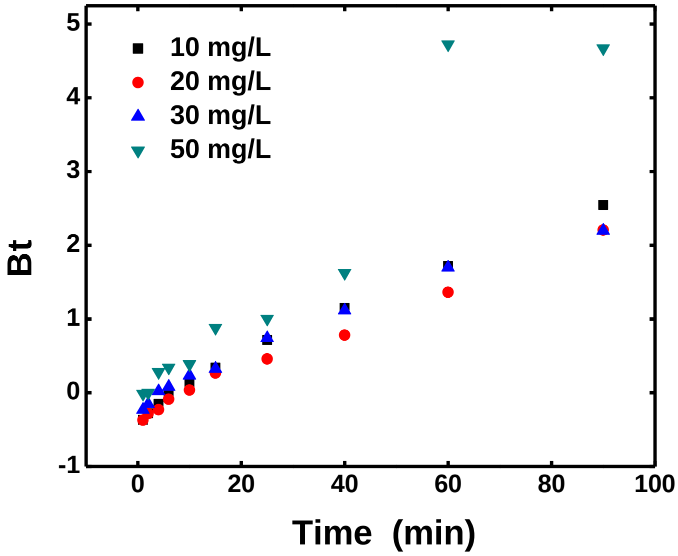

Fig. 4.31: Boyd's plots for sorption of cesium ions onto KCuHCF-Gel beads at 293 K, for four different initial concentrations of Cs^+ ions

4.5.2.5 Effect of interfering ions

The influence of interfering cations (Na^+, K^+, Ca^{2+} and Ba^{2+}) on the sorption of cesium ions onto the KCuHCF-Gel beads was investigated by keeping the concentration of cesium ions constant (5 mg/L), and varying concentration of the interfering ions, at neutral pH, at 298 K. Fig. 4.32 depicts the effect of the interfering metal ions on % removal of cesium ions from the solution. The presence of both the monovalent and the divalent interfering ions decreases the sorption of cesium ions, but the effect is more in the case of divalent ions. About 5% decrease in the removal efficiency of the beads is observed in the case of Na^+ and K^+ ions (Fig. 4.32(a)), whereas, decrease of 9 and 10% takes place in the presence of Ca^{2+} and Ba^{2+} ions, respectively (Fig. 4.32(b)), at the highest studied concentration (48 mg/L) of the interfering ions.

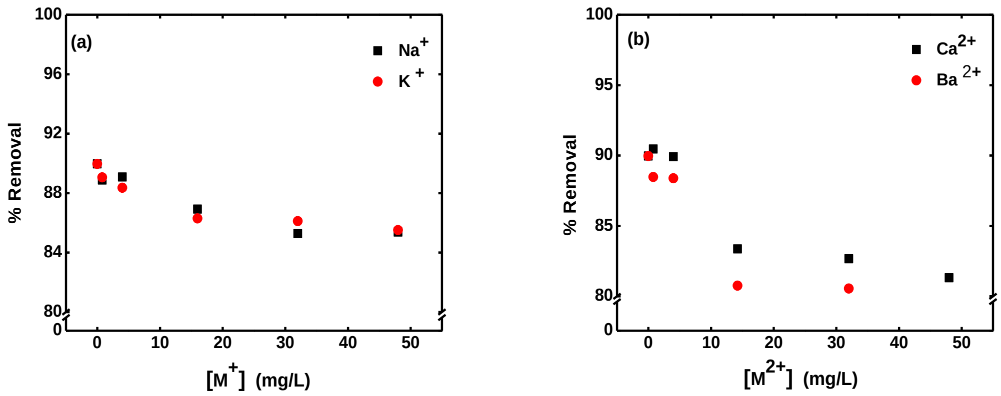

Fig. 4.32: Effect of interfering ions (a) Na^+& K^+, and (b) Ca^{2+}& Ba^{2+} on the sorption of cesium ions onto the KCuHCF Gel beads

The observed smaller decrease, in the case of alkali metal ions, could be due to the lower hydration energy of the cesium ions. The relatively higher effect of Ca^{2+} and Ba^{2+} ions on the sorption of cesium ions could be due to the other processes involved, such as complexation, or nonspecific surface sorption.[183] Moreover, Ba^{2+} ions may also replace Ca^{2+} ions in the beads, as reported by Mandal et al.[190] Even in the presence of these interfering metal ions, the % removal of cesium ions from the solution is quite high, which indicates that these beads can be used effectively for the removal of cesium ions even in the presence of the usual interfering metal ions.

4.5.2.6 Effect of pH sorption kinetics

The effect of pH on the kinetics of the sorption of cesium ions onto the synthesized beads was also studied (Fig. 4.33). The pH of the solution was maintained by using dilute solutions of NaOH (0.1M) and HCl (0.1M). It can be seen from this figure, that the equilibrium uptakes (q_e) are similar at the pH 5 and 7, while a slight increase in the q_e value is observed at pH 9. The data were also analyzed by fitting to the pseudo first-order and the pseudo second-order kinetic models. The values of the kinetic parameters thus obtained, along with that of the correlation coefficient, are given in Table 4.5.

Table 4.5: Kinetic parameters for the sorption of cesium ions onto the KCuHCF-Gel beads at different pH

Kinetic model	Parameters	C_o= 10 mg/L		
		pH=5	pH= 7	pH=9
Pseudo –1st order	k_1 (L/min)	0.0299	0.0322	0.0307
	q_e (mg/g)	0.682	0.609	0.774
	R^2	0.9956	0.9867	0.9951
Pseudo -2nd order	k_2 (g/mg/min)	0.07058	0.1031	0.0635
	q_e (mg/g)	0.888	0.853	1.016
	R^2	0.9936	0.9974	0.9953

The values of the correlation coefficients and q_e (Table 4.5) suggest that the sorption of cesium ions onto the beads follows pseudo second-order kinetics in the studied concentration and pH range.

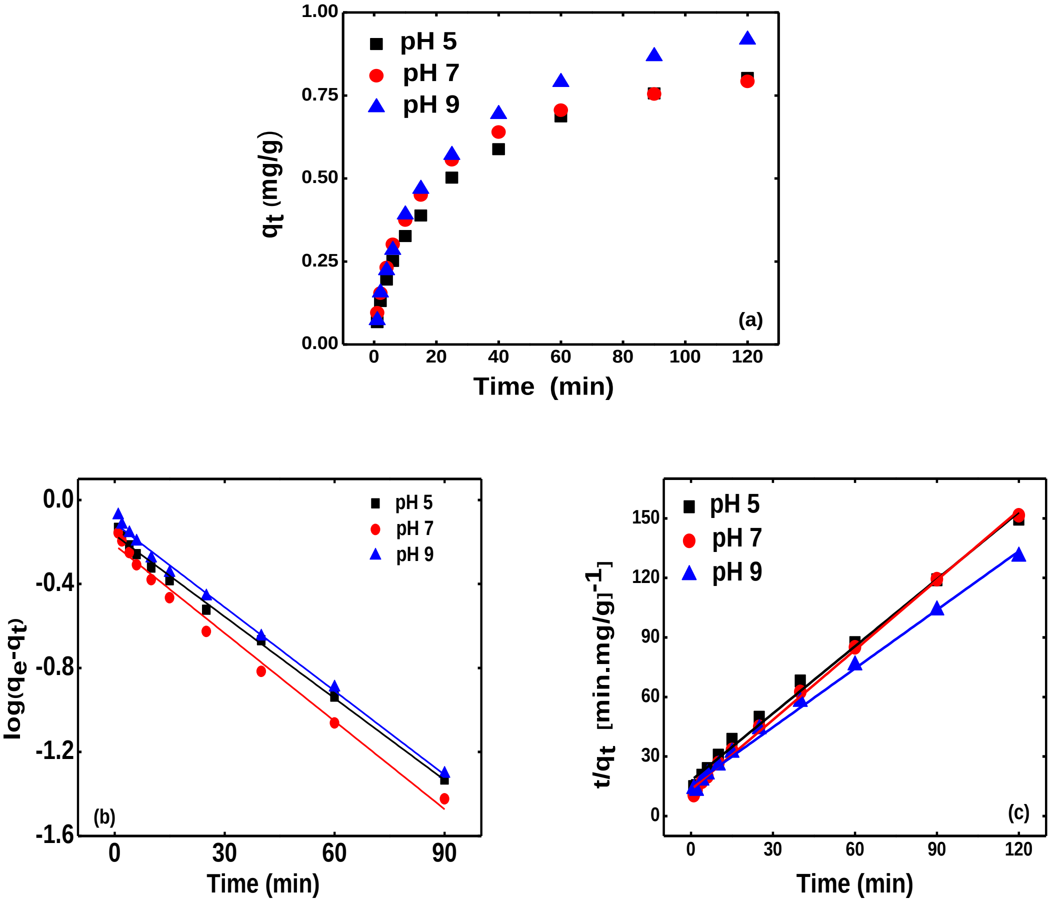

Fig. 4.33:(a) The effect of equilibration time, (b) pseudo first-order plots and (c) pseudo second-order plots, for the sorption of Cs^+ ions onto the KCuHCF-Gel beads, at different pH with C_o =10mg/L

4.6 Comparison of the Sorbent Beads

The physical characteristics of the synthesized sorbent-polymer composite beads, CuHCF-PES and KCuHCF-Gel beads, are quite different, but the sorption behaviors have many points of similarities. In the case of CuHCF-PES beads, the water content is only 83.52%, whereas the KCuHCF-Gel beads, being hydrogel, have about 93% water content. The effect of the water holding capacity of the beads is reflected in the sorption kinetics. Surface area of the CuHCF-PES beads is ~ 479 m^2/g, which is greater than that of KCuHCF-Gel beads (304.6 m^2/g). The methods of preparation of the both the inorganic sorbents are different, which determine their stability and cesium sorption capacity. The chemical stability of the CuHCF-PES beads is expected to be more than that of the KCuHCF-Gel beads. The reason being, the polyethersulfone matrix is less hydrophilic and less likely to be affected by strongly acidic and alkaline environment, whereas PVA-alginate matrix, being very hydrophilic, can be easily degraded by harsh alkaline and acidic conditions. Moreover, the chemical stability of the active component KCuHCF itself is reported to be less than that of CuHCF.[191] The mechanisms of uptake of cesium ions by the two sorbents are quite different. In the case of CuHCF-PES, it is mainly the incorporation of cesium and nitrate ion pairs into the sites, which ultimately leads to phase change, while in the case of KCuHCF-Gel beads, ion exchange, involving exchange of potassium ions with cesium ions, prevails. Depending on the loading of the components and their nature, the capacities of the two sorbent composites are different from each other. The kinetics of sorption is quite fast in the case of KCuHCF-Gel beads, as the hydrophilicity and the water content of the beads is quite high. However, sorption of cesium ions onto both the beads follows pseudo second-order kinetics, and the mechanistic steps involved are complex, and involve both intraparticle diffusion and film diffusion, with the latter as rate controlling step.

4.7 Conclusion

The present study shows that CuHCF-PES composite beads can be easily synthesized by phase inversion technique, and can be used as a sorbent for removal of cesium ions from waste water. Copper hexacyanoferrate can be prepared in the form of fine powder by using PVA as a stabilizer. TGA showed that the water content of the blank and the sorbent composite bead was comparable. The effective incorporation of the CuHCF powder into the beads was also confirmed by IR and EDXRF studies. The surface morphology investigated by SEM technique indicated the porous nature of the beads. These results were also supported by the surface area analysis (surface area = 407 m^2/g). The potential of the beads for removal of cesium was checked in batch mode radioanalytically. The beads were found to work effectively in the pH range 3-9. The equilibrium capacity of the swollen beads was determined to be 1.56 mg/g, which corresponds to ~10 mg/g of the dry beads. The equilibrium sorption data were analyzed, using different sorption isotherm models. The equilibrium data was best explained by the Langmuir isotherm, confirming the monolayer coverage of cesium ions onto the composite beads. From Temkin model, it was inferred that the sorption of cesium ions onto the beads also involve ion exchange, and is a spontaneous process. Among the different kinetic equations applied, the kinetics data fitted well to the pseudo second-order rate model. Analysis of the mechanistic steps involved in the sorption process reveals the complex nature of the sorption process, involving both film diffusion and surface sorption.

In the case of potassium copper hexacyanoferrate-Gel beads also, the particle size of KCuHCF particles was controlled by using PVA as a stabilizer, but the active inorganic sorbent was loaded into a hydrogel matrix of cross-linked PVA and alginate. An interpenetrating network of PVA and alginate, containing KCuHCF particles, was formed, and drawn into spherical bead form, using a syringe with a pump. TGA analysis showed that the beads are stable for use upto 226ºC, and are quite hydrophilic in nature.

BET surface area of the beads was determined to be 304.6 m^2/g. The equilibrium sorption studies showed that the synthesized beads have good potential as a sorbent for the removal of radioactive cesium ions from low-level liquid nuclear waste in the pH range 3-9. The monolayer capacity determined by applying Langmuir sorption isotherm is ~1.6 mg/g of the swollen beads, which corresponds to ~20 mg/g of the dry beads. The kinetics of sorption of the cesium ions onto the synthesized beads was quite fast, and the sorption process reaches equilibrium in the first 60 minutes. The kinetic data were represented well by the pseudo second-order rate model. Analysis of the mechanistic steps involved in the sorption process reveals the complex nature of the sorption process, which comprising both film diffusion and intraparticle diffusion. The effect of interfering ions (Na^+, K^+, Ca^{2+} and Ba^{2+}) on the sorption of cesium ions, from aqueous solution, was found to be quite low, i.e., about 5 and 10 % decrease in the sorption capacity was observed, for the studied alkali and alkaline earth metal ions, respectively, in the studied concentration range. Thus, both the synthesized composites have shown good potential for removal of cesium ions from the near neutral aqueous waste in the pH range of 5 to 9.

Chapter-5

Potassium cobalthexacyanoferrate-Gel Beads & Potassium nickelhexacyanoferrate-Gel Beads

5.1 Introduction

Transition metal hexacyanoferrates are a unique class of inorganic compounds, containing exchangeable alkali and divalent metal ions in their crystal lattice. These compounds have better selectivity for cesium ions as compared to organic resins and zeolites, and can be used for removal of cesium ions over a wide pH range, and even in the presence of high salt loadings. Various transition metal hexacyanoferrates are suggested for removal of cesium, and among these, hexacyanoferrates of copper, cobalt and nickel are extensively studied. Both potassium cobalt hexacyanoferrate (KCoHCF) and potassium nickel hexacyanoferrate (KNiHCF) have a cubic structure (FCC). Iron and transition metal (Co or Ni) ions are located at the corners of the elementary cubes, and the cyano groups are present on the edges.[192] The exchangeable potassium ions are located in the body center. The lattice parameter 'a' of the unit cell is 1.006 nm, for KCoHCF, and 1.012 nm, for KNiHCF. Depending on the method of preparation, the product is either stoicheiometric, with the potassium as the only exchangeable ion, or non-stoicheiometric, with both potassium and transition metal ions available for exchange. Letho et al. have reported that the unit cell parameter 'a' of $Cs_2[CoFe(CN)_6]$, formed, after exchange of K^+ with Cs^+ in KCoHCF, increases to only 1.030 nm, suggesting that no drastic rearrangement of the lattice is involved in the sorption of cesium ions.[93] Various researchers have stated that the sorption of cesium ions onto both KCoHCF and KNiHCF takes place mainly by ion exchange mechanism.[193-197]

These sorbents can be easily prepared in insoluble form, by reacting alkali metal hexacyanoferrate with transition metal salts in aqueous medium. These hexacyanoferrates are difficult to use in column mode, as these sorbents are either obtained in a fine powder form, or tend to become colloidal in aqueous solution. In order to improve their mechanical properties, deposition of insoluble hexacyanoferrates on various supports has been suggested as a possible solution. Mimura et al. prepared KNiHCF by precipitation on chabazite, a kind of natural zeolite, and evaluated the ion exchange performance, for separation of cesium ions from radioactive waste solutions.[195, 198] Ali and co workers prepared composites of KCoHFC, using silica and polymer coated silica as a support material.[199] By using such supporting materials, the operation and hydrodynamic characteristics of the process can be significantly improved. In general, the conventional method of synthesis of these composites involves precipitation of the metal hexacyanoferrates on the supporting matrix, or loading of the synthesized fine powder in some polymer matrix. But, these methods also have their disadvantages, like difficulties in controlling the precipitation step, immobilization of large amounts of inorganic materials, variation of the sorbing properties from one preparation to the other, etc. Considering these problems, we have developed a new method for the synthesis of the KCoHCF and KNiHCF composite beads, by loading the slurry of these compounds into a bio-polymeric matrix in the form of a hydrogel. The synthesized sorbent-hydrogel beads have high hydrophilicity, and work very well in the pH range 1-12.

The synthesized spherical beads were characterized, using TGA technique, XRD, SEM and BET surface area analysis techniques. The sorption of cesium ions by these beads was evaluated by radioanalytic method. The effect of various system parameters, such as the initial cesium ion concentration, time, pH and sorbent dosage, were studied, and the data obtained were analyzed, using different sorption isotherms and kinetic models.

5.2 Materials

All the reagents used were analytical grade chemicals. A stock solution of cesium ions (1000 mg/L) was prepared by dissolving appropriate amount of $CsNO_3$. Sodium alginate and poly vinyl alcohol (Molecular weight 1,25,000) were purchased from SD Fine chemicals, India. Cesium nitrate, potassium hexacyanoferrate (KHCF), cobalt sulphate, nickel sulphate and nitrate salts of sodium, potassium, calcium and barium were obtained from Merck. All the chemicals used were of analytical grade.

5.3 Synthesis of Sorbent-Gel Beads

The KCoCHF-Gel beads used in this study were prepared indigenously, using sodium alginate as a binding matrix. KCoHCF was prepared by the reaction of 5 ml of $CoSO_4$ (0.1M) and 3 ml of KHCF (0.1M), in the presence of 5ml of 10 % PVA solution. PVA acts as stabilizer, and controls the size of the KCoHCF particles formed. To this solution, 10 ml aqueous solution of 4% sodium alginate was added. This solution was used to prepare KCoHCF containing polymer composite beads, by dropping it into 4 wt % $CaCl_2$ aqueous solution, through 0.8 mm diameter needle, using a syringe with a pump. Thus formed beads were kept in the same $CaCl_2$ solution, for 3 hours, for complete conversion of sodium alginate to calcium alginate. Then, the beads were separated from the solution, and washed with water. KNiHCF-loaded hydrogel beads were prepared in the similar fashion, by using $NiSO_4$ as a source of nickel ions, and the KNiHCF slurry was mixed in 8 ml 4 wt % sodium alginate solution. Tthe blank polymer gel beads were prepared by mixing PVA and alginate solution in similar compositions as in the case of the respective sorbent gel beads. This blank polymer solution was dropped into 4 wt % $CaCl_2$ aqueous solution, through 0.8 mm diameter needle, as explained earlier to form blank gel beads. Swollen beads were used in TGA and all the sorption experiments, whereas SEM, EDX, and BET surface area analyses were carried out with air-dried sorbent beads.

5.3.1 Effect of PVA concentration on KCoHCF particle size

The effect of the presence of PVA on the size of the synthesized KCoHCF particles was studied, by varying the concentration of PVA, from 0 to 10 wt%, and keeping the concentrations of KHCF and $CoSO_4$ constant (Fig. 5.1). The rate of reaction was not altered due to the presence of PVA. The reaction was observed to be instantaneous, and a significant decrease in the size of the KCoHCF particles was noticed in the presence of PVA. Variation in the size of the KCoHCF particles was observed, from 3.8 μm to 0.41 μm, by increasing the concentration of PVA, from 0 to 10 wt%. Fig. 5.1 depicts the plot of the average diameter, measured by the particle size analyzer, vs. PVA concentration.

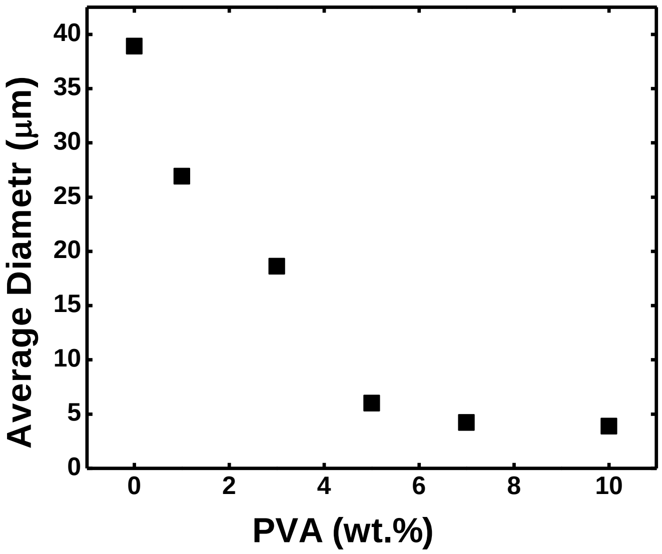

Fig. 5.1: Effect of PVA concentration on the size of the KCoHCF particles

From this plot, it is clear that the size of the KCoHCF particle can be effectively controlled by introducing PVA in the reaction mixture. The particle size decreases as the PVA concentration increases from 0 to 7%, and thereafter, no significant changes in the size of the KCoHCF particles is seen. The synthesis of the KCoHCF particles was carried out in the presence of 10% PVA, to adjust the viscosity of the polymeric solution for the formation of beads.

5.3.2 Effect of PVA concentration on KNiHCF particle size

The stabilizing effect of PVA on the size of KNiHCF particles was studied, by varying the concentration of PVA, from 0 to 10 wt%, and keeping the concentrations of KHCF and $NiSO_4$ constant. The mean size of the KNiHCF particles obtained, by carrying out the reaction in the presence of different concentrations of PVA, was smaller than that obtained in the absence of PVA. It was observed that, KNiHCF particles of mean size 1.4 μm were formed in the absence of PVA, whereas in the presence of 3% PVA, the mean size of the particle was reduced to 0.4 μm. Further increase in the concentration of PVA did not cause any significant reduction in the size of the KNiHCF particles, in the studied range. However, 10 wt % solution of PVA was used in the synthesis of KNiHCF particles, to maintain the optimum viscosity of the polymer slurry, for efficient formation of the sorbent-gel beads. The average size of the KNiHCF particles under the conditions of the beads formation was determined to be 0.4 μm. The technique of dynamic light scattering was used to determine size of the sorbate particles directly in the aqueous sol used for the synthesis of the beads. The hydration sphere associated with particles is generally responsible for the observed higher particle size by the dynamic light scattering technique, as compared to that obtained by other techniques, such as AFM, SEM, TEM, etc. So, the actual size of the particles may be smaller than 0.4 μm.

5.4 Sorption Studies

The cesium stock solution of 1000 mg/L was diluted as required, to obtain standard solutions, containing 1–150 mg/L of cesium. 5 ml of the cesium ion solution, of desired concentration, spiked with known amount of ^{137}Cs, (0.5μCi/L) radiotracer, was taken in each of the equilibration tubes of 20 ml capacity, and 0.05 g of KCoHCF-Gel beads was added in each. pH of the solution was adjusted by using dilute solutions of hydrochloric acid, or sodium hydroxide, depending on the requirement. The solutions were agitated, for a predetermined period at 20 ± 0.5 °C, at a fixed speed of 150 rpm. After equilibration, sample aliquots were taken in the counting voils, and counted for gamma activity. For sorption isotherm studies, the initial concentrations of the solution taken for the studies were in the range of 1-150 mg/L. The equilibrium sorption capacity, $q_{e,}$ was calculated, using the equation

$$q_e = \frac{(C_o - C_e)V}{m} \tag{5.1}$$

where, C_o and C_e are the initial and the equilibrium concentrations, respectively, of cesium ions in the solution, V is the volume of the aqueous solution, and m is the weight of the sorbent. The effect of the sorbent dose on the equilibrium capacity q_e was investigated, to choose optimum sorbent dose, which was used in all the experiments.

Kinetic experiments were conducted, by using a known weight of sorbent, and employing cesium ion concentration in the range 1–20 mg/L. The samples were taken at different time intervals (0–180 min). Suitable aliquots were analyzed for cesium concentration, and recorded. The rate constants were calculated by using the conventional rate expression. The amount of metal ions sorbed at time t, q_t, was calculated from

$$q_t = \frac{(C_o - C_t)V}{m} \tag{5.2}$$

where C_t is the concentration of cesium ions in solution at time t.

5.5 Results and Discussion

The cross-linking of the alginate chains occurs, which fixes the metal hexacyanoferrate particles inside the spherical and dense polymeric matrix almost uniformly. The cross-linking mechanism of the alginate by calcium ions is often explained by "egg-box" model, in which α -l-guluronic acid (G) units bind to calcium ions. Binding of calcium ions takes place with the carboxyl groups by primary valencey, and with the hydroxyl groups via secondary valencies, resulting in a three-dimensional network. Optical microscope images of the KCoHCF-Gel and the KNiHCF-Gel beads are shown in Fig. 5.2. The diameter of both types of the beads is ~2 mm.

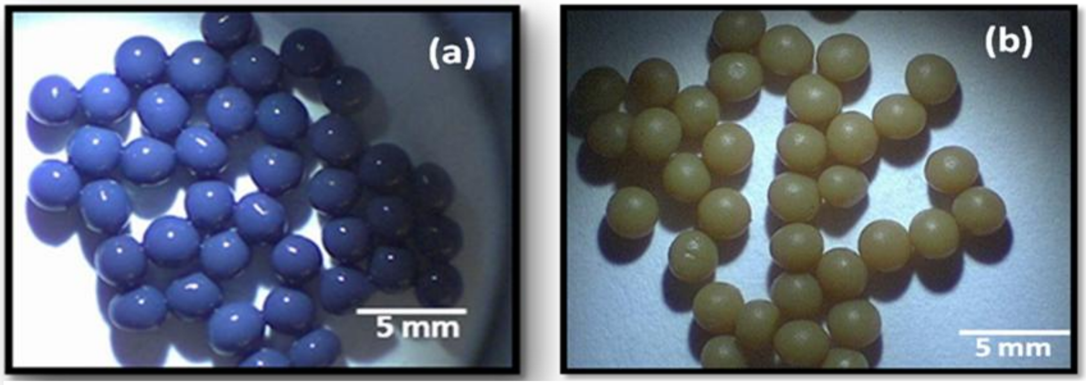

Fig. 5.2: Optical microscope images of the (a) KCoHCF-Gel beads,and (b) KNiHCF -Gel beads, at 10X magnification

5.5.1 KCoHCF-Gel beads

5.5.1.1 Characterization

5.5.1.1.1 Thermogravimetric analysis

Thermo gravimetric analysis (TGA) of the synthesized beads was performed at a heating rate of 10 °C/min, in nitrogen atmosphere, from ambient conditions upto 750 °C. Fig. 5.3 shows typical TGA profiles of the blank gel beads and the KCoHCF-Gel beads.

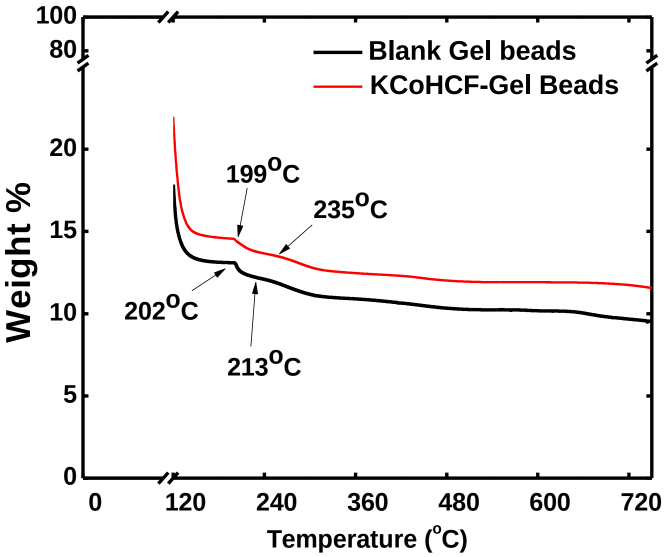

Fig. 5.3: TGA profiles of the blank alginate beads and the KCoHCF-Gel beads

The first step in the TGA profile of the blank gel beads, from room temperature to 151 °C, corresponds to a weight loss of ~86%, due to the absorbed water in the water-swollen beads. After this step, the degradation of the beads starts at 202 °C, and another step in the TGA profile is observed at 213 °C. After this temperature, the blank beads degrade gradually. At the end, ~ 11% residue is left as charred mass. TGA profile of KCoHCF-Gel beads also shows similar weight loss of ~ 87% in the first step, due to the absorbed water. After that, the thermal degradation of the sorbent beads starts at 199 °C. The subsequent degradation step starts at 235 °C, as compared to that at 213 °C, in the case of the blank beads. The early onset of this degradation step could be due to the presence of KCoHCF in the matrix. The individual degradation peaks are not visible in the TGA profile of the synthesized beads, due to the small amounts, and overlapping thermal degradation profiles of the components present therein. After heating upto 750 °C, ~9.5% residue is left. From these results, it can be concluded that the synthesized

KCoHCF-Gel beads are stable upto ~ 200 °C, and the water content of these beads is very high, indicating extremely hydrophilic and porous nature, while the water content of the metal hexacyanoferrate composites, synthesized by using other conventional polymeric supports, is much lower.[183] Such sorbent beads are expected to show enhanced sorption efficiency for the metal ions from the aqueous waste solutions.

5.5.1.1.2 XRD study

In the X-ray powder diffraction pattern of the synthesized KCoHCF-Gel beads, three main diffraction peaks were observed at 2θ values of 17.57º, 20.43º and 25.01º, and some low intensity peaks at 30.99º and 36.33º, which match well with those of $K_2Co[Fe(CN)_6]$ (JCPDS Card No. 75-0038). The powder diffraction XRD pattern of the synthesized beads didn't have sharp peaks, indicating the amorphous nature of KCoHCF crystallites. Thus, it can be concluded that the synthesized sorbent beads contain amorphous KCoHCF.

5.5.1.1.3 SEM and EDX Study

The SEM images of the outer surface and a cross-section of a KCoHCF-Gel bead are shown in Figs. 5.4(a) and (b), respectively. The outer surface of the synthesized beads is quite porous, which is a desirable property for any sorbent. From Fig. 5.4(b), it is clear that large pores are also present in the interior of the bead. Almost uniform distribution of KCoHCF in the synthesized beads was further confirmed by EDX measurement.

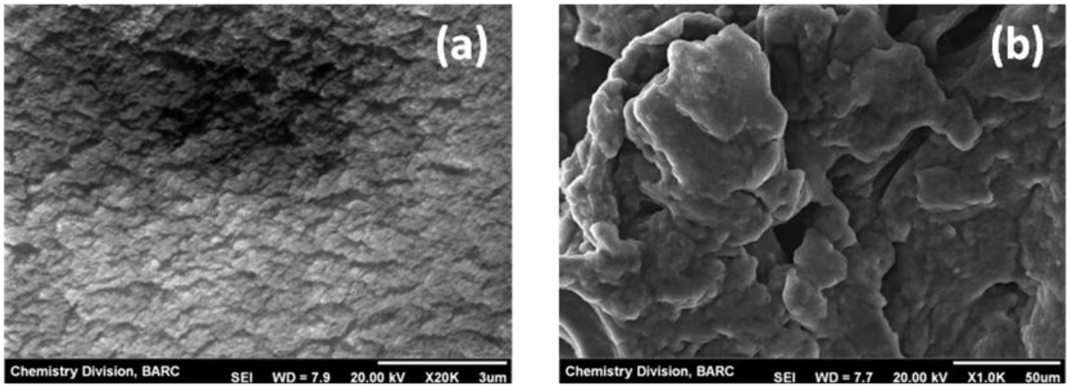

Fig. 5.4: SEM Image of (a) the outer surface, and (b) cross-section of a KCoHCF-Gel bead

5.5.1.1.4 BET surface area analysis

The specific surface area and the pore volume of the beads were determined by BET N_2 sorption method. The nitrogen adsorption-desorption isotherms were measured at 77 K, and at a relative partial pressure (i.e. P/P_o) of N_2 of 0.98, after degassing the samples at 100ºC, for 5 hours. The surface area was found to be 498.33 m^2/g, and the pore volume was found to be 1.469 cc/g. The surface area and the pore volume measured are for the dried beads, but the actual sorption experiments are carried out, using the swollen beads. Therefore, the effective surface area and the pore volume of the swollen beads are expected to be much higher than these values for the dried beads. The higher surface area will lead to higher sorption capacity of the beads.

5.5.1.2 Sorption studies

The sorption of cesium ions on potassium cobalt hexacyanoferrate proceeds via stoichiometric ion exchange between the potassium and the cesium ions. Letho et al. investigated the sorption of cesium ions onto potassium cobalt hexacyanoferrates, and reported that the ion exchange process probably involves only the crystallites of KCoHCF closer to the surface.[93, 200] To investigate the potential of the synthesized beads as an efficient sorbent for cesium ions, the effect of sorbent dose, pH, cesium ion concentration and contact time was investigated in detail.

5.5.1.2.1 Effect of sorbent dose

Different known amounts of the KCoHCF-Gel beads were equilibrated with 5 ml of the cesium ion solution of a suitable concentration, and the equilibrium sorption capacity for cesium, q_e, was determined at each sorbent dose. The effect of the sorbent dose on the q_e value is shown in Fig. 5.5. With increase in the mass of the sorbent beads, the sorption capacity increases till sorbent dose of 0.05 g, i.e., 10 g/L, and after that, the sorption capacity starts decreasing sharply. The initial increase in the apparent sorption capacity with sorbent dose is, because probably, the sorption equilibrium is not attained during the experimental contact time. As the sorbent dose increases, more number of active sites and surface area are available for sorption of cesium ions, which results in the increase in the rate of sorption. So, the system approaches towards equilibrium much faster with increase in the sorbent dose, manifesting in increase in the sorption capacity. Once the sorbent dose is sufficient, and the equilibrium is attained in the experimental contact time, there will be decrease in sorption capacity with further increase in the sorbent dose due to the fixed number of the sorbent ions initially present in the solution. Once equilibrium is reached during the contact time, the relation between q_e value and the sorbent dose can be derived as follows

Distribution coefficient K can be represented as

$$K = \frac{C_s}{C_e} \tag{5.4}$$

where C_s is the concentration of the solute sorbed and C_e is the equilibrium solute concentration of the solution, at equilibrium.

If W_s is the amount of the solute sorbed and W_l is the amount of solute in the solution at equilibrium, V_s is the volume of sorbent and M is molecular weight of the sorbate, K can be expressed as

$$K = \frac{W_S/M}{V_S} \times \frac{V}{W_l/M} \tag{5.5}$$

Further, W_l can be represented as (W-W_s), where W is the total inital amount of the solute in the solution. Using this, equation (5.5) can be solved for W_s as

$$W_s = WK\left(\frac{V_S}{KV_S+V}\right) \tag{5.6}$$

The above equation can be further written as

$$W_s = WK\left(\frac{m}{Km+V\rho_S}\right) \tag{5.7}$$

where m is the mass and ρ_s is the density of the sorbent.

q_e in mg/g can be represented as $q_e = W_s/m$,

Using equation (5.7), q_e can be written as

$$q_e = \frac{W}{m+V\rho_S/K} \tag{5.8}$$

It is clear from the equation (5.8) that, with increase in the mass of the sorbent, the value of q_e decreases in a non linear fashion. The rate of decrease of sorption capacity with the increase in the sorbent dose is given by

$$\frac{dq_e}{dm} = -W\ (m_s + V\rho_s/K)^{-2} \tag{5.9}$$

So, the main reason for the decrease in sorption capacity with increase in the sorption dose is the decrease in the fraction of the occupied sites in the sorbent. The additional effect could be due to the interference between the binding sites at higher sorbent doses.[201-202] Therefore, an optimum sorbent dose of 0.05 g was chosen for the subsequent experiments.

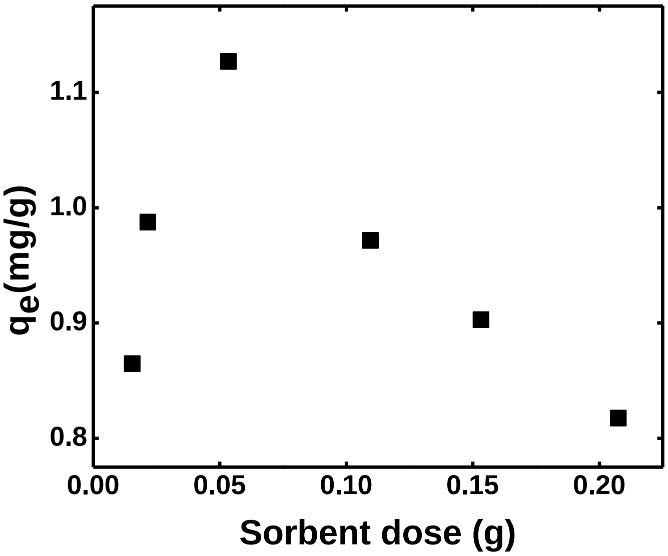

Fig. 5.5: Effect of sorbent dose on the sorption of cesium ions onto the KCoHCF-Gel beads

5.5.1.2.2 Effect of pH

Fig. 5.6 depicts the effect of pH of the sample solution on the sorption behavior of the synthesized beads. It is clear from the figure that the q_e value changes from 0.99 mg/g to 0.92 mg/g of the swollen beads, in the entire pH range investigated. The observed change in the equilibrium capacity value is not much. This result indicates that the sorption efficiency of the synthesized beads is quite good almost in the entire pH range of 1 to 12, and the beads can be used effectively for sorption/separation of cesium over a wide pH range.

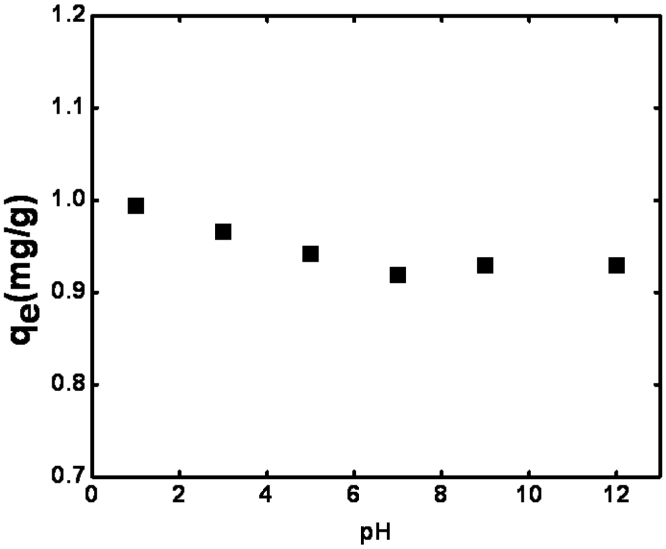

Fig. 5.6: Effect of pH on the sorption of cesium ions onto the KCoHCF-Gel beads

5.5.1.2.3 Effect of cesium ion concentration

The effect of cesium ion concentration on the sorption capacity of the beads was studied, by varying the concentration of cesium, from 1 to 150 mg/L, under neutral condition. Figs. 5.7 (a) & (b) show the effect of the initial cesium ion concentration on the sorption capacity and the % removal of cesium from the sample solution, respectively. The sorption capacity, q_e, increases almost linearly with increase in the initial cesium ion concentration upto 30 mg/L, and then, it increases less than linearly upto ~90 mg/L, and thereafter, it starts reaching saturation. A q_e value of 1.87 mg/g of the swollen beads is observed at the highest studied initial cesium concentration of 150 mg/L.

This is because the total number of active sites is finite due to the fixed amount of the resin taken for sorption studies. However, the percentage uptake shows a decreasing trend, as the initial concentration of the cesium ion increases from 1 to 150 mg/L. As the swollen beads, used in the present study, contain ~ 87% water, the equilibrium amount of the cesium ions sorbed with respect to the dry weights will be more than 7 times of these values. The initial linear increase in q_e value with increase in C_o could be due to the fact that, the mass transfer resistance experienced by the cesium ions, while diffusing from the aqueous phase to the solid phase, is minimized by the driving forces provided by the higher initial cesium ion concentration, and more number of active sites are available. But, at high C_o values, the number of active sites is reduced quickly, and consequently, the competition between the cesium ions for interaction with the available active sites increases, and the increase in the sorption capacity with concentration reduces, and finally, it reaches a saturation value.

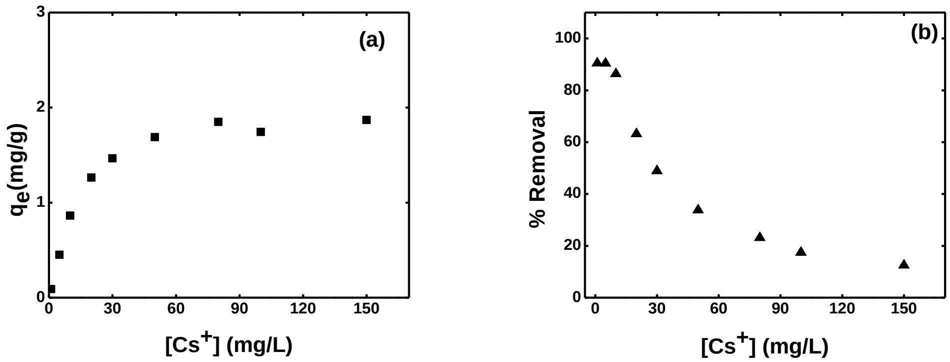

Fig. 5.7: Effect of cesium ion concentration on its sorption onto KCoHCF-Gel beads

5.5.1.3 Sorption isotherms

The analysis of the results of sorption process is required for better understanding of the sorption process. The quantity of the metal ions that could be taken up by a sorbent is a function of both the concentration of the metal ions and the temperature. The amount of solute sorbed is determined as a function of the concentration of the solute at a constant temperature, which could be explained in sorption isotherms. The sorption isotherm provides fundamental physiochemical data for evaluating the applicability of the sorption process as a unit operation. The experimental isotherm data are usually analyzed by the Langmuir and the Freundlich isotherms.[130, 154]

The linearized forms of the Freundlich and the Langmuir isotherm expressions can be written as follows:

Freundlich isotherm: $\log q_e = \log K_F + \frac{1}{n} \log C_e$ (5.10)

where K_F (mg/g) is the Freundlich constant and ‘n’ the Freundlich exponent

Langmuir isotherm: $\frac{1}{q_e} = \frac{1}{q_m} + \frac{1}{K_L q_m C_e}$ (5.11)

where K_L and q_m are the sorption coefficient and maximum monolayer capacity, respectively.

Fig. 5.8 shows the plot of log q_e versus log C_e. The values of constants K_F and n, and R^2 value, obtained by fitting the data of the sorption of cesium ions onto the KCoHCF-Gel beadsto equation (5.10), are presented in Table 5.1. The Langmuir isotherm, equation (5.11), was also applied to the sorption of cesium ions onto the KCoHCF-Gel beads. The plots of $1/q_e$ versus $1/C_e$, as shown in Fig. 5.9, is linear, with R^2

value of 0.9977, which indicates that the sorption process can be explained best by the Langmuir sorption isotherm. From the slope and the intercept of the Langmuir plot, the values of K_L and q_m, respectively, are determined. These values, along with that of R^2, are listed in Table 5.1. The maximum uptake of cesium ions, q_m, is about 1.95 mg/g of the swollen KCoHCF-Gel beads. This capacity value will be ~15 mg/g, if the dry weight of the beads is considered.

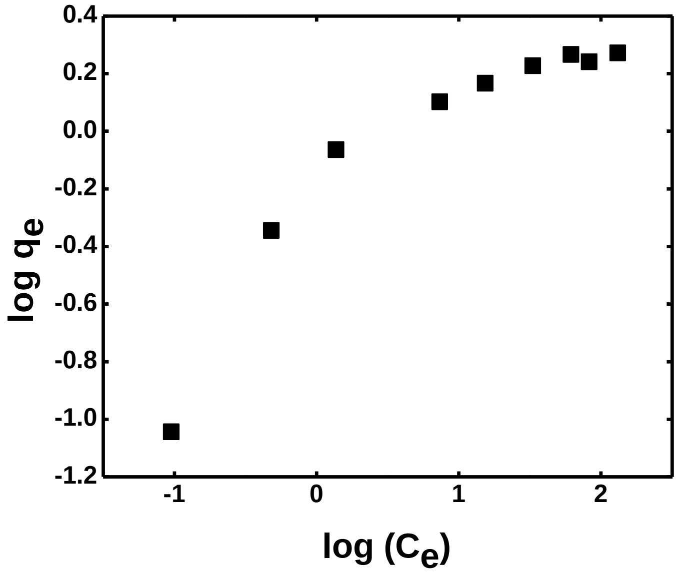

Fig. 5.8: Freundlich sorption isotherm plot for sorption of cesium ions onto KCoHCF-Gel beads at 293K

The favorability of sorption of Cs^+ ions onto the KCoHCF-Gel beads can also be expressed in terms of a dimensionless constant, (R_L), called separation factor, using the essential features of the Langmuir isotherm, as given below

$$R_L = 1/(1 + K_L C_o) \tag{5.12}$$

The parameter R_L indicates the nature of the sorption isotherm. Depending on the value of R_L, it is considered unfavorable ($R_L > 1$), favorable ($0 < R_L < 1$), irreversible ($R_L = 0$), or linear ($R_L = 1$) sorption. The calculated value of R_L, for the gel beads, lies between 0 and 1, for the concentration range investigated in this work, which indicates that the KCoHCF-Gel beads are good sorbent for Cs^+ ions, and the sorption process is favorable for efficient removal of Cs^+ ions from aqueous waste solutions.

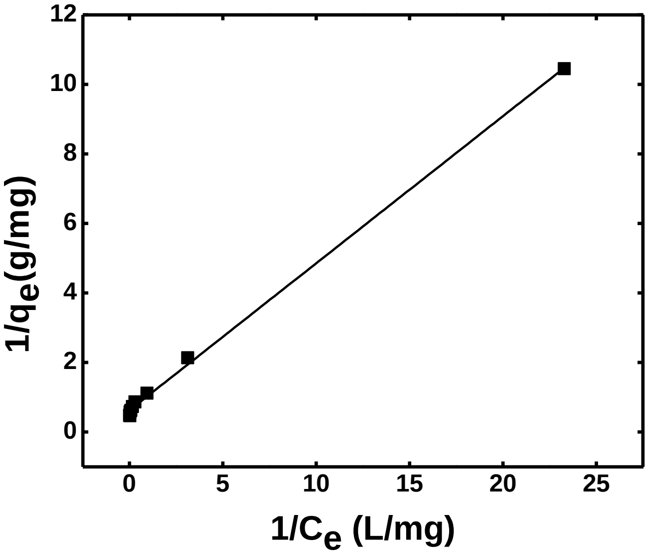

Fig. 5.9: Langmuir sorption isotherm plot for the sorption of cesium ions onto the KCoHCF-Gel beads at 293K

Table 5.1 Freundlich and Langmuir isotherm parameters for sorption of cesium ions onto the KCoHCF-Gel beads at 293K

Freundlich isotherm parameters			Langmuir isotherm parameters		
K_F (mg/g)	n	R^2	q_m(mg /g)	K_L (L /mg)	R^2
0.45	2.74	0.8210	1.952	0.05	0.9977

5.5.1.4 Sorption kinetics

The knowledge of the kinetics of sorbate uptake is required for selecting optimum operating conditions for a full-scale batch process.[203] Fig. 5.10 shows that the rate of sorption of cesium ions onto the KCoHCF-Gel beads is very fast initially, for all the initial metal ion concentrations taken; about 38-90% of the total cesium ions present initially get sorbed in ~ 40 minutes of equilibration in the studied concentration range of 1-20 mg/L. Thereafter, the sorption proceeds at a slower rate until equilibrium is reached. The equilibrium time is found to be ~180 min, for the initial cesium ion concentration range studied. The kinetics of the sorption process was analyzed, using different kinetic models, such as the pseudo first-order and the pseudo second-order models.

The kinetic data were first analyzed by the pseudo first-order rate expression given by the Lagergren, which, in the linerized form, can be written as [133]

$$\log(q_e - q_t) = \log(q_e) - \frac{k_1}{2.303}t \tag{5.13}$$

where q_t is the amount of the cesium ions sorbed at time t, and k_1 is the rate constant of the pseudo first-order sorption process. The values of k_1 and q_e can be determined from the slope and intercept, respectively, of the straight line plot of log (q_e - q_t) versus t.

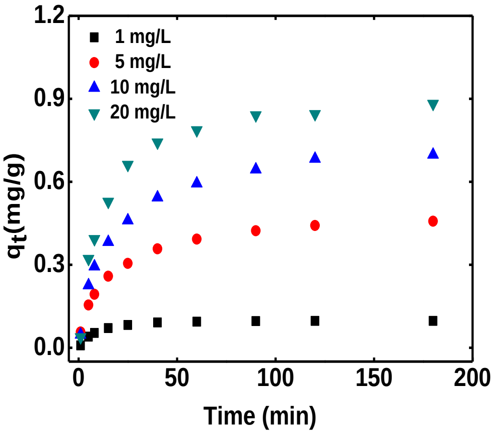

Fig. 5.10: Effect of contact time on the sorption of cesium ions onto the KCoHCF-Gel beads at different cesium ion concentrations

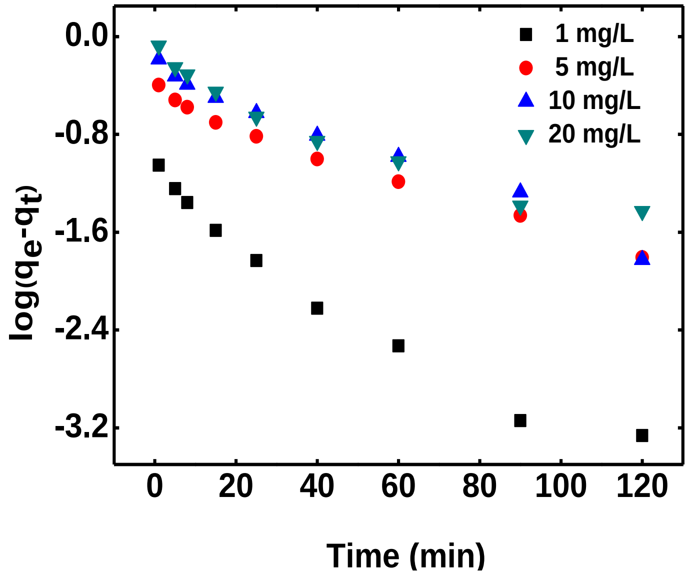

Fig. 5.11: Pseudo first-order kinetic plots for sorption of cesium ions onto the KCoHCF-Gel beads at different cesium ion concentrations

Fig. 5.11 shows that the pseudo first-order kinetics model does not apply for the entire sorption period investigated in this work. It is applicable only over the initial 1-60 min sorption period. After that, a considerable deviation of the plot of log (q_e - q_t) versus "time" from linearity is observed at different sorbate concentrations (Fig. 5.11). Thus, the model represents the initial stages well, where rapid sorption occurs, but cannot be applied to the entire studied time scale. A similar trend was previously observed by Ho and McKay, for sorption of dyes on peat particles.[204] Ho and McKay reported that the sorption data are represented well by the Lagergren first-order kinetic model only for the initial rapid sorption stage that occurs for a contact time of 0–30 min.[142, 156, 204]

Also from Table 5.2, it is evident that the values of the correlation coefficients for pseudo first-order rate model are not very good, for all the concentrations of cesium ions studied. Furthermore, the values of q_e calculated from the equation differ substantially from those measured experimentally. Thus, sorption of cesium ions onto KCoHCF-Gel beads cannot be explained satisfactorily by the pseudo first-order model.

Table 5.2: The pseudo first-order rate constants, theoretical and experimental q_e values for sorption of cesium ions onto the KCoHCF-Gel beads at different initial concentrations of cesium ions

C_o (mg/L)	k_1 (min^{-1})	$q_{e\ theoretical}$ (mg/g)	$q_{e\ experimental}$ (mg/g)	R^2
1	0.044	0.06	0.097	0.94791
5	0.027	0.32	0.457	0.98575
10	0.029	0.54	0.698	0.98239
20	0.026	0.55	0.882	0.92167

The kinetic data were further analyzed, using the pseudo second-order kinetic model proposed by Ho and McKay,[156] which is represented, in its linearized form, as

$$\frac{t}{q_t} = \frac{1}{k_2 q_e^2} + \frac{1}{q_e} t \qquad (5.14)$$

where k_2 is the rate constant of the pseudo second-order sorption process (g/mg min). The slope and the intercept of the plot of t/q_t versus t give the values of the constants q_e and k_2, respectively.

Fig. 5.12 shows the pseudo second-order plots for the sorption of cesium ions onto the KCoHCF-Gel beads. The results show that, at all the initial cesium concentrations investigated, and for the entire sorption period, the linear regression correlation coefficient R_2^2 values, obtained for fitting the sorption data to equation (5.14), are very high, >0.995, and the values of q_e thus calculated are in agreement with the experimental data (Table 5.3). The calculated q_e values increase with increase in the initial cesium ion concentration, and the pseudo second-order rate constant (k_2) decreases with increase in the initial concentration. The higher R_2^2 values suggest that the sorption data are well represented by the pseudo second-order kinetics, for the entire sorption period.

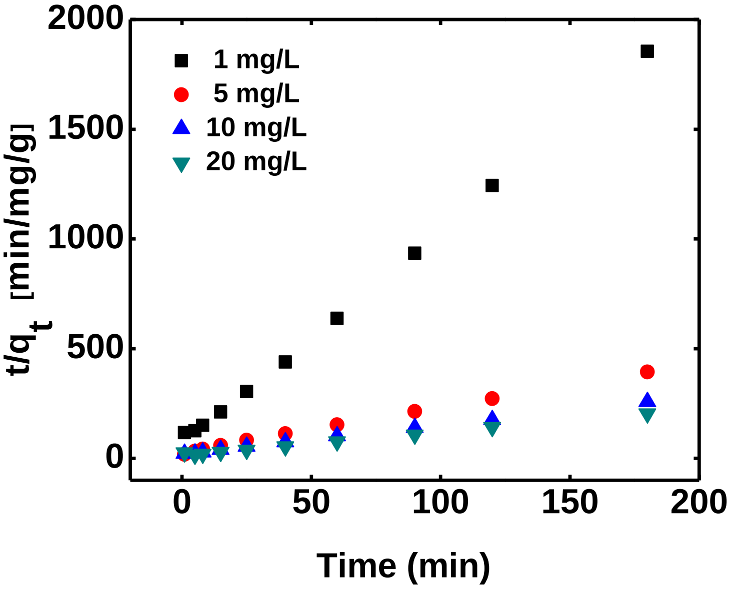

Fig. 5.12: Pseudo second-order kinetic plots for sorption of cesium ions onto the KCoHCF-Gel beads at different cesium ion concentrations

5.5.1.5 Mechanism

The experimental data were also analyzed by the intraparticle diffusion kinetic model, to find out whether the sorption process is described better by the film diffusion or the intraparticle diffusion. The prediction of the rate-limiting step is an important factor to be considered in the sorption process.[205] For a solid–liquid sorption process, the solute transfer is usually characterized by external mass transfer (film diffusion), or intraparticle diffusion, or a combination of both. The sorption of cesium ions onto the synthesized beads may be controlled by film diffusion at earlier stages, and later by the intraparticle diffusion. According to the Weber-Morris model, a plot of sorbate uptake q_t versus the square root of time, $t^{1/2}$, should be linear, if intraparticle diffusion is involved in the sorption system, and if the line passes through the origin, then the intraparticle diffusion is the only rate-limiting step. The intraparticle diffusion model is mathematically defined as [145]

$$q_t = K_{id}t^{1/2} + I \tag{5.15}$$

where K_{id} is the intraparticle diffusion rate constant (mg/g/min$^{1/2}$) and I gives an idea about the boundary layer thickness. The second gentle-sloped portion of the q_t vs $t^{½}$ plot is attributed to gradual sorption due to intraparticle diffusion (Fig. 5.13).

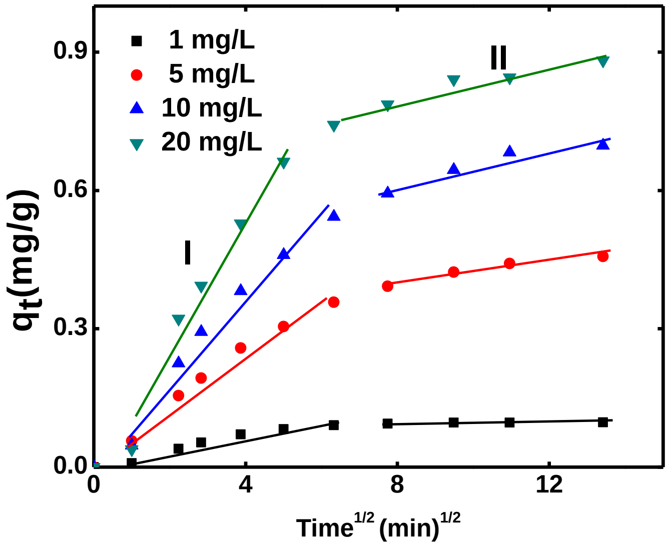

Fig. 5.13: Intraparticle diffusion plots for sorption of cesium ions onto the KCoHCF-Gel beads

The intraparticle diffusion rate is obtained from the slope of the second stage portion (Table 5.3). The K_{id} value is higher at the higher initial cesium ion concentrations. With decrease in the cesium ion concentration in the solution, the diffusion rate becomes lower and lower, and the diffusion process reaches the final equilibrium stage. The values of K_{id} and I determined for different Cs^+ ion concentrations are given in Table 5.3. The multilinearity of all the plots indicates some degree of boundary layer control, and also that intraparticle diffusion is not the only rate-limiting step. Therefore, in order to characterize what the actual rate-controlling step involved in the cesium sorption process is, the sorption data were further analyzed by the kinetic expression given by Boyd et al.,[146] the solutions of which, depending on the values of F, the fractional attainment of equilibrium, are

$$Bt = 2\pi - \frac{\pi^2 F}{3} - 2\pi\left(1 - \frac{\pi F}{3}\right)^{1/2} \tag{5.16}$$

$$Bt = -0.4977 - \ln(1 - F) \tag{5.17}$$

The value of Bt was calculated for each value of F, using Eq. (5.16), for F values upto 0.85, and, equation (5.17) was used for higher F values.[147] The calculated Bt values were plotted against time (Fig. 5.14). The linearity of this plot provides useful information to distinguish between the film diffusion and the intraparticle-diffusion rates of sorption.[148] A straight line passing through the origin is indicative of the sorption process being governed by intraparticle-diffusion mechanism.[149] All the plots obtained are linear, but do not pass through origin, indicating some degree of boundary layer control, and also that, the sorption process is of complex nature, consisting of both film diffusion and intraparticle diffusion, and rate of sorption is governed by film diffusion step.

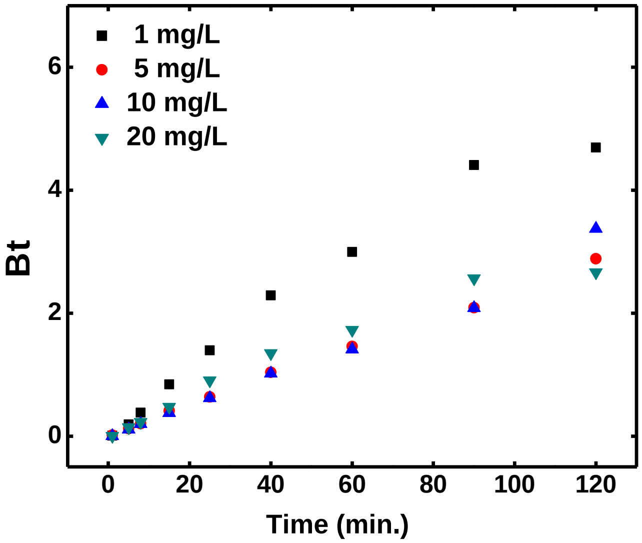

Fig. 5.14: Boyd's plots for sorption of cesium ions onto the KCoHCF-Gel beads

Table 5.3 The pseudo second-order rate constants, calculated q_e values and intraparticle diffusion values, for sorption of cesium ions onto the KCoHCF-Gel beads, at different initial cesium ion concentrations

C_o (mg/L)	k_2 (g/mg min)	R^2	q_e (mg/g) (calculated)	K_{id} (mg/gmin$^{1/2}$)	I (mg/L)
1	1.4144	0.9988	0.102	7.940×10^{-4}	0.280
5	0.1705	0.9985	0.483	0.0135	0.415
10	0.0932	0.9992	0.752	0.0222	0.636
20	0.0794	0.9950	0.952	0.0191	0.087

5.5.1.6 Effect of interfering ions

The influence of interfering cations (Na^+, Ca^{2+} and Ba^{2+}) on the sorption of cesium ions onto the KCoHCF-Gel beads was investigated, keeping the concentration of cesium ions constant (5 mg/L), and varying the concentration of Na^+, Ca^{2+} and Ba^{2+} ions, under neutral pH, at 298 K. Table 5.4 gives the effect of the metal ions on % removal of cesium ions from the solution. On increasing the concentration of the interfering metal ions from 0 to 32 mg/L, about 3 % decrease in the removal efficiency of the beads is observed in the case of Na^+ ions, whereas negligible decrease in the % removal of cesium ions is observed in the presence of Ca^{2+} and Ba^{2+} ions. The observed smaller decrease in the case of alkali metal ions could be due to the lower hydration energy of the cesium ions, which contributes to the selectivity of the sorbent for cesium. The effect of Ca^{2+} and Ba^{2+} ions on the sorption of cesium ions is very small, which could be due to the other processes involved, such as complexation, nonspecific surface sorption, or partial replacement of Ca^{2+}ions of the calcium alginate gel by Ba^{2+}ions.[183, 190] So, even in the presence of other metal ions, the % removal of cesium ions from the solution is quite good, which indicates that these beads can be used effectively for removal of cesium ions in the presence of the interfering metal ions also.

Table 5.4: Effect of interfering ion concentration on the sorption of cesium ions onto KCoHCF- Gel beads

Metal ion concentration (mg/L)	**% Removal of Cs^+ ion in presence interfering ions**		
	Na^+	**Ca^{2+}**	**Ba^{2+}**
0	88.33%	85.33%	85.33%
4	88.04%	83.86%	86.61%
16	86.90%	84.36%	86.47%
32	85.08%	85.17%	85.72%

5.5.2 KNiHCF-Gel beads

5.5.2.1 Characterization

The synthesized KNiHCF-Gel beads were characterized, for their thermal stability, water content, surface morphology and surface area, by using various techniques described below.

5.5.2.1.1 SEM & EDX study

Figs. 5.15(a) & (b), respectively, show the SEM images of the outer surface and a cross-section of a KNiHCF-Gel bead. The outer surface of the dried bead is quite rough, and some large pores are visible in the SEM image. The cross-sectional image of the bead shows the presence of pores of even smaller size. The peaks corresponding to K, Ni and Fe in the EDX spectrum confirms the presence of KNiHCF particles in the synthesized beads (Fig. 5.15(c)).

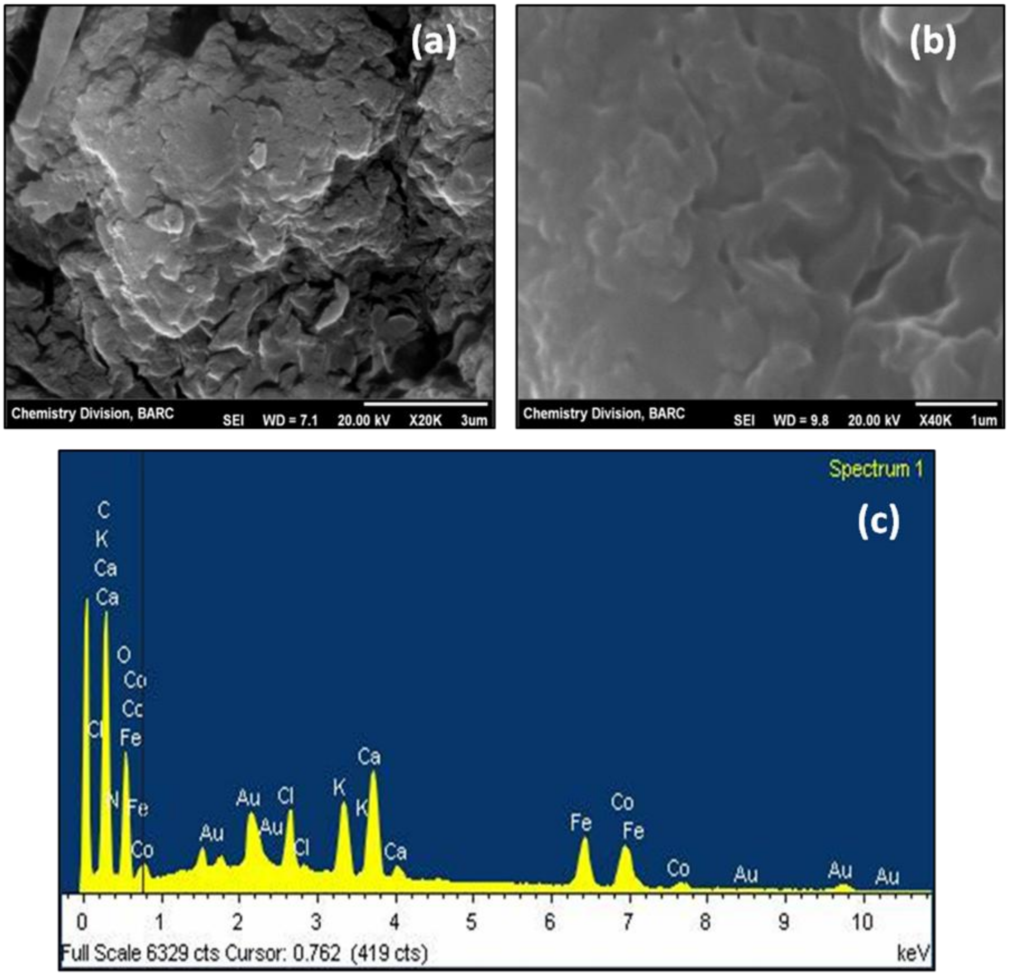

Fig. 5.15: SEM image of (a) the outer surface & (b) a cross-section of the KNiHCF-Gel beads; (c) EDX spectra of the KNiHCF-Gel beads

5.5.2.1.2 Thermogravimetric analysis

The thermal stability of the beads, and their water content, were determined by thermogravimetry. A known amount of the surface-dried swollen beads was heated in an alumina crucible, at a heating rate of 10 °C/min, in nitrogen atmosphere, from ambient conditions upto 750 °C. TGA profiles of the blank gel beads and the KNiHCF-Gel beads are shown in Fig. 5.16. In the TGA profile of the blank beads, a huge weight loss of ~ 85% is observed upto 150 °C, due to the loss of the absorbed water molecules. A degradation step is observed from 198 to 339 °C, corresponding to a very small weight loss of 2%. After 339 °C, a continuous degradation of the blank beads takes place, and at the end of 750 °C, ~ 11.6% charred mass is left. TGA profile of KNiHCF-Gel beads is similar to that of the blank alginate beads. The first weight loss step, corresponding to the loss of the absorbed and structural water (87%), is observed upto 150 °C. Then, the degradation step is observed from 200 to 324 °C, with a small weight loss of ~2%. The shifts of about +2 °C in the onset temperature and -15 °C in the offset temperature are observed in the TGA profile of the sorbent beads, as compared to that of the blank beads. These shifts could be due to the presence of the KNiHCF particles in the polymeric matrix. At the end of 750 °C, 9.5 % of the mass is left as a residue.

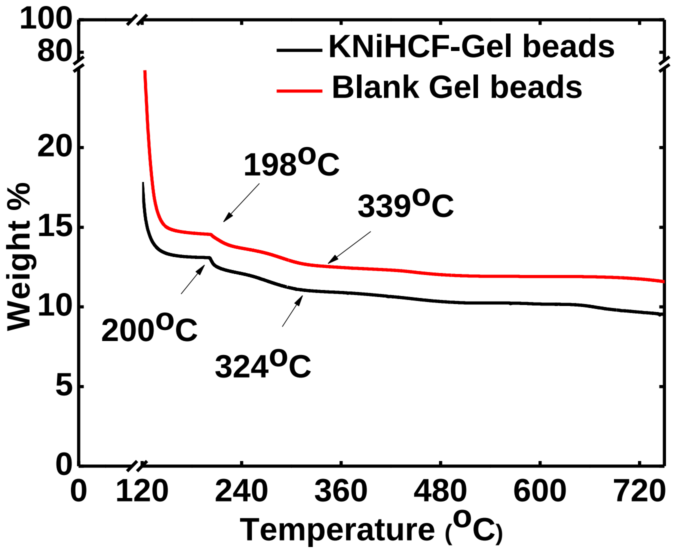

Fig. 5.16: TGA profiles of the blank alginate beads and the KNiHCF-Gel beads

From these results, it can be inferred that the sorbent beads are stable upto ~200 °C, and the water content (87%) of these beads is much higher as compared to that of the sorbents reported in literature, which are prepared by using conventional supports.[183] These synthesized sorbent-hydrogel composite beads are expected to have faster kinetics for sorption of the metal ions from the aqueous waste solutions, as compared to that for the conventional polymeric composites.

5.5.2.1.3 XRD Study

The X-ray powder diffraction (XRD) pattern of the synthesized KNiHCF-Gel beads was recorded, using CuKα radiation. The diffraction pattern obtained had broad diffraction peaks, indicating amorphous nature of the KNiHCF particles. The main diffraction peaks were observed at 2θ values of 15.19°, 17.56°, 25.05° and 35.49, which match well with those reported for $K_2Ni[Fe(CN)_6]$ (JCPDS Card No. 20-0915). So, the results of the XRD study confirmed the presence of amorphous KNiHCF in the synthesized beads.

5.5.2.1.4 BET Surface area analysis

The specific surface area and the pore volume of the beads were determined by BET N_2 adsorption method. The surface area was determined to be 178.97 m^2/g, and the pore volume was found to be 0.564 cc/g. The surface area and the pore volume measured are for the dried beads, but the actual extraction experiments are carried out using swollen beads. Therefore, the effective surface area and the pore volume of the swollen beads are expected to be much higher, which will give higher sorption capacity.

5.5.2.2 Sorption studies

KNiHCF has a cubic structure (FCC), in which iron and Ni ions are located at the corners of the elementary cubes, and cyano groups are present on the edges. The exchangeable potassium ions are located in the body center. The lattice parameter ‘a’ of the unit cell is 1.012 nm for KNiHCF, which gives it ion-sieving ability towards larger hydrated ions, and is also responsible for its selectivity towards cesium ions.[198] Therefore, sorption of cesium ions onto the KNiHCF particles takes place by ion-exchange mechanism, in which generally, potassium ion of KNiHCF is exchanged by cesium ion. The synthesized sorbent beads, being hydrogel in nature, have high water content, and can freely exchange their water with that in the aqueous waste solution outside. Thus, it is expected that all the KNiHCF particles, even present deep inside the beads, to be accessible and contributing in the removal of cesium ions, by the ion-exchange process. The sorption capacity of the blank polymer beads was determined at cesium ion concentration of 5 mg/L, keeping mass of the blank polymer beads and the sample volume same, as in the case of the sorbent beads. The q_e value for the blank polymer beads was determined to be 0.002 mg/g of the swollen beads. This capacity value is very low, hence, the sorption due to the polymeric binding matrix can be assumed to be negligible in all the sorption experiments. The synthesized beads were used, to remove cesium ions from its aqueous solution, and the effect of pH, sorbent dose, interfering ions and cesium ion concentrations on the sorption efficiency of the beads was investigated.

5.5.2.2.1 Effect of sorbent dose

The effect of the sorbent dose on the percentage removal of cesium ions from its solution is shown in Fig. 5.17 (a). With increase in the mass of the sorbent beads, a gradual increase in the percentage removal values is observed. With the increase of sorbent dosage, from 2 to 40 g/L, the percentage of cesium ions sorbed increases from 30 to 99.9%. The increase in the percentage removal can be due to the fact that the high sorbent dosage offers more number of active sites and surface area, for sorption of cesium ions. However, the determined sorption capacity value decreases with increase in the sorbent dose (Fig. 5.17 (b)). The main reason for the decrease in sorption capacity is the decrease in the fraction of occupied sites in the sorbent due to fixed number of the sorbate ions initially present in the solution. This capacity is given by equation (5.8). The additional effect could be due to the interference between the binding sites at higher sorbent doses. [201-202] Therefore, an optimum sorbent dose of 0.05g per 5 ml of the sorbate solution, i.e, 10g/L, was chosen for the subsequent experiments.

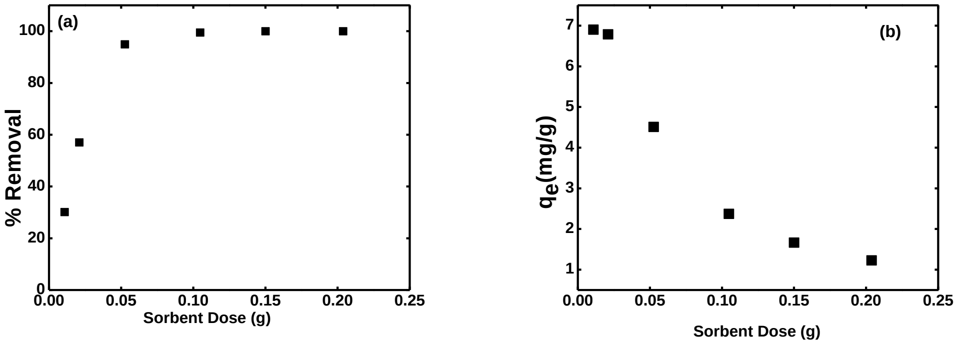

Fig. 5.17: Effect of sorbent dose on the (a) % removal of cesium ions, and (b) sorption capacity of the KNiHCF-Gel beads for cesium ions

5.5.2.2.2 Effect of pH

The effect of pH on the equilibrium uptake capacity was studied, by varying pH of the sorbate solution, using dilute NaOH and HNO_3. From Fig. 5.18, it can be seen that, q_e value does not change much in the pH range 1-12. These results suggest that these beads can be used effectively for sorption of cesium ions over a wide pH range.

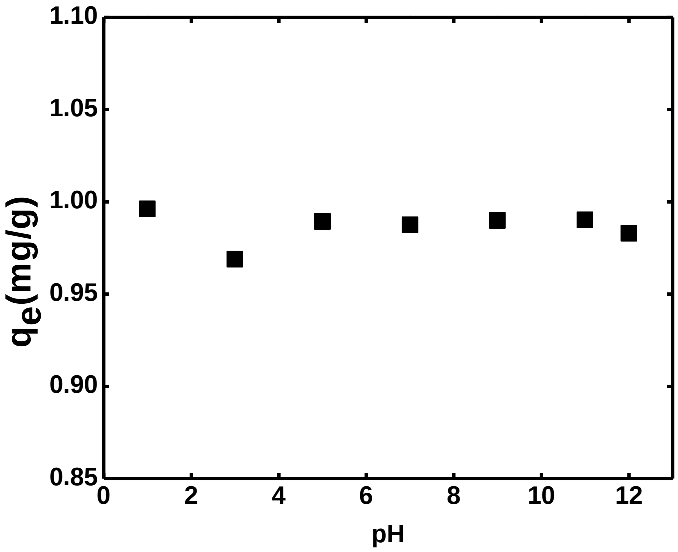

Fig. 5.18: Effect of pH on the sorption of cesium ions onto the KNiHCF-Gel beads

5.5.2.2.3 Effect of cesium ion concentration

The effect of cesium ion concentration on the sorption capacity of the beads was studied, by varying the initial concentration of cesium ions from 1 to150 mg/L, in neutral solution. Fig. 5.19(a) shows the effect of initial cesium ion concentration on the sorption capacity (q_e). A gradual increase in the sorption capacity of the beads is observed upto cesium ion concentration of about 80 mg/L, and thereafter, the q_e value starts saturating. The q_e value of 7.19 mg/g, of the swollen beads is observed at the highest studied C_o value of 150 mg/L. However, the percentage uptake shows a decreasing trend, as the initial concentration of the cesium is increased (Fig. 5.19(b)). The maximum capacity, in terms of the dry weight of the sorbent beads, will be almost eight times more than the value of 7.19 mg/g obtained for the swollen beads, as these contain 87% water. The initial cesium ion concentration plays an important role in the uptake of cesium by the beads, by providing necessary driving force to overcome all the mass resistances from the liquid to the solid phase. But, when the concentration of cesium ions becomes very high, the competition between the cesium ions, for interacting with the active sites, also intensifies, and further uptake of cesium ions decreases, due to lower number of the vacant sites available on the sorbent beads.

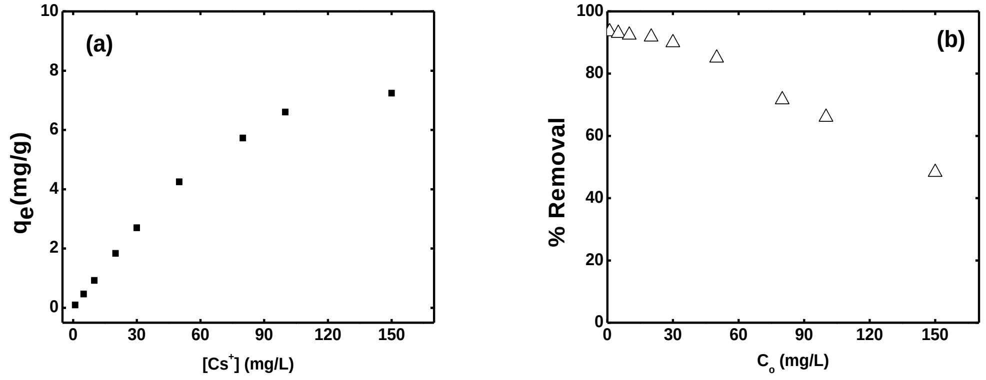

Fig. 5.19: Effect of cesium ion concentration on the sorption of cesium ions onto the KNiHCF-Gel beads

5.5.2.3 Sorption isotherms

Application of the sorption isotherm models to the sorption data are helpful in describing how the solute interacts with the sorbent, and hence, helps in optimizing the conditions for efficient use of the sorbent. The experimental isotherm data were analyzed by the Langmuir and the Freundlich isotherms.[154, 206] The Langmuir sorption isotherm is the simplest isotherm model for sorption of a solute from a liquid solution onto a surface, containing a finite number of identical active sites, and assumes monolayer sorption.[154] The data were fitted to the linearized form of the Langmuir model, equation (5.11). The plot of $1/q_e$ vs $1/C_e$ is a straight line (Fig. 5.20), with correlation coefficient (R^2) value of 0.9999, which indicates a good correlation between the experimental data and the Langmuir sorption model. The values of q_m and K_L can be determined from the intercept and the slope, respectively, of the plot. The maximum monolayer sorption capacity, q_m, of the beads, for Cs^+ ions, is determined to be 6.86 mg/g of the swollen beads.

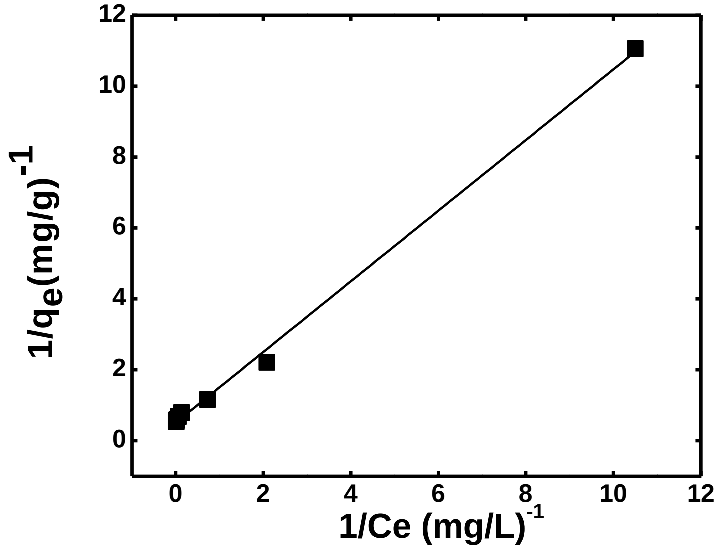

Fig. 5.20: Langmuir sorption isotherm plot for sorption of cesium ions onto the KNiHCF-Gel beads at 293K

The favorability of the sorption of Cs^+ ions onto KNiHCF-Gel beads was checked, by calculating separation factor (R_L), given by equation (5.12). Fig. 5.21 depicts the plot of the calculated R_L values at different initial cesium ion concentrations. All the R_L values, for the synthesized beads, lie between 0 and 1, indicating that the sorption of cesium ions onto the beads is favorable for efficient removal of Cs^+ ions from aqueous waste solutions under the studied conditions.[207] However, a steep decrease in the R_L values is observed with the increase in the initial concentration, from 1 to 50 mg/L. This indicates that the sorption of cesium ions onto the beads is more favourable at higher initial cesium ion concentrations.

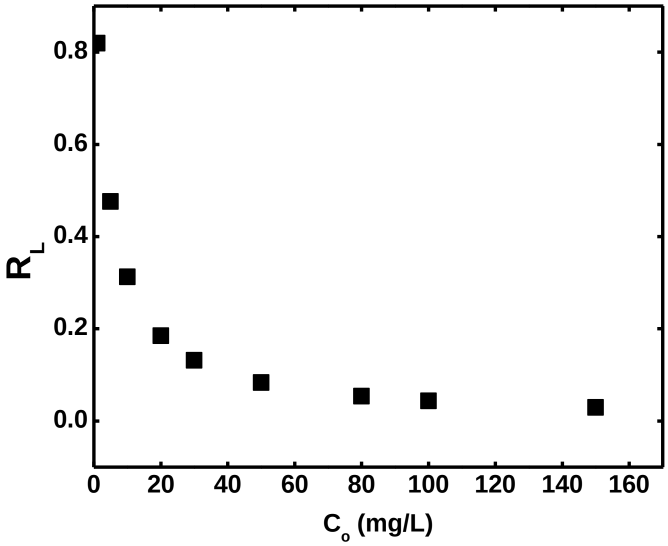

Fig. 5.21: Effect of initial cesium ion concentration on the R_L value at 293K

The Freundlich isotherm is well known, and is one of the oldest empirical sorption model. It assumes that all the active sites on the sorbent are not equal, and the stronger binding sites are occupied first, and that the binding strength decreases with the increase in the degree of site occupation. The data were analyzed, using the linerized form of the Freundlich isotherm, given by equation (5.10). Fig. 5.22 shows the plot of log (q_e) vs log (C_e). The value of K_F and n are determined by fitting the sorption data to equation (5.10), with correlation coefficient (R^2) value of 0.9186, are 0.89 mg/g and 1.66, respectively. R^2 value of 0.9186 suggests a poor correlation between the experimental data and the Freundlich isotherm model, as compared to that with the Langmuir sorption model. The results of both the sorption isotherm studies are summarized in Table 5.5.

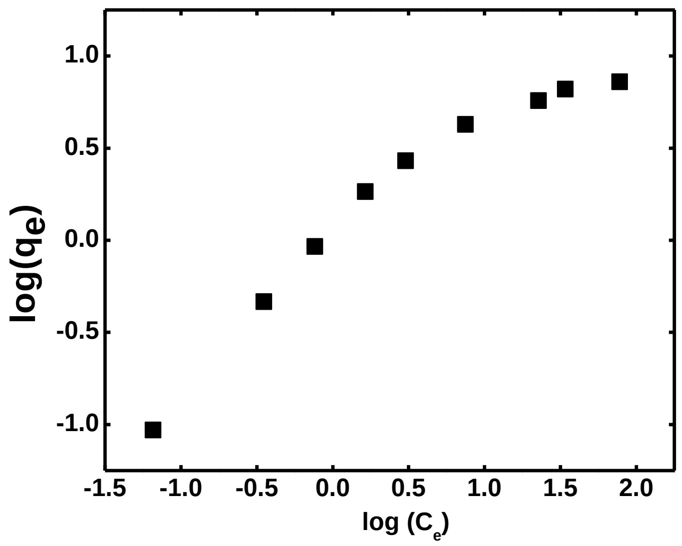

Fig. 5.22: Freundlich sorption isotherm plot for the sorption of cesium ions onto the KNiHCF-Gel beads at 293K

Table 5.5: Langmuir and Freundlich isotherm parameters for sorption of cesium ions onto the KNiHCF-Gel beads at 293K

Langmuir isotherm constants			**Freundlich isotherm constants**		
K_L (L /mg)	**q_m(mg /g)**	**R^2**	**n**	**K_F (mg/g)**	**R^2**
0.22	6.86	0.9999	1.66	0.89	0.9186

5.5.2.4 Sorption kinetics

The sorption of metal ions onto the polymeric composites is a complex process, and the rate of uptake of the metal ions depends upon the physical properties of both the sorbate and the sorbent. Fig. 5.23 shows the effect of contact time on the sorption of cesium ions onto the synthesized beads, at different initial cesium ion concentrations. It is observed that the amount of cesium ions sorbed onto the beads increases with increase in the initial cesium ion concentration. A major fraction (~ 90 %) of the cesium ions, present in the solution, is sorbed within the first 40 min. This could be due to the fact that, after the initial fast sorption, the competition for the available active sites intensifies greatly, and the rate of sorption starts decreasing until equilibrium is reached. The kinetic sorption data were analyzed, using different kinetic models, such as the pseudo first-order and the pseudo second-order models, in order to understand the sorption rate law for sorption of cesium ions onto the beads.

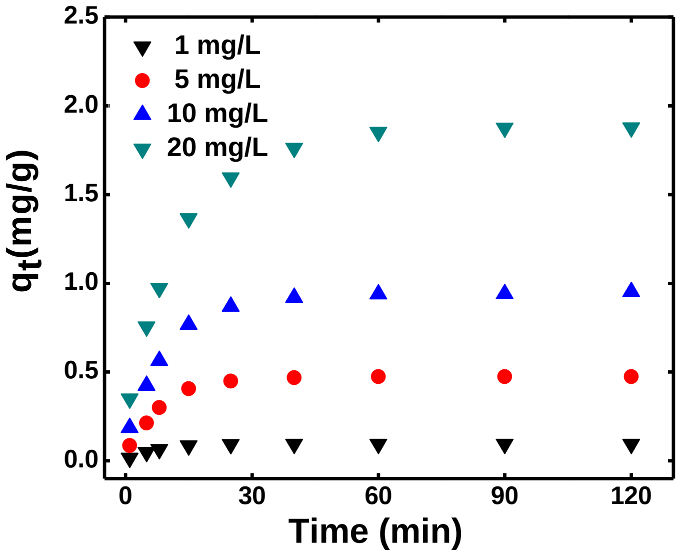

Fig. 5.23: Effect of contact time on the sorption of cesium ions onto the KNiHCF-Gel beads at different cesium ion concentrations

The kinetic data were analyzed, using the pseudo first-order model equation (5.13), and the pseudo second-order model equation (5.14).The values of k_1 and q_e obtained by fitting the sorption data to the pseudo first-order kinetic model, along with that of the R^2 are given in Table 5.6. The pseudo-second-order rate constants k_2 and q_e, respectively, can be determined from the slope and the intercept of the straight line plot of t/q_t vs t (Fig. 5.24(b)). These values of k_1, k_2, R^2 and q_e, determined from pseudo first-order and the pseudo second-order rate models are given in Table 5.6. The R^2 values for the pseudo first-order model are quite small as compared to those for the pseudo second-order rate model. Moreover, the equilibrium capacities, q_e, obtained from pseudo second-order rate model are closely in line with the experimental values. Therefore, it can be concluded that, the sorption of cesium ions onto the sorbent beads follows pseudo second-order kinetics for the entire period of time, and for all the studied initial concentrations.

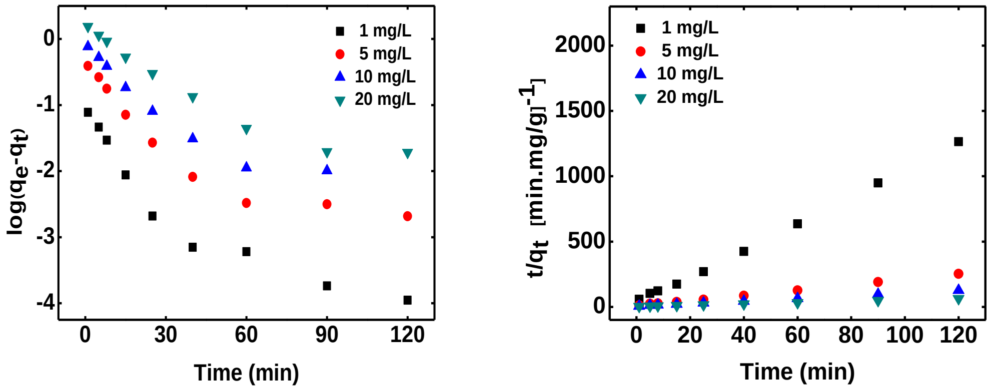

Fig. 5.25: (a) Pseudo first order and (b) pseudo second order kinetic plots for sorption of cesium ion onto the KNiHCF-Gel beads at different cesium ion concentrations

Table 5.6: The pseudo first-order and pseudo second-order rate constants, and theoretical and experimental q_e values, for the removal of cesium ions by the KNiHCF-Gel beads, at different initial concentrations

C_o (mg/L)	Pseudo first-order			Pseudo second-order			q_e experimental (mg/g)
	k_1 (min^{-1})	R_1^2	$q_{e(1)}$ Theoretical (mg/g)	k_2 (g/mg min)	R_2^2	$q_{e(2)}$ Theoretical (mg/g)	
1	0.054	0.8278	0.026	3.572	0.9993	0.097	0.095
5	0.447	0.7988	0.161	0.539	0.9992	0.490	0.477
10	0.052	0.8731	0.473	0.238	0.9994	0.987	0.950
20	0.039	0.9076	1.014	0.083	0.9992	1.974	1.896

5.5.2.5 Mechanism

The transport of the sorbate from the solution phase to the sorbent particles takes place gradually, and involves many steps.[148] These steps include external or film diffusion and intraparticle diffusion. To study the mechanistic steps involved in the present sorption system, the kinetic data were analyzed, using intraparticle diffusion model (equation 5.15) According to this model, a plot of the uptake q_t versus the square root of time $t^{1/2}$ should be linear, if intraparticle diffusion is involved in the sorption process, and if the line passes through the origin, then, the intraparticle diffusion is the only rate-limiting step. From Fig. (5.25), it can be seen that the plots of q_t vs $t^{1/2}$ are multilinear, each with a sharp slope for the initial fast sorption stage, and a gentle slope for the second relatively slower sorption stage. The values of K_{id} and I are determined from the slope and intercept of the second stage, and given in Table 5.7.

The results from this model imply that the intraparticle diffusion is also involved in the sorption of cesium ions onto the beads, but it is not the only rate governing step. Therefore, in order to understand the steps involved in the sorption process, the sorption data were further analyzed by the solutions, equation (5.16) and (5.17), of the kinetic expression given by Boyd et al. The calculated Bt values were plotted against time (Fig. 5.26). The linearity of the plots provides useful information to distinguish between the film diffusion and intraparticle diffusion-controlled rates of sorption.[148] A straight line passing through the origin is indicative of sorption process governed by intraparticle-diffusion mechanism, otherwise, it is governed by film diffusion.[149] In the present case, the plots were reasonably linear, but do not pass through the origin, indicating towards the complex nature of the sorption process, and involvement of film diffusion in the mechanistic step.

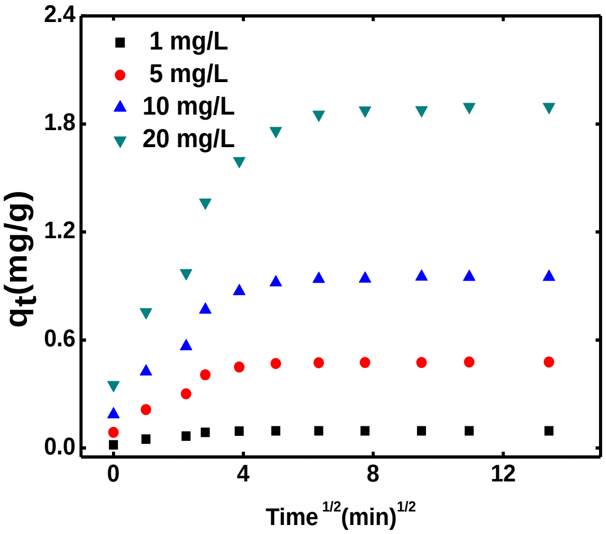

Fig. 5.25: Intraparticle diffusion plots for sorption of cesium onto the KNiHCF-Gel beads

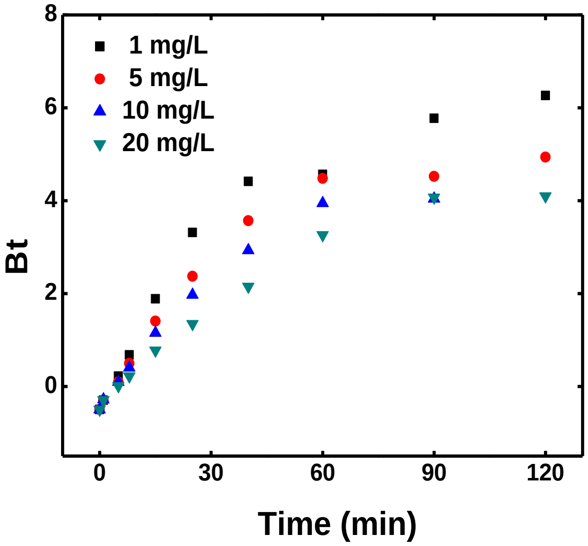

Fig. 5.26: Boyd's plots for sorption of cesium ions onto the KNiHCF Gel beads at different initial cesium ion concentrations

Table 5.7 The intraparticle diffusion parameters, at different initial concentrations of cesium ions, for its removal by the KNiHCF-Gel beads

C_o (mg/L)	K_{id} (mg/g/min$^{1/2}$)	I (mg/L)
1	1.06x 10^{-4}	0.093
5	9.88x 10^{-4}	0.463
10	0.004	0.901
20	0.016	1.697

5.6 Comparison of the Sorbent Beads

In this study, KCoHCF and KNiHCF-loaded hydrogel beads were synthesized, using cross-linked alginate as a polymeric matrix. The metal hexacyanoferrate (MHCF) particles were prepared in the presence of PVA, which acts as stabilizer. It was observed that, size of these MHCF particles can be effectively controlled by using PVA stabilizer. The loadings of KCoHCF and KNiHCF in the gel beads were different. But, still there was only a slight difference in their thermal stabilities and water contents. KCoHCF-Gel beads contained 87% water, and were stable upto 202°C, whereas KNiHCF-Gel beads contained 89% as absorbed water, and were stable upto 200°C. The XRD patterns of both the sorbents confirmed amorphous nature of the respective constituent MHCF particles. The surface morphology, as viewed in SEM images, appeared to be similar for both the types of the beads. The images of the outer surface and the cross-sectional part suggested rough surface and porous nature of the beads. However, the surface area of the KNiHCF-Gel beads was found to be considerably less than that of the KCoHCF-Gel beads. This could be due to the lower loading of KCoHCF in the KCoHCF-Gel beads. The higher polymeric content in the beads might have made the surface of the beads more porous, leading to the higher surface area. But, the lower loading of the active component, i.e, MHCF particles, is reflected in the observed lower sorption capacity for cesium ions. The effect of sorbent dose in the sorption of cesium ions was also different for both of the sorbents beads. In the case of KCoHCF-Gel beads, the equilibrium sorption capacity, q_e, of the KNiHCF-Gel beads increased with the increase in the sorbent dose initially, and then, started decreasing. Whereas, in the case of the KNiHCF-Gel beads, there was a continuous decrease in the q_e value under the studied experimental conditions. This could be due to the equilibrium not being attained in the contact time at lower sorbent dose in the case of the KCoHCF-Gel beads due to slower sorption kinetics. The sorption capacities of both of the sorbents were found to be unaltered in the pH range 1-12. The sorption isotherm data were explained best by the Langmuir sorption isotherm, and the sorption process was found to follow pseudo second-order kinetics. The kinetics of sorption was faster in the case of KNiHCF-Gel beads. The mechanism of sorption process, investigated by using intraparticle diffusion model and Boyd's plot, suggests that sorption of cesium ions onto both these sorbent beads is a complex process, with film diffusion as the rate limiting step.

5.7 Conclusion

In this study, hydrogel beads were synthesized by using cross-linked alginate containing PVA, as a binding matrix. The size of the KNiHCF and the KCoHCF particles was controlled by reacting the precursors in aqueous medium, in the presence of aqueous solution of PVA, which acts as a stabilizer. The characterization of the synthesized beads suggests that the beads are quite porous and hydrophilic, with high water content and large surface area. The efficiency of the beads for removal of cesium ions from the waste waters was evaluated under various experimental conditions. The results of the sorption study indicate that, the beads can be used effectively for removal of cesium ions over a wide pH range 1-12. The maximum sorption capacities of the dry beads of the KCoHCF-

Gel beads and the KNiHCF-Gel beads were determined to be ~ 15 mg/g and ~ 63 mg/g, respectively. The equilibrium sorption data were best explained by Langmuir sorption isotherm, and the pseudo second-order kinetics was followed for the studied initial cesium ion concentrations. The mechanism of the sorption of the cesium ions onto the beads was found to be complex, including intraparticle diffusion and film diffusion steps, with the latter being the rate limiting step.

Chapter-6

Mesoporous Titania Beads

6.1 Introduction

Titanium dioxide (titania) has attracted a considerable interest in the last couple of decades because of its excellent performance as catalyst, sensor, energy converter, an alternative support material to silica, for column packing in HPLC, etc. [208-211] Titania is also known to be a good adsorbent for toxic metal ions, like Cs^{+}, As^{3+}, Pu^{4+}, etc. [212-214] Titania has a stable chemical structure, and it is biocompatible, nontoxic and cost effective. It is the most commonly used photo-catalyst for degradation of many organic contaminants, such as dyes and volatile organic compounds.[215-216] As we know, the dye pollutants from the various industries, such as textiles, rubber, paper, plastics, cosmetics, etc., are some of the main sources of environmental contamination, which have strong impact on the ecosystem. Many techniques are employed to remove dyes from waste waters. These techniques include coagulation and/or flocculation, membrane technologies, such as reverse osmosis, nanofiltration and dialysis, chemical oxidation technologies, including Fenton's reagent with hydrogen peroxide, photocatalysis with UV radiation), biochemical oxidation and adsorbents utilization, e.g., activated carbon, inorganic adsorbents, such as silica, clays, synthetic ion-exchange resins, chitin-based adsorbents and other similar ones.[217-219] Among these, the photo-degradation of dyes is one of the effective and popular way. Many researchers across the globe have used titania in different forms as photo-catalyst for degradation of various dyes. The advantage of photo-degradation is that it can break these into carbon dioxide, water and some simple acids, using easily available photons.[220] Photo degradation, using titania as photo-catalysis, can take place by either excitation of titania or excitation of the dye, depending on the photon energy vis-à-vis band gap of titanium dioxide and absorption spectra of the dye.

Another major problem associated with industrial waste is the heavy metal ion pollutants, like cadmium, mercury, lead, arsenic, etc. Especially, arsenic contamination in potable water is the burning issue in the East Asian region.[221] Long-term exposure to inorganic arsenic compounds from drinking water may lead to various diseases, such as conjunctivitis, hyperkeratosis, hyper pigmentation, cardiovascular diseases, disturbances in peripheral vascular and nervous systems, skin cancer, gangrene in the limbs, etc.[221-222] There are several methods available for removal of arsenic from water in large conventional treatment plants. The most commonly used technologies include oxidation, co-precipitation, sorption onto coagulated flocs, or sorptive media, lime treatment, ion exchange resins and membranes.[223-226] The physical form of the resin is very important for its effective utilization. For applications in waste water treatment, like degradation of dyes and removal of toxic ions, it is beneficial to have titania in the form of spherical beads of good mechanical strength and porosity. An additional advantage of the bead-form is their easy separation from waste water, after the treatment, whereas separation and reuse of TiO_2 powder is difficult and tedious due to its fine morphology. Therefore, extensive work is going on, to develop new methodologies for the synthesis of titania in granular form, with good control over its crystallinity and physical properties, like mechanical strength, porosity, interconnectivity of pores, high surface area, etc.

Antonelli and Ying were the first to report synthesis of mesoporous titania.[227] Since then, several works have been published on different strategies to prepare titania, with tailored porosities. These include polymerization-induced colloid aggregation (PICA), oil emulsion method (OEM) and spray-drying method.[209, 228-230] These techniques have some disadvantages, like broad particle size distribution, smaller pore diameter and poor pore connectivity. For catalytic applications, pore size, surface area and pore connectivity are very important parameters, and control over these can be achieved by sol-gel templating method. In a typical procedure, the sacrificial template is put, along with the precursor, to allow its infiltration into the pre-formed interstices, and subsequent removal of the template by calcination, or extraction. Meyer and co-workers prepared porous titania beads, employing commercial polystyrene beads as a template.[231] These commercial beads are costly, and are of some specific sizes only. In addition, the beads has poor mechanical strength. These shortcomings seriously affect their use in various applications, like in chromatographic packings and column operations, involving many extraction-stripping cycles.

The present chapter describes the synthesis of mesoporous titania spherical beads, using calcium alginate beads as a sacrificial template, and titanium (IV) isoporpoxide (TIP) as titanium precursor. Removal of the template has been carried out in different atmospheres and at different temperatures, to observe their effect on the physical properties of the synthesized titania microspheres. These beads have a diameter of ~0.5 mm. The method is simple and highly reproducible. The application of these mesoporous beads have been demonstrated by photo-catalytic degradation of methylene blue dye by visible light.

6.2 Materials

Sodium alginate, calcium chloride, ethanol and isopropyl alcohol (IPA) were purchased from SD Fine chemicals, India. Methylene blue was obtained from Fisher Scientific. Arsenous oxide of 99% purity and titanim (IV) isoporpoxide (TIP) of 97% purity were obtained from Alderich and Merck, respectively. Commercial P25-TiO_2 powder, procured from local market, was used for comparative degradation experiments. All the other solvents and the chemicals used were of analytical grade. Nanopure water, with conductivity < 0.3 μS/cm, obtained from Millipore-Q water purification system, was used for the preparation of aqueous solutions.

6.3 Synthesis of Titania Microspheres

Aqueous solutions of sodium alginate, with three different weight percentages, were prepared, by dissolving 2.0, 1.4 and 0.8 g of sodium alginate, each in 100 ml of water. The sodium alginate solution was dropped into a calcium chloride solution (2.0%) through a 0.8 mm internal diameter syringe needle, forming gelified calcium alginate microspheres (A1). Similarly, other calcium alginate microspheres, A2 and A3, were prepared, using the 1.4% and 0.8 % polymer solutions, respectively. The average size of these beads was ~2 mm. If required, the alginate beads of much smaller size can be produced by using a syringe needle of appropriate internal diameter and an electromagnetic drop breaking mechanism. The beads were kept overnight in the calcium chloride solution, for complete curing, washed with water, and then, dehydrated by equilibrating with ethanol and IPA successively, to obtain IPA-swollen alginate beads, M1, M2 and M3, from A1, A2 and A3 beads, respectively. Fig. 6.1 illustrates schematic of the sol-gel templating procedure employed for the synthesis of the titania beads, from the IPA swollen beads, along with the optical microscope images of the corresponding products.[232]

In the first step, IPA-swollen alginate beads were equilibrated with TIP. For this, the IPA-equilibrated alginate microspheres, M1, M2 and M3, were soaked in the 97% TIP solution, for 48 hours, at room temperature in different containers, under closed conditions. The TIP molecules diffused into the interwoven polymeric matrix. The beads were separated from the solution. In the second step, TIP impregnated in the beads was hydrolyzed, by equilibrating with excess of water, for 24 hours. During this process, polycondensation took place inside the polymeric matrix. Thereafter, these beads were washed with water, to remove loose titanium hydroxide present on the surface of the beads. Then, the polymeric template was burnt off, and the inorganic precursor crystallized, forming a dense inorganic network of titanium dioxide in the form of beads (T1, T2 and T3). To study the effect of temperature and calcining atmosphere on the physical characteristics of the synthesized beads, these alginate-titanium hydroxide composite microspheres were calcined upto different temperatures (400, 700, 1000 and 1200 ºC) in different atmospheres (N_2, O_2 and air), at a heating rate of 10 ºC/min.

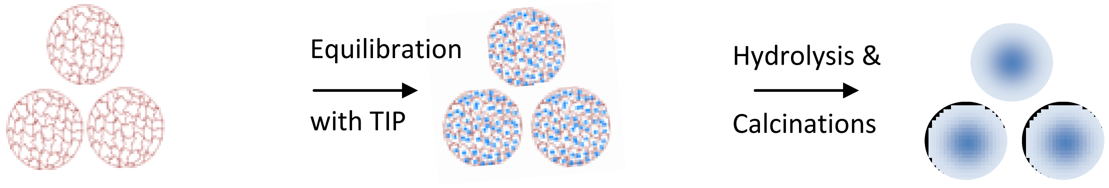

IPA-equilibrated calcium alginate beads (M1/M2/M3) TIP-loaded alginate beads Titania beads (T1/T2/T3)

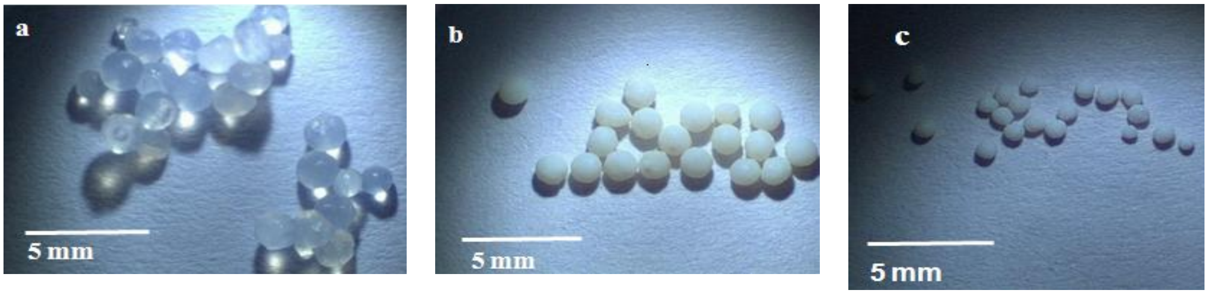

Fig. 6.1: Schematic diagram of the sol gel templating procedure, and optical microscope images of the beads at the corresponding steps at 10x magnification

6.4 Photo-catalytic Activity

Photo-catalytic activity of the synthesized titania beads was evaluated, by investigating photo-degradation of methylene blue (MB), in the presence of the anatase titania beads T1, obtained by calcining TIP-saturated M1 beads at 700 °C under air atmosphere. The aqueous solution of MB (20 µM), in a quartz cell, in air atmosphere, was irradiated in a photo-reactor in the presence and absence of the titania beads (50 g/l). The samples were irradiated in a circular chamber of internal diameter 44 cm and height 46 cm, fitted with eight ordinary day-light fluorescent lamps (Wipro, 36 W each, emissive length of the tube ~37 cm, and radius 1.5 cm) symmetrically on the walls. The spectrum of the lamp consisted of fluorescent emission, predominantly in the visible region, along with a UV contribution of ~3%. Photo-degradation of MB dye was quantified, by recording the change in the optical absorption at λ_{max}= 664 nm (ε=74028 $M^{-1}cm^{-1}$).

6.5 Results and Discussion

6.5.1 Characterization

Typical optical microscope (OM) images of IPA-equilibrated alginate beads, M1, and the corresponding TIP-impregnated beads are shown in Figs. 6.1(a) & (b), respectively. These beads are spherical in shape. The diameter of IPA and TIP-equilibrated beads are ~1.5 and ~1.0 mm, respectively. The diameter of the IPA equilibrated alginate beads is reduced by ~0.5 mm, on equilibration with TIP, i.e., the size of TIP equilibrated beads is ~75% of the original size, and its volume is reduced to ~43% of the original volume. When these beads were suspended in water, these almost swelled back to their original size. These results indicate that, the alginate microspheres have a large number of voids, which allow easy infiltration of the precursor molecules inside, and the shrinking property checks leaching of the precipitated solid out of the matrix. These characteristics strongly support candidature of the alginate beads as a templating material. Fig. 6.1(c) depicts the OM image, of the titania microspheres, T1, which indicates spherical shape of the beads. But, there is a considerable shrinking from the original size. The size of the calcined titania beads is ~ 0.5 mm, which is ~ 25% of the original size (~2.0 mm) of the water-swollen calcium alginate beads used as the template.

Shrinkage is a commonly observed phenomenon in the sol-gel synthesis of titanium oxide also.

6.5.1.1 Thermogravimetric analysis

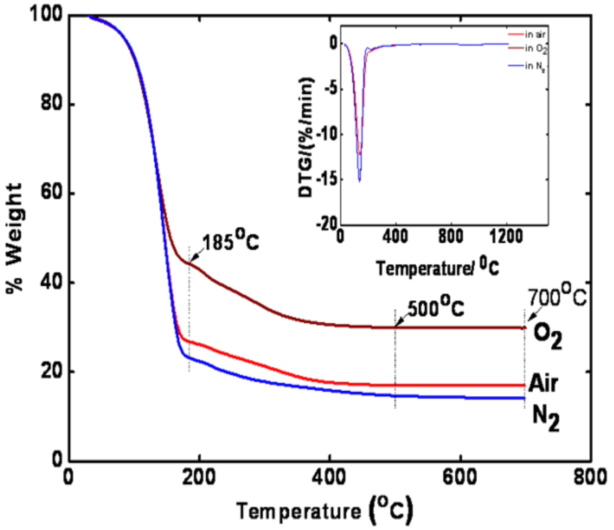

Fig. 6.2: TGA profiles obtained on calcination upto 700 °C under O_2, air and N_2 atmospheres during the preparation of T1 beads (Inset shows the corresponding DTG profiles).

Thermogravimetric analysis (TGA) of the hydrolysed beads was performed at a heating rate of 10 °C/min in oxygen, nitrogen and air atmospheres, from ambient conditions upto different temperatures in the range 400-1200 °C. Fig. 6.2 shows typical TGA profiles upto 700 °C, for the TIP-loaded M1 beads, after hydrolysis in air, O_2 and N_2 atmospheres. The TGA profiles can be divided into three stages. The first stage is from 30 °C to 185 °C, over which a mass loss of about 73% is observed due to dehydration.[233] The second stage, from 185 °C to 500 °C, experiences an additional mass decrease of about 10 %, due to pyrolysis of the alginate template, further condensation of TiO_2 oligomer and the unreacted TiO_2 precursor. This is followed by a third stage above 500 °C, where essentially constant mass, comprising 17 wt% inorganic solid, is left as a residue. The DTG traces (inset, Fig.6.2) exhibit an endothermic peak at 150°C due to water loss.

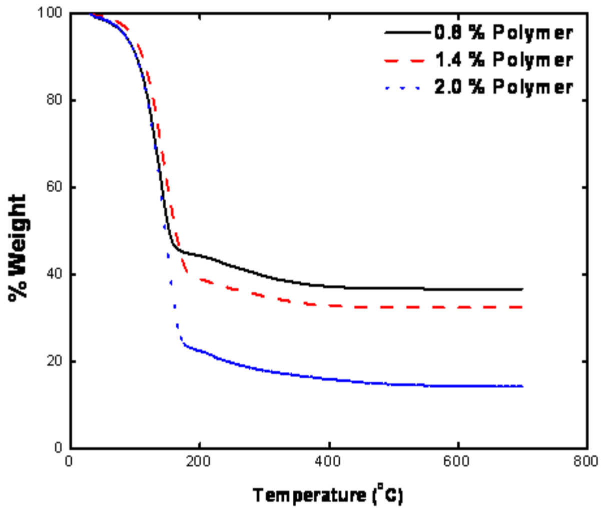

Fig. 6.3: TGA profiles obtained on calcination upto 700 °C during the preparation of T1, T2 and T3 beads, under N_2 atmosphere

The percentage thermal degradation of the composite beads, with lower polymeric content, i.e., TIP-loaded M2, is less as compared to that of the beads, with higher polymeric content, i.e., TIP-loaded M1 (Fig. 6.3). This could be due to fact that the template beads prepared with higher initial polymeric concentration have a fewer voids in comparison to those with lower polymeric content, as a result of which these beads imbibe less amount of TIP. In addition to that, the steric hindrance imposed by dense polymeric structure is more (as in TIP-loaded M1), which limits the growth of TiO_2, due to the presence of higher number of Ti-OR and Ti-OH unreacted groups, resulting in decreased mechanical stability of the tiatnia beads. The yield of titania, after heating at 700 ºC, was ~37 wt % in 1.4 % polymer-inorganic composite, whereas in 2% polymer-inorganic composite, it was only 17 wt %, which is due to the difference in TIP loading in the two cases.

6.5.1.2 XRD studies

The effect of the calcination temperature and the atmosphere on the phase content and crystallite size of the titania beads formed was investigated by XRD technique. Fig. 6.4 shows the XRD patterns of the titania beads (T1), formed by calcining under different atmospheric conditions and at different temperatures.

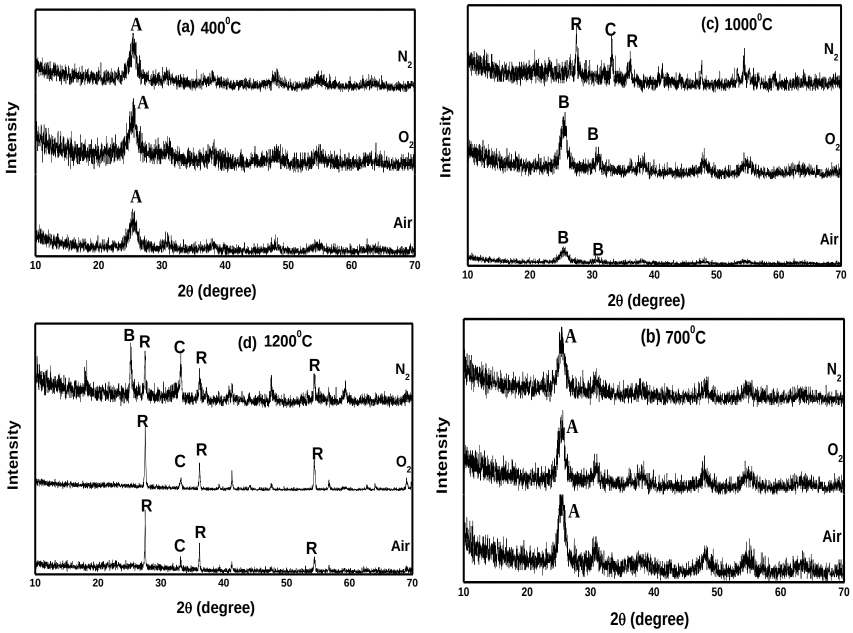

Fig. 6.4: Powder XRD patterns of the T1 samples, obtained by calcination under air, O_2 and N_2 atmospheres at (a) 400 ºC, (b) 700 ºC, (c) 1000 ºC and (d) 1200 ºC, where A, B, C and R represent anatase, brookite, calcium titanate and rutile phases, respectively

The average crystallite size (d) of anatase and rutile grains was determined, using Scherer formula (equation 6.2)

$$d = \frac{0.9\lambda}{\beta\cos\theta} \qquad (6.2)$$

Where λ, β and θ represent Cu Kα wavelength (0.15418 nm), full width at half maxima of anatase (101), or rutile (110) peak, in radians, and Braggs diffraction angle, after correcting for instrumental broadening, respectively. The average size of the crystallites was quantitatively determined from the relative intensities of (101) diffraction peak of anatase and (110) diffraction peak of rutile (R) phase, obtained at different temperatures and atmospheres. The experimentally determined crystallite size of the different titania beads synthesized, by calcining at different temperature and environments, are shown in Fig. 6.5.

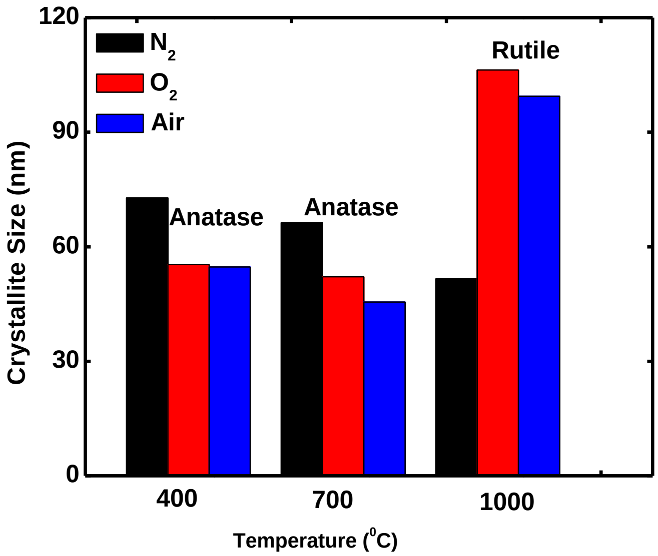

Fig. 6.5: Bar graph showing crystallite size of titania (T1) formed under different calcination atmospheres at different temperatures

It is observed that, crystallinity and average crystallite size of anatase titania decrease with increase in calcination temperature. The effect of calcination atmosphere is also important (as explained in the SEM observations later). The crystallinity increases, if the atmosphere is changed from air to O_2, and it is maximum in N_2. Phase stability of titania is also different under different atmospheres. Calcination in air and oxygen atmospheres results in anatase (A)-to -brookite (B) phase transition at 1000°C, which is an intermediate stage in the anatase-to-rutile phase transformation,[234] but under N_2 atmosphere at 1000 °C, calcium titanate ($CaTiO_3$) peak at $2\theta = 33.06$, corresponding to (112) plane, is also observed (JCPDS 76-1936). Whereas a low intensity peak of calcium titanate, along with an intense rutile phase peak, is observed at 1200 °C in air and O_2 atmospheres (Fig. 6.4). At this high temperature, brookite phase is completely converted to rutile phase. The early formation of calcium titanate under nitrogen flow can be due to the reason that, at high temperature (at 1000 °C and above), titania becomes oxygen deficient, as the oxygen from TiO_2 is captured by the calcium present in the matrix, forming calcium oxide, which, in turn, reacts with titania, forming calcium titanate.[235] The complete anatase-to-rutile transformation is observed at 1000 °C in N_2 atmosphere, whereas anatase-to-brookite transformation takes place at 1000 °C in air and O_2. This could be due to the presence of carbon in the beads (explained in section 6.3.1.4).

6.5.1.3 EDX and SEM studies

The results of the compositional analysis of the T1 titania beads, formed by calcination under N_2 atmosphere at different tempertures, as obtained from EDX measurements, are shown in Fig. 6.6. Generally, the carbon content of the beads decreases with increase in calcination temperature. The beads calcined at 400 and 700 °C show the presence of carbon (Fig. 6.6 (a & b)), while it is absent in the beads calcined at 1000 °C (Fig. 6.6(c)).

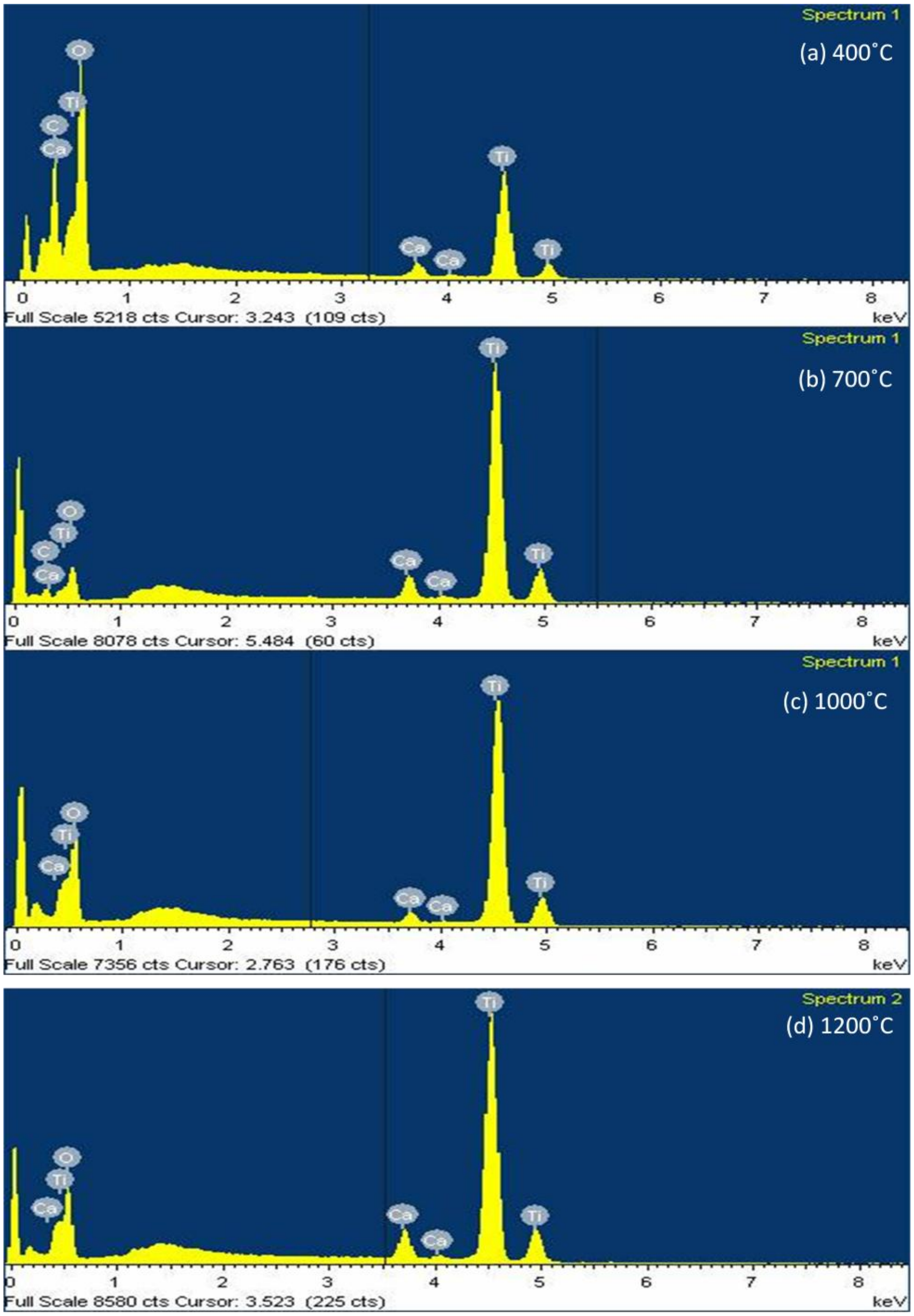

Fig. 6.6: EDX spectra of T1 microspheres, obtained after calcining at (a) 400 °C, (b) 700 °C, and (c) 1000 °C and (d) 1200 °C temperature under N_2 atmosphere

Carbon content seems to favor formation of the rutile phase. Under similar conditions, calcination in air, or oxygen, results in titania beads, with lower carbon content, as compared to that under N_2 atmosphere. The rutile phase was found to be the preferred one in the beads formed by calcining under N_2 atmosphere at 1000 °C. Whereas, those formed under Air/O_2 atmosphere showed anatase-to-rutile conversion only at 1200 °C. The difference in the anatase and the rutile phases lies in the ratio of the corner-sharing octahedrons to the edge-sharing octahedrons. In the anatase phase, the ratio is higher. In presence of oxygen, or air, carbon present in the matrix reacts with atmospheric oxygen, forming CO, or CO_2, but under N_2 environment, carbon reacts with oxygen from the titania matrix, generating oxygen vacancies, which may destroy the two corner sharing octahedrons, and favor the formation of two edge sharing units.[236] This decreases the ratio of the corner-sharing octahedrons to the edge-sharing octahedrons, leading to formation of thermodynamically stable rutile phase.[236]

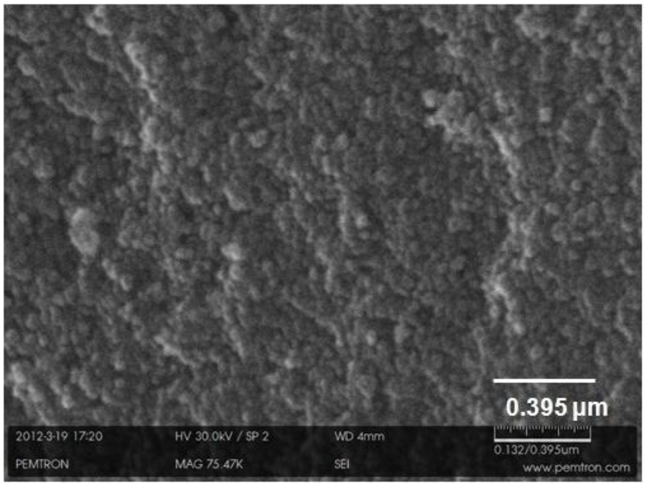

Fig. 6.7: SEM image of the outer surface of a T1 microsphere obtained on calcination under air atmosphere at 700ºC

The effect of calcination temperature and atmosphere on the morphology of the titania beads formed was also investigated by SEM technique. Fig. 6.7 depicts the SEM image of the outer surface of a T1 microsphere, calcined at 700 °C in air atmosphere. This image shows the porous nature of the synthesized beads. Fig. 6.8(a) shows the cross-sectional image of the titania beads, formed by calcining at 400 °C in air atmosphere. It reveals the porous structure of the beads, along with titania particles.

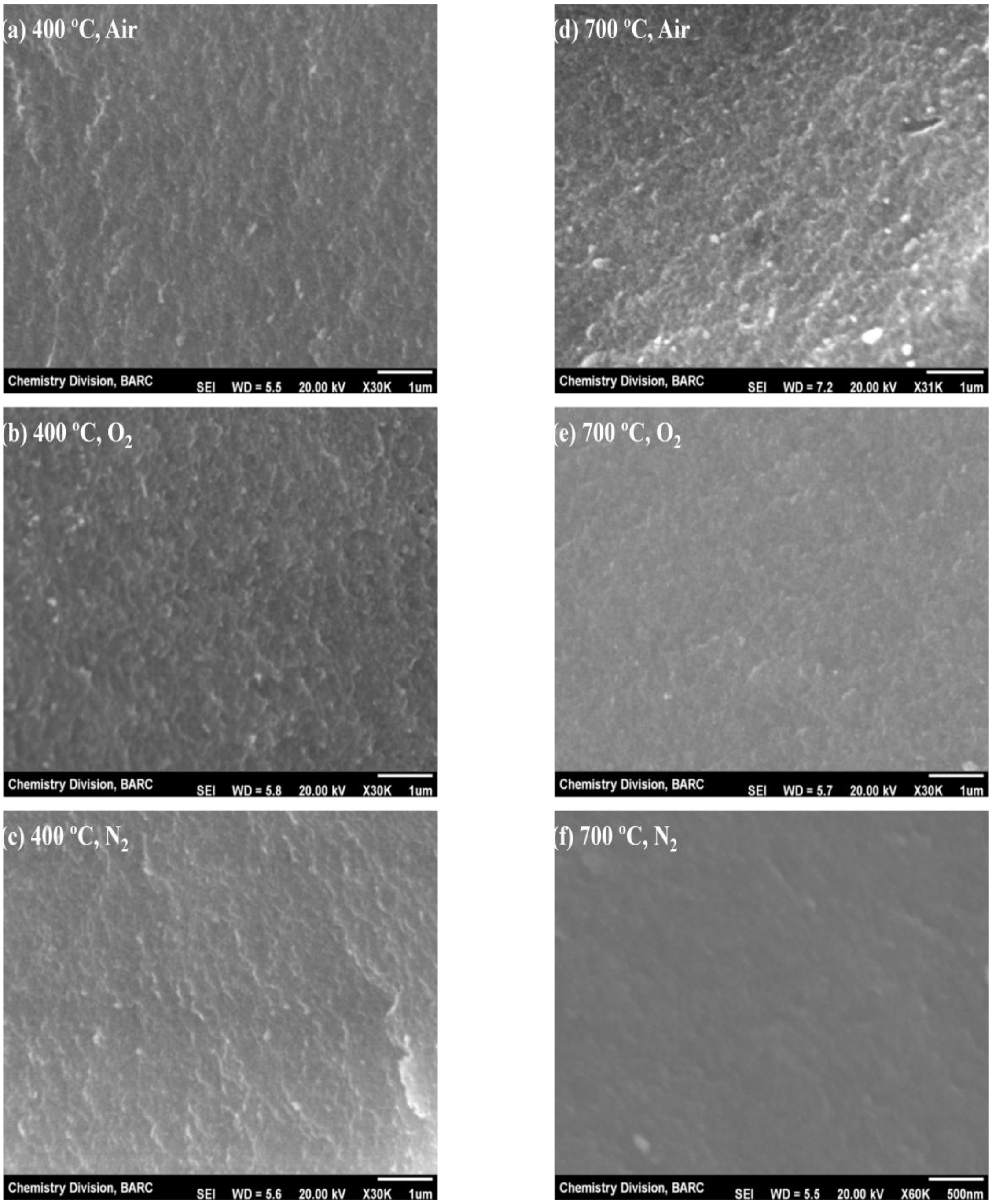

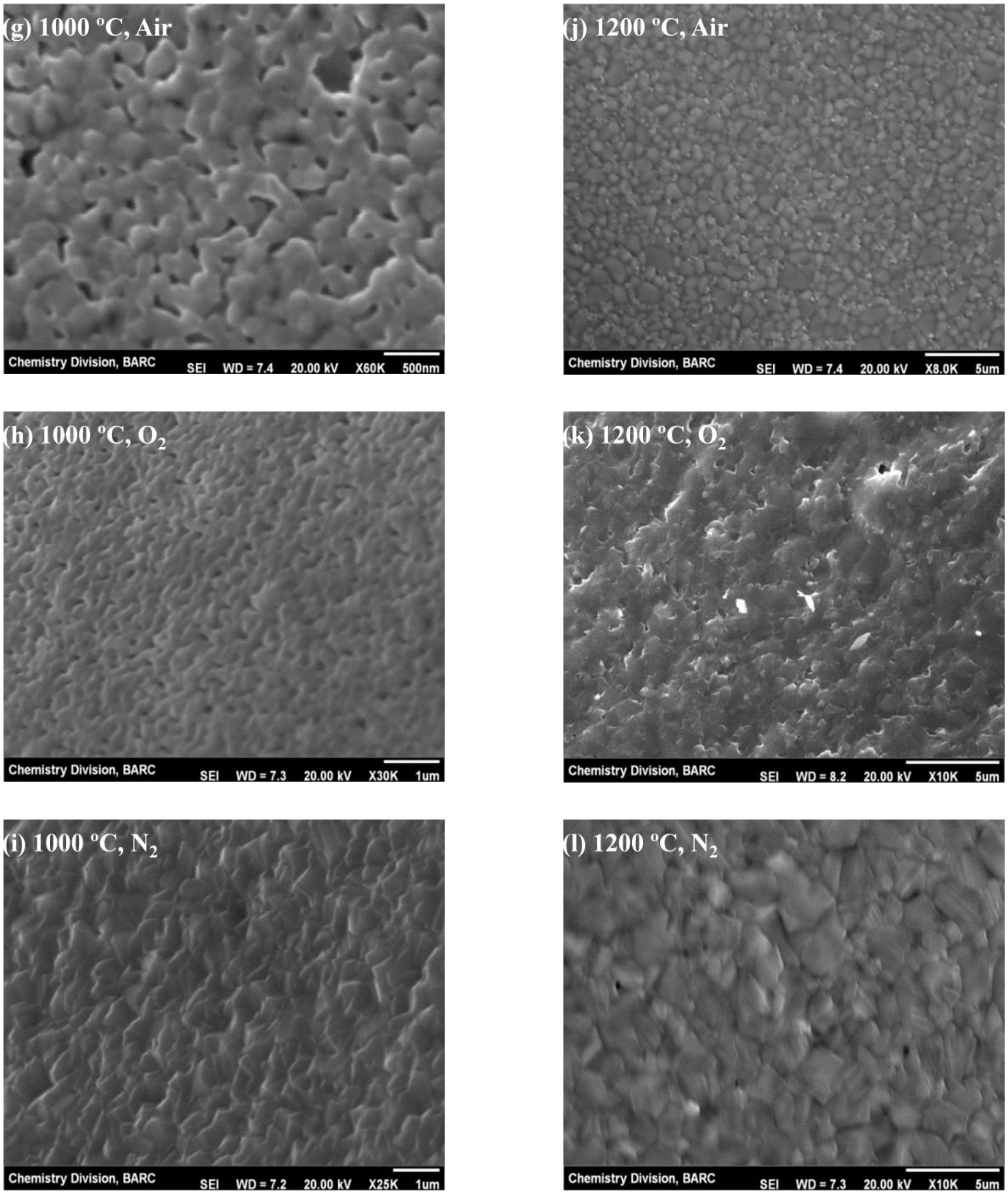

Fig. 6. 8: SEM images of the cross-section of the titania microspheres (T1), formed after calcining at different temperature and under different atmospheres (a) 400 ºC, air, (b) 400 ºC, O_2, (c) 400 ºC, N_2, (d) 700 ºC, air (e) 700 ºC, O_2, (f) 700 ºC, N_2, (g) 1000 ºC, air, (h) 1000 ºC, O_2, (i) 1000 ºC, N_2 (j) 1200 ºC, air, (k) 1200 ºC, O_2, and (l) 1200 ºC, N_2 atmosphere

The cross-sectional morphology of the other samples calcined at 400 °C and 700 °C in different atmospheres (O_2, N_2 and air) is also very similar (Figs. 6.8(a)-(f)), indicating that there are not much changes in sintering and grain growth in this temperature range. Figs. 6.8(g)-(l) show the cross-sectional images of the samples calcined at 1000 and 1200 °C, in various atmospheres. With increase in temperature, from 700 to1000 °C, and then to 1200 °C, the extent of sintering increases significantly. At 1000 °C, uniformly porous and dense microstructure is observed in the samples calcined under air and O_2 atmospheres (Fig. 6.8(g) & (h)). While in the beads calcined under N_2 atmosphere, the structure is dense and pore-free, with coarser titania grains of size ~ 0.5 µm (Fig. 6.8(i)). At 1200 °C, the extent of sintering is quite high, and the microstructure is mainly pore-free and denser, and in the beads calcined under air (Fig. 6.8(j)) and O_2 atmospheres (Fig. 6.8(k)), with larger grains of size 1-3 µm, surrounded by titania flakes. The grain growth is even more in the samples calcined under N_2 atmosphere (Fig. 6.8(l)). The microstructure of the beads calcined in N_2 flow shows larger lumps of TiO_2 of size 2-5 µm. These pores can grow by coalescence, along with increase in the particle size.[237] Anatase phase has lower surface energy than rutile phase, and, therefore, the presence of pores stabilizes the anatase phase, by reducing the volume and increasing the surface area. With heat treatment, the pores grow by coalescence, and the surface area of the anatase phase decreases, resulting in its destabilization. This is consistent with the XRD data, which shows that, above 700 °C temperature, anatase phase starts disappearing (Fig. 6.5). At even higher temperatures (1000 °C), rutile phase, with big-sized pores, is expected, which has grown at the expense of anatase phase. At 1200 °C, rutile particles also grow to bigger size, by coalescences of the smaller ones.

These are general observations in all the atmospheres investigated in the present work. The extent of grain growth, and disappearance of the pores are more pronounced under N_2 atmosphere, even at 1000 °C, because of the presence of C and Ca in the matrix, as explained earlier. These results show that, both the atmosphere and the temperature of calcination significantly affect the morphology of the titania beads formed.[232]

6.5.1.4 Surface area analysis

Fig. 6.9 depicts the N_2 adsorption/desorption isotherms of T1 and T3 beads, formed by calcination at 700 °C in the air. Barrett-Joyner-Halenda (BJH) analysis of the desorption isotherms shows clear hysteresis loop at high relative pressure, indicative of the capillary condensation associated with the large pore channels. Standard Brunauer-Emmett-Teller (BET) method was used to determine the specific surface area. The total pore volume of the beads T1 and T3 was also evaluated, by converting the volume of the adsorbed nitrogen at relative pressure (p/p_o) of approximately 0.99, to that of the liquid adsorbate. The BET surface area, the pore diameter, and the pore volume of the synthesized mesoporous titania beads are summarized in Table 6.1, and compared with the results reported in literature. The results show that the effect of polymer content on the specific surface area is not very significant, but it affects the total pore volume and pore diameter significantly.

The comparison with the reported results shows that both the average pore diameter and the pore volume of the synthesized titania microspheres (T1 and T3 beads obtained after calcining at 700°C in air atmosphere) are somewhat larger than the corresponding reported values for the TiO_2 beads synthesized by OEM [209] and sol-gel method.[238] The surface area of the synthesized beads is also found to be higher than that of P25, the commercially available titanium dioxide powder.[239-240]

Table 6.1: Surface area, pore diameter and pore volume of the titania beads.

Type of the beads	Surface area (m^2/g)	Pore diameter (nm)	Pore volume (ml/g)
T3 beads (synthesized using 0.8% Polymer)[232]	67.2	19.8	0.33
T1 beads (synthesized using 2.0% Polymer)[232]	69.7	24.9	0.42
TiO_2 beads (using agrose gel as template at 700°C) [238]	6.7	14.0	0.02
TiO_2 beads (by OEM) [209]	78.0	8.0	0.23
P25[239-240]	50-56	-	-

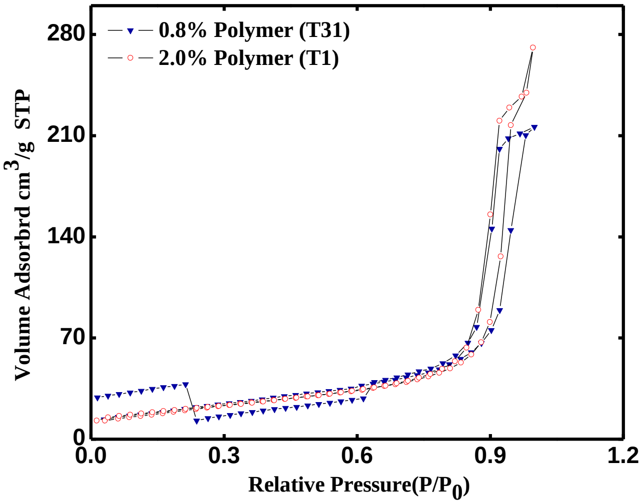

Fig. 6.9: The nitrogen adsorption-desorption isotherms of mesoporous titanium dioxide beads T1 and T3, obtained after calcining at 700 ºC under air flow

6.5.1.5 UV-vis diffuse reflectance spectroscopy

The synthesized titania beads (T1) were also characterized by UV-visible diffuse reflection spectroscopy and the result was compared with that of P25 degussa powder.

Fig. 6.10 shows the UV-vis DRS plot of both T1 and P25. A red shift of about ~ 20 nm is observed in the absorption edge of the synthesized titania beads, as compared to that of the commercial anatase powder. The increased absorption in visible light and the red shift in the UV-Vis DRS spectrum can be due to the presence of calcium and carbon in the titania matrix (confirmed by EDX studies, Fig. 6.6(b)). Carbon and calcium are reported in literature as dopants for titania matrix, to increase its light absorption efficiency in visible light region.[241-242] The observed higher absorption of the beads in the visible region is very important from the viewpoint of practical applications.

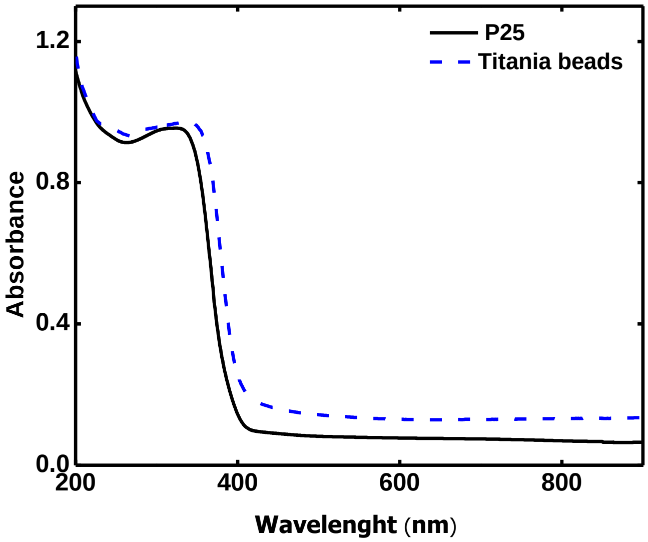

Fig. 6.10: UV-Vis diffuse reflectance spectrum of the synthesized titania beads (T1), calcined at 700°C under air flow, and commercial P25 TiO_2 powder

6.5.2 Photolytic degradation of dye

In order to evaluate the photo-catalytic activity of the synthesized titania beads, photo-degradation of methylene blue dye (Fig. 6.11) was studied, using T1 beads calcined at 700 °C in air atmosphere. Particularly, these beads were chosen for the application studies, because these beads had appropriate mechanical strength, surface area, and were prepared under normal atmosphere conditions. When these titania beads are added to dye solution, some amount of the dye gets adsorbed on the beads, depending on the concentration of the dye in the solution and the amount of beads taken. Since the dye exists in solution, as well as on the beads, it can undergo degradation due to absorption of light by it, both in the solution and on the beads.

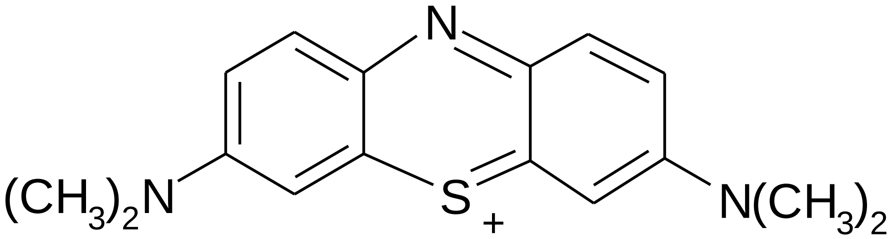

Fig. 6.11: Chemical structure of methylene blue dye

In order to resolve these two components, and to evaluate photo-catalytic activity of the titania beads, photo-degradation of MB dye was investigated, both with and without the synthesized beads, and the results are shown in Fig. 6.12. Trace ‘a’ shows the absorbance of MB dye at 664 nm, after different times of irradiation with light, in the absence of titania beads, in N_2 atmosphere. It indicates a negligible change in the concentration of the dye. Traces ‘b’ and ‘c’ show the absorbance of MB dye as a function of irradiation time in the absence and the presence of titania beads, respectively, in air atmosphere, indicating degradation of the dye.

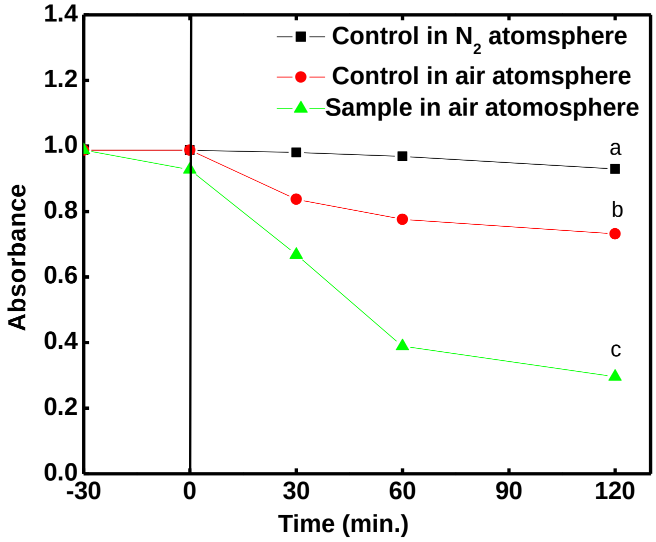

Fig. 6.12: Photo-degradation of MB in aqueous medium using the synthesized TiO_2 microspheres

6.5.2.1 Adsorption of methylene blue on titania beads

On addition of titania beads to a dye solution, the fraction of the active sites of the beads covered by the dye molecules, θ, is given as

$$\theta = \frac{n_b}{n_o} = \frac{KC_e}{1+KC_e} \tag{6.3}$$

where 'K' is the binding constant, C_e is the concentration of the dye at equilibrium, n_o and n_b are the total number of adsorption sites and the number of the sites covered by the dye molecules, respectively. Equation (6.3) can be written as

$$\frac{1}{n_b} = \frac{1}{n_0} + \frac{1}{n_o K C_e} \tag{6.4}$$

The above equation can also be expressed as

$$\frac{1}{q_e} = \frac{1}{q_m} + \frac{1}{Kq_m C_e} \qquad (6.5)$$

where q_e is the equilibrium adsorption capacity, and q_m is the maximum equilibrium adsorption capacity. Equilibrium adsorption capacity was calculated, using the equation

$$q_e = \frac{(C_o - C_e)V}{m} \qquad (6.6)$$

where C_o is the initial concentration of MB dye, V is volume of the dye solution and m is weight of the adsorbent. The plot of $1/q_e$ vs. $1/C_e$ gives a straight line, with $1/q_m$ and $1/q_mK$ as intercept and slope, respectively.

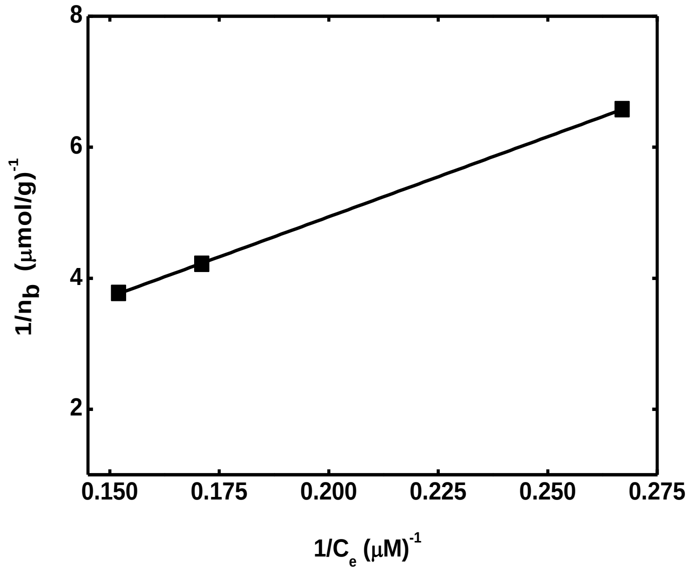

Fig. 6.13: Linearized Langmuir adsorption isotherm of MB dye by titania beads

The adsorption of MB dye on the titania beads was investigated by equilibrating a known weight of the beads with different initial concentrations of the dye, in dark, for 3 hours. It was observed that the equilibrium adsorption was reached in ~30 minutes, for the various initial concentrations used. Fig. 6.13 shows the linearized Langmuir adsorption isotherm of MB dye by titania beads, i.e., plot of ($1/q_e$) vs.($1/C_e$). The value of q_m, i.e., the maximum capacity of the beads for the adsorption of the dye, determined from the intercept of the plot, has been found to be 2.0137 µmol/g, which is equivalent to 0.0175 sites/nm^2. Knowing the value of q_m, the value of K has been determined from the slope as 2.626×10^2 Lmol^{-1}.

6.5.2.2 Photo-degradation of dye in solution

Upon irradiation with light, the dye is excited to singlet state, S_1, which can give fluorescence, or undergo intersystem crossing, giving triplet state, and once in the triplet state, the dye can generate singlet oxygen ($^1O_2$), by energy transfer to the dissolved oxygen.[243] This $^1O_2$ can react with the dye itself, and bring about its degradation. Also, the dye in the triplet state can react with ground state oxygen, and undergo degradation.[244] The rate of change of concentration of the dye, on exposure to light, is given as

$$-\frac{d[C]}{dt} = k_{app(s)}[C] \tag{6.7}$$

Where $k_{app(s)}$ is the apparent first-order rate constant for the degradation of the dye due to absorption of light by it in the solution.

The equation (6.7) can be integrated as follows

$$-\int_{C_0}^{C} \frac{dC}{C} = k_{app(s)} \int_0^t dt \tag{6.8}$$

$$-\ln\left(\frac{C}{C_0}\right) = k_{app(s)}t \tag{6.9}$$

Where C_0 is the initial concentration of MB dye and ‘t’ is the time of exposure to light.

Fig. 6.14 (trace a) shows that the plot of ln (C/Co) vs. time is a straight line, passing through origin, indicating that photo-degradation of dye in the solution follows first-order kinetics. The value of the first-order rate constant, $k_{app(s)}$, determined from the slope of the plot is 0.00293 min^{-1}.

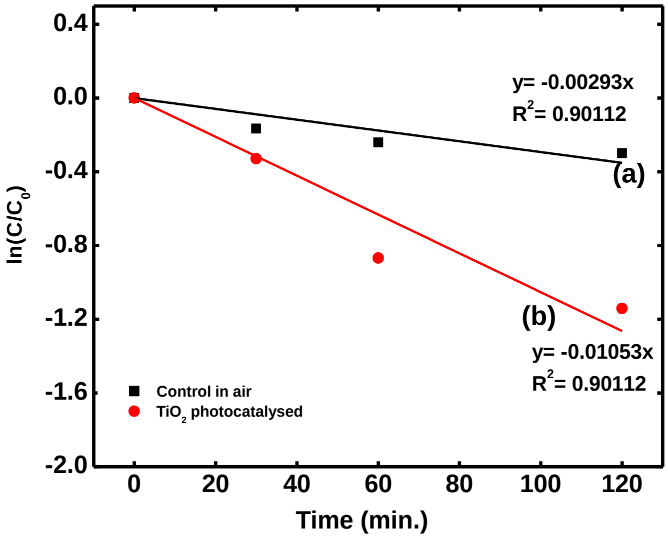

Fig. 6.14: Plots of ln (C/C_0) vs. time for degradation of MB dye under visible light irradiation in air atmosphere: (a) in the absence of titania beads, and (b) in the presence of titania beads

6.5.2.3 Photo-catalytic degradation

The mechanism of photo-catalytic degradation of organic dyes, under visible irradiation, is proposed as as shown in Fig. 6.15.[245] The excited dye molecule (S_1) injects an electron to the conduction band of TiO_2, where it is scavenged by the pre-adsorbed O_2, forming active radicals, $O_2^{\cdot-}$, $HO_2^{\cdot}$, or $OH^{\cdot}$. These radicals, then, attack the dye molecules, and bring about further degradation and mineralization.

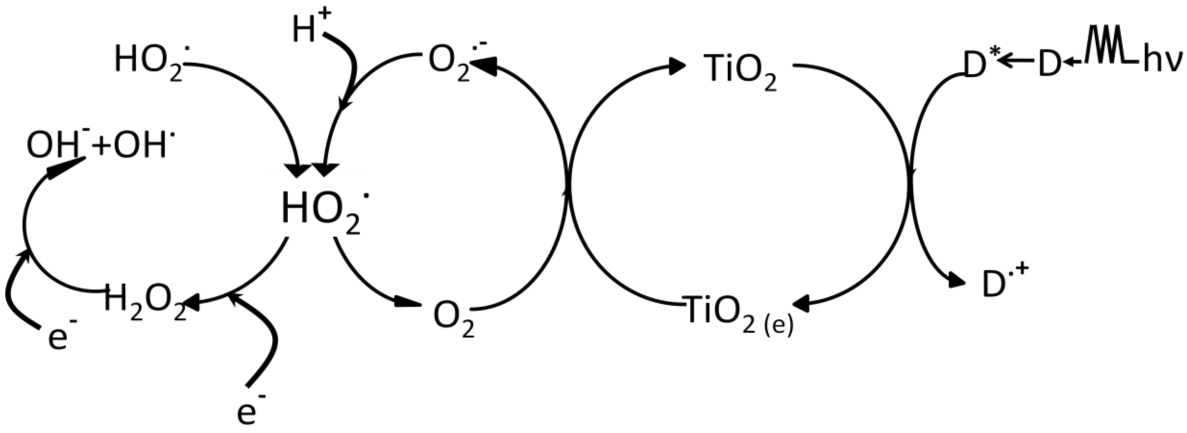

Fig. 6.15: Schematic of degradation of organic dye, in the presence of the TiO_2, under visible light irradiation; D is the organic dye molecule

It is well known that the photo-catalytic degradation of organic dyes, like MB, follows the Langmuir–Hinshelwood kinetics, which may be expressed as

Rate of degradation = $\frac{-dc}{dt} = k\theta = \frac{kKC_e}{1+KC} \approx kKC_e \approx k_{app(a)}C_e$ (6.10)

$-\frac{d[C]}{dt} = k_{app(a)}[C_e]$ (6.11)

where, $k_{app(a)}$ is the apparent first-order reaction rate constant for photo-catalytic degradation of the dye.

The integrated form of the equation (6.11) can be written as

$-\ln\left(\frac{C_e}{C_0}\right) = k_{app(a)}t$ (6.12)

Fig. 6.14 (trace b) shows that the plot of $\ln(C_e/C_0)$ versus time, obtained from the data given in the Fig. 6.12(c), is a fairly good straight line, passing through the origin, indicating that the photo-degradation of MB, in the presence of titania beads, follows a first-order kinetics. The apparent first-order rate constant obtained from the plot is 0.01053 min $^{-1}$. It is sum of two rate constants, the apparent first-order rate constant for photo-degradation of dye in the solution, $k_{app(s)}$, and the apparent first-order rate constant for photo-catalytic degradation of the dye, $k_{app(a).}$ Since $k_{app(s)}$ = 0.00293 min $^{-1}$, the value of $k_{app(a)}$ is determined to be 0.00760 min $^{-1}$. The value of $k_{app(a)}$ suggests that the photo-catalysis can be triggered by visible light, using synthesized titania beads in air atmosphere. The photo-catalytic activity of the synthesized titania beads (T1) was compared with that of P25 Degussa under similar conditions. The results show that the synthesized beads are equally efficient in photo-degradation, as compared to P25, which could be due to the combined effect of presence of calcium and carbon in the titania matrix and high surface area. The additional advantage of the synthesized beads over P25 is their easy separation from the treated solution.

6.6 Conclusion

In this work, mesoporous titania beads have been synthesized by sol-gel templating method, using pre-formed alginate beads as a sacrificial template. Alginate polymer behaves as a directing agent, and consequently, controls the growth of the inorganic part during the preparation process. Calcination temperature and atmosphere are found to affect the size, morphology and phase of the titania nanocrystals. Anatase phase is stabilized upto 700 ºC in oxygen and air atmospheres, and rutile phase is observed only at 1200 ºC, while in N_2 atmosphere, anatase phase completely disappears at 1000 ºC. Polymer content of the sacrificial template also governs the specific surface area, the pore volume and the average pore size. The use of lower polymer content can easily give mesoporous beads, with higher pore diameter. Finally, applicability of these beads in photo-catalyzed degradation of methylene blue dye has been studied. The results indicate that the synthesized titania beads have good photo-catalytic activity in air atmosphere. The reported results suggest that the substantial porosity and the ease of preparation of these materials make the procedure attractive for a number of applications.

Refernces

1. A. J. Hunt, E. H. K. Sin, R. Marriott and J. H. Clark, *ChemSusChem*, 2010, **3**, 306-322.
2. D. Angel and M. T. Rock, *Technological Forecasting and Social Change*, 2009, **76**, 229-240.
3. J. Roy and S. Pal, *Current Opinion in Environmental Sustainability*, 2009, **1**, 192-200.
4. *Disposition of High-Level Waste and Spent Nuclear Fuel: The Continuing Societal and Technical Challenges*, The National Academies Press, Washington, D.C., USA, 2001.
5. C. F. Schmidt, W. K. Nank and R. V. Lechowich, *Journal of Food Science*, 1962, **27**, 77-84.
6. P. Warde, *Medicine*, 2008, **36**, 15-18.
7. http://cndpindia.org/e107_plugins/content/content.php?content.28.
8. R. Rhodes and D. Beller, *IAEA Bulletin* 2000, vol. 42.
9. *End Points for Spent Nuclear Fuel and High-Level Radioactive Waste in Russia and the United States*, The National Academies Press, Washington, D.C., USA, 2003.
10. D. Zdenek, *Disposal of Radioactive Wastes*. (*Studies in Environmental Science Sr. No. 15)*, Scientific Publishing Co., Elsevier, Amsterdam 1982, pp. 30-64.
11. M. I. Ojovan and W. E. Lee., *An Introduction to Nuclear Waste Immobilisation*, Elsevier, 2005, pp. 92.
12. http://www.world-nuclear.org/info/inf04.html.

13. M. I. Ojovan and W. E. Lee., *An Introduction to Nuclear Waste Immobilisation*, Elsevier, 2005, pp. 94.

14. http://www.world-nuclear.org/education/wast.htm.

15. http://www.evs.anl.gov/pub/doc/cesium.pdf.

16. M. I. Ojovan and W. E. Lee, *An Introduction to Nuclear Waste Immobilisation*, Elsevier, 2005, pp. 112.

17. R. F. Morrissey and C. M. Herring, *Radiation Physics and Chemistry*, 2002, **63**, 217-221.

18. http://www.qsa-global.com/sources/industrial-isotopes/cesium-137.aspx.

19. S. B. Ahlstrom, *Radiation Physics and Chemistry*, 1985, **25**, 1-10.

20. J. S. Sivinski, *Radiation Physics and Chemistry*, 1983, **22**, 99-118.

21. H. S. Chang, W. Um, K. Rod, R. J. Serne, A. Thompson, N. Perdrial, C. I. Steefel and J. Chorover, *Environmental Science and Technology*, 2011, **45**, 8313-8320.

22. M. Bouby, H. Geckeis, J. Lützenkirchen, S. Mihai and T. Schäfer, *Geochimica et Cosmochimica Acta*, 2011, **75**, 3866-3880.

23. M. N. Sabodina, S. N. Kalmykov, Y. A. Sapozhnikov and E. V. Zakharova, *Journal of Radioanalytical and Nuclear Chemistry,* 2006, **270**, 349-355.

24. B. J. Howard, N. A. Beresford and K. Hove, *Health Physics*, 1991, **61**, 715-725.

25. W. L. Robison and E. L. Stone, *Health Physics*, 1992, **62**, 496-511.

26. K. Stark and H. B. L. Pettersson, *Radiation and Environmental Biophysics*, 2008, **47**, 481-489.

27. H. K. Bates, *Metal Finishing*, 2010, **108**, 28-32.

28. D. V. Vassallo, M. R. Simoes, L. B. Furieri, M. Fioresi, J. Fiorim, E. A. S. Almeida, J. K. Angeli, G. A. Wiggers, F. M. Pecanha and M. Salaices, *Brazilian Journal of Medical and Biological Research*, 2011, **44**, 939-946.

29. D. H. Jang and R. S. Hoffman, *Neurologic Clinics*, 2011, **29**, 607-622.

30. L. Jarup, *British Medical Bulletin*, 2003, **68**, 167-182.

31. M. N. Chong, B. Jin, C. W. K. Chow and C. Saint, *Water Research*, 2010, **44**, 2997-3027.

32. J.-C. Sin, S.-M. Lam, A. R. Mohamed and K.-T. Lee, *International Journal of Photoenergy*, 2012, **2012,** Article ID 720491.

33. A. Mollah, A. Begum and M. Rahman, *Journal of Radioanalytical and Nuclear Chemistry*, 1998, **229**, 187-189.

34. E. H. Lee, J. G. Lim, D. Y. Chung, H. B. Yang and K. W. Kim, *Journal of Radioanalytical and Nuclear Chemistry*, 2010, **284**, 387-395.

35. L. Mow Lee, and L. L Kilpatrik, *A Precipitation Process for Supernate Decontamination*, Report DP-1636, E.I. DuPont de Nemours & Co., Savannah River Laboratory, Aiken, SC, 1982.

36. D. D. Walker and M. A. Schmitz, *Technical Data Summary: In-Tank Precipitation Processing of Soluble High-Level Waste*, Report DPSTD-84-103, Savannah River Plant, May 1984

37. M. Meisters, J. T. Vandeberg, F. P. Cassaretto, H. Posvic and C. E. Moore, *Analytica Chimica Acta*, 1970, **49**, 481-485.

38. E. J. Birch, in *Encyclopedia of Separation Science*, Academic Press, 2000.

39. G. R. Choppin, *Solvent Extraction Research and Development*, 2005, **12**, 1-10.

40. J. F. Dozol, M. Dozol and R. M. Macias, *Journal of Inclusion Phenomena and Macrocyclic Chemistry*, 2000, **38**, 1-22.

41. W. J. McDowell, B. A. Moyer, G. N. Case and F. I. Case, *Solvent Extraction and Ion Exchange*, 1986, **4**, 217-236.

42. N. Fontanals, R. M. Marce, F. Borrull and P. A. G. Cormack, *Trends in Analytical Chemistry*, 2010, **29**, 765-779.

43. L. Vidal, M.-L. Riekkola and A. Canals, *Analytica Chimica Acta*, 2012, **715**, 19-41.

44. W. J. Thomas and B. D. Crittenden, *Adsorption Technology and Design*, Oxford, 1998.

45. A. Dabrowski, *Advances in Colloid and Interface Science*, 2001, **93**, 135-224.

46. D. H. Everett, *Special Publication Royal Society of Chemistry*, 1982, **43**, 71.

47. S. J. Gregg and K. S. W. Sing, *Adsorption, Surface Area and Porosity*, 1982.

48. C. E. Harland, *Ion Exchange: Theory and Practice*, Royal Society of Chemistry,1997.

49. F. Helfferich, *Ion Exchange*, Mc-Graw Hill, New York, 1962.

50. V. J. Inglezakis, M. M. Loizidou and H. P. Grigoropoulou, *Journal of Colloid and Interface Science*, 2004, **275**, 570-576.

51. F. S. Zhang, J. O. Nriagu and H. Itoh, *Water Research*, 2005, **39**, 389-395.

52. E. Yavuz, B. F. Senkal and N. Bicak, *Reactive and Functional Polymer*, 2005, **65**, 121-125.

53. I. K. Tonle, E. Ngameni, D. Njopwouo, C. Carteret and A. Walcarius, *Physical Chemistry Chemical Physics*, 2003, **5**, 4951-4961.

54. A. Walcarius and C. Delacôte, *Analytica Chimica Acta*, 2005, **547**, 3-13.

55. E. Fourest and J. C. Roux, *Applied Microbiology and Biotechnology*, 1992, **37**, 399-403.

56. B. Volesky, *Trends in Biotechnology*, 1987, **5**, 96-101.

57. B. Volesky, *Biosorbent Materials*, Troy, NY, USA, 1986.

58. N. Kuyucak and B. Volesky, *Biotechnology Letters*, 1988, **10**, 137-142.

59. D. Chakraborty, S. Maji, A. Bandyopadhyay and S. Basu, *Bioresource Technology*, 2007, **98**, 2949-2952.

60. Y. Mao, H. Hu and Y. Yan, *Journal of Environmental Sciences*, 2011, **23**, 1104-1112.

61. S. P. Mishra, S. K. Prasad, R. S. Dubey, M. Mishra, D. Tiwari and S.-M. Lee, *Applied Radiation and Isotopes*, 2007, **65**, 280-286.

62. A. Clearfield, *Solvent Extraction and Ion Exchange*, 2000, **18**, 655-678.

63. K. G. Bhattacharyya and S. S. Gupta, *Separation and Purification Technology*, 2006, **50**, 388-397.

64. G. E. Christidis, P. W. Scott and A. C. Dunham, *Applied Clay Science*, 1997, **12**, 329-347.

65. S. H. Lin and R. S. Juang, *Journal of Hazardous Materials*, 2002, **92**, 315-326.

66. B. I. Olu-Owolabi and E. I. Unuabonah, *Applied Clay Science*, 2011, **51**, 170-173.

67. E. I. Unuabonah, K. O. Adebowale and B. I. Olu-Owolabi, *Journal of Hazardous Materials*, 2007, **144**, 386-395.

68. O. Yavuz, Y. Altunkaynak and F. Guzel, *Water Research*, 2003, **37**, 948-952.

69. P. Sylvester and A. Clearfield, *Separation Science and Technology*, 1998, **33**, 1605-1615.

70. B. Ma, S. Oh, W. S. Shin and S. J. Choi, *Desalination*, 2011, **276**, 336-346.

71. Z. Zheng, C. V. Philip, R. G. Anthony, J. L. Krumhansl, D. E. Trudell and J. E. Miller, *Industrial and Engineering Chemistry Research*, 1996, **35**, 4246-4256.

72. N. R. Mann and T. A. Todd, *Separation Science and Technology*, 2004, **39**, 2351-2371.

73. T. A. Todd, K. N. Brewer, D. J. Wood, P. A. Tullock, N. R. Mann and L. G. Olson, *Separation Science and Technology*, 2001, **36**, 999-1016.

74. P. Singh, J. P. Rawat and N. Rahman, *Talanta*, 2003, **59**, 443-452.

75. W. A. Siddiqui and S. A. Khan, *Bulletin of Materials Science*, 2007, **30**, 43-49.

76. K. M. Parida, B. B. Sahu and D. P. Das, *Journal of Colloid and Interface Science*, 2004, **270**, 436-445.

77. G. Alberti and E. Torracca, *Journal of Inorganic and Nuclear Chemistry*, 1968, **30**, 3075-3080.

78. R. Thakkar and U. Chudasama, *Journal of Hazardous Materials*, 2009, **172**, 129-137.

79. S. P. Mishra, D. Tiwari, S. K. Prasad, R. S. Dubey and M. Mishra, *Journal of Radioanalytical and Nuclear Chemistry*, 2006, **268**, 191-199.

80. K. Moosavi, S. Setayeshi, M. G. Maragheh, S. Javadahmadi, M. R. Kardan and S. Nosrati, *Journal of Applied Sciences*, 2009, **9**, 2180-2184.

81. S. S. Kumar, M. V. Sivaiah, K. A. Venkatesan, R. M. Krishna, G. S. Murthy and P. Sasidhar, *Journal of Radioanalytical and Nuclear Chemistry*, 2003, **258**, 321-327.
82. K. A. Kraus, T. A. Carlson and J. S. Johnson, *Nature*, 1956, **177**, 1128-1129.
83. J. Satyanarayana, G. S. Murthy and P. Sasidhar, *Journal of Radioanalytical and Nuclear Chemistry*, 1999, **242**, 11-16.
84. J. F. Walker Jr, P. A. Taylor and D. D. Lee, *Separation Science and Technology*, 1999, **34**, 1167-1181.
85. J. V. R. Smit, *Nature*, 1958, **181**, 1530-1531.
86. J. van R. Smit, W. Robb and J. J. Jacobs, *Journal of Inorganic and Nuclear Chemistry*, 1959, **12**, 104-112.
87. J. L. Kassner, H. P. Crammer and M. A. Ozier, *Analytical Chemistry*, 1948, **20**, 1052-1055.
88. J. Krtil, *Journal of Inorganic and Nuclear Chemistry*, 1962, **24**, 1139-1144.
89. H. L. Caron and T. T. Sugihara, *Analytical Chemistry*, 1962, **34**, 1082-1086.
90. R. Chakravarty, R. Ram, K. T. Pillai, Y. Pamale, R. V. Kamat and A. Dash, *Journal of Chromatography A*, 2012, **1220**, 82-91.
91. N. R. De Tacconi, K. Rajeshwar and R. O. Lezna, *Chemistry of Materials*, 2003, **15**, 3046-3062.
92. J. Lehto, S. Haukka, R. Harjula and M. Blomberg, *Journal of the Chemical Society, Dalton Transactions*, 1990, 1007-1011.
93. J. Lehto, R. Harjula and J. Wallace, *Journal of Radioanalytical and Nuclear Chemistry, Articles*, 1987, **111**, 297-304.

94. S. Ayrault, B. Jimenez, E. Garnier, M. Fedoroff, D. J. Jones and C. Loos-Neskovic, *Journal of Solid State Chemistry*, 1998, **141**, 475-485.

95. C. Loos-Neskovic and M. Fedoroff, *Solvent Extraction and Ion Exchange*, 1989, **7**, 131-158.

96. R. O. Lezna, R. Romagnoli, N. R. De Tacconi and K. Rajeshwar, *Journal of Physical Chemistry B*, 2002, **106**, 3612-3621.

97. W. E. Prout, E. R. Russell and H. J. Groh, *Journal of Inorganic and Nuclear Chemistry*, 1965, **27**, 473-479.

98. W. D. King, F. F. Fondeur, W. R. Wilmarth, M. E. Pettis and S. W. McCollum, *Separation Science and Technology*, 2006, **41**, 2475-2486.

99. T. W. G. Solomons, *Organic Chemistry*, John Wiley & Sons, New York, 1992.

100. C. Lin and J. A. Ritter, *Carbon*, 1997, **35**, 1271-1278.

101. R. W. Pekala, *Journal of Materials Science*, 1989, **24**, 3221-3227.

102. A. M. Elkhatat and S. A. Al-Muhtaseb, *Advanced Materials*, 2011, **23**, 2887-2903.

103. E. Pretsch, P. Buhlmann and C. Affolter, *Structure Determination of Organic Compounds*, Springer-Verlag, Berlin, 2000.

104. S. K. Samanta, M. Ramaswamy and B. M. Misra, *Separation Science and Technology*, 1992, **27**, 255-267.

105. S. T. Mayer, F. Kong, R. W. Pekala and J. L. Kaschmitter, *US Patent No. 3850868*, 1999.

106. C. Bondy, *U.S. Patent No.* 3989661, 1976.

107. J. T. Stephan, *U.S. Patent No*. 2675336, 1954.

108. R. J. Sphar and W. R. Moffitt and E. H. Pryde, *U.S. Patent No.* 2489336, 1949.

109. M. Wismer, G. K. F. Schimel, Verona R. G. Temple, and Gibsonia, *U.S. Patent No.* 3850868, 1973.

110. P. Kopf, *U. S. Patent No.* 4366303, 1981.

111. J. Wynstra and S. J. Schultz, *U. S. Patent No.* 4206095, 1978.

112. J. Gillot, S. F. Excell and B. Lux, *U. S. Patent No.* 4237107, 1980.

113. H. F. Cosway, *U. S. Patent No.* 4317901, 1982.

114. S. T. Tennison, J. R. Tunbridge, R. N. Place, A. J. Blackburn and A. M. Giles, *U. S. Patent Application No*. 12/444840, 2010.

115. R. W. Pekala, *U. S. Patent No.* 4873218, 1989.

116. A. W. Hull, *Journal of the American Chemical Society*, 1919, **41**, 1168-1175.

117. H. P. Klug and L. E. Alexander, *X-ray Diffraction Procedures*, Wiley-Interscience Publication, New York, 1974.

118. B. D. Cullity, *Elements of X-ray Diffraction*, Addison-Wilson Publishing Comp. Inc., USA, 1959.

119. H. Borchert, E. V. Shevchenko, A. Robert, I. Mekis, A. Kornowski, G. Grübel and H. Weller, *Langmuir*, 2005, **21**, 1931-1936.

120. A. R. West, *Solid State Chemistry and its Applications*, John Wiley & Sons, New York, 1984.

121. www.icdd.com.

122. P. J Goodhew, F. J. Humphreys and R. Beanland, *Electron Microscopy and Analysis*, Taylor and Francis, London, 1988.

123. M. E. Brown, *Introduction to Thermal Analysis: Techniques and Applications*, Kluwer Academic Publishers, 2001.

124. G. R. Choppin, J. Liljenzin and R. Jan, *Radiochemistry and Nuclear Chemistry*, Elsevier, 2002.

125. C. W. Sensen, *Advanced Imaging in Biology and Medicine:Technology, Software Environments, Applications*, Springer, 2008.

126. G. F. Knoll, *Radiation Detection and Measurement, Fourth Edition*, University of Michigan, Ann Arbor, 2010.

127. H. A. Barnes, J. F. Hutton and K. Walters, *An Introduction to Rheology* Elsevier, Amsterdam, 1989.

128. G. McKay and J. F. Porter, *Process Safety and Environmental Protection*, 1997, **75**, 171-180.

129. D. Das, N. Das and L. Mathew, *Journal of Hazardous Materials*, 2010, **184**, 765-774.

130. S. J. Allen, Q. Gan, R. Matthews and P. A. Johnson, *Bioresource Technology*, 2003, **88**, 143-152.

131. R. R. Sheha and E. Metwally, *Journal of Hazardous Materials,* 2007, **143**, 354-361.

132. Y. S. Ho, *Scientometrics,* 2004, **59**, 171-177.

133. W. Rudzinski and W. Plazinski, *Langmuir*, 2008, **24**, 5393-5399.

134. W. Rudzinski and W. Plazinski, *Journal of Physical Chemistry C*, 2007, **111**, 15100-15110.

135. S. J. Allen, Q. Gan, R. Matthews and P. A. Johnson, *Journal of Colloid and Interface Science*, 2005, **286**, 101-109.

136. J. Febrianto, A. N. Kosasih, J. Sunarso, Y. H. Ju, N. Indraswati and S. Ismadji, *Journal of Hazardous Materials*, 2009, **162**, 616-645.

137. G. McKay, Y. S. Ho and J. C. Y. Ng, *Separation and Purification Methods*, 1999, **28**, 87-125.

138. W. Plazinski, W. Rudzinski and A. Plazinska, *Advances in Colloid and Interface Science*, 2009, **152**, 2-13.

139. Y. S. Ho, *Water Research*, 2006, **40**, 119-125.

140. W. Rudzinski and W. Plazinski, *Journal of Physical Chemistry B*, 2006, **110**, 16514-16525.

141. Y. S. Ho and G. McKay, *Adsorption Science and Technology*, 1998, **16**, 243-255.

142. Y. S. Ho and G. McKay, *Water Research*, 2000, **34**, 735-742.

143. S. Sen Gupta and K. G. Bhattacharyya, *Advances in Colloid and Interface Science*, 2011, **162**, 39-58.

144. F.-C. Wu, R.-L. Tseng and R.-S. Juang, *Chemical Engineering Journal*, 2009, **150**, 366-373.

145. G. E. Boyd, A. W. Adamson and L. S. Myers Jr, *Journal of the American Chemical Society*, 1947, **69**, 2836-2848.

146. D. Reichenberg, *Journal of the American Chemical Society*, 1953, **75**, 589-597.

147. B. K. Singh and N. S. Rawat, *Journal of Chemical Technology & Biotechnology*, 1994, **61**, 57-65.

148. M. Sankar, G. Sekaran, S. Sadulla and T. Ramasami, *Journal of Chemical Technology and Biotechnology*, 1999, **74**, 337-344.

149. N. M. Hassan and K. Adu-Wusu, *Solvent Extraction and Ion Exchange*, 2005, **23**, 375-389.

150. C. Dwivedi, K. K. Singh, M. Kumar, I. Singh and P. N. Bajaj, *Patent in process*, 2011.

151. C. Dwivedi, A. Kumar, J. K. Ajish, K. K. Singh, M. Kumar, P. K. Wattal and P. N. Bajaj, *RSC Advances*, 2012, **2**, 5557-5564.

152. C. Dwivedi, A. Kumar, K. A. Juby, M. Kumar, P. K. Wattal and P. N. Bajaj, *Chemical Engineering Journal*, 2012, **200–202**, 491-498.

153. K. R. Hall, L. C. Eagleton, A. Acrivos and T. Vermeulen, *Industrial and Engineering Chemistry Fundamentals*, 1966, **5**, 212-223.

154. S. Eftekhari, A. Habibi-Yangjeh and S. Sohrabnezhad, *Journal of Hazardous Materials*, 2010, **178**, 349-355.

155. Y. S. Ho and G. McKay, *Canadian Journal of Chemical Engineering*, 1998, **76**, 822-827.

156. S. Azizian, *Journal of Colloid and Interface Science*, 2004, **276**, 47-52.

157. C. R. Phillips and H. Lin Pai, *Water, Air, & Soil Pollution*, 1977, **8**, 145-163.

158. G. Prohl and A. Ulanovsky, *Radiation and Environmental Biophysics*, 2009, **48**, 243-244.

159. W. C. Camplin, G. P. Brownless, G. D. Round, K. Winpenny and G. J. Hunt, *Journal of Radiological Protection*, 2002, **22**, 371-388.

160. M. Adabbo, D. Caputo, B. De Gennaro, M. Pansini and C. Colella, *Microporous and Mesoporous Materials*, 1999, **28**, 315-324.

161. Y. G. Zhu and G. Shaw, *Chemosphere*, 2000, **41**, 121-128.

162. O. M. Vatutsina, V. S. Soldatov, V. I. Sokolova, J. Johann, M. Bissen and A. Weissenbacher, *Reactive and Functional Polymers*, 2007, **67**, 184-201.

163. G. S. Klisuranov, G. Gradev, I. Stefanova and A. Milusheva, *Use of Inorganic Sorbents for Treatment of Liquid Radioactive Waste and Backfill of Underground Repositories*, IAEA-TEC DOC-675, Vienna, 1992.

164. A. Nilchi, M. G. Maragheh and A. R. Khanchi, *Separation Science and Technology*, 1999, **34**, 1833-1843.

165. T. Moller, R. Harjula and A. Paajanen, *Separation Science and Technology*, 2003, **38**, 2995-3007.

166. S. P. Mishra and Vijaya, *Separation and Purification Technology*, 2007, **54**, 10-17.

167. S. Inan and Y. Altas, *Separation Science and Technology*, 2010, **45**, 269-276.

168. E. H. Tusa, A. Paavola, R. Harjula and J. Lehto, *Nuclear Technology*, 1994, **107**, 279-284.

169. J. B. Ayers and W. H. Waggoner, *Journal of Inorganic and Nuclear Chemistry*, 1971, **33**, 721-733.

170. W. F. Hendrickson and G. K. Riel, *Health Physics*, 1975, **28**, 17-21.

171. M. M. Ishfaq, H. M. A. Karim and M. A. Khan, *Journal of Radioanalytical and Nuclear Chemistry*, 1992, **159**, 335-342.

172. H. Loewenschuss, *Radioactive Waste Management*, 1982, **2**, 327-341.

173. E. H. Tusa, A. Paavola, R. Harjula and J. Lehto, *Proceedings of the Symposium on Waste Management*, 1993, **2**, 1687-1691.

174. C.-T. Huang and G. Wu, *Waste Management*, 1999, **19**, 263-268.

175. S. Milonji, I. Bispo, M. Fedoroff, C. Loos-Neskovic and C. Vidal-Madjar, *Journal of Radioanalytical and Nuclear Chemistry*, 2002, **252**, 497-501.

176. T. Koichi, *Reports of the Kyushu National Industrial Research Institute*, 1999, **62**, 3855-3863.

177. A. Nilchi, H. Atashi, A. H. Javid and R. Saberi, *Applied Radiation and Isotopes*, 2007, **65**, 482-487.

178. L. Wang, M. Feng, C. Liu, Y. Zhao, S. Li, H. Wang, L. Yan, G. Tian and S. Li, *Separation Science and Technology*, 2009, **44**, 4023-4035.

179. I. S. Byun, I. C. Kim and J. W. Seo, *Journal of Applied Polymer Science*, 2000, **76**, 787-798.

180. I. J. Singh and B. M. Misra, *Separation Science and Technology*, 1996, **31**, 1695-1705.

181. J. L. Collins, B. Z. Egan, K. K. Anderson, C. W. Chase, J. E. Mrochek, J. T. Bell and G. E. Jernigan, *ORNL/TM-12938, Martin Marietta Energy Systems, Oak Ridge National Laboratory*, 1995.

182. A. Nilchi, R. Saberi, M. Moradi, H. Azizpour and R. Zarghami, *Chemical Engineering Journal*, 2011, **172**, 572-580.

183. H. S. Mansur, C. M. Sadahira, A. N. Souza and A. A. P. Mansur, *Materials Science and Engineering: C*, 2008, **28**, 539-548.

184. K. Wang and Z. He, *International Journal of Pharmaceutics*, 2002, **244**, 117-126.

185. S. K. Papageorgiou, E. P. Kouvelos, E. P. Favvas, A. A. Sapalidis, G. E. Romanos and F. K. Katsaros, *Carbohydrate Research*, 2010, **345**, 469-473.

186. C. Loos-Neskovic, C. Vidal-Madjar, B. Jimenez, A. Pantazaki, V. Federici, A. Tamburini, M. Fedoroff and E. Persidou, *Radiochimica Acta*, 1999, **85**, 143-148.

187. J. L. Collins, B.Z. Egan, C. W. Chase, K. K. Anderson, and J. T. Bell, *Interim letter report to C. P. McGinnis,* Oak Ridge National Laboratory, 1994.

188. Q. Wang, J. Li, C. Chen, X. Ren, J. Hu and X. Wang, *Chemical Engineering Journal*, 2011, **174**, 126-133.

189. A. Mandal and S. Lahiri, *Journal of Radioanalytical and Nuclear Chemistry*, 2011, **290**, 115-118.

190. P. A. Haas, *Separation Science and Technology*, 1993, **28**, 2479-2506.

191. S. Ayrault, C. Loos-Neskovic, M. Fedoroff, E. Garnier and D. J. Jones, *Talanta*, 1995, **42**, 1581-1593.

192. M. M. Ishfaq, H. M. A. Karim and M. A. Khan, *Journal of Radioanalytical and Nuclear Chemistry*, 1993, **170**, 321-331.

193. D. L. Jacobi and M. Streat, *Institution of Chemical Engineers Symposium Series*, 1990, 107-118.

194. H. Mimura, N. Kageyama, K. Akiba, M. Yoneya and Y. Miyamoto, *Solvent Extraction and Ion Exchange*, 1998, **16**, 1013-1031.

195. H. Mimura, M. Kimura, K. Akiba and Y. Onodera, *Journal of Nuclear Science and Technology*, 1999, **36**, 307-310.

196. J. K. Moon, E. H. Lee and H. T. Kim, *Korean Journal of Chemical Engineering*, 2004, **21**, 1026-1031.

197. H. Mimura, J. Lehto and R. Harjula, *Journal of Nuclear Science and Technology*, 1997, **34**, 484-489.

198. A. Mardan, R. Ajaz, A. Mehmood, S. M. Raza and A. Ghaffar, *Separation and Purification Technology*, 1999, **16**, 147-158.

199. J. Lehto, S. Haukka, P. Koskinen and M. Blomberg, *Thermochimica Acta*, 1990, **160**, 343-347.

200. B. Benguella and H. Benaissa, *Water Research*, 2002, **36**, 2463-2474.

201. M. N. Zafar, R. Nadeem and M. A. Hanif, *Journal of Hazardous Materials*, 2007, **143**, 478-485.

202. V. K. Gupta and S. Sharma, *Industrial and Engineering Chemistry Research*, 2003, **42**, 6619-6624.

203. Y. S. Ho and G. McKay, *Chemical Engineering Journal*, 1998, **70**, 115-124.

204. M. Sarkar, P. K. Acharya and B. Bhattacharya, *Journal of Colloid and Interface Science*, 2003, **266**, 28-32.

205. P. Saha, S. Chowdhury, S. Gupta and I. Kumar, *Chemical Engineering Journal*, 2010, **165**, 874-882.

206. I. A. W. Tan, A. L. Ahmad and B. H. Hameed, *Journal of Hazardous Materials*, 2009, **164**, 473-482.

207. E. Sotter, X. Vilanova, E. Llobet, A. Vasiliev and X. Correig, *Sensors and Actuators B: Chemical*, 2007, **127**, 567-579.

208. U. Trudinger, G. Muller and K. K. Unger, *Journal of Chromatography A*, 1990, **535**, 111-125.

209. O. K. Varghese and C. A. Grimes, *Solar Energy Materials and Solar Cells*, 2008, **92**, 374-384.

210. J. Winkler and S. Marme, *Journal of Chromatography A*, 2000, **888**, 51-62.

211. D. S. Han, A. Abdel-Wahab and B. Batchelor, *Journal of Colloid and Interface Science*, 2010, **348**, 591-599.

212. I. Pius, R. Bhanushali, Y. Bamankar, S. Mukerjee and V. Vaidya, *Journal of Radioanalytical and Nuclear Chemistry*, 2004, **261**, 547-550.

213. Y. Altas, H. Tel and G. Yaprak, *Radiochimica Acta*, 2003, **91**, 603-606.

214. Y. Ao, J. Xu, D. Fu and C. Yuan, *Journal of Hazardous Materials*, 2009, **167**, 413-417.

215. L. M. S. Colpini, H. J. Alves, O. A. A. d. Santos and C. M. M. Costa, *Dyes and Pigments*, 2008, **76**, 525-529.

216. A. A. Attia, W. E. Rashwan and S. A. Khedr, *Dyes and Pigments*, 2006, **69**, 128-136.

217. G. McKay, H. Blair and J. R. Gardiner, *Journal of Applied Polymer Science*, 1989, **28**, 1499-1544.

218. C. T. Hsieh and H. Teng, *Journal of Chemical Technology and Biotechnology*, 2000, **75**, 1066-1072.

219. C. Galindo, P. Jacques and A. Kalt, *Journal of Photochemistry and Photobiology A: Chemistry*, 2000, **130**, 35-47.

220. N. K. Mandal and R. Biswas, *Indian Journal of Public Health*, 2004, **48**, 30-33.

221. W. P. Tseng, *Environmental Health Perspectives*, 1977, **19**, 109-119.

222. E. O. Kartinen Jr and C. J. Martin, *Desalination*, 1995, **103**, 79-88.

223. R. C. Cheng, S. Liang, H.-C. Wang and M. D. Beuhler, *Journal of American Water Works Association*, 1994, **86**, 79-90.

224. J. G. Hering, P. Y. Chen, J. A. Wilkie, M. Elimelech and S. Liang, *Journal-American Water Works Association*, 1996, **88**, 155-167.

225. J. G. Hering, P. Y. Chen, J. A. Wilkie and M. Elimelech, *Journal of Environmental Engineering*, 1997, **123**, 800-807.

226. D. M. Antonelli and J. Y. Ying, *Angewandte Chemie International Edition in English*, 1995, **34**, 2014-2017.

227. Z.-T. Jiang and Y.-M. Zuo, *Analytical Chemistry*, 2000, **73**, 686-688.

228. H. Oveisi, N. Suzuki, A. Beitollahi and Y. Yamauchi, *Journal of Sol-Gel Science and Technology*, 2010, **56**, 212-218.

229. L. Sun, M. J. Annen, F. Lorenzano-Porras, P. W. Carr and A. V. McCormick, *Journal of Colloid and Interface Science*, 1994, **163**, 464-473.

230. U. Meyer, A. Larsson, H. P. Hentze and R. A. Caruso, *Advanced Materials*, 2002, **14**, 1768-1772.

231. C. Dwivedi, N. Raje, J. Nuwad, M. Kumar and P. N. Bajaj, *Chemical Engineering Journal*, 2012, **193–194**, 178-186.

232. A. A. Said and R. M. Hassan, *Polymer Degradation and Stability*, 1993, **39**, 393-397.

233. J. Ovenstone and K. Yanagisawa, *Chemistry of Materials*, 1999, **11**, 2770-2774.

234. K. T. Jacob and S. Gupta, *Bulletin of Materials Science* 2009, **32**, 611–616.

235. P.-W. Chou, Y.-S. Wang, C.-C. Lin, Y.-J. Chen, C.-L. Cheng and M.-S. Wong, *Surface and Coatings Technology*, 2009, **204**, 834-839.

236. G. H. Lee and J.-M. Zuo, *Journal of the American Ceramic Society* 2004, **87**, 473-479.

237. K.-F. Du, D. Yang and Y. Sun, *Industrial & Engineering Chemistry Research*, 2008, **48**, 755-762.

238. K. J. A. Raj and B. Viswanathan, *Indian Journal of Chemisry A*, 2009, **48**, 1378-1382.

239. A. D. Belapurkar, P. Sherkhane and S. P. Kale, *Current Science*, 2006, **91**, 73-76.

240. U. G. Akpan and B. H. Hameed, *Journal of Colloid and Interface Science*, 2011, **357**, 168-178.

241. P. W. Chou, S. Treschev, P. H. Chung, C. L. Cheng, Y. H. Tseng, Y. J. Chen and M. S. Wong, *Applied Physics Letters*, 2006, **89,** 131919(1)-131919(3).

242. M. Stylidi, D. I. Kondarides and X. E. Verykios, *Applied Catalysis B: Environmental*, 2004, **47**, 189-201.

243. M. Yamashita and H. Kashiwagi, *IEEE Journal of Quantum Electronics*, 1976, **QE-12**, 90-95.

244. D. R. Liu, Y. S. Jiang and G. M. Gao, *Chemosphere*, 2011, **83**, 1546-1552.

List of Publications included in the present thesis

Patent

1. A new method for synthesis of resol beads with good control over their size **C. Dwivedi**, K. K. Singh, M.Kumar, I. J. Singh, P. N. Bajaj, Patent Application submmited (2012).

Journal

1. Resorcinol-Formaldehyde Coated XAD Resin Beads for Removal of Cesium Ions from Radioactive Waste: Synthesis Adsorption and Kinetic Studies

   C. Dwivedi, A. Kumar, K. A. Juby, K. K. Singh, M. Kumar, P. K. Wattal, P. N. Bajaj, *RSC Advances* 2012, **2**, 5557-5564.

2. Synthesis and Characterization of Mesoporous Titania Microspheres and their Applications

   C. Dwivedi, N. Raje, J. Nuwad, M. Kumar, P. N. Bajaj, *Chemical Engineering Journal*, 2012, **193–194**, 178-186.

3. Preparation and Evaluation of Alginate Assisted Spherical Resorcinol-Formaldehyde Resin Beads for Removal of Cesium From Waste

   C. Dwivedi, A. Kumar, K. A. Juby, M. Kumar, P. K. Wattal, P. N. Bajaj, *Chemical Engineering Journal*, 2012, 200-202, 491-498.

4. Copperhexacyanoferrate-Polymer Composite Beads for Cesium Ion Removal: Synthesis, Characterization, Sorption and Kinetic Studies

   C. Dwivedi, A. Kumar , K. A. Juby, K. K. Singh, M. Kumar, P. K. Wattal, P. N. Bajaj, *Journal of Applied Polymer Science*, 2012, DOI: 10.1002/app.38707.

5. Removal of Cesium by Spherical Resorcinol-Formaldehyde Resin Beads: Sorption and Kinetic Studies

   C. Dwivedi, S. K. Pathak, M. Kumar, S. C. Tripathi, P. N. Bajaj, *Journal of Radioanalytical and Nuclear Chemistry*, 2012, DOI 10.1007/s10967-012-2320-y.

6. Uptake Studies of Arsenic [(III) and (V)] on Synthesized Mesoporous Titania Microspheres

   C. Dwivedi, N. Raje, M Kumar, A. V. R. Reddy, P. N. Bajaj, *Journal of Radioanalytical and Nuclear Chemistry* 2012, **294**, 131-136.

7. Preparation and Characterization of Potassium Nickelhexacyanoferrate Loaded Hydrogel Beads for the Removal of Cesium Ions

   C. Dwivedi, S. K. Pathak, M. Kumar, S. C. Tripathi, P. N. Bajaj, (Communicated, 2012).

8. Potassium copperhexacyanoferrate-Hydrogel Beads: Synthesis, Characterization and Applications

   C. Dwivedi, S. K. Pathak, M. Kumar, S. C. Tripathi, P. N. Bajaj, (To be communicated, 2012).

9. Selective Removal of Cesium Ions by Potassium Cobalthexacyanoferrate-Gel beads: Kinetics, and Sorption Isotherms Studies

   C. Dwivedi, S. K. Pathak, M. Kumar, S. C. Tripathi, P. N. Bajaj, (To be communicated, 2012).